Appendix A

Air Quality Modeling

2016 Moderate Area Plan for the 2012 PM2.5 Standard

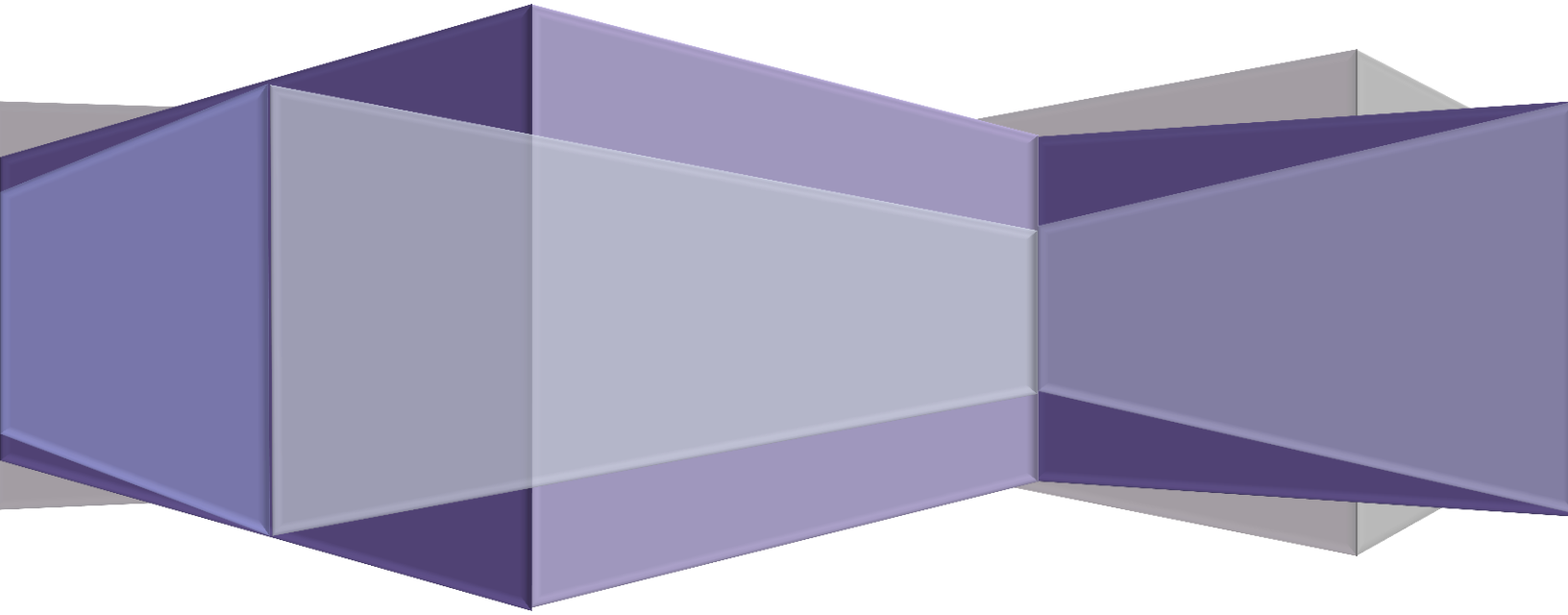

[This Appendix provided by the California Air Resources Board]

This page intentionally blank.

MODELING ASSESSMENT

Photochemical Modeling for the 2016 San Joaquin Valley Annual $PM_{2.5}$ State Implementation Plan

Prepared by

California Air Resources Board
San Joaquin Valley Air Pollution Control District

Prepared for

United States Environmental Protection Agency Region IX

July 26, 2016

TABLE OF CONTENTS

1 INTRODUCTION 8
2 APPROACHES 8
2.1 METHODOLOGY 8
2.2 MODELING PERIOD 9
2.3 BASELINE DESIGN VALUES 9
2.4 BASE, REFERENCE, AND FUTURE YEARS 11
2.5 $PM_{2.5}$ SPECIES CALCULATIONS 12
2.6 FUTURE YEAR DESIGN VALUES 14
3 METEOROLOGICAL MODELING 15
3.1 WRF MODEL SETUP 15
3.2 WRF MODEL RESULTS AND EVALUATION 18
3.2.1 PHENOMENOLOGICAL EVALUATION 30
4 EMISSIONS 34
4.1 EMISSIONS SUMMARIES 34
5 $PM_{2.5}$ MODELING 36
5.1 CMAQ MODEL SETUP 36
5.2 CMAQ MODEL EVALUATION 39
5.3 FUTURE YEAR DESIGN VALUES 48
5.4 PRECURSOR SENSITIVITY ANALYSIS 51
5.5 DISCUSSION ON PRECURSOR SENSITIVITY 55
6 REFERENCES 60
SUPPLEMENTAL MATERIALS 66

List of Figures

Figure 1. WRF modeling domains (D01 36km; D02 12km; and D03 4km). 16

Figure 2. Meteorological observation sites in San Joaquin Valley. The numbers correspond to the sites listed in Table 7. 19

Figure 3. Distribution of model daily mean bias for Modesto, Fresno, Visalia, Bakersfield and SJV. Results are shown for wind speed (top), temperature (middle), and Relative Humidity (bottom). 26

Figure 4. Distribution of model daily mean error for Modesto, Fresno, Visalia, Bakersfield and SJV. Results are shown for wind speed (top), temperature (middle), and Relative Humidity (bottom). 27

Figure 5. Comparison of modeled and observed hourly wind speed (left column), 2-meter temperature (middle column), and relative humidity (right column). Results for Modesto are shown in the top row, Fresno in the middle row, and Visalia in the bottom row. 28

Figure 6. Comparison of modeled and observed hourly wind speed (left column), 2-meter temperature (middle column), and relative humidity (right column). Results for Bakersfield are shown in the top row and SJV in the bottom row. 29

Figure 7. Surface wind field at 13:00 PST January 20, 2013. 31

Figure 8. Surface wind field at 01:00 PST January 21, 2013. 32

Figure 9. Surface wind field at 08:00 PST January 21, 2013. 33

Figure 10. Monthly average biogenic ROG emissions for 2013. 36

Figure 11. CMAQ modeling domains utilized in the modeling assessment. 37

Figure 12. Bugle plot of annual $PM_{2.5}$ model performance in terms of MFB and MFE at four CSN sites in the SJV (i.e., Bakersfield, Fresno, Modesto, and Visalia). 45

Figure 13. Comparison of annual $PM_{2.5}$ model performance to other modeling studies in Simon et al. (2012). Red symbols represent performance at the four CSN sites in the SJV 46

Figure 14. Excess NH_3 in the SJV on January 18 (Left) and January 20 (Right) based on NASA aircraft measurements in 2013. 56

List of Tables

Table 1. Illustrates the data from each year that are utilized in the baseline Design Value calculation. 10

Table 2. Average baseline DVs for each FRM monitoring site in the SJV, as well as the yearly design values from 2012-2014 utilized in calculating the baseline DVs. 10

Table 3. Description of CMAQ model simulations used to evaluate model performance and project baseline design values to the future. 12

Table 4. $PM_{2.5}$ speciation data used for each $PM_{2.5}$ design site. 13

Table 5. WRF vertical layer structure. 17

Table 6. WRF Physics Options. 17

Table 7. Meteorological monitor location and parameter(s) measured. 20

Table 8. Hourly surface wind speed, temperature and relative humidity statistics in Modesto. 21

Table 9. Hourly surface wind speed, temperature and relative humidity statistics in Fresno. 22

Table 10. Hourly surface wind speed, temperature and relative humidity statistics in Visalia. 23

Table 11. Hourly surface wind speed, temperature and relative humidity statistics in Bakersfield (valid RH data available from January through May only; statistics are based on the available data). 24

Table 12. Hourly surface wind speed, temperature and relative humidity statistics in the San Joaquin Valley. 25

Table 13. SJV Annual Planning Emissions for 2013, 2021, and 2025 35

Table 14. CMAQ configuration and settings. 38

Table 15. Quarterly and annual $PM_{2.5}$ model performance based on CSN measurement at Fresno – Garland. 41

Table 16. Quarterly and annual $PM_{2.5}$ model performance based on CSN measurement at Visalia. 42

Table 17. Quarterly and annual $PM_{2.5}$ model performance based on CSN measurement at Bakersfield. 43

Table 18. Quarterly and annual $PM_{2.5}$ model performance based on CSN measurement at Modesto. 44

Table 19. Model performance for 24-hour $PM_{2.5}$ concentrations measured from continuous $PM_{2.5}$ monitors 48

Table 20. Projected future year $PM_{2.5}$ DVs at each monitor 49

Table 21. Annual RRFs for $PM_{2.5}$ components 49

Table 22. Base year $PM_{2.5}$ compositions* 50

Table 23. Projected future year $PM_{2.5}$ compositions 51

Table 24. Difference in $PM_{2.5}$ and ammonium nitrate DVs from a 30% perturbation in anthropogenic NO_x emissions. 52

Table 25. Difference in $PM_{2.5}$ and components (including sulfate, OM, EC, and other) DVs from a 30% perturbation in anthropogenic $PM_{2.5}$ emissions 53

Table 26. Difference in $PM_{2.5}$ and ammonium nitrate DVs from a 30% perturbation in ammonia emissions 53

Table 27. Difference in $PM_{2.5}$ and SOA DVs from a 30% perturbation in VOCs emissions 54

Table 28. Difference in $PM_{2.5}$ and sulfate DVs from a 30% perturbation in SO_x emissions 54

ACRONYMS

ARB – Air Resources Board

BCs – Boundary Conditions

CMAQ Model – Community Multi-scale Air Quality Model

CRPAQS – California Regional Particulate Air Quality Study

CSN – Chemical Speciation Network

DISCOVER-AQ – Deriving Information on Surface Conditions from Column and Vertically Resolved Observations Relevant to Air Quality

DV – Design Value

EC – Elemental Carbon

FEM – Federal Equivalent Method

FRM – Federal Reference Method

GEOS-5 – Goddard Earth Observing System Model, Version 5

GMAO – Global Modeling and Assimilation Office

ICs – Initial Conditions

MEGAN – Model of Emissions of Gases and Aerosols from Nature

MFB – Mean Fractional Bias

MFE – Mean Fractional Error

MOZART – Model for Ozone and Related chemical Tracers

NARR – North American Regional Reanalysis

NASA – National Aeronautics and Space Administration

NCR – National Center for Atmospheric Research

NMB – Normalized Mean Bias

NME – Normalized Mean Error

NO_x – Oxides of Nitrogen

OC – Organic Carbon

OM – Organic Matter

$PM_{2.5}$ – Particulate Matter of Aerodynamic Diameter less than 2.5 micrometers

RMSE – Root Mean Square Error

ROG – Reactive Organic Gases

RRF – Relative Response Factors

SANWICH – Sulfate, Adjusted Nitrate, Derived Water, Inferred Carbon Hybrid material balance

SAPRC – Statewide Air Pollution Research Center

SIP – State Implementation Plan

SJV – San Joaquin Valley

SOA – Secondary Organic Aerosol

SO_x – Sulfur oxides

U.S. EPA – United States Environmental Protection Agency

VOCs – Volatile Organic Compounds

WRF – Weather and Research Forecasting

1 INTRODUCTION

The purpose of this document is to summarize the findings of the modeling assessment for the annual $PM_{2.5}$ (12 µg/m^3) standard in the San Joaquin Valley nonattainment area (SJV or the Valley), which forms the scientific basis for the SJV 2016 annual $PM_{2.5}$ SIP. The 12 µg/m^3 standard was promulgated by the U.S. EPA in 2012, and EPA issued final designations in 2014. Currently, the Valley is designated as a Moderate nonattainment area for this standard with an attainment date of 2012. However, recent $PM_{2.5}$ trends in the Valley brought on by a sustained drought coupled with the modeling assessment described below, illustrates the impracticability of attaining the standard by 2021. This would lead to a reclassification of the Valley from a Moderate to Serious nonattainment area, as well as a new SIP timeline and attainment date of 2025.

The remainder of the document is organized as follows: Section 2 describes the general approach for projecting design values (DVs) to the future (2021), Section 3 discusses the meteorological modeling and evaluation, while Sections 4 and 5 describe the emissions inventory and $PM_{2.5}$ modeling and evaluation, respectively. A more detailed description of the modeling and development of the model-ready emissions inventory can be found in the Photochemical Modeling Protocol Appendix.

2 APPROACHES

This section briefly describes the Air Resources Board's (ARB's) procedures, based on U.S. EPA guidance (U.S. EPA, 2014), for projecting future year annual $PM_{2.5}$ Design Values (DVs) using model output and a Relative Response Factor (RRF) approach.

2.1 METHODOLOGY

The U.S. EPA modeling guidance (U.S. EPA, 2014) outlines the approach for using models to predict future year annual $PM_{2.5}$ DVs. The guidance recommends using model predictions in a "relative" rather than "absolute" sense. In this relative approach, the fractional change (or ratio) in $PM_{2.5}$ concentration between the model future year and model baseline year are calculated for all valid monitors. These ratios are called relative response factors (RRFs). Since $PM_{2.5}$ is comprised of different chemical species, which respond differently to changes in emissions of various pollutants, separate RRFs are calculated for the individual $PM_{2.5}$ species. Baseline DVs are then projected to the future on a species-by-species basis, where the DV is separated into individual $PM_{2.5}$ species and each species is multiplied by its corresponding RRF. The individual species are then summed to obtain the future year $PM_{2.5}$ DV.

A brief summary of the modeling procedures utilized in this attainment analysis, as prescribed by the U.S. EPA modeling guidance (U.S. EPA, 2014), is provided below. A

more detailed description can be found in the Photochemical Modeling Protocol Appendix.

2.2 MODELING PERIOD

Based on analysis of recent years' ambient $PM_{2.5}$ levels and meteorological conditions leading to elevated $PM_{2.5}$ concentrations, the year 2013 was selected for baseline modeling calculations. The National Aeronautics and Space Administration (NASA) launched the DISCOVER-AQ (Deriving Information on Surface Conditions from Column and Vertically Resolved Observations Relevant to Air Quality) field campaign in the SJV from January 16th to Mid-February, 2013. This field study provided unprecedented observations of wintertime $PM_{2.5}$ and its precursors not available in the SJV since the CRPAQS (i.e., California Regional Particulate Air Quality Study) study more than 15 years ago. These observations aided in development of the modeling platform used in this SIP work.

2.3 BASELINE DESIGN VALUES

Specifying the baseline DV is a key consideration in the model attainment test, because this value is projected forward to the future and used to test for future attainment of the standard at each monitor. U.S. EPA guidance (2014) defines the annual $PM_{2.5}$ DV for a given year as the 3-year average (ending in that year) of the annual average $PM_{2.5}$ concentrations, where the annual average is calculated as the average of the quarterly averages for each calendar quarter (e.g., January-March, April-June, July-September, October-December). For example, the 2012 $PM_{2.5}$ DV is the average of the annual $PM_{2.5}$ concentrations from 2010, 2011, and 2012.

To minimize the influence of year-to-year variability in demonstrating attainment, the U.S. EPA (2014) optionally allows the averaging of three DVs, where one of the years is the baseline emissions inventory and modeling year. This average DV is referred to as the baseline DV. For a baseline modeling year of 2013, this would typically mean that the average of the 2013, 2014, and 2015 DVs would be used. However, at the time of this work the 2015 DVs were still preliminary (i.e., 2015 measurements had not been finalized), so the average DV will instead include 2012, 2013, and 2014. Since each DV represents an average over three years, observational data from 2010, 2011, 2012, 2013, and 2014 will influence the average DV, with each year receiving a different weighting. Table 1 illustrates the observational data from each year that goes into the baseline DV.

Table1. Illustrates the data from each year that are utilized in the baseline Design Value calculation.

DV Year	Years averaged for the DV (average of quarterly average $PM_{2.5}$)				
2012	2010	2011	2012		
2013		2011	2012	2013	
2014			2012	2013	2014
Yearly weighting for the baseline DV calculation					
$2012-2014\ Average = \frac{PM2.5_{2010} + 2 \times PM2.5_{2011} + 3 \times PM2.5_{2012} + 2 \times PM2.5_{2013} + PM2.5_{2014}}{9}$					

Table 2 shows the 2012-2014 average DVs (or baseline DVs) for each Federal Reference Method (FRM) /Federal Equivalent Method (FEM) site in the SJV. For three sites with incomplete data, assumptions were made to calculate the baseline DVs and those assumptions were annotated following Table 2. The highest DV occurred at the Bakersfield – Planz site with a baseline DV of 17.3 µg/m^3.

Table 2. Average baseline DVs for each FRM monitoring site in the SJV, as well as the yearly design values from 2012-2014 utilized in calculating the baseline DVs.

AQS site ID	Monitoring Site Name	2012	2013	2014	2012-2014 Average Baseline
60290016	Bakersfield - Planz	15.6	16.9	19.3	17.3
60392010	Madera		18.1	15.8	16.9*
60311004	Hanford	15.8	17.0	16.8	16.5
60310004	Corcoran				16.3*
61072002	Visalia	14.8	16.6	17.2	16.2
60195001	Clovis	16.0	16.4	16.0	16.1
60290014	Bakersfield – California Ave.	14.5	16.4	17.2	16.0
60190011	Fresno –Garland	14.2	15.4	15.3	15.0
60990006	Turlock	14.9	15.7	14.1	14.9
60195025	Fresno –Hamilton & Winery	13.9	14.7	14.1	14.2

60771002	Stockton	11.6	13.8	14.1	13.1
60470003	Merced - Coffee	14.3	13.3	11.7	13.1
60990005	Modesto	12.9	13.6	12.5	13.0
60472510	Merced -Main Street	10.4	11.1	11.4	11.0
60772010	Manteca		10.2	9.9	10.1*
60192009	Tranquility	7.5	7.9	7.7	7.7

*: Because of incomplete data, at Madera and Manteca, only DVs from 2013 and 2014 were averaged to determine the baseline DV; at Corcoran, annual average concentrations from 2010, 2013, and 2014 were averaged to obtain baseline DV.

2.4 BASE, REFERENCE, AND FUTURE YEARS

The modeling assessment consists of the following three primary model simulations, which all used the same model inputs for meteorology, chemical boundary conditions, and biogenic emissions. The only difference between the simulations was the year represented by the anthropogenic emissions (2013 or 2021) and certain day-specific emissions.

1. *Base Year (or Base Case) Simulation*
   The base year simulation for 2013 was used to assess model performance and includes as much day-specific detail as possible in the emissions inventory such as hourly adjustments to the motor vehicle and biogenic inventories based on observed local meteorological conditions, as well as known wildfire and agricultural burning events.

2. *Reference (or Baseline) Year Simulation*
   The reference year simulation was identical to the base year simulation, except that certain emissions events which are either random and/or cannot be projected to the future were removed from the emissions inventory. For the 2013 reference year modeling, the only category/emissions source that was excluded was wildfires, which are difficult to predict in the future and can significantly influence the model response to anthropogenic emissions reductions in regions with large fires.

3. *Future Year Simulation*
   The future year simulation is identical to the reference year simulation, except that projected future year (2021) anthropogenic emission levels were used rather than 2013 emission levels. All other model inputs (e.g., meteorology, chemical

boundary conditions, biogenic emissions, and calendar for day-of-week specifications in the inventory) are the same as those used in the reference year simulation.

To summarize (Table 3), the base year 2013 simulation was used for evaluating model performance, while the reference (or baseline) 2013 and future year 2021 simulations were used to project the average DVs to the future as described in the Photochemical Modeling Protocol Appendix and in subsequent sections of this document.

Table 3. Description of CMAQ model simulations used to evaluate model performance and project baseline design values to the future.

Simulation	Anthropogenic Emissions	Biogenic Emissions	Meteorology	Chemical Boundary Conditions
Base year (2013)	2013 w/ wildfires	2013 MEGAN	2013 WRF	2013 MOZART
Reference year (2013)	2013 w/o wildfires	2013 MEGAN	2013 WRF	2013 MOZART
Future year (2021)	2021 w/o wildfires	2013 MEGAN	2013 WRF	2013 MOZART

2.5 $PM_{2.5}$ SPECIES CALCULATIONS

Since $PM_{2.5}$ consists of different chemical components, it is necessary to assess how each individual component will respond to emission reductions. As a first step in this process, the measured total $PM_{2.5}$ must be separated into its various components. In the SJV, the primary components on the filter based $PM_{2.5}$ measurements include sulfates, nitrates, ammonium, organic carbon (OC), elemental carbon (EC), particle-bound water, other primary inorganic particulate matter, and passively collected mass (blank mass). Species concentrations were obtained from the four chemical speciation network (CSN) sites in the SJV. These four CSN sites are located at: Bakersfield – California Avenue, Fresno – Garland, Visalia – North Church, and Modesto – 14th Street. Chemical species were measured once every three or six days at those sites. Since not all of the 16 FRM $PM_{2.5}$ sites in the Valley have collocated speciation monitors, it was necessary to utilize the speciated $PM_{2.5}$ measurements at one of the four CSN sites to represent the speciation profile at each of the FRM sites. The choice of which CSN site to represent the speciation profile at a given FRM monitor (Table 4) was determined based on geographic proximity, analysis of local emission sources, and

measurements from previous field studies (e.g., CRPAQS), and is consistent with previous $PM_{2.5}$ SIPs in the Valley.

Table 4. $PM_{2.5}$ speciation data used for each $PM_{2.5}$ design site.

AQS Site ID	$PM_{2.5}$ Design Site (FRM/FEM Monitor)	$PM_{2.5}$ Speciation Site
60290016	Bakersfield – Planz	Bakersfield – California
60392010	Madera	Fresno – Garland
60311004	Hanford	Visalia – Church
60310004	Corcoran	Visalia – Church
61072002	Visalia	Visalia – Church
60195001	Clovis	Fresno – Garland
60290014	Bakersfield – California Ave.	Bakersfield – California
60190011	Fresno – Garland	Fresno – Garland
60990006	Turlock	Modesto – 14th
60195025	Fresno – Hamilton & Winery	Fresno – Garland
60771002	Stockton	Modesto – 14th
60470003	Merced – Coffee	Modesto – 14th
60990005	Modesto	Modesto – 14th
60472510	Merced – Main Street	Modesto – 14th
60772010	Manteca	Modesto – 14th
60192009	Tranquility	Fresno – Garland

Since the FRM $PM_{2.5}$ monitors do not retain all of the $PM_{2.5}$ mass that is measured by the speciation samplers, the U.S. EPA (2014) recommends using the SANDWICH approach (Sulfate, Adjusted Nitrate, Derived Water, Inferred Carbon Hybrid material balance) described by Frank (2006) to apportion the FRM $PM_{2.5}$ mass to individual $PM_{2.5}$ species based on nearby CSN speciation data. A detailed description of the SANDWICH method can be found in the modeling protocol and in the U.S. EPA (2014) modeling guidance. In addition, based on completeness of the data, $PM_{2.5}$ speciation data from 2010 – 2013 were utilized. For each quarter, percent contributions from individual chemical species to FRM $PM_{2.5}$ mass were calculated as the average of the corresponding quarter from 2010-2013. In general, the inter-annual variability of the species fractions is small compared to the variability in the species concentrations and so the use of average data from 2010 – 2013 is appropriate.

2.6 FUTURE YEAR DESIGN VALUES

Projecting baseline annual $PM_{2.5}$ DVs to the future is a multi-step process as outlined below. See U.S. EPA (2014) and the Photochemical Modeling Protocol Appendix for additional details.

Step 1: Compute observed quarterly weighted average concentrations (consistent with the weighted average DV calculation) at each monitor for the following species: ammonium, nitrate, sulfate, organic carbon, elemental carbon, and other primary PM. This is done by multiplying quarterly weighted average FRM $PM_{2.5}$ concentrations by the fractional composition of $PM_{2.5}$ species for each quarter.

Step 2: Compute the component-specific RRF for each quarter and each species at each monitor based on the reference and future year modeling. The RRF for a specific component *j* is calculated using the following expression:

$$RRF_j = \frac{[C]_{j,\ future}}{[C]_{j,\ reference}} \quad (1)$$

Where $[C]_{j,\ future}$ is the modeled quarterly mean concentration for component *j* predicted for the future year averaged over the 3x3 array of grid cells surrounding the monitor, and $[C]_{j,reference}$ is the same, but for the reference year simulation. An RRF was calculated for each species in Step 1 and at each monitor and for each quarter.

Step 3: Apply the component specific RRF from Step 2 to the observed quarterly weighted average concentrations from Step 1 to obtain projected quarterly species concentrations.

Step 4: Use the online E-AIM model (http://www.aim.env.uea.ac.uk/aim/aim.php) to calculate future year particle-bound water for each quarter at each monitor based on projected ammonium sulfate and ammonium nitrate concentrations.

Step 5: The projected concentration for each quarter is summed over all species, including particle bound water from Step 4, as well as a blank mass of 0.5 µg/m^3 to obtain the future quarterly average $PM_{2.5}$ concentration. Finally, the future annual $PM_{2.5}$ DVs are calculated as the average of the projected $PM_{2.5}$ concentrations from the four quarters.

Projected future year $PM_{2.5}$ DVs are discussed in Section 5.3.

3 METEOROLOGICAL MODELING

California's proximity to the ocean, complex terrain, and diverse climate represent a unique challenge for developing meteorological fields that adequately represent the synoptic and mesoscale features of the regional meteorology. In summertime, the majority of the storm tracks are far to the north of the state and a semi-permanent Pacific high typically sits off the California coast. Interactions between this eastern Pacific subtropical high pressure system and the thermal low pressure further inland over the Central Valley or South Coast lead to conditions conducive to pollution buildup (Fosberg and Schroeder, 1966; Bao et al., 2008). In wintertime, periods of high atmospheric pressure bring light winds and, sometimes, low solar insolation (Daly et al. 2009) to the Central Valley. Because of the topographical features surrounding San Joaquin Valley, under such conditions, a layer of cold and wet air can be overlaid by warm air aloft creating strong and long-lasting stagnation in the area (Whiteman et al. 2001). It is under such conditions that high surface particulate matter concentrations typically occur (Gilles et al. 2010; Baker et al. 2011).

In the past, the ARB has utilized both prognostic and diagnostic meteorological models, as well as hybrid approaches in an effort to develop meteorological fields for use in air quality modeling that most accurately represent the meteorological processes which are important to air quality (e.g., Jackson et al., 2006). In this work, the state-of-the-science Weather and Research Forecasting (WRF) prognostic model (Skamarock et al., 2005) version 3.6 was utilized to develop the meteorological fields used in the subsequent photochemical model simulations.

3.1 WRF MODEL SETUP

The WRF meteorological modeling domain consisted of three nested Lambert projection grids of 36-km (D01), 12-km (D02), and 4-km (D03) uniform horizontal grid spacing (Figure 1). WRF was run simultaneously for the three nested domains with two-way feedback between the parent and the nest grids. The D01 and D02 grids were used to resolve the larger scale synoptic weather systems, while the D03 grid resolved the finer details of the atmospheric conditions and was used to drive the air quality model simulations. All three domains utilized 30 vertical sigma layers (defined in Table 5), with the major physics options for each domain listed in Table 6.

Initial and boundary conditions (IC/BCs) for the WRF modeling were based on the 32-km horizontal resolution North American Regional Reanalysis (NARR) data that are archived at the National Center for Atmospheric Research (NCAR). Boundary conditions to WRF were updated at 6-hour intervals for the 36-km grid (D01). In addition, surface and upper air observations obtained from NCAR were used to further refine the analysis data that were used to generate the IC/BCs. Analysis nudging was

employed in the outer 36-km grid (D01) to ensure that the simulated meteorological fields were adequately constrained and did not deviate from the observed meteorology. No nudging was used on the two inner domains to allow model physics to work fully without externally imposed forcing (Rogers et al., 2013).

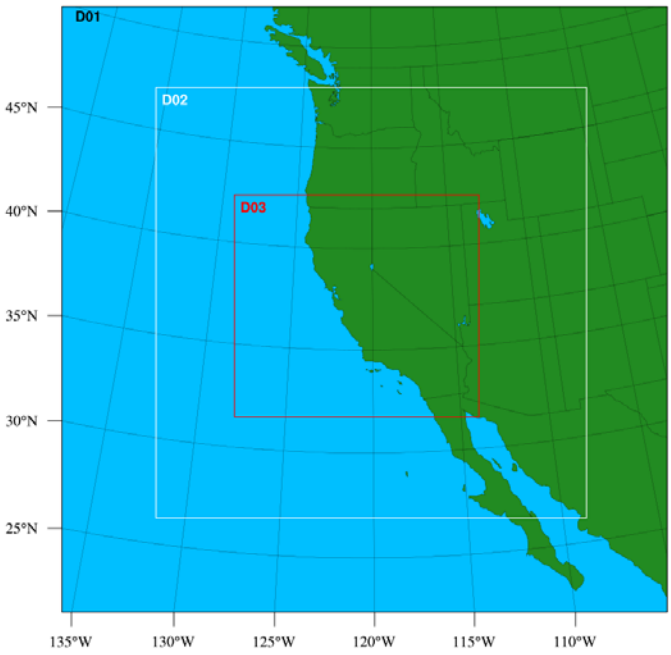

Figure 1. WRF modeling domains (D01 36km; D02 12km; and D03 4km).

Table 5. WRF vertical layer structure.

Layer Number	Height (m)	Layer Thickness (m)	Layer Number	Height (m)	Layer Thickness (m)
30	16082	1192	14	1859	334
29	14890	1134	13	1525	279
28	13756	1081	12	1246	233
27	12675	1032	11	1013	194
26	11643	996	10	819	162
25	10647	970	9	657	135
24	9677	959	8	522	113
23	8719	961	7	409	94
22	7757	978	6	315	79
21	6779	993	5	236	66
20	5786	967	4	170	55
19	4819	815	3	115	46
18	4004	685	2	69	38
17	3319	575	1	31	31
16	2744	482	0	0	0
15	2262	403			

Note: Shaded layers denote the subset of vertical layers used in the CMAQ photochemical model simulations.

Table 6. WRF Physics Options.

Physics Option	**Domain**		
	D01 (36 km)	**D02 (12 km)**	**D03 (4 km)**
Microphysics	WSM 6-class graupel scheme	WSM 6-class graupel scheme	WSM 6-class graupel scheme
Longwave radiation	RRTM	RRTM	RRTM
Shortwave radiation	Dudhia scheme	Dudhia scheme	Dudhia scheme
Surface layer	Revised MM5 Monin-Obukhov	Revised MM5 Monin-Obukhov	Revised MM5 Monin-Obukhov
Land surface	TD Scheme (Jan., Feb., Nov. and Dec.) Pleim-Xiu LSM (others)	TD Scheme (Jan., Feb., Nov. and Dec.) Pleim-Xiu LSM (others)	TD Scheme (Jan., Feb., Nov. and Dec.) Pleim-Xiu LSM (others)
Planetary Boundary Layer	YSU	YSU	YSU
Cumulus Parameterization	Kain-Fritsch scheme	Kain-Fritsch scheme	None

3.2 WRF MODEL RESULTS AND EVALUATION

Simulated surface wind speed, temperature, and relative humidity from the 4 km domain were validated against hourly observations at 77 surface stations in the SJV. Observational data for the surface stations were obtained from the ARB's archived meteorological database (http://www.arb.ca.gov/aqmis2/aqmis2.php). Table 7 lists the observational stations and the parameters measured at each station, including wind speed and direction (wind), temperature (T) and relative humidity (RH). The location of each of these sites is shown in Figure 2. Quarterly and annual quantitative performance metrics for 2013 were used to compare hourly surface observations and modeled estimates: mean bias (MB), mean error (ME) and index of agreement (IOA) based on recommendations from Simon et al. (2012). A summary of these statistics by performance region is shown in Tables 8 through 12. The performance regions cover roughly the Modesto, Fresno, Visalia, and Bakersfield regions, as well as one for the entire San Joaquin Valley (SJV), respectively. The region around Modesto includes sites 5737, 2833, and 2080. The region surrounding Fresno encompasses sites 5741, 2449, 2013, and 2844. The region around Visalia includes sites 2032, 5386, and 3250, while the region covering Bakersfield includes sites 5287 and 3146 (note that valid relative humidity observations in the Bakersfield area were only available at site 5287 for the months of January through May 2013). Model performance statistical metrics were calculated using all of the available data. All the sites in the valley are included in the SJV performance region (in addition to the sites mentioned above). The distribution of daily mean bias and mean error are shown in Figures 3 and 4. Figures 5 and 6 show observed vs. modeled scatter plots.

From a valley-wide perspective, the wind speed biases were positive in each quarter of 2013. At Bakersfield the biases turn slightly negative throughout the year, and are mostly less than 0.6 m/s. The annual temperature biases are less than 1 K in all performance regions, with the quarterly temperature biases reaching as high as -1.87 K in Bakersfield during the second quarter of 2013. Simulated temperature is generally in good agreement with the observations in all regions with the index of agreement (IOA) above 0.90 (1.0 represents perfect agreement). Relative humidity biases are positive except in the Modesto region. The annual bias values range from -1.53% to 12.47%, with the largest bias occurring in Visalia. These results are comparable to other recent WRF modeling efforts in California investigating ozone formation in Central California (e.g., Hu et al., 2012) and modeling analysis for the CalNex and CARES field studies (e.g., Fast et al., 2014; Baker et al., 2013; Kelly et al., 2014; Angevine et al., 2012). Detailed hourly time-series of surface temperature, relative humidity, wind speed, and wind direction for SJV can be found in the supplementary material, together with 2013 quarterly mean bias and mean error distributions of these parameters.

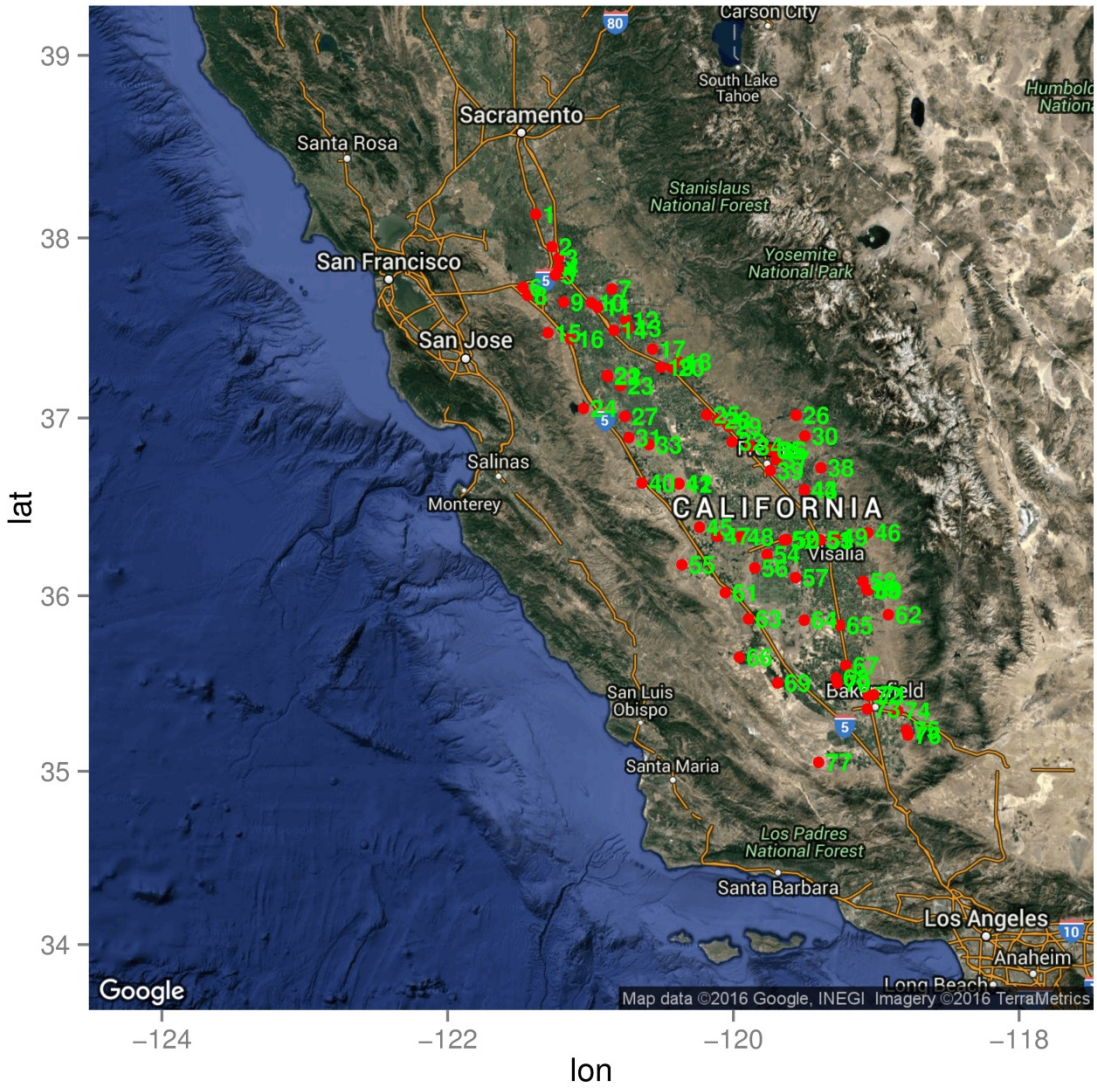

Figure 2. Meteorological observation sites in San Joaquin Valley. The numbers correspond to the sites listed in Table 7.

Table 7. Meteorological monitor location and parameter(s) measured.

Site	Site ID	Site Name	Parameter Measured	Site	Site ID	Site Name	Parameter Measured
1	5809	LodiWest	T, RH	40	3309	PanocheRd	Wind, T, RH
2	2094	Stockton-Haz	Wind, T, RH	41	3759	Tranquility	Wind, T
3	5362	StocktonArpt	Wind, T	42	5757	Westlands	T, RH
4	5736	Manteca	T, RH	43	5723	Parlier2	T, RH
5	3772	Manteca-Fish	Wind, T	44	2114	Parlier	Wind, T, RH
6	5810	Tracy	T, RH	45	5828	FivePointsSW	T, RH
7	5831	Oakdale2	T, RH	46	5746	Lindcove	T, RH
8	3696	Tracy_Air	Wind, T	47	5708	FivePoints2	T, RH
9	5737	Modesto3	T, RH	48	2544	Lemoore-Met	Wind, T
10	2833	Modesto-14th	Wind	49	2032	Visalia-NChu	Wind, T
11	2080	Modesto-Met	Wind, T	50	5308	HanfordMuni	Wind, T
12	7233	DenairII	T, RH	51	5386	VisaliaMuni	Wind, T
13	3303	RosePeak	Wind, T, RH	52	3129	Hanford-Irwn	Wind, T
14	2996	Turlock-SMin	Wind, T	53	3250	Visalia-Airp	Wind, T, RH
15	3449	Pulgas	Wind, T, RH	54	3712	StRosaRnchria	Wind, T
16	5805	Patterson2	T, RH	55	6028	CoalingaCIM	T, RH
17	2814	Merced-AFB	Wind, T	56	5715	Stratford2	T, RH
18	5793	Merced	T, RH	57	3194	Corcoran-Pat	Wind, T
19	5318	MercedMuni	Wind, T	58	5812	Portervl	T, RH
20	3022	Merced-SCofe	Wind, T	59	5351	PortervlMuni	Wind, T
21	6079	MERCED 23WSW	T	60	3763	Portrvlle-Ne	Wind, T
22	5752	Kesterson	T, RH	61	3330	KettlemanHls	Wind, T, RH
23	3647	SanLuisNWR	Wind, T, RH	62	3350	FountnSpr	Wind, T, RH
24	3307	LosBanos	Wind, T, RH	63	5717	Kettleman	T, RH
25	5790	Madera	T, RH	64	6813	Alpaugh	T, RH
26	3522	Hurley1	Wind, T, RH	65	5823	Delano2	T, RH
27	5730	LosBanos2	T, RH	66	5729	BlackwllCnr	T, RH
28	5317	MaderaMuni	Wind, T	67	5783	Famoso	T, RH
29	3771	Madera-Av14	Wind, T, RH	68	5709	ShafterUSDA	T, RH
30	3346	FancherCreek	Wind, T, RH	69	5791	Belridge	T, RH
31	5770	Panoche	T, RH	70	2981	Shafter-Wlkr	Wind, T, RH
32	3211	Madera-Rd29	Wind, T, RH	71	2772	Oildale-3311	Wind, T
33	5711	Firebgh-Tel	T, RH	72	5287	MeadowsFld	Wind, T
34	2844	Fresno-Sky#2	Wind, T	73	3146	Baker-5558Ca	Wind, T, RH
35	5741	FSU2	T, RH	74	2312	Edison	Wind, T
36	3026	Clovis	Wind, T, RH	75	3758	Arvin-DiG	Wind, T
37	2449	Fresno-FAT	Wind, T	76	5771	Arvin-Edison	T, RH
38	5787	OrangeCove	T, RH	77	2919	Maricopa-Stn	Wind, T
39	2013	Fresno-Drmnd	Wind, T				

Table 8. Hourly surface wind speed, temperature and relative humidity statistics in Modesto.

Quarter	Observed Mean	Modeled Mean	Mean Bias	Mean Error	IOA
		Wind Speed (m/s)			
Q1	2.08	2.62	0.54	1.16	0.74
Q2	3.04	3.51	0.46	1.43	0.73
Q3	2.64	2.94	0.30	1.18	0.65
Q4	1.66	2.35	0.69	1.23	0.68
Annual	2.41	2.89	0.49	1.26	0.73
		Temperature (K)			
Q1	282.62	282.93	0.31	2.16	0.94
Q2	293.18	292.86	-0.32	2.07	0.96
Q3	295.98	297.06	1.07	2.35	0.93
Q4	283.95	285.73	1.78	2.73	0.93
Annual	288.93	289.65	0.71	2.33	0.97
		Relative Humidity (%)			
Q1	73.52	74.38	0.86	9.14	0.89
Q2	57.03	53.28	-3.75	10.99	0.86
Q3	62.17	55.26	-6.91	13.98	0.72
Q4	67.75	71.40	3.66	11.48	0.85
Annual	65.10	63.57	-1.53	11.40	0.86

Table 9. Hourly surface wind speed, temperature and relative humidity statistics in Fresno.

Quarter	Observed Mean	Modeled Mean	Mean Bias	Mean Error	IOA
		Wind Speed (m/s)			
Q1	1.47	1.90	0.43	1.11	0.56
Q2	2.54	3.12	0.58	1.53	0.59
Q3	2.14	2.65	0.51	1.42	0.47
Q4	1.12	1.69	0.57	1.05	0.52
Annual	1.85	2.37	0.52	1.29	0.61
		Temperature (K)			
Q1	283.76	282.90	-0.86	1.79	0.96
Q2	295.23	294.04	-1.19	2.16	0.95
Q3	299.69	299.22	-0.47	2.22	0.94
Q4	285.65	286.01	0.36	1.93	0.96
Annual	291.18	290.65	-0.53	2.03	0.98
		Relative Humidity (%)			
Q1	71.46	76.39	4.93	10.71	0.86
Q2	48.01	53.07	5.06	11.88	0.83
Q3	45.12	51.45	6.33	14.95	0.65
Q4	64.03	70.79	6.77	13.49	0.83
Annual	57.09	62.87	5.78	12.77	0.86

Table 10. Hourly surface wind speed, temperature and relative humidity statistics in Visalia.

Quarter	Observed Mean	Modeled Mean	Mean Bias	Mean Error	IOA
		Wind Speed (m/s)			
Q1	1.48	1.64	0.16	0.82	0.55
Q2	2.07	2.53	0.45	1.04	0.65
Q3	1.91	2.22	0.31	0.86	0.59
Q4	1.62	1.58	-0.04	0.73	0.60
Annual	1.77	2.00	0.24	0.88	0.65
		Temperature (K)			
Q1	283.66	282.87	-0.79	1.85	0.95
Q2	294.38	293.09	-1.29	2.23	0.95
Q3	298.73	298.42	-0.31	2.56	0.91
Q4	285.19	286.03	0.84	2.11	0.95
Annual	290.03	289.55	-0.48	2.16	0.97
		Relative Humidity (%)			
Q1	73.28	80.72	7.44	11.11	0.82
Q2	47.80	59.94	12.13	17.23	0.73
Q3	47.08	63.07	15.99	21.49	0.49
Q4	61.22	75.43	14.21	16.36	0.77
Annual	57.37	69.84	12.47	16.56	0.76

Table 11. Hourly surface wind speed, temperature and relative humidity statistics in Bakersfield (valid RH data available from January through May only; statistics are based on the available data).

Quarter	Observed Mean	Modeled Mean	Mean Bias	Mean Error	IOA
		Wind Speed (m/s)			
Q1	1.84	1.80	-0.04	0.88	0.59
Q2	2.63	2.47	-0.15	1.03	0.74
Q3	2.12	2.10	-0.02	1.10	0.68
Q4	2.23	1.86	-0.37	0.98	0.61
Annual	2.21	2.09	-0.12	1.00	0.70
		Temperature (K)			
Q1	284.94	283.97	-0.97	1.91	0.95
Q2	295.66	293.78	-1.87	2.44	0.94
Q3	301.17	299.54	-1.63	2.63	0.90
Q4	286.85	286.97	0.12	1.73	0.97
Annual	291.33	290.17	-1.16	2.16	0.97
		Relative Humidity (%)			
Q1	62.65	72.70	10.04	15.15	0.81
Q2	36.94	51.46	14.52	16.82	0.74
Annual	52.27	64.12	11.85	15.83	0.83

Table 12. Hourly surface wind speed, temperature and relative humidity statistics in the San Joaquin Valley.

Quarter	Observed Mean	Modeled Mean	Mean Bias	Mean Error	IOA
		Wind Speed (m/s)			
Q1	2.08	2.62	0.54	1.16	0.74
Q2	3.04	3.51	0.46	1.43	0.73
Q3	2.64	2.94	0.30	1.18	0.65
Q4	1.66	2.35	0.69	1.23	0.68
Annual	2.41	2.89	0.49	1.26	0.73
		Temperature (K)			
Q1	283.31	283.30	-0.01	2.17	0.94
Q2	294.23	293.42	-0.81	2.46	0.94
Q3	298.22	298.21	-0.02	2.82	0.90
Q4	285.08	286.20	1.12	2.65	0.93
Annual	290.19	290.25	0.07	2.52	0.96
		Relative Humidity (%)			
Q1	69.36	71.65	2.29	12.87	0.81
Q2	47.95	52.53	4.57	13.73	0.79
Q3	46.35	54.48	8.12	17.33	0.59
Q4	58.62	68.35	9.72	16.00	0.75
Annual	55.70	61.84	6.14	14.96	0.79

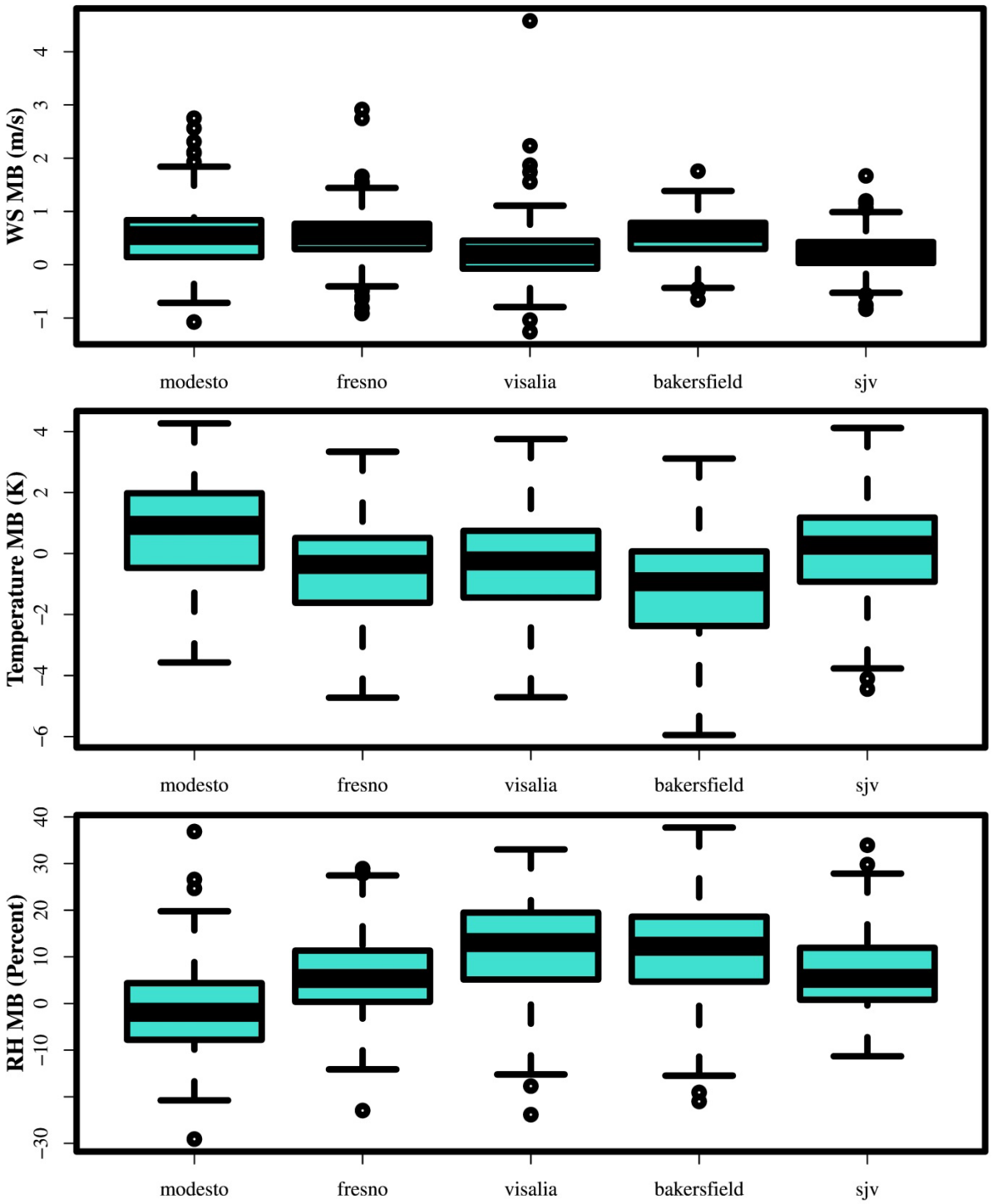

Figure 3. Distribution of model daily mean bias for Modesto, Fresno, Visalia, Bakersfield and SJV. Results are shown for wind speed (top), temperature (middle), and Relative Humidity (bottom).

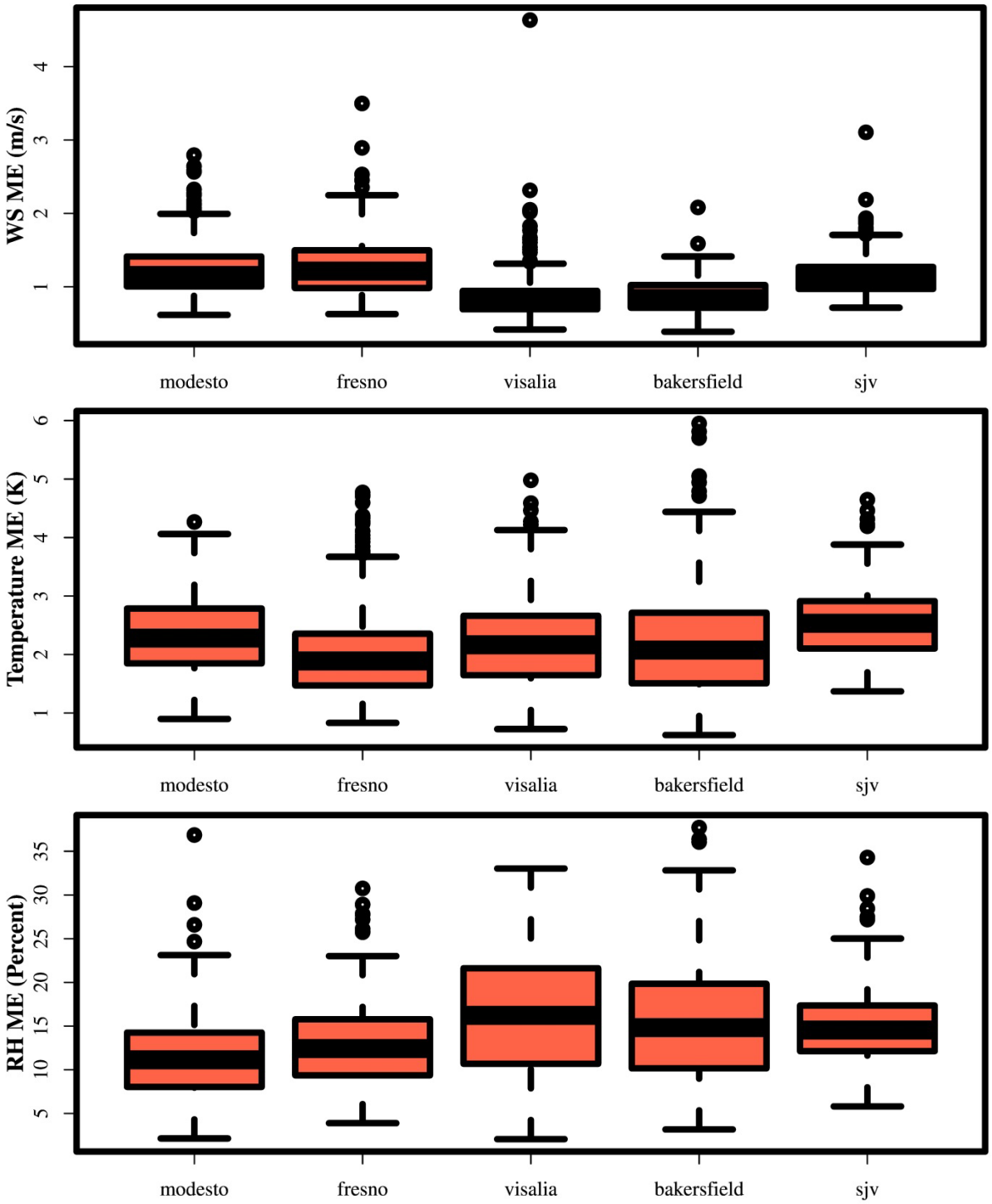

Figure 4. Distribution of model daily mean error for Modesto, Fresno, Visalia, Bakersfield and SJV. Results are shown for wind speed (top), temperature (middle), and Relative Humidity (bottom).

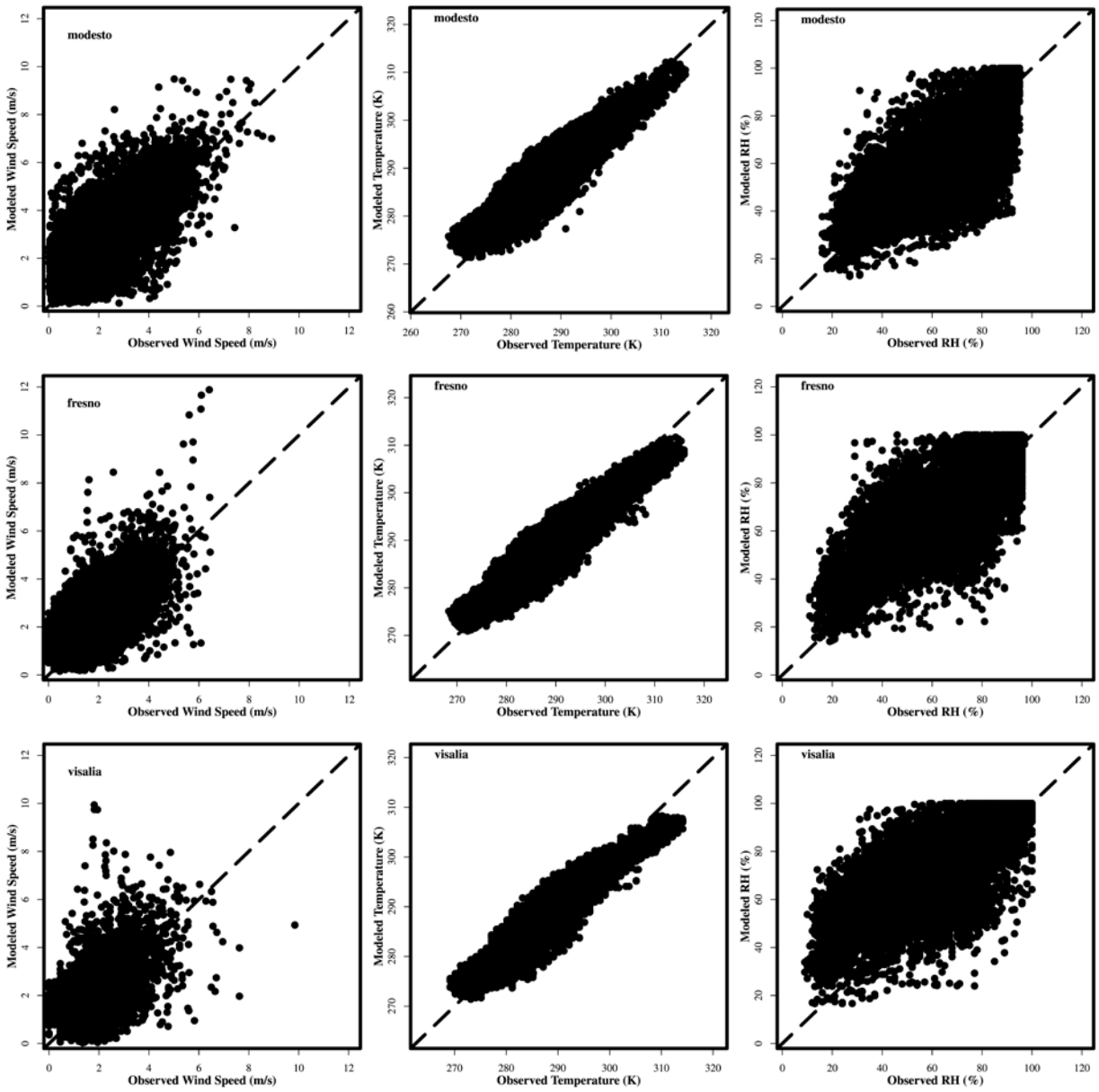

Figure 5. Comparison of modeled and observed hourly wind speed (left column), 2-meter temperature (middle column), and relative humidity (right column). Results for Modesto are shown in the top row, Fresno in the middle row, and Visalia in the bottom row.

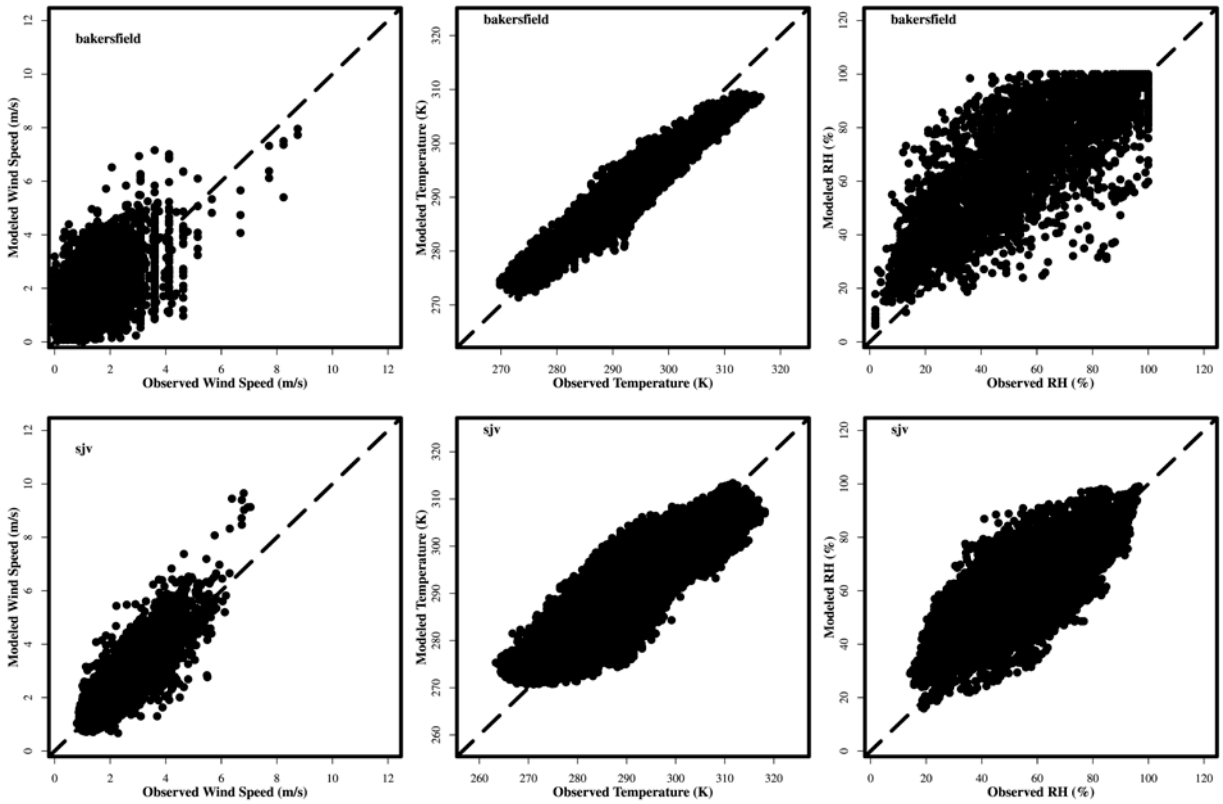

Figure 6. Comparison of modeled and observed hourly wind speed (left column), 2-meter temperature (middle column), and relative humidity (right column). Results for Bakersfield are shown in the top row and SJV in the bottom row.

3.2.1 PHENOMENOLOGICAL EVALUATION

Conducting a detailed phenomenological evaluation for all modeled days can be resource intensive given that the entire year was modeled. However, some insight and confidence that the model is able to reproduce the meteorological conditions leading to elevated particulate matter can be gained by investigating the meteorological conditions during a period of peak PM within the Valley in more detail. The highest $PM_{2.5}$-conducive meteorological conditions in the Valley occurred around January 20, 2013. Surface weather analysis shows that on January 20, the western US was under a typical Great Basin high pressure system. In the 500 hPa map (not shown), a strong high pressure ridge extends from Northern California along the west Pacific coast all the way to Alaska. As shown in Figures 7, 8, and 9, the winds, though weak, are mainly offshore along the northern California coast. Under this type of weather system, conditions in SJV are driven by diurnal cycles of the local winds. Figure 7 shows that at 13:00 PST, January 20, the upslope flows along the eastern side of the Coastal Ranges and the western side of the Sierras, lead to a weak northwesterly flow on the floor of the valley. The downslope winds form at nighttime and in the early morning (Figure 8 and Figure 9). They converge towards the valley and the winds in the center of the valley floor turn southeasterly. At the southern end of the valley, an eddy-like pattern occurs due to the interaction of the katabatic flows. The surface wind distributions of the modeled and observed winds indicate the model was able to capture many of the important features of the meteorological fields in the SJV.

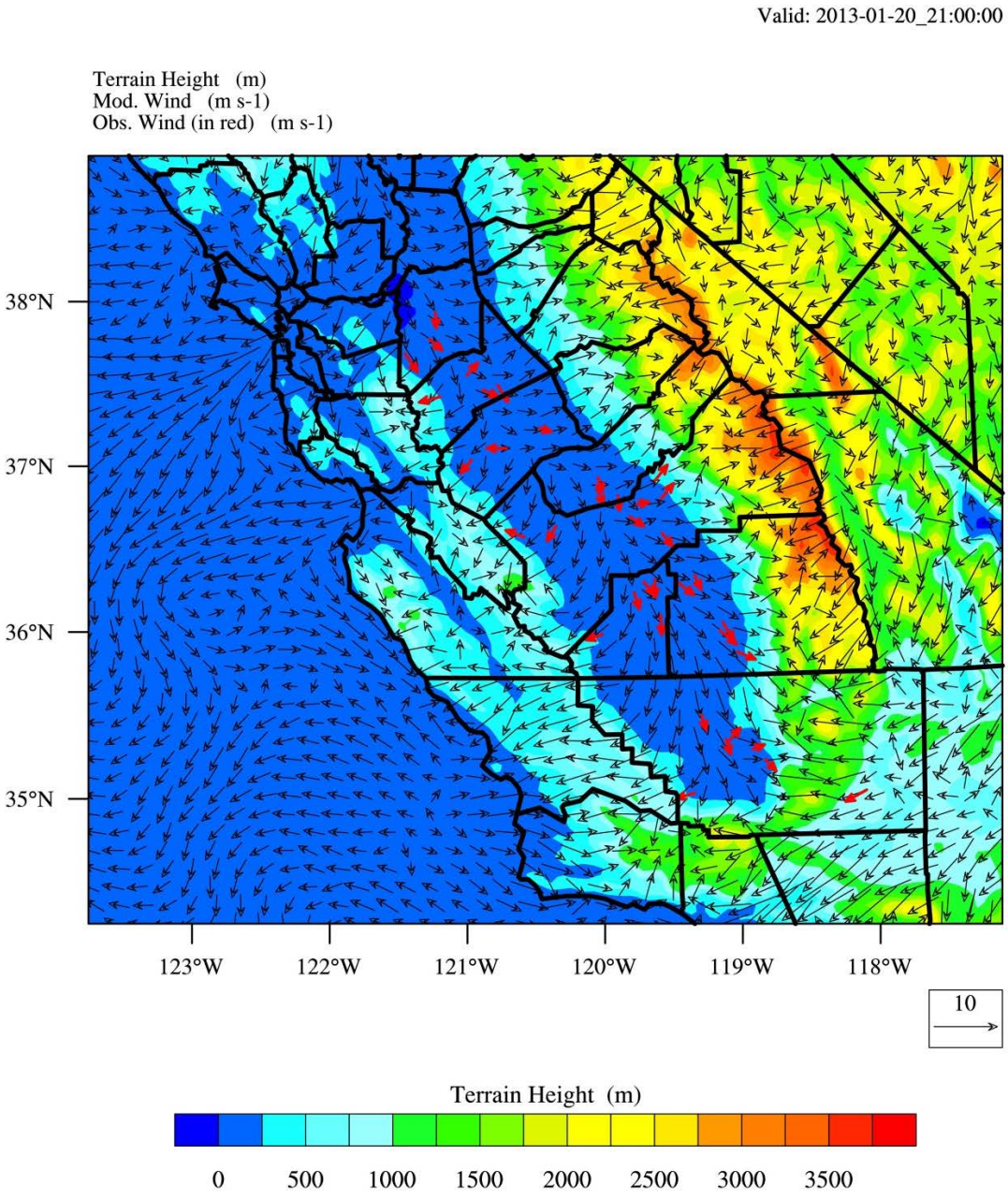

Figure 7. Surface wind field at 13:00 PST January 20, 2013.

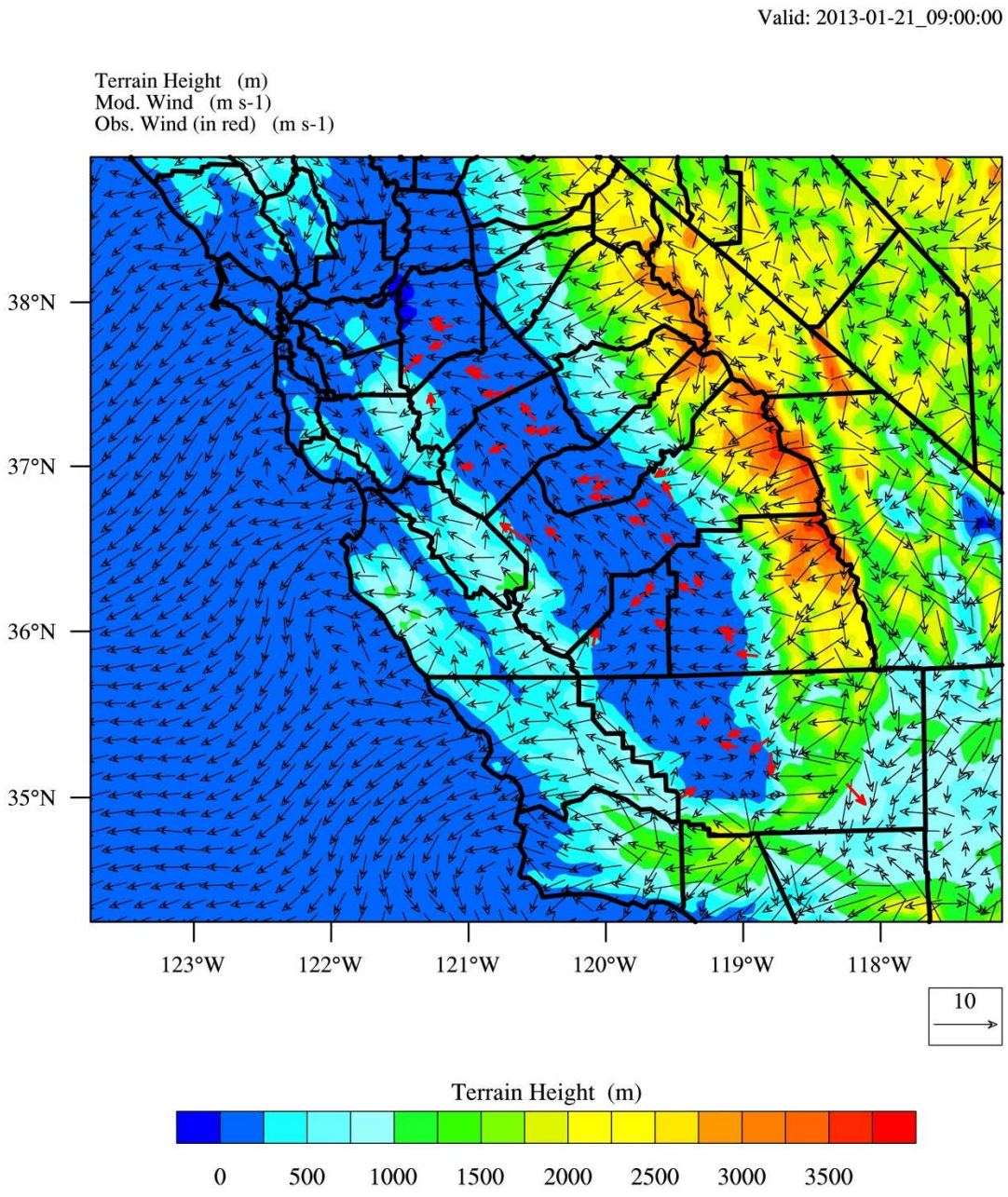

Figure 8. Surface wind field at 01:00 PST January 21, 2013.

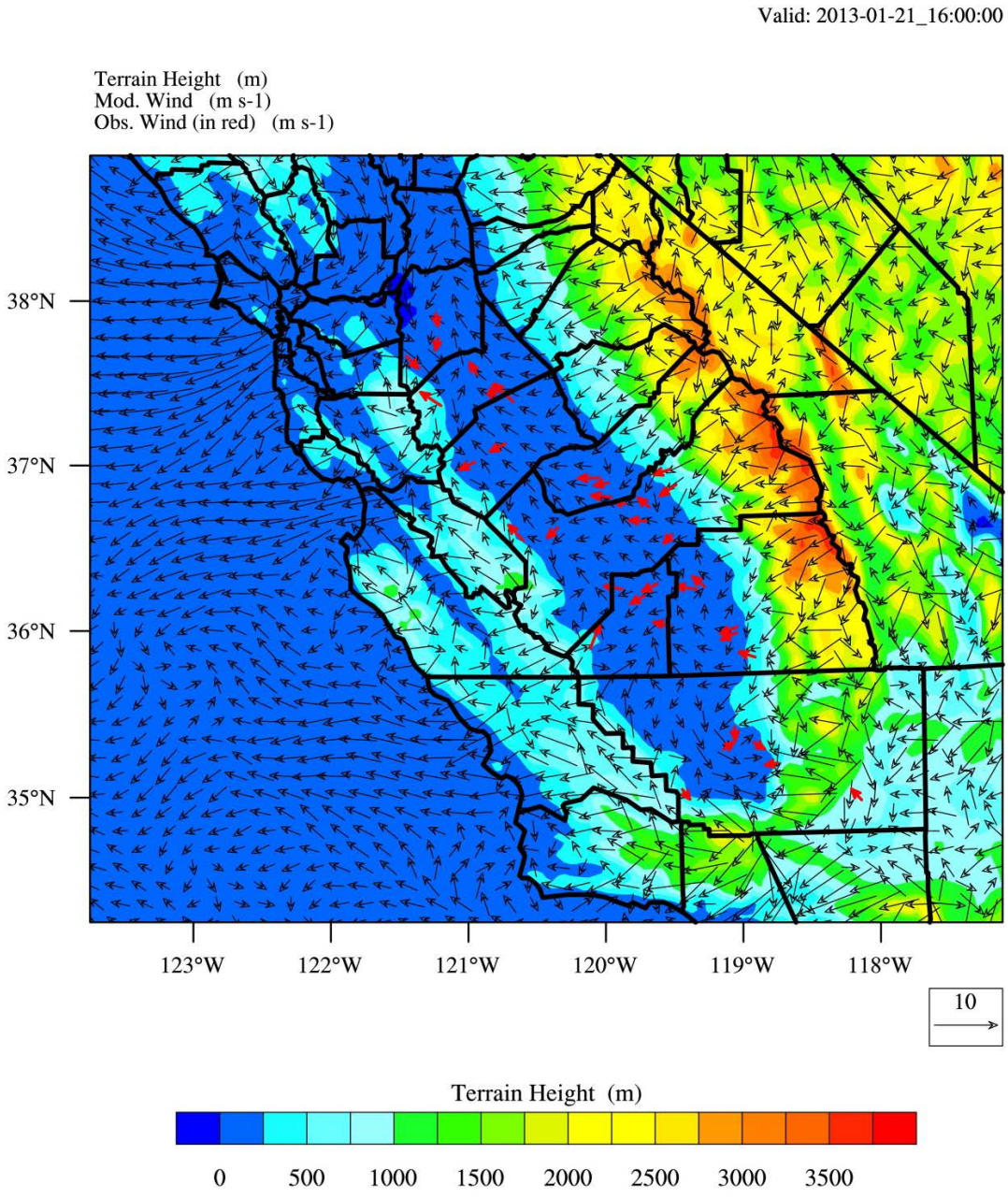

Figure 9. Surface wind field at 08:00 PST January 21, 2013.

4 EMISSIONS

The emissions inventory used in this modeling was based on the most recent inventory submitted to the U.S. EPA, with base year 2012 and projected to 2013 under growth and control conditions (http://www.arb.ca.gov/planning/sip/2012iv/2012iv.htm). For a detailed description of the emissions inventory, updates to the inventory, and how it was processed from the planning totals to a gridded inventory for modeling, see the Modeling Emissions Inventory Appendix.

4.1 EMISSIONS SUMMARIES

Table 13 summarizes 2013, 2021, and 2025 SJV annual anthropogenic emissions for the five $PM_{2.5}$ precursors. Emissions totals in Table 13 do not reflect reductions to residential wood burning (RWC) emissions applied to the modeling inventory to reflect actual no burn days in 2013 and projected no burn days in 2021/2025. Under the 2014 amendment to the RWC rule (two curtailment levels), 2021 emissions were reduced by 85% (level 1: no burning unless registered) and 90% (level 2: no burning for all) on projected no burn days. In addition, emissions totals also do not reflect the 20% reduction in commercial charbroiling applied to the modeling inventory per commitments made in the SJV 2012 24-hour $PM_{2.5}$ SIP. From 2013 to 2021, anthropogenic emissions in the SJV will drop approximately 38%, 8%, 7%, 2%, and 1% for NO_x, ROG, primary $PM_{2.5}$, SO_x, and NH_3, respectively. Among these five precursors, anthropogenic NO_x emissions show the largest relative reduction, dropping from 318.2 tons/day in 2013 to 196.1 tons/day in 2021. Anthropogenic ROG emissions will drop from 319.2 tons/day to 292.8 tons/day, reflecting an 8% reduction from 2013 to 2021. From 2021 to 2025, NO_x emissions will further drop by 24%, while emissions of other pollutants will stay nearly flat. Monthly biogenic ROG totals for 2013 in the SJV are shown in Figure 10 (note that the 2013 biogenic emissions were used for all model runs). Biogenic ROG emissions are highest in the summer at nearly 1800 tons/day in July when temperature, insolation, and leaf area are generally at their peak, and drop to near zero during winter months.

Table 13. SJV Annual Planning Emissions for 2013, 2021, and 2025

Category	NO_x	ROG	$PM_{2.5}$	SO_x	NH_3
2013 (tons/day)					
Stationary	38.6	85.1	8.9	7.2	13.8
Area	8.1	150.3	42.3	0.3	310.7
On-road Mobile	183.2	49.9	6.4	0.6	4.5
Other Mobile	88.3	33.9	5.8	0.2	0.0
Total	318.2	319.2	63.5	8.4	329.1
2021 (tons/day)					
Stationary	29.8	90.5	9.1	6.9	15.3
Area	8.1	152.4	41.9	0.3	306.4
On-road Mobile	88.0	23.3	3.3	0.6	4.2
Other Mobile	70.2	26.7	5.0	0.3	0.0
Total	196.1	292.8	59.3	8.2	325.9
2025 (tons/day)					
Stationary	29.2	94.3	9.3	7.1	16.3
Area	8.0	154.1	42.2	0.3	304.3
On-road Mobile	54.3	18.9	3.3	0.6	4.3
Other Mobile	58.3	24.1	4.3	0.3	0.0
Total	149.8	291.4	59.1	8.4	324.9

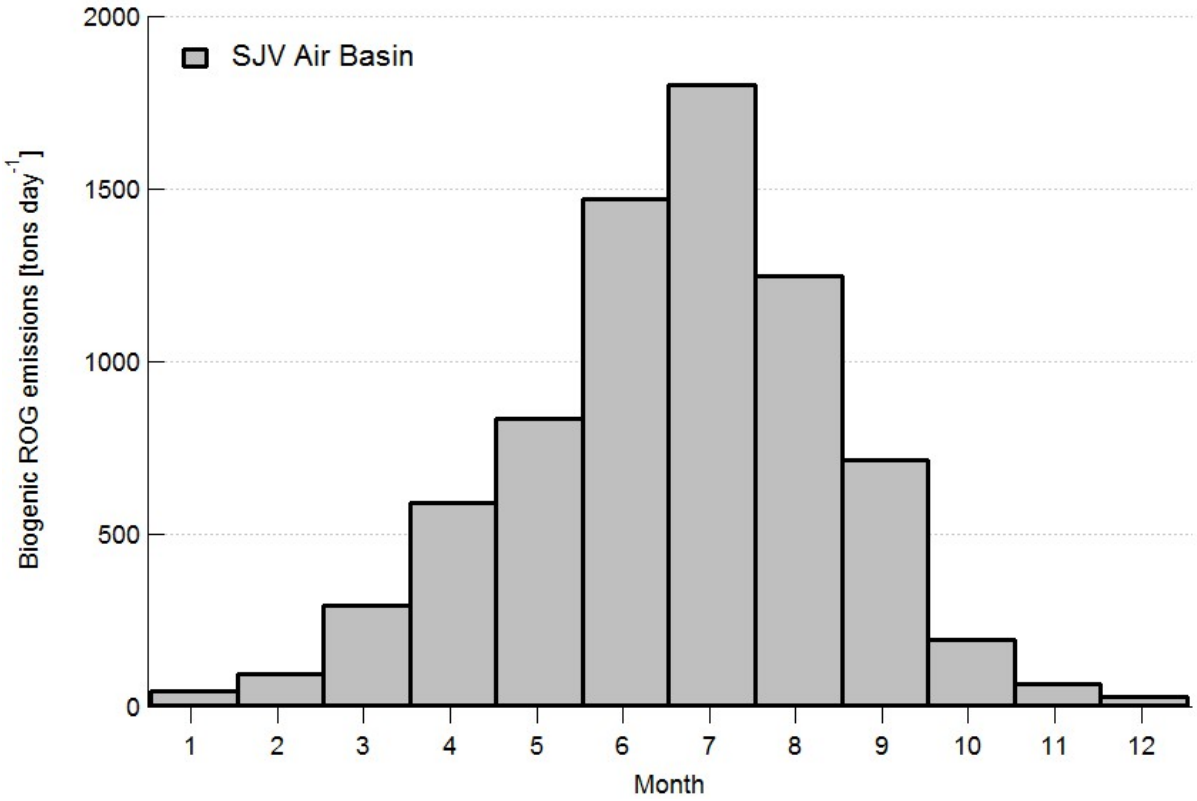

Figure 10. Monthly average biogenic ROG emissions for 2013.

5 $PM_{2.5}$ MODELING

5.1 CMAQ MODEL SETUP

Figure 11 shows the CMAQ modeling domains used in this work. The larger domain covering all of California has a horizontal grid resolution of 12 km with 107 x 97 lateral grid cells for each vertical layer and extends from the Pacific Ocean in the west to Eastern Nevada in the east and runs from the U.S.-Mexico border in the south to the California-Oregon border in the north. The smaller nested domain covering the SJV region has a finer scale 4 km grid resolution and includes 87 x 103 lateral grid cells. While the nested domain is smaller than that used for ozone modeling in the Valley (see the Photochemical Modeling Protocol), as long as the larger statewide 12 km domain is utilized to provide dynamic boundary condition inputs to the smaller 4 km domain, there is no appreciable difference in simulated $PM_{2.5}$ predictions between the smaller domain utilized for $PM_{2.5}$ modeling and the larger domain used for ozone modeling. Both the 12 km and 4 km domains are based on a Lambert Conformal Conic projection with reference longitude at – 120.5ºN and 60ºN, which is consistent with WRF domain settings. The 30 vertical layers from WRF were mapped onto 18 vertical layers for CMAQ, extending from the surface to 100 mb such that a majority of the vertical layers

fall within the planetary boundary layer (see the Photochemical Modeling Protocol for details).

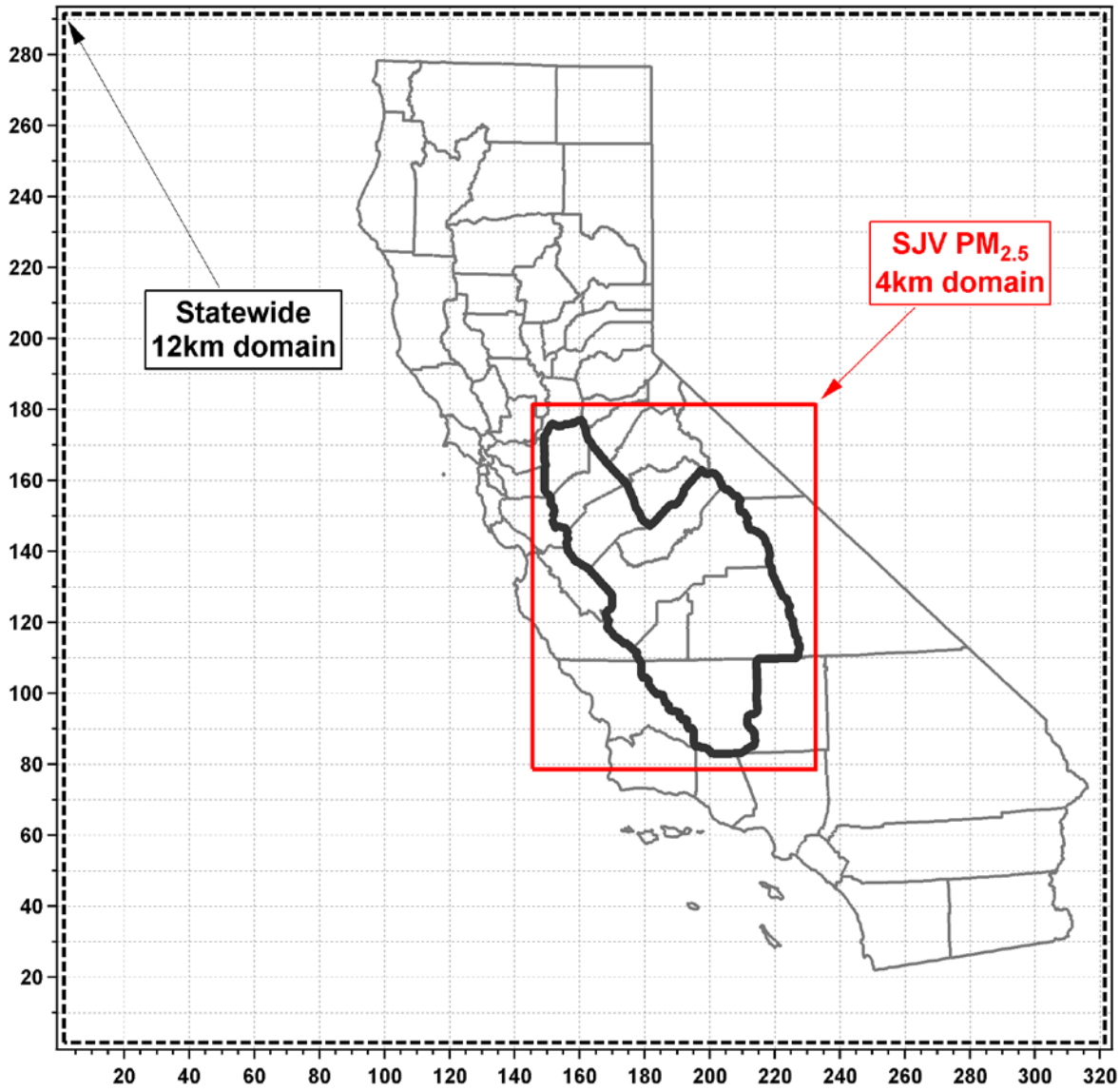

Figure 11. CMAQ modeling domains utilized in the modeling assessment.

The CMAQ model version 5.0.2 (http://www.airqualitymodeling.org/cmaqwiki/index.php?title=CMAQ_version_5.0.2_%28April_2014_release%29_Technical_Documentation) released by the U.S. EPA in May 2014 was used for all air quality model simulations. The SAPRC07 chemical mechanism and aerosol module aero6 were selected as the gas-phase and aerosol modules, respectively. Further details of the CMAQ configuration can be found in

Table14 and in the Photochemical Modeling Protocol. The same configuration was used for all simulations.

Annual simulations were conducted on a simultaneous month-by-month basis, rather than one single continuous simulation. For each month, the CMAQ simulations included a seven day spin-up period (i.e., the last seven days of the previous month) for the outer 12 km domain, where initial conditions were set to the default CMAQ initial conditions. These outer domain simulations were used to provide initial and lateral boundary conditions for the inner 4 km simulation, which utilized a three day spin-up period.

Chemical boundary conditions for the outer 12 km domain were extracted from the global chemical transport Model for Ozone and Related chemical Tracers, version 4 (MOZART-4; Emmons et al., 2014). The MOZART-4 model output for 2013 was obtained from the National Center for Atmospheric Research (NCAR; https://www2.acom.ucar.edu/gcm/mozart) using the simulations driven by meteorological fields from the NASA GMAO GEOS-5 model. The same MOZART derived BCs for the 12 km outer domain were used in all simulations.

Table 14. CMAQ configuration and settings.

Process	Scheme
Horizontal advection	Yamo (Yamartino scheme for mass-conserving advection)
Vertical advection	WRF-based scheme for mass-conserving advection
Horizontal diffusion	Multi-scale
Vertical diffusion	ACM2 (Asymmetric Convective Model version 2)
Gas-phase chemical mechanism	SAPRC-07 gas-phase mechanism version “B”
Chemical solver	EBI (Euler Backward Iterative solver)
Aerosol module	Aero6 (the sixth-generation CMAQ aerosol mechanism with extensions for sea salt emissions and thermodynamics; includes a new formulation for secondary organic aerosol yields)

Cloud module	ACM_AE6 (ACM cloud processor that uses the ACM methodology to compute convective mixing with heterogeneous chemistry for AERO6)
Photolysis rate	phot_inline (calculate photolysis rates in-line using simulated aerosols and ozone concentrations)

5.2 CMAQ MODEL EVALUATION

CMAQ model performance was evaluated for $PM_{2.5}$ mass, individual $PM_{2.5}$ chemical species, as well as a number of gas-phase species based on observations from an extensive network of monitors in the SJV.

Time series of observed and modeled $PM_{2.5}$ chemical species based on CSN measurements are shown in the supplemental material (Figures S37-S40 of the supplemental materials for Bakersfield, Fresno, Modesto, and Visalia, respectively). $PM_{2.5}$ species are measured every 3 or 6 days at these sites. Generally, observed $PM_{2.5}$ concentrations are higher in winter months and are much lower in summer months. During winter months, $PM_{2.5}$ in the SJV is dominated by ammonium nitrate and directly emitted OC. The CMAQ model was able to reasonably reproduce these key characteristics of $PM_{2.5}$ pollution in the SJV, including successfully capturing many elevated wintertime nitrate events, which is key for accurately simulating both peak wintertime $PM_{2.5}$ as well as annual average $PM_{2.5}$ in the SJV.

Tables 15-18 summarize the key model performance metrics for major $PM_{2.5}$ chemical species at the four CSN sites. Model performance was evaluated quarterly as well as on an annual basis. Average observations, average modeled values, mean bias, mean error, mean fractional bias (MFB), and mean fractional error (MFE) are given for individual $PM_{2.5}$ species at these four sites. Detailed definitions for these metrics can be found in the Photochemical Modeling Protocol Appendix. In general, model performance was consistent across different quarters and at different monitors. Mean bias of the simulated annual average $PM_{2.5}$ was within +/-1 $\mu g/m^3$ at all the CSN sites except Bakersfield, which showed an annual mean bias of -2.5 $\mu g/m^3$. The larger negative bias at Bakersfield was the result of a slight over prediction during winter months, which was offset by a larger under prediction during summer months (likely due to uncertainty in the unspecified $PM_{2.5}$ category – not shown). This is consistent with the other sites, which also generally showed over predictions in the first and fourth quarters, and under predictions in the second and third quarters. The two primary components of $PM_{2.5}$ in

the SJV, nitrate and OC, exhibited somewhat different quarterly biases, with nitrate closely following total $PM_{2.5}$ and OC being under predicted during most quarters and at most sites.

A graphical representation of the annual MFB and MFE values in Tables 15-18 is shown in Figure 12 for each CSN site, along with suggested model performance goals and criteria (green and red lines, respectively) from Boylan and Russell (2006). According to Boylan and Russell (2006), model performance goals are defined as the level of accuracy that is considered to be close to the best a model can achieve while model performance criteria are defined as the level of accuracy that is considered to be acceptable for modeling applications. Based on these metrics, the current CMAQ modelling system met the model performance criteria and in many instances exceeded model performance goals.

Table 15. Quarterly and annual $PM_{2.5}$ model performance based on CSN measurement at Fresno – Garland.

Quarter	Species	# of Obs.	Avg. Obs. (µg/m^3)	Avg. Mod. (µg/m^3)	Mean bias (µg/m^3)	Mean error (µg/m^3)	MFB	MFE
1	$PM_{2.5}$	30	21.1	22.7	1.6	6.5	0.18	0.36
1	Ammonium	30	1.7	2.8	1.1	1.3	0.56	0.67
1	Nitrate	30	5.8	9.4	3.6	4.1	0.46	0.60
1	Sulfate	30	0.8	1.0	0.2	0.3	0.28	0.41
1	OC	28	4.9	4.1	-0.8	1.6	-0.03	0.34
1	EC	28	1.2	1.4	0.1	0.5	0.27	0.45
2	$PM_{2.5}$	30	7.8	6.4	-1.4	2.4	-0.23	0.37
2	Ammonium	30	0.4	0.3	-0.2	0.2	-0.50	0.62
2	Nitrate	30	0.9	0.6	-0.2	0.4	-0.53	0.72
2	Sulfate	30	1.1	0.7	-0.4	0.4	-0.37	0.46
2	OC	29	1.8	1.9	0.2	0.5	0.02	0.25
2	EC	29	0.3	0.6	0.3	0.3	0.61	0.62
3	$PM_{2.5}$	30	9.4	6.4	-3.0	3.7	-0.35	0.44
3	Ammonium	30	0.4	0.2	-0.2	0.2	-0.61	0.77
3	Nitrate	30	0.7	0.3	-0.4	0.5	-1.18	1.25
3	Sulfate	30	0.9	0.8	-0.2	0.3	-0.10	0.33
3	OC	30	2.4	1.8	-0.6	0.9	-0.21	0.34
3	EC	30	0.5	0.6	0.1	0.2	0.23	0.32
4	$PM_{2.5}$	29	25.8	25.1	-0.7	8.5	0.07	0.36
4	Ammonium	29	2.9	2.7	-0.2	1.4	0.06	0.52
4	Nitrate	28	9.0	9.4	0.4	3.6	0.02	0.43
4	Sulfate	28	1.0	1.0	-0.1	0.3	-0.03	0.26
4	OC	29	6.0	4.6	-1.4	2.1	-0.13	0.38
4	EC	29	1.6	1.6	0.0	0.5	0.14	0.41
Annual	$PM_{2.5}$	119	16.0	15.1	-0.9	5.2	-0.08	0.38
Annual	Ammonium	119	1.3	1.5	0.2	0.8	-0.12	0.65
Annual	Nitrate	118	4.0	4.9	0.9	2.1	-0.32	0.75
Annual	Sulfate	118	1.0	0.9	-0.1	0.3	-0.06	0.36
Annual	OC	116	3.8	3.1	-0.7	1.3	-0.09	0.33
Annual	EC	116	0.9	1.0	0.1	0.4	0.31	0.45

Table 16. Quarterly and annual $PM_{2.5}$ model performance based on CSN measurement at Visalia.

Quarter	Species	# of Obs.	Avg. Obs. ($\mu g/m^3$)	Avg. Mod. ($\mu g/m^3$)	Mean bias ($\mu g/m^3$)	Mean error ($\mu g/m^3$)	MFB	MFE
1	$PM_{2.5}$	15	20.5	22.8	2.4	4.9	0.17	0.29
1	Ammonium	15	2.0	3.1	1.2	1.4	0.50	0.65
1	Nitrate	15	6.7	10.6	4.0	4.4	0.45	0.55
1	Sulfate	15	1.0	0.8	-0.3	0.4	-0.20	0.36
1	OC	15	4.6	3.5	-1.1	1.3	-0.18	0.27
1	EC	15	0.9	1.1	0.3	0.3	0.37	0.40
2	$PM_{2.5}$	15	9.8	8.0	-1.8	2.6	-0.30	0.37
2	Ammonium	15	0.7	0.5	-0.2	0.2	-0.33	0.45
2	Nitrate	10	2.2	1.9	-0.2	0.8	-0.21	0.48
2	Sulfate	15	1.6	0.7	-0.9	0.9	-0.77	0.77
2	OC	17	2.6	1.8	-0.8	0.8	-0.46	0.46
2	EC	17	0.4	0.6	0.2	0.2	0.36	0.37
3	$PM_{2.5}$	17	10.5	7.4	-3.2	3.8	-0.31	0.41
3	Ammonium	17	0.6	0.3	-0.2	0.3	-0.47	0.63
3	Nitrate	17	1.6	0.7	-0.9	1.0	-0.91	0.95
3	Sulfate	17	1.4	0.8	-0.5	0.5	-0.41	0.43
3	OC	17	2.9	1.8	-1.1	1.3	-0.49	0.53
3	EC	17	0.5	0.6	0.2	0.2	0.26	0.30
4	$PM_{2.5}$	16	33.1	33.1	-0.1	13.0	0.11	0.38
4	Ammonium	16	4.3	4.0	-0.3	2.1	0.11	0.48
4	Nitrate	16	14.3	13.9	-0.4	6.9	0.14	0.48
4	Sulfate	16	1.4	1.0	-0.4	0.6	-0.28	0.41
4	OC	16	5.8	4.4	-1.4	1.8	-0.27	0.36
4	EC	16	1.3	1.5	0.3	0.5	0.17	0.32
Annual	$PM_{2.5}$	63	18.5	17.7	-0.7	6.1	-0.09	0.37
Annual	Ammonium	63	1.9	2.0	0.1	1.0	-0.06	0.55
Annual	Nitrate	58	6.5	7.1	0.6	3.5	-0.15	0.64
Annual	Sulfate	63	1.4	0.8	-0.5	0.6	-0.41	0.49
Annual	OC	65	3.9	2.8	-1.1	1.3	-0.36	0.41
Annual	EC	65	0.7	1.0	0.2	0.3	0.29	0.35

Table 17. Quarterly and annual $PM_{2.5}$ model performance based on CSN measurement at Bakersfield.

Quarter	Species	# of Obs.	Avg. Obs. ($\mu g/m^3$)	Avg. Mod. ($\mu g/m^3$)	Mean bias ($\mu g/m^3$)	Mean error ($\mu g/m^3$)	MFB	MFE
1	$PM_{2.5}$	21	20.5	23.2	2.7	8.7	0.34	0.49
1	Ammonium	21	2.2	2.8	0.7	1.6	0.57	0.74
1	Nitrate	19	7.9	9.4	1.5	3.9	0.28	0.47
1	Sulfate	21	0.9	0.9	0.1	0.4	0.26	0.52
1	OC	22	3.9	4.6	0.7	1.3	0.27	0.36
1	EC	22	1.1	1.5	0.4	0.4	0.36	0.41
2	$PM_{2.5}$	25	11.0	7.8	-3.3	4.0	-0.36	0.45
2	Ammonium	25	0.6	0.4	-0.2	0.3	-0.52	0.59
2	Nitrate	25	1.1	0.9	-0.2	0.6	-0.46	0.74
2	Sulfate	25	1.4	0.8	-0.6	0.6	-0.49	0.54
2	OC	22	2.2	2.4	0.2	0.5	0.09	0.24
2	EC	22	0.4	0.7	0.4	0.4	0.75	0.75
3	$PM_{2.5}$	19	15.5	8.2	-7.3	8.0	-0.55	0.60
3	Ammonium	19	0.5	0.3	-0.2	0.3	-0.61	0.68
3	Nitrate	19	0.8	0.6	-0.2	0.6	-0.69	0.93
3	Sulfate	19	1.3	0.9	-0.5	0.5	-0.38	0.38
3	OC	17	2.6	2.5	0.0	0.9	-0.05	0.33
3	EC	17	0.5	0.8	0.4	0.4	0.58	0.58
4	$PM_{2.5}$	0	NA	NA	NA	NA	NA	NA
4	Ammonium	0	NA	NA	NA	NA	NA	NA
4	Nitrate	0	NA	NA	NA	NA	NA	NA
4	Sulfate	0	NA	NA	NA	NA	NA	NA
4	OC	0	NA	NA	NA	NA	NA	NA
4	EC	0	NA	NA	NA	NA	NA	NA
Annual	$PM_{2.5}$	65	15.4	12.9	-2.5	6.7	-0.19	0.50
Annual	Ammonium	65	1.1	1.2	0.1	0.7	-0.19	0.67
Annual	Nitrate	63	3.0	3.4	0.3	1.6	-0.30	0.71
Annual	Sulfate	65	1.2	0.9	-0.3	0.5	-0.22	0.49
Annual	OC	61	2.9	3.2	0.3	0.9	0.11	0.31
Annual	EC	61	0.7	1.0	0.4	0.4	0.56	0.58

Table 18. Quarterly and annual $PM_{2.5}$ model performance based on CSN measurement at Modesto.

Quarter	Species	# of Obs.	Avg. Obs. ($\mu g/m^3$)	Avg. Mod. ($\mu g/m^3$)	Mean bias ($\mu g/m^3$)	Mean error ($\mu g/m^3$)	MFB	MFE
1	$PM_{2.5}$	15	17.3	18.4	1.1	4.2	0.18	0.34
1	Ammonium	15	1.0	2.2	1.2	1.2	0.70	0.73
1	Nitrate	15	5.0	7.1	2.1	2.3	0.27	0.42
1	Sulfate	15	0.8	1.1	0.3	0.4	0.31	0.41
1	OC	14	5.5	3.9	-1.6	2.2	-0.09	0.37
1	EC	14	1.2	1.2	0.0	0.4	0.21	0.42
2	$PM_{2.5}$	15	6.5	5.4	-1.1	2.2	-0.18	0.36
2	Ammonium	15	0.3	0.4	0.1	0.1	0.27	0.48
2	Nitrate	13	0.7	0.6	-0.1	0.4	-0.35	0.63
2	Sulfate	15	1.0	0.8	-0.1	0.3	-0.10	0.33
2	OC	15	1.6	1.3	-0.3	0.4	-0.20	0.27
2	EC	15	0.3	0.4	0.1	0.1	0.38	0.38
3	$PM_{2.5}$	14	7.9	6.0	-1.8	3.2	-0.13	0.37
3	Ammonium	15	0.3	0.2	0.0	0.1	0.22	0.50
3	Nitrate	15	0.7	0.2	-0.5	0.5	-1.12	1.12
3	Sulfate	15	1.1	1.0	-0.1	0.3	-0.04	0.28
3	OC	15	2.6	1.7	-1.0	1.1	-0.29	0.36
3	EC	15	0.4	0.5	0.1	0.2	0.18	0.34
4	$PM_{2.5}$	17	25.6	30.3	4.7	6.5	0.25	0.31
4	Ammonium	17	2.4	3.3	0.9	1.0	0.50	0.53
4	Nitrate	17	8.2	11.2	3.0	3.5	0.42	0.48
4	Sulfate	17	1.1	1.2	0.1	0.3	0.12	0.25
4	OC	17	6.2	4.7	-1.6	1.8	-0.20	0.29
4	EC	17	1.6	1.5	-0.1	0.3	0.02	0.24
Annual	$PM_{2.5}$	61	14.8	15.7	0.9	4.1	0.04	0.34
Annual	Ammonium	62	1.0	1.6	0.6	0.6	0.43	0.56
Annual	Nitrate	60	3.9	5.1	1.2	1.8	-0.17	0.66
Annual	Sulfate	62	1.0	1.0	0.0	0.3	0.07	0.32
Annual	OC	61	4.0	2.9	-1.1	1.4	-0.19	0.32
Annual	EC	61	0.9	0.9	0.0	0.2	0.19	0.34

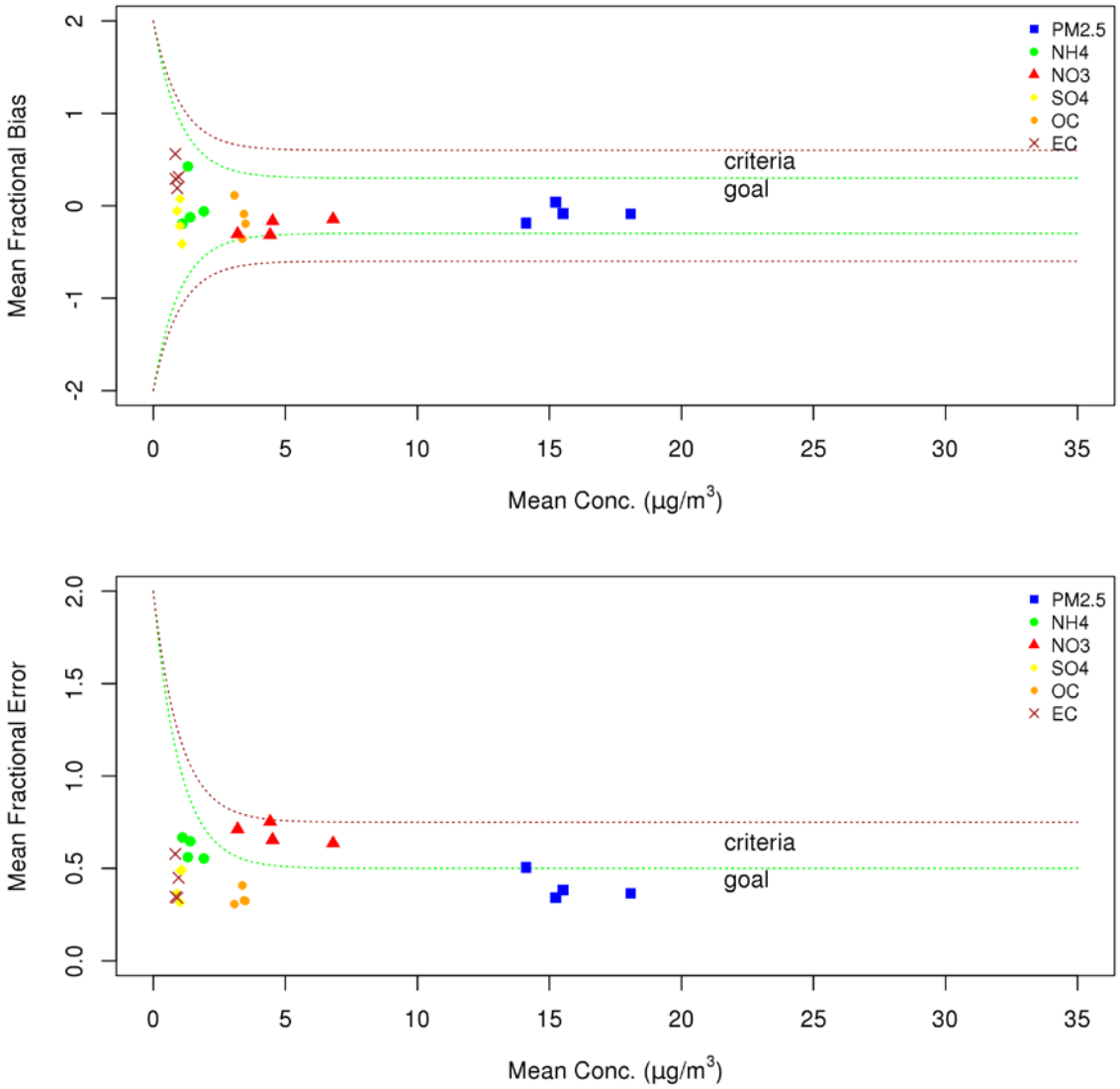

Figure 12. Bugle plot of annual $PM_{2.5}$ model performance in terms of MFB and MFE at four CSN sites in the SJV (i.e., Bakersfield, Fresno, Modesto, and Visalia).

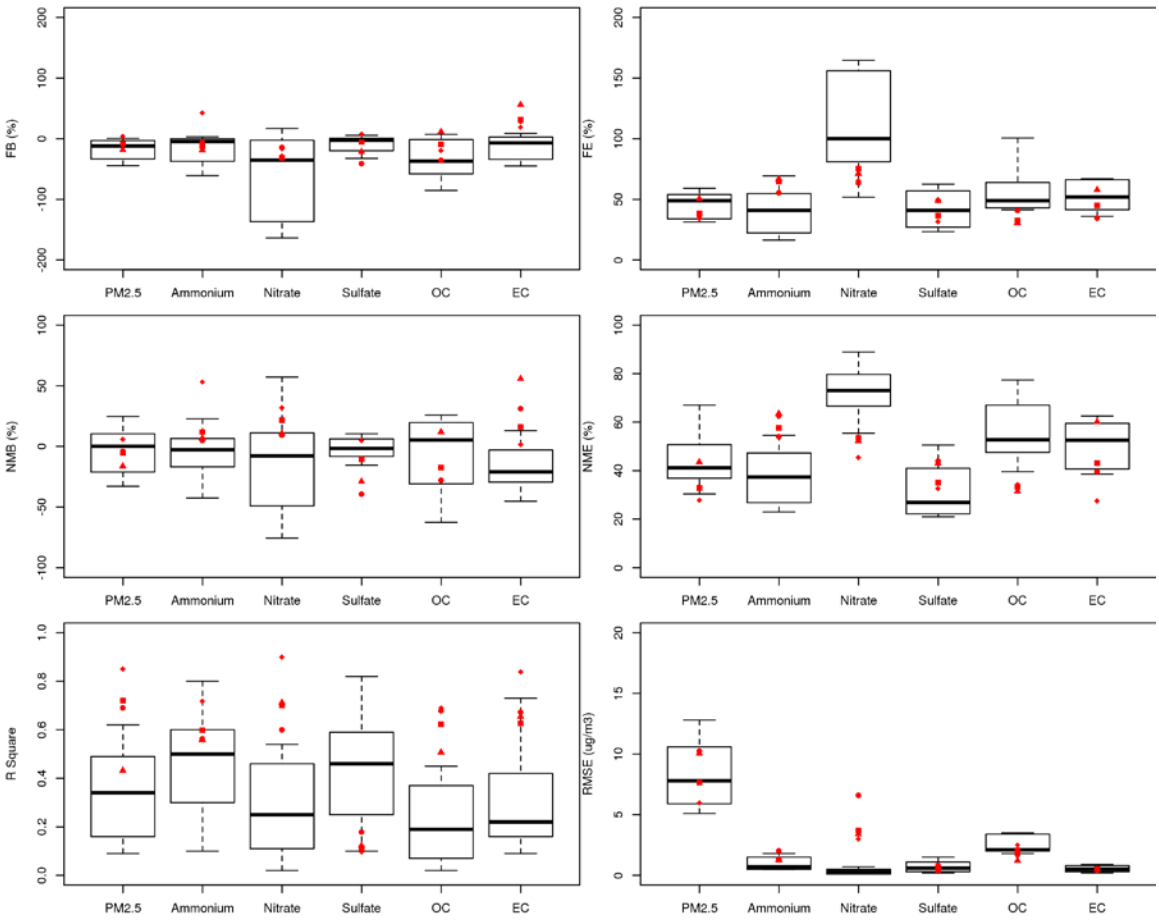

Figure 13. Comparison of annual $PM_{2.5}$ model performance to other modeling studies in Simon et al. (2012). Red symbols represent performance at the four CSN sites in the SJV.

In addition to evaluating the standard statistical performance metrics, it is also informative to put these performance statistics in the context of other studies published in the scientific literature. Figure 13 compares key performance statistics from the modeling platform presented in this document to the range of published performance statics from 2006 to 2012 and summarized in Simon et al. (2012). In Figure 13, the black centerline shows the median value (i.e., median model performance) from those studies, the boxes outline the 25th and 75th percentile values, and the whiskers show the 10th and 90th percentile values. The model performance for each of the four CSN sites in the SJV is shown in red. Performance metrics including MFB, MFE, normalized mean bias (NMB), normalized mean error (NME), R squared, and root mean square error (RMSE) are compared. Definitions of the statistics can be found in the Photochemical

Modeling Protocol or Simon et al. (2012). Model performance metrics in the SJV are typically equal to or better than the corresponding statistics from other studies. One exception is the higher RMSE for nitrate in the SJV, which is simply a reflection of the higher nitrate concentrations in the SJV compared to other regions. In fact, MFB, MFE, NME, and R squared for nitrate in the SJV is consistently better than the majority of the model studies summarized in Simon et al. (2012).

Since CSN monitors do not measure $PM_{2.5}$ on a daily basis, it is also advantageous to compare modeled 24-hour average $PM_{2.5}$ concentrations to observations from continuous $PM_{2.5}$ samplers, which typically report 24-hour average $PM_{2.5}$ concentrations on a daily basis. Figures S-41 – S-52 show the time series of modeled and observed 24-hour average $PM_{2.5}$ concentrations at these sites located throughout the SJV. Distinct seasonal variations in $PM_{2.5}$ concentrations are observed throughout the Valley, and are also reasonably captured by the model. Of particular importance, the modeling system was able to capture the elevated $PM_{2.5}$ events during the winter months and the lower $PM_{2.5}$ common in the summer months. In addition, Table 19 summarizes the corresponding model performance statistics at these sites. All the sites met or exceeded the $PM_{2.5}$ model performance criteria defined in Boyland and Russell (2006).

In addition to the $PM_{2.5}$ performance evaluation, gas phase model performance was also evaluated for NO_2 and ozone, which are key products of the photochemical processes in the atmosphere. Scatter plots of observed and modeled one-hour NO_2 mixing ratios at 16 sites are shown in Figures S-53 to S-68 in the supplemental materials. On average, there is good agreement between observed and modeled NO_2 mixing ratios. The slope of the regression line between the observed and modeled hourly NO_2 mixing ratios is within ±30% of the 1:1 line at most of the sites. Scatter plots of observed and modeled hourly O_3 mixing ratios at 25 sites are shown in Figures S-69 to S-93 in the supplemental materials. Modeled O_3 mixing ratios showed excellent agreement with observed mixing ratios and the slopes of the regression lines between observed and modeled O_3 are all within ±15% of the 1:1 line.

Table 19. Model performance for 24-hour $PM_{2.5}$ concentrations measured from continuous $PM_{2.5}$ monitors

Sites	# of Obs.	Avg. Obs. (µg/m^3)	Avg. Mod. (µg/m^3)	Mean bias (µg/m^3)	Mean error (µg/m^3)	MFB	MFE
Fresno-Drummond Street	246	14.8	13.5	-1.2	4.4	-0.16	0.36
Clovis	300	16.4	14.5	-1.9	5.6	-0.22	0.42
Bakersfield-California Avenue	267	20.2	16.2	-4.0	7.0	-0.29	0.44
Tranquility	301	8.5	10.1	1.5	5.0	-0.11	0.52
Fresno-Garland	312	19.3	15.7	-3.6	6.1	-0.33	0.44
Stockton	302	18.0	13.1	-4.9	7.3	-0.55	0.63
Merced	326	13.2	13.3	0.1	5.3	-0.14	0.44
Hanford	329	18.0	15.8	-2.2	5.9	-0.27	0.46
Madera	323	18.0	13.1	-4.9	7.7	-0.51	0.64
Manteca	325	11.7	13.4	1.7	6.2	-0.10	0.55
Visalia	309	18.6	19.1	0.5	6.9	-0.09	0.41
Modesto	315	14.4	14.5	0.1	5.0	-0.05	0.42
Turlock	316	14.8	14.6	-0.2	4.5	-0.05	0.41

5.3 FUTURE YEAR DESIGN VALUES

Future DVs for each site are given in Table 20. Correspondingly, Relative Response Factors (RRFs) and the base and the projected future year annual $PM_{2.5}$ composition at each monitor are given in Tables 21-23 (Note that the annual RRFs and composition are for reference only and that in the actual future year DV calculation, separate calculations were performed for each quarter and not on the annual average). The Bakersfield-Planz site has the highest projected future year DV at 14.8 µg/m^3, which is well above the 2012 annual $PM_{2.5}$ standard of 12 µg/m^3, but below the 2006 annual $PM_{2.5}$ standard of 15 µg/m^3. From the base to future year, there are significant reductions projected for ammonium nitrate and EC, modest reduction in OM, almost no change in sulfate, and a slight increase in crustal material (i.e., other primary $PM_{2.5}$ such as fugitive dust emissions).

Table 20. Projected future year $PM_{2.5}$ DVs at each monitor

Site AQS ID	Name	Base DV ($\mu g/m^3$)	Future 2021 DV ($\mu g/m^3$)
60290016	Bakersfield - Planz	17.3	14.8
60392010	Madera	16.9	14.4
60311004	Hanford	16.5	13.4
60310004	Corcoran	16.3	14.4
61072002	Visalia	16.2	13.7
60195001	Clovis	16.1	14.1
60290014	Bakersfield - California	16.0	13.6
60190011	Fresno-Garland	15.0	12.9
60990006	Turlock	14.9	12.8
60195025	Fresno - Hamilton & Winery (H &W)	14.2	12.2
60771002	Stockton	13.1	11.7
60470003	Merced - S Coffee	13.1	11.2
60990005	Modesto	13.0	11.2
60472510	Merced - Main Street	11.0	9.7
60772010	Manteca	10.1	8.8
60192009	Tranquility	7.7	6.5

Table 21. Annual RRFs for $PM_{2.5}$ components

Site	RRF for $PM_{2.5}$	RRF for NH_4	RRF for NO_3	RRF for SO_4	RRF for OM	RRF for EC	RRF for Crustal
Bakersfield - Planz	0.85	0.68	0.69	0.97	0.90	0.51	1.02
Madera	0.85	0.74	0.70	1.00	0.93	0.69	1.01
Hanford	0.81	0.71	0.67	1.02	0.94	0.70	0.92
Corcoran	0.88	0.70	0.68	1.04	0.97	0.76	0.95
Visalia	0.85	0.69	0.70	1.01	0.89	0.63	1.02
Clovis	0.87	0.70	0.70	1.00	0.91	0.66	1.07
Bakersfield - California	0.85	0.67	0.67	0.97	0.90	0.52	1.03
Fresno-Garland	0.86	0.72	0.72	0.99	0.89	0.59	1.05
Turlock	0.86	0.77	0.75	1.00	0.92	0.67	1.05

Fresno - H&W	0.86	0.74	0.74	0.99	0.89	0.58	1.05
Stockton	0.89	0.80	0.76	1.02	0.95	0.70	1.05
Merced - S Coffee	0.85	0.73	0.71	1.01	0.93	0.68	1.04
Modesto	0.86	0.77	0.74	1.01	0.92	0.67	1.05
Merced - Main Street	0.88	0.72	0.71	1.01	0.93	0.69	1.04
Manteca	0.87	0.81	0.77	1.02	0.92	0.68	1.04
Tranquility	0.84	0.69	0.63	1.00	0.96	0.73	1.02

Table 22. Base year $PM_{2.5}$ compositions*

Name	Base $PM_{2.5}$ ($\mu g/m^3$)	Base NH_4 ($\mu g/m^3$)	Base NO_3 ($\mu g/m^3$)	Base SO_4 ($\mu g/m^3$)	Base OM ($\mu g/m^3$)	Base EC ($\mu g/m^3$)	Base Crustal ($\mu g/m^3$)
Bakersfield - Planz	17.3	1.1	2.6	1.7	7.0	1.0	2.5
Madera	16.9	1.4	4.1	1.5	6.4	0.9	1.2
Hanford	16.5	1.9	5.5	1.5	4.1	0.7	1.2
Corcoran	16.3	1.2	2.9	1.5	7.4	0.7	1.2
Visalia	16.2	1.2	3.0	1.4	7.3	0.7	1.2
Clovis	16.1	0.9	2.1	1.3	8.7	0.9	1.1
Bakersfield – California	16.0	1.1	2.6	1.5	6.4	0.9	2.2
Fresno - Garland	15.0	0.9	2.2	1.1	8.0	0.8	0.9
Turlock	14.9	1.4	3.9	1.2	5.4	0.8	0.9
Fresno - H&W	14.2	0.8	2.1	1.0	7.6	0.8	0.8
Stockton	13.1	1.1	3.3	1.1	4.9	0.7	0.8
Merced - S Coffee	13.1	1.1	3.3	1.1	4.8	0.7	0.8
Modesto	13.0	1.2	3.4	1.1	4.7	0.7	0.8
Merced – Main Street	11.0	0.7	1.7	0.9	5.6	0.6	0.6
Manteca	10.1	0.9	2.6	0.8	3.6	0.5	0.6
Tranquility	7.7	0.6	1.9	0.6	2.8	0.4	0.5

*: Base year $PM_{2.5}$ compositions were based on CSN speciation measurement adjusted by the EPA SANDWICH method. Particle-bound water and blank mass are not shown.

Table 23. Projected future year $PM_{2.5}$ compositions

Name	Future $PM_{2.5}$ ($\mu g/m^3$)	Future NH_4 ($\mu g/m^3$)	Future NO_3 ($\mu g/m^3$)	Future SO_4 ($\mu g/m^3$)	Future OM ($\mu g/m^3$)	Future EC ($\mu g/m^3$)	Future Crustal ($\mu g/m^3$)	Future Water ($\mu g/m^3$)	Blank ($\mu g/m^3$)
Bakersfield - Planz	14.8	0.8	1.8	1.6	6.2	0.5	2.6	0.7	0.5
Madera	14.4	1.1	2.8	1.5	5.9	0.6	1.2	0.8	0.5
Hanford	13.4	1.4	3.6	1.5	3.8	0.5	1.1	0.9	0.5
Corcoran	14.4	0.8	2.0	1.5	7.1	0.5	1.1	0.7	0.5
Visalia	13.7	0.8	2.1	1.5	6.5	0.4	1.2	0.7	0.5
Clovis	14.1	0.6	1.5	1.3	7.9	0.6	1.1	0.6	0.5
Bakersfield - California	13.6	0.7	1.7	1.4	5.8	0.5	2.3	0.6	0.5
Fresno - Garland	12.9	0.6	1.6	1.1	7.1	0.5	0.9	0.5	0.5
Turlock	12.8	1.0	3.0	1.2	4.9	0.5	0.9	0.7	0.5
Fresno - H&W	12.2	0.6	1.5	1.0	6.7	0.4	0.9	0.5	0.5
Stockton	11.7	0.9	2.5	1.2	4.6	0.5	0.9	0.6	0.5
Merced - S Coffee	11.2	0.8	2.3	1.1	4.5	0.5	0.8	0.6	0.5
Modesto	11.2	0.9	2.5	1.1	4.3	0.4	0.8	0.6	0.5
Merced – Main Street	9.7	0.5	1.2	0.9	5.2	0.4	0.6	0.4	0.5
Manteca	8.8	0.7	2.0	0.8	3.3	0.3	0.6	0.5	0.5
Tranquility	6.5	0.4	1.2	0.6	2.7	0.3	0.5	0.3	0.5

5.4 PRECURSOR SENSITIVITY ANALYSIS

To evaluate the impact of reducing emissions of different $PM_{2.5}$ precursors on the projected future $PM_{2.5}$ DVs, a series of model sensitivity simulations were conducted, where emissions of the precursor species were scaled by ±15% from the future year baseline emissions. Comparing the difference in $PM_{2.5}$ DVs from the ±15% perturbations essentially produces the sensitivity of the future year $PM_{2.5}$ DVs to a 30% change in future year baseline precursor emissions. Specifically, the effect of reductions in the following $PM_{2.5}$ precursors was investigated: direct $PM_{2.5}$ (or primary $PM_{2.5}$), nitrogen oxides (NO_x), sulfur oxides (SO_x), ammonia, and volatile organic compounds (VOCs). For each precursor, only anthropogenic emissions in California were perturbed. Natural emissions and emissions outside of California (e.g., Mexico) were not perturbed.

Tables 24-28 show the change in $PM_{2.5}$ DV at each site from the 30% perturbation of controllable NO_x, direct $PM_{2.5}$, NH_3, VOCs, and SO_x emissions, respectively. The DV change is calculated as the difference in the projected DV from the +15% perturbation minus the projected DV from the -15% perturbation case. In addition, the differences are calculated for both the aggregate $PM_{2.5}$ DV as well as the component specific portion of the DV that is directly linked to each precursor. The $PM_{2.5}$ component(s) corresponding to each emissions precursor are as follows: NO_x is linked to ammonium nitrate; direct $PM_{2.5}$ is linked to primary sulfate, organic matter (OM), EC, and other primary $PM_{2.5}$ components; NH_3 is linked to ammonium nitrate plus the ammonium associated with ammonium sulfate (i.e., all ammonium); VOCs are linked to secondary organic aerosol (SOA); and SO_x is linked to the sulfate component of ammonium sulfate.

A threshold of 0.2 µg/m^3 for the annual $PM_{2.5}$ DV was used to determine the significance of a precursor to $PM_{2.5}$ formation (e.g., if a 30% change in precursor emissions leads to a change in component DV less than or equal to 0.2 µg/m^3 then the precursor is deemed not significant). For NO_x (Table 24), a 30% change in emissions resulted in a response of the component DV that is greater than 0.2 µg/m^3 at all sites, so NO_x is deemed a significant precursor. The same is true for direct $PM_{2.5}$ (Table 25), where sites show a response between 0.8 µg/m^3 at Tranquility and 2.8 µg/m^3 at Bakersfield-Planz and Clovis. For the other major precursors, ammonia, VOC, and SO_x (Tables 26-28), all are shown to be not significant based on the 0.2 µg/m^3 threshold and a 30% change in precursor emissions.

Table 24. Difference in $PM_{2.5}$ and ammonium nitrate DVs from a 30% perturbation in anthropogenic NO_x emissions.

Site	Difference in $PM_{2.5}$ DVs (µg/m^3)	Difference in component (i.e., ammonium nitrate, µg/m^3)
Bakersfield - Planz	0.8	0.7
Madera	1.1	1.0
Hanford	1.5	1.3
Corcoran	0.9	0.8
Visalia	0.9	0.8
Clovis	0.7	0.5
Bakersfield - California	0.8	0.7
Fresno-Garland	0.6	0.5
Turlock	1.1	1.0
Fresno - Hamilton & Winery	0.6	0.5
Stockton	0.9	0.8
Merced - S Coffee	0.9	0.8
Modesto	0.9	0.8
Merced - Main Street	0.5	0.4
Manteca	0.7	0.6
Tranquility	0.5	0.4

Table 25. Difference in $PM_{2.5}$ and components (including sulfate, OM, EC, and other) DVs from a 30% perturbation in anthropogenic $PM_{2.5}$ emissions

Site	Difference in $PM_{2.5}$ DVs ($\mu g/m^3$)	Difference in component (including sulfate, OM, EC, and other $PM_{2.5}$, $\mu g/m^3$)
Bakersfield - Planz	2.9	2.8
Madera	2.3	2.1
Hanford	1.6	1.5
Corcoran	2.4	2.3
Visalia	2.4	2.3
Clovis	2.9	2.8
Bakersfield - California	2.7	2.6
Fresno-Garland	2.7	2.6
Turlock	2.0	1.9
Fresno - Hamilton & Winery	2.6	2.5
Stockton	1.9	1.8
Merced - S Coffee	1.7	1.6
Modesto	1.8	1.7
Merced - Main Street	1.8	1.8
Manteca	1.3	1.2
Tranquility	0.9	0.8

Table 26. Difference in $PM_{2.5}$ and ammonium nitrate DVs from a 30% perturbation in ammonia emissions

Site	Difference in $PM_{2.5}$ DVs ($\mu g/m^3$)	Difference in component (i.e., ammonium nitrate, $\mu g/m^3$)
Bakersfield - Planz	0.1	0.1
Madera	0.2	0.2
Hanford	0.2	0.2
Corcoran	0.1	0.1
Visalia	0.1	0.1
Clovis	0.1	0.1
Bakersfield - California	0.1	0.1
Fresno-Garland	0.1	0.1
Turlock	0.2	0.1
Fresno - Hamilton & Winery	0.1	0.1
Stockton	0.1	0.1
Merced - S Coffee	0.1	0.1
Modesto	0.1	0.1
Merced - Main Street	0.1	0.1
Manteca	0.1	0.1
Tranquility	0.1	0.1

Table 27. Difference in $PM_{2.5}$ and SOA DVs from a 30% perturbation in VOCs emissions

Site	Difference in $PM_{2.5}$ DVs ($\mu g/m^3$)	Difference in component (i.e., SOA, $\mu g/m^3$)
Bakersfield - Planz	0.0	0.1
Madera	0.0	0.1
Hanford	-0.1	0.1
Corcoran	0.0	0.1
Visalia	0.0	0.1
Clovis	0.1	0.1
Bakersfield - California	0.0	0.1
Fresno-Garland	0.1	0.1
Turlock	0.0	0.0
Fresno - Hamilton & Winery	0.0	0.1
Stockton	0.0	0.0
Merced - S Coffee	0.0	0.1
Modesto	0.0	0.0
Merced - Main Street	0.0	0.1
Manteca	0.0	0.0
Tranquility	0.0	0.0

Table 28. Difference in $PM_{2.5}$ and sulfate DVs from a 30% perturbation in SO_x emissions

Site	Difference in $PM_{2.5}$ DVs ($\mu g/m^3$)	Difference in component (i.e., sulfate only, $\mu g/m^3$)
Bakersfield - Planz	0.1	0.1
Madera	0.2	0.1
Hanford	0.2	0.1
Corcoran	0.1	0.1
Visalia	0.2	0.1
Clovis	0.1	0.1
Bakersfield - California	0.1	0.1
Fresno-Garland	0.1	0.1
Turlock	0.2	0.1
Fresno - Hamilton & Winery	0.1	0.1
Stockton	0.2	0.1
Merced - S Coffee	0.2	0.1
Modesto	0.2	0.1
Merced - Main Street	0.1	0.1
Manteca	0.2	0.1
Tranquility	0.1	0.0

5.5 DISCUSSION ON PRECURSOR SENSITIVITY

In this section, we address three questions regarding precursor sensitivity:

1.) NO_x as the limiting precursor for ammonium nitrate vs. benefits of ammonia reductions on ammonium nitrate formation;
2.) On VOCs' indirect role in ammonium nitrate formation;
3.) Current status of secondary organic aerosol (SOA)

Ammonia's role in ammonium nitrate formation in the SJV

During the DISCOVER-AQ field campaign, aircraft measurements of $PM_{2.5}$ and its precursors were made in the planetary boundary layer over agricultural and urban areas within the SJV. Among the suite of measurements made, the measurements of total nitric acids (gas + particle phases, or g + p), gaseous ammonia, particulate ammonium, and sulfate allowed for an observation based evaluation of the precursor limitation for ammonium nitrate formation. The excess NH_3 in the atmosphere can be defined as the sum of gaseous NH_3 and particulate ammonium minus 2x particulate sulfate and total nitric acids (g + p) (Blanchard et al., 2000). While the calculation of excess NH_3 in Blanchard et al. (2000) also incorporated the impact from other ions, such as calcium, magnesium, potassium and chloride, those species should only have a minor effect on the analysis and so were not considered in order to maximize the data availability. If the value of excess NH_3 is greater than zero, this indicates that secondary particulate nitrate is in a NO_x-limited regime. Conversely, a value less than zero demonstrates an ammonia-limited regime.

Figure 14 shows the excess NH_3 in the bottom 1 km of the atmosphere, collected by NASA aircraft in the SJV on January 18 and 20, during which $PM_{2.5}$ concentrations in the SJV were elevated. Each data point of excess NH_3 was calculated based on 10 second observational data with no further averaging. For nearly all data points, excess NH_3 is clearly above zero, indicating that nitrate formation in the SJV is in a NO_x-limited regime, which is consistent with past observations (Lurmann et al., 2006; Markovic, 2014).

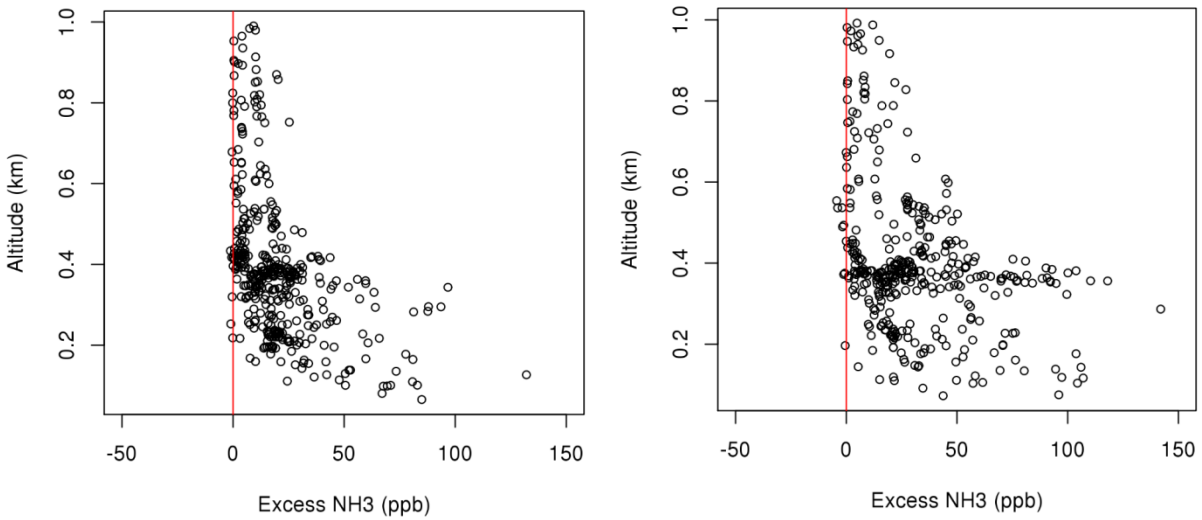

Figure 14. Excess NH_3 in the SJV on January 18 (Left) and January 20 (Right) based on NASA aircraft measurements in 2013.

While ammonium nitrate formation is in a NO_x limited regime, this does not conflict with modeling results that showed a small sensitivity of ammonium nitrate formation to ammonia emission reductions. At equilibrium state, the product of gaseous nitric acid and ammonia mixing ratios in the atmosphere is a constant, and the equilibrium constant depends on ambient conditions as well as particulate compositions (Seinfeld and Pandis, 2006). Even in a NO_x-limited regime, the perturbation of ammonia mixing ratios influences the partitioning of nitric acids. As ammonia becomes more and more excessive, the partitioning of nitric acids shifts towards the particulate phase. After the vast majority of nitric acids are in the particulate phase (e.g., > 98% of nitric acids in particulate phase), the formation of ammonium nitrate becomes far less sensitive to the excessive ammonia. In addition, the dry deposition velocity difference between gaseous nitric acid and particulate nitrate further adds to the complexity. When the partitioning of gaseous and particulate nitric acids is perturbed by changing ammonia, due to the different removal rates of gaseous and particulate nitric acids (Meng et al., 1997; Pusede et al., 2016), the mass of total nitric acids is perturbed as well, which could amplify the response to ammonia emissions changes. In the SJV, because of the excessive ammonia, the formation of ammonium nitrate is much more sensitive to the reductions of NO_x than to the reductions of ammonia, which has been widely documented in past modeling studies. Nevertheless, limited sensitivity of ammonium nitrate formation to large ammonia reductions has been shown in previous modeling studies as well (Kleeman et al., 2005). Overall, modeling demonstrated that ammonia is not a significant precursor to $PM_{2.5}$ as $PM_{2.5}$ DVs only exhibited a limited sensitivity to a reasonable level of ammonia reductions.

Indirect role of VOCs in ammonium nitrate formation

The integrated reaction rate (IRR) analysis in CMAQv5.0.2 was used to understand the impact of VOC emission reductions on nitrate formation in the model. IRR outputs the production or loss rates for individual gas-phase chemical pathways. Heterogeneous nitric acid formation rates were obtained from the aerosol module. Two separate simulations using the January 2013 meteorological fields were conducted for two future year emission scenarios. One utilized the baseline future year emissions inventory for 2025 and the other involved a 25% reduction in VOC emissions from the baseline scenario. When VOC emissions were reduced by 25%, daytime and nighttime nitric acid formation rates were only slightly impacted by the VOC emission reductions. Daytime homogeneous nitric acid formation is primarily through the gas-phase reaction of NO_2 and the hydroxyl radical. When VOC emissions were reduced, at urban locations such as Bakersfield, the daytime nitric acid formation rate decreased slightly because of the slight decrease in hydroxyl radical mixing ratios associated with VOC reductions. More specifically, reduced hydroxyl radical mixing ratio was due to reduced photolysis from formaldehyde (Pusede et al., 2016).

In addition to the effect that VOCs can have on daytime nitric acid formation rates, they can also indirectly affect nighttime heterogeneous nitric acid formation, which involves the heterogeneous reaction of N_2O_5 on particles. N_2O_5 is formed from NO_2 and NO_3, the latter of which is a product of the reaction between NO_2 and O_3 (Seinfeld and Pandis, 2006). In places like Visalia, the nighttime heterogeneous nitric acid formation rate above the surface was slightly enhanced when VOC emissions were reduced. Model output showed reduced peroxyacetyle nitrate (PAN) formation under reduced VOC emissions. The reduced PAN formation then resulted in increased availability of NO_2, which in turn enhanced N_2O_5 formation (Meng et al., 1997) and slightly increased its heterogeneous formation rate.

Overall, reducing VOC emissions by 25% increased ammonium nitrate only slightly (~ 1%) at $PM_{2.5}$ design sites, which is the net outcome of different chemical processes in competition with each other, as well as the physical transport and mixing processes in the atmosphere.

Current status of secondary organic aerosol (SOA)

Secondary organic aerosol (SOA) is formed in the atmosphere by oxidation of VOCs followed by gas to particle partitioning of the oxidation products (Kanakidou et al., 2005). In general, the importance of SOA is higher during the ozone season when VOC emissions are at their peak (e.g., Foley et al., 2010; Liu et al., 2012; Rollins et al., 2012;

Zhao et al., 2013) and is much smaller in winter (Lurmann et al., 2006). However, in the SJV, $PM_{2.5}$ concentrations are typically lower in summer compared to winter. In recent years, Aerosol Mass Spectrometer (AMS) measurements made in Fresno during winter showed that approximately a third of organic aerosol is oxygenated organic aerosol (OOA) and the remaining is primary (Ge et al., 2013; Young et al., 2016).At present, the sources and/or formation processes for OOA are not known yet. Potential sources for OOA could include SOA, atmospherically processed POA, or directly emitted POA as well.

In the CMAQ model, SOA is simulated using the two-product absorption model (Odum et al., 1996). Detailed description of the SOA model in CMAQ can be found in Carlton et al. (2010) and Simon et al. (2012). Briefly, CMAQ considers SOA formation from the following precursors: long chain alkanes, high-yield aromatics (e.g., toluene), low-yield aromatics (e.g., xylene), benzene, isoprene, monoterpenes, and sesquiterpenes. For most anthropogenic VOCs, SOA is formed via oxidation by the hydroxyl radical. For biogenic VOCs, such as monoterpenes and sesquiterpenes, SOA is also formed from oxidation by nitrate and ozone, in addition to oxidation by the hydroxyl radical (Carlton et al., 2010). CMAQ also incorporates a NO_x dependence on SOA yield, in-cloud SOA formation from glyoxal and mythylglyoxal, particle-phase oligomerization (Carlton et al., 2010) and aging of primary organic aerosol (Simon et al., 2012). Overall, CMAQ's SOA module represents a state-of-the-science treatment of known SOA precursors and processes. Various daytime and nighttime formation processes of SOA considered important at Bakersfield (Liu et al., 2012; Rollins et al., 2012; Zhao et al., 2013) are treated in the CMAQ model.

In general, current state-of-the-science SOA models are believed to under-predict the levels of SOA formation in the atmosphere. The under-prediction of SOA is not limited to the two-product SOA model used in CMAQ. Other SOA modeling formulations, such as the volatility bin based model (e.g., Ciarelli et al., 2015; Woody et al., 2015) and the statistical oxidation model (e.g., Jathar et al., 2016) under-predict SOA concentrations to a similar degree, especially when these models are calibrated to the same chamber SOA yield data and are based on the same SOA precursors

Two important issues have emerged in recent years that were deemed to be promising in reducing the gaps between modeled and observed SOA concentrations in the atmosphere. Robinson et al. (2007) demonstrated that SOA formation from emissions of intermediate-volatile/semi-volatile organic compounds (IVOCs/SVOCs) from combustion sources far exceeded known SOA precursors and that those emissions were not accounted for in the current emission inventories. Characterization and quantification of the emission factors and SOA formation potentials of the IVOCs/SVOCs are not trivial. In the past several years, collaborations among Professor Robinson's group at

Carnegie Mellon University (CMU), EPA, and CARB have been focusing on the characterization of IVOCs/SVOCs emissions from mobile sources. Follow-up studies have demonstrated the importance of SOA formation from motor vehicle emitted IVOCs/SVOCs (e.g., Jathar et al., 2014; Zhao et al., 2015), although these studies were based on 0-D calculations. Given the challenge of characterizing those emissions and SOA formation potentials, there is also a discrepancy regarding the relative importance of SOA formation from different motor vehicle sources (Bahreini et al., 2012; Gentner et al., 2012; Jathar et al., 2014; Zhao et al., 2015). However, CMU's latest 3-D air quality modeling assessment in Southern California including those IVOCs/SVOCs emissions shows only modest difference of OA prediction compared to the traditional method in CMAQv4.7 and that mobile sources (including gasoline and diesel vehicles/equipments) only contributed one-quarter of the OA burden in Southern California, as strict regulations have dramatically reduced motor vehicle emissions (Robinson, 2016). Zhang et al. (2014) found that SOA yield data measured from laboratory chamber experiments may be substantially suppressed due to losses of SOA-forming vapors to chamber walls. This can lead to an underestimate of SOA in air quality models because parameterizations in SOA models are calibrated against chamber measured SOA yields. While the significance of vapor wall loss has been recognized, more work is needed to understand the mechanisms of vapor wall loss and to correct the vapor wall loss for past experimental data (Krechmer et al., 2016; Yeh and Ziemann, 2015; Zhang et al., 2015).

Many ambient or laboratory measurements have demonstrated potential SOA formation from different chemical pathways beyond the absorption process treated in typical SOA models. For example, Zhao et al (2013) showed that SOA production from phthalic acid was substantially increased by reaction with ammonia to form ammonium salts that favor their partitioning into the particle phase. Smith (2014) demonstrated that aqueous oxidation of phenols can lead to SOA formation. While those findings are important under certain conditions, more coordinated ambient measurement, laboratory experiments, and computational modeling are needed to develop models that describe those formation pathways rigorously under different atmospheric conditions. From there, the importance of those processes and the implication to control programs can be assessed. Arbitrary use of findings may itself lead to simulated SOA formation that is not a true representation of the relevant atmospheric processes, even though the model performance of SOA/OA is improved. For example, Jathar et al. (2016) cautioned that the use of an unconstrained multi-generational aging scheme, commonly adopted in models recently (e.g., Lane et al., 2008; Shrivastava et al., 2008), is not an indication of improved representation of atmospheric chemistry, though it improved the agreement between observed and modeled OA concentrations. Hayes et al. (2015) showed that including SOA formation from IVOCs/SVOCs based on three different parameterizations

shows very large differences (e.g., a factor of 3 in SOA mass concentrations), which underscored the uncertainties associated with the current understanding. These all demonstrated that caution needs to be taken in terms of development and choice of parameterizations of SOA precursors/formation, particularly when these models are used for regulatory purposes.

Overall, continued assessment of SOA formation in the SJV is warranted as the scientific understanding of SOA contributing sources and formation mechanisms continues to be improved. However, based on modeling result from the current state-of-the-science SOA module in CMAQv5.0.2, VOC is not a significant precursor to $PM_{2.5}$ formation in the SJV based on its contribution to SOA formation.

6 REFERENCES

Angevine, W. M., Eddington, L., Durkee, K., Fairall, C., Bianco, L., Brioude, J., 2012: Meteorological model evaluation for CalNex 2010, Monthly Weather Review, 140, 3885-3906.

Bahreini, R., et al., 2012: Gasoline emissions dominate over diesel in formation of secondary organic aerosol mass, Geophysical Research Letters, 39, doi:10.1029/2011GL050718.

Baker, K. R., H. Simon, and J. T. Kelly, 2011: Challenges to modeling “cold pool” meteorology associated with high pollution episodes. Environ. Sci. and Technol., 45(17), 7118–9.

Baker, K. R., Misenis, C., Obland, M. D., Ferrare, R. A., Scarino, A. J., and Kelly, J. T., 2013: Evaluation of surface and upper air fine scale WRF meteorological modeling of the May and June 2010 CalNex period in California, Atmos. Environ., 80, 299-309.

Bao, J.W., Michelson, S.A., Persson, P.O.G., Djalalova, I.V., Wilczak, J.M., 2008: Observed and WRF-simulated low-level winds in a high-ozone episode during the Central California ozone study, Journal of Applied Meteorology and Climatology, 47, 2372-2394.

Blanchard, C.L., Roth, P.M., Tanenbaum, S.J., Ziman, S.D., Seinfeld, J.H., 2000, The use of ambient measurements to identify which precursor species limit aerosol nitrate formation, Journal of Air Waste Management Association, 50, 2073-2084.

Boylan, J.W. and Russell, A.G., 2006, PM and light extinction model performance metrics, goals, and criteria for three-dimensional air quality models, Atmospheric Environment, 40, 4946-4959.

Carlton, A. G., P. V. Bhave, S. L. Napelenok, E. O. Edney, G. Sarwar, R. W. Pinder, G. A. Pouliot, and M. Houyoux, 2010, Model Representation of Secondary Organic Aerosol in CMAQv4.7., Env. Sci. & Techno., 44, 8553-8560.

Ciarelli, G., et al., 2015, European air quality modelled by CAMx including the volatility basis set scheme, Atmospheric Chemistry Physics Discussion, 15, 35645-35691.

Daly, C., D. Conklin, and M. Unsworth, 2009: Local atmospheric decoupling in complex topography alters climate change impacts. Int. J. Climatol., 30, 1857–1864.

Emmons, L. K., Apel, E.C., Lamarque, J.F., Hess, P.G., Avery, M., Blake, D., Brune, W., Campos, T., Crawford, J., DeCarlo, P.F., Hall, S., Heikes, B., Holloway, J., Jimenez, J.L., Knapp, D.J., Kok, G., Mena-Carrasco, M., Olson, J., O'Sullivan, D., Sachse, G., Walega, J., Weibring, P., Weinheimer, A., and Wiedinmyer, C., 2010, Impact of Mexico City emissions on regional air quality from MOZART-4 simulations, Atmospheric Chemistry and Physics, 10, 6195-6212.

Fast, J. D., Gustafson Jr, W. I., Berg, L. K., Shaw, W. J., Pekour, M., Shrivastava, M., Barnard, J. C., Ferrare, R. A., Hostetler, C. A., Hair, J. A., Erickson, M., Jobson, B. T., Flowers, B., Dubey, M. K., Springston, S., Pierce, R. B., Dolislager, L., Pederson, J., and Zaveri, R. A., 2012: Transport and mixing patterns over Central California during the carbonaceous aerosol and radiative effects study (CARES), Atmos. Chem. Phys., 12, 1759-1783, doi:10.5194/acp-12-1759-2012.

Foley, K. M., et al., 2010, Incremental testing of the Community Multiscale Air Quality (CMAQ) modeling system version 4.7, Geosci. Model Dev., 3, 205-226, doi:10.5194/gmd-3-205-2010.

Fosberg, M.A., Schroeder, M.J., 1966: Marine air penetration in Central California, Journal of Applied Meteorology, 5, 573-589.

Frank, N.H., 2006, Retained nitrate, hydrated sulfates, and carbonaceous mass in federal reference method fine particulate matter for six eastern U.S. cities, Journal of Air & Waste Management Association, 56, 500-511.

Ge, X. L., A. Setyan, Y. L. Sun, Q. Zhang, 2012, Primary and Secondary Organic Aerosols in Fresno California during Wintertime: Results from High Resolution Aerosol Mass Spectrometry, Journal of Geophysical Research – Atmospheres, 117, D19301, 15p,10.1029/2012JD018026.

Gentner, D.R., et al., 2012, Elucidating secondary organic aerosol from diesel and gasoline vehicles through detailed characterization of organic carbon emissions, Proceedings of the National Academy of Sciences, 109, 18318-18323.

Gillies, R. R., S. Wang, and M. R. Booth, 2010: Atmospheric scale interaction on wintertime intermountain west low-level inversions. Weather Forecasting, 25, 1196–1210.

Hayes, P.L., et al., 2015, Modeling the formation and aging of secondary organic aerosols in Los Angeles during CalNex 2010, Atmospheric Chemistry Physics, 15, 5773-5801.

Hu, J., Howard, C. J., Mitloehner, F., Green, P. G., and Kleeman, M. J., 2012: Mobile Source and Livestock Feed Contributions to Regional Ozone Formation in Central California, Environmental Science & Technology, 46, 2781-2789.

Jackson, B.S., Chau, D., Gurer, K., Kaduwela, A., 2006: Comparison of ozone simulations using MM5 and CALMET/MM5 hybrid meteorological fields for the July/August 2000 CCOS episode, Atmos. Environ., 40, 2812-2822.

Jathar, S. H., Cappa, C. D., Wexler, A. S., Seinfeld, J. H., and Kleeman, M. J., 2016, Simulating secondary organic aerosol in a regional air quality model using the statistical oxidation model – Part 1: Assessing the influence of constrained multi-generational ageing, Atmos. Chem. Phys., 16, 2309-2322.

Jathar, S.H., Gordon, T.D., Hennigan, C.J., Pye, H.O.T., Pouliot G., Adams, P.J., Donahue, N.M., Robinson, A.L., 2014, Unspeciated organic emissions from combustion sources and their influence on the secondary organic aerosol budget in the United State, Proceedings of the National Academy of Sciences, 111, 10473-10478.

Kanakidou et al., 2005, Organic aerosol and global climate modeling: a review, Atmospheric Chemistry Physics, 5, 1053-1123.

Kelly, J. T., Baker, K. R., Nowak, J. B., Murphy, J. G., Milos, Z. M., VandenBoer, T. C., Ellis, R. A., Neuman, J. A., Weber, R. J., Roberts, J. M., Veres, P. R., de Gouw, J. A., Beaver, M. R., Newman, S., and Misenis, C., 2014: Fine-scale simulation of ammonium and nitrate over the South Coast Air Basin and San Joaquin Valley of California during CalNex-2010, J. Geophysical Research, 119, 3600-3614, doi:10.1002/2013JD021290.

Kleeman, M.J., Ying, Q., and Kaduwela, A., 2005, Control strategies for the reduction of airborne particulate nitrate in California's San Joaquin Valley, Atmospheric Environment, 39, 5325-5341.

Krechmer, J., Pagonis, D., Ziemann, P.J., Jimenez, J.L., 2016, Quantification of gas-wall partitioning in Teflon environmental chambers using rapid bursts of low-volatility oxidized species generated in situ, Environmental Science & Technology, doi:10.1021/acs.est.6b00606.

Lane, T.E., Donahue, N.M., Pandis, S.N., 2008, Simulating secondary organic aerosol formation using the volatility basis-set approach in a chemical transport model, Atmospheric Environment, 42, 7439-7451.

Liu, S., et al., 2012, Secondary organic aerosol formation from fossil fuel sources contribute majority of summertime organic mass at Bakersfield, J. Geophys. Res., 117, D00V26, doi:10.1029/2012JD018170.

Lurmann, F.W., Brown, S.G., McCarthy, M.C., and Roberts, P.T., 2006, Processes Influencing Secondary Aerosol Formation in the San Joaquin Valley during Winter, Journal of Air and Waste Management Association, 56, 1679-1693.

Markovic, M. Z., VandenBoer, T. C., Baker, K. R., Kelly, J. T., and Murphy, J. G., 2014, Measurements and modeling of the inorganic chemical composition of fine particulate matter and associated precursor gases in California's San Joaquin Valley during CalNex 2010, Journal of Geophysical Research - Atmosphere,119, 6853–6866, doi:10.1002/2013JD021408.

Meng, Z., Dabdub, D., Seinfeld, J.H., 1997, Chemical coupling between atmospheric ozone and particulate matter, Science, 277, 116-119.

Odum, J.R., T. Hoffmann, F. Bowman, D. Collins, R.C. Flagan, J.H. Seinfeld, 1996, Gas/particle partitioning and secondary organic aerosol yields, Environmental Science & Technology, 30, 2580-2585.

Pusede, S.E., et al., 2016, On the effectiveness of nitrogen oxide reductions as a control over ammonium nitrate aerosol, Atmospheric Chemistry Physics, 16, 2575-2596.

Robinson, A. 2016, Linking Tailpipe to Ambient: Phase 4 Executive Summary, prepared by Carnegie Mellon University for the Coordinating Research Council, Inc., available at http://www.crcao.com/reports/recentstudies2016/A-74_E-96%20Phase%204/A-74-E-96%20Phase%204%20Executive%20Summary.pdf, accessed in July 2016.

Rogers, R.E., Deng, A., Stauffer, D. Gaudet, B.J., Jia, Y., Soong, S.-T., Tanrikulu, S., 2013, Application of the Weather Research and Forecasting model for air quality modeling in the San Francisco Bay area, Journal of Applied Meteorology and Climatology, 52, 1953-1973.

Rollins, A. W., et al., 2012, Evidence for NOx Control over Nighttime SOA Formation, Science, 337, 1210-1212, doi:10.1126/science.1221520.

Seinfeld, J.H., Pandis, S.N., 2006, Atmospheric Chemistry and Physics: From Air Pollution to Climate Change, 2nd Edition, Wiley, Inc., New York.

Shrivastava, M.K., Lane, T.E., Donahue, N.M., Pandis, S.N., Robinson, A.L., 2008, Effects of gas particle partitioning and aging of prigram emissions on urban and regional organic aerosol concentrations, Journal of Geophysical Research, 113, D18301, doi:10.1029/2007JD009735.

Skamarock, W. C., J. B. Klemp, J. Dudhia, D. O. Gill, D. M. Barker, W. Wang, and J. G. Powers, 2005: A description of the Advanced Research WRF Version 2. NCAR Tech Notes-468+STR.

Simon, H., Baker, K.R., and Phillips, S., 2012, Compilation and interpretation of photochemical model performance statistics published between 2006 and 2012, Atmospheric Environment, 61, 124-139.

Simon, H., Bhave, P.V., 2012, Simulating the degree of oxidation in atmospheric organic particles. Environ. Sci. Technol., 46, 331-339.

Smith, J.D., Sio, V., Yu, L., Zhang, Q., Anastasio, C., 2014, Secondary organic aerosol production from aqueous reactions of atmospheric phenols with an organic triplet excited state, Environmental Science & Technology, 48, 1049-1057.

Whiteman, C. D., S. Zhong, W. J. Shaw, J. M. Hubbe, X. Bian, and J. Mittelstadt, 2001: Cold pools in the Columbia Basin. Weather Forecasting, 16, 432–447.

Woody, M. C., Baker, K. R., Hayes, P. L., Jimenez, J. L., Koo, B., and Pye, H. O. T., 2015: Understanding sources of organic aerosol during CalNex-2010 using the CMAQ-VBS, Atmos. Chem. Phys. Discuss., 15, 26745-26793, doi:10.5194/acpd-15-26745-2015.

Yeh, G.K., Ziemann, P.J., 2015, Gas-wall partitioning of oxygenated organic compounds: Measurements, structure-activity relationships, and correlation with gas chromatographic retention factor, Aerosol Science & Technology, 49, 727-738.

Young, D., Kim, H. J., Parworth, C., Zhou, S., Zhang, X. L., Cappa, C., Seco, R., Kim, S., and Zhang, Q., 2016, Influences of emission sources and meteorology on aerosol chemistry in a polluted urban environment: Results from DISCOVER-AQ California, Atmospheric Chemistry & Physics, 16, 5427-5451.

Zhao, Y., et al., 2013, Sources of organic aerosol investigated using organic compounds as tracers measured during CalNex in Bakersfield, J. Geophys. Res. Atmos., 118, doi:10.1002/jgrd.50825.

Zhao, Y., Nguyen, N.T., Presto, A.A., Hennigan C.J., May A.A., Robinson, A.L., 2015, Intermediate volatility organic compound emissions from on-road diesel vehicles: chemical composition, emission factors, and estimated secondary organic aerosol production, Environmental Science Technology, 49, 11516-11526.

Zhang, X., Schwantes, R.H., McVay, R.C., Lignell, H., Coggon, M.M., Flagan, R.C., Seinfeld, J.H., 2015, Vapor wall deposition in Teflon chambers, Atmospheric Chemistry Physics, 15, 4197-4214.

Zhang, X., Cappa, C.D., Jathar, S.H., McVay, R.C., Ensberg, J.J., Kleeman, M.J., and Seinfeld, J.H., 2014, Influence of vapor wall loss in laboratory chambers on yields of secondary organic aerosol, Proceedings of the National Academy of Sciences of the United States of America, 111, 5802-5807, doi:10.1073/pnas.1404727111.

U.S. EPA, 2014, Draft Modeling Guidance for Demonstrating Attainment of Air Quality Goals for Ozone, PM2.5 and Regional Haze, available at http://www.epa.gov/scram001/guidance/guide/Draft_O3-PM-RH_Modeling_Guidance-2014.pdf

SUPPLEMENTAL MATERIALS

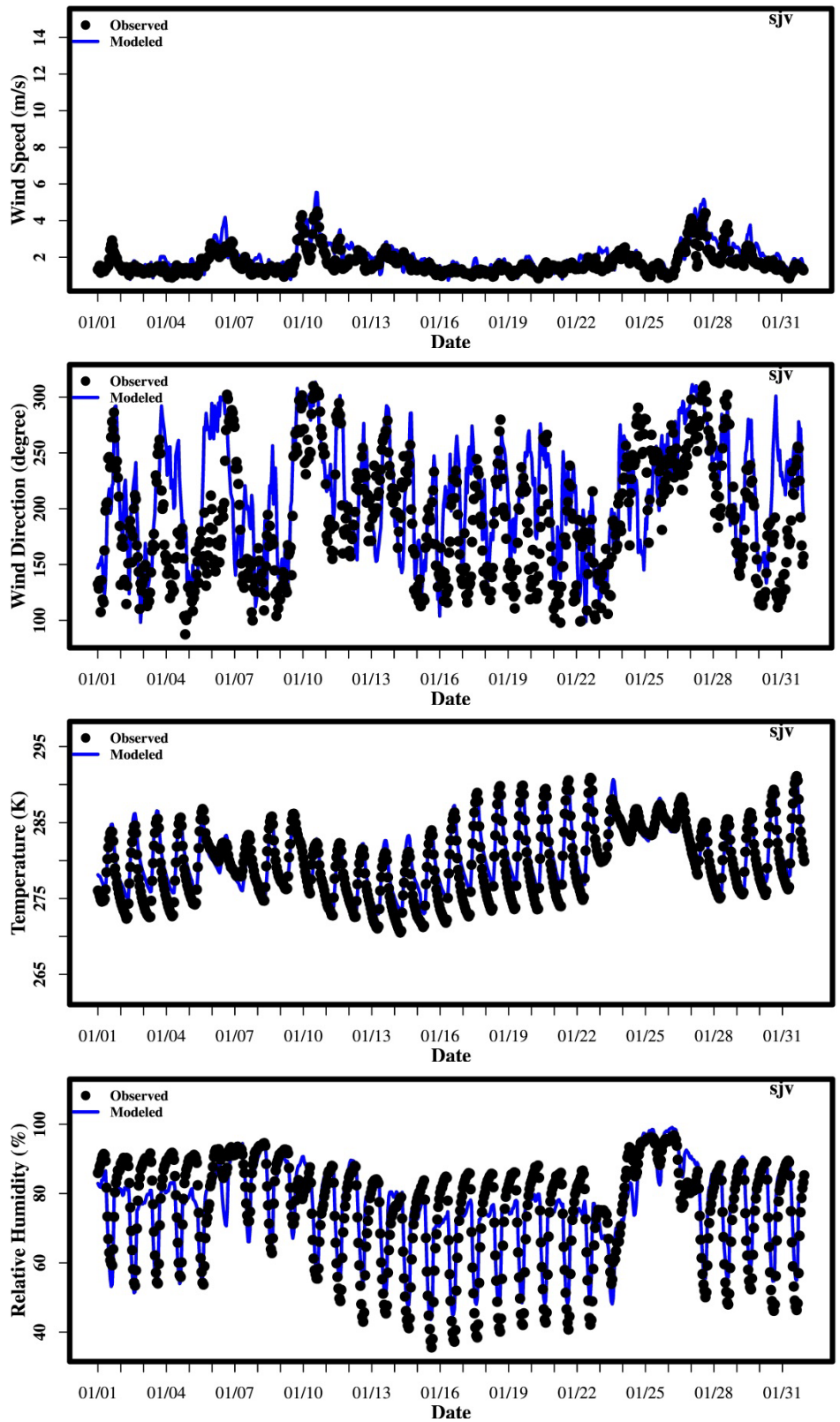

Figure S. 1 Time series of wind speed, direction, temperature and relative humidity for San Joaquin Valley in January 2013.

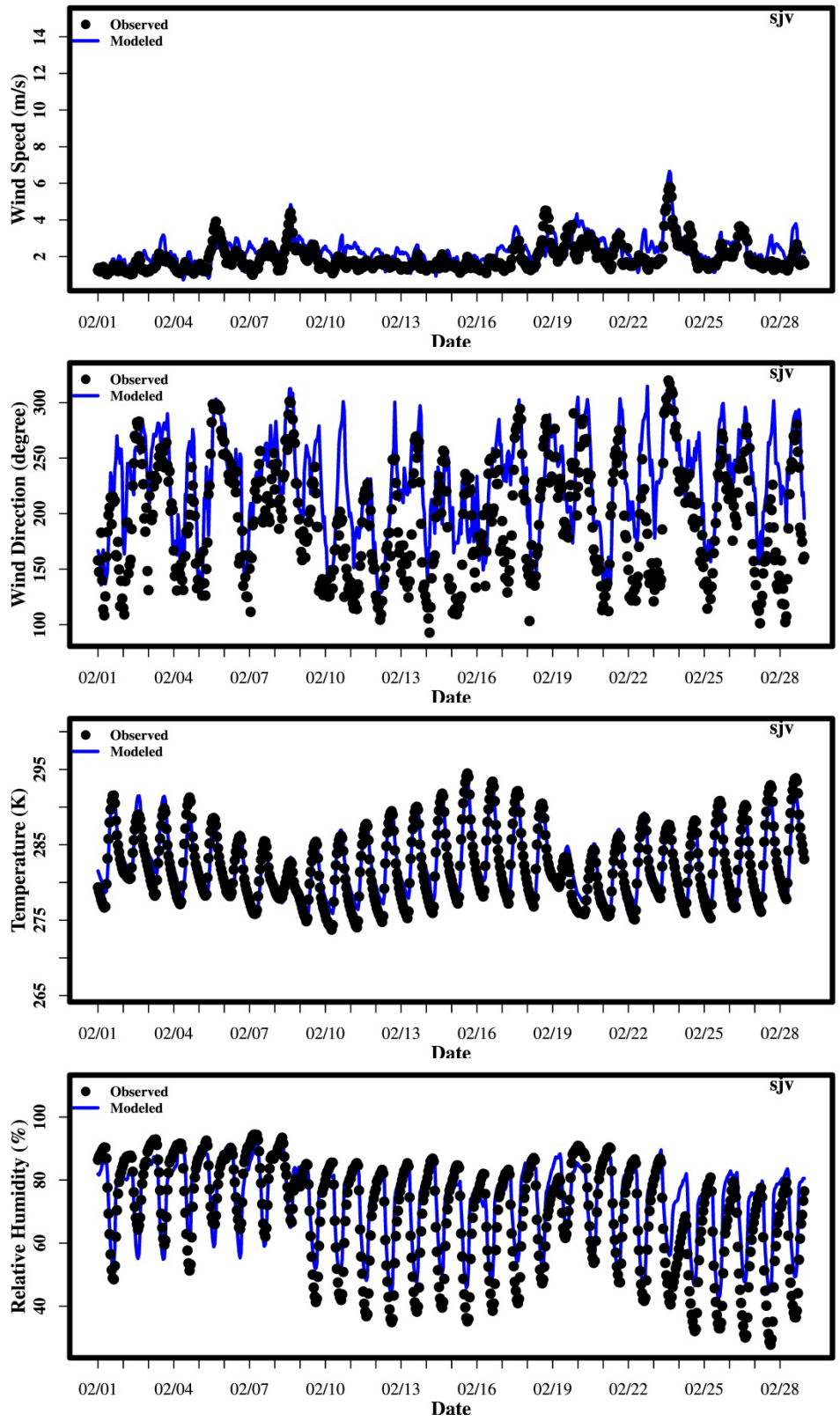

Figure S. 2 Time series of wind speed, direction, temperature and relative humidity for San Joaquin Valley in February 2013.

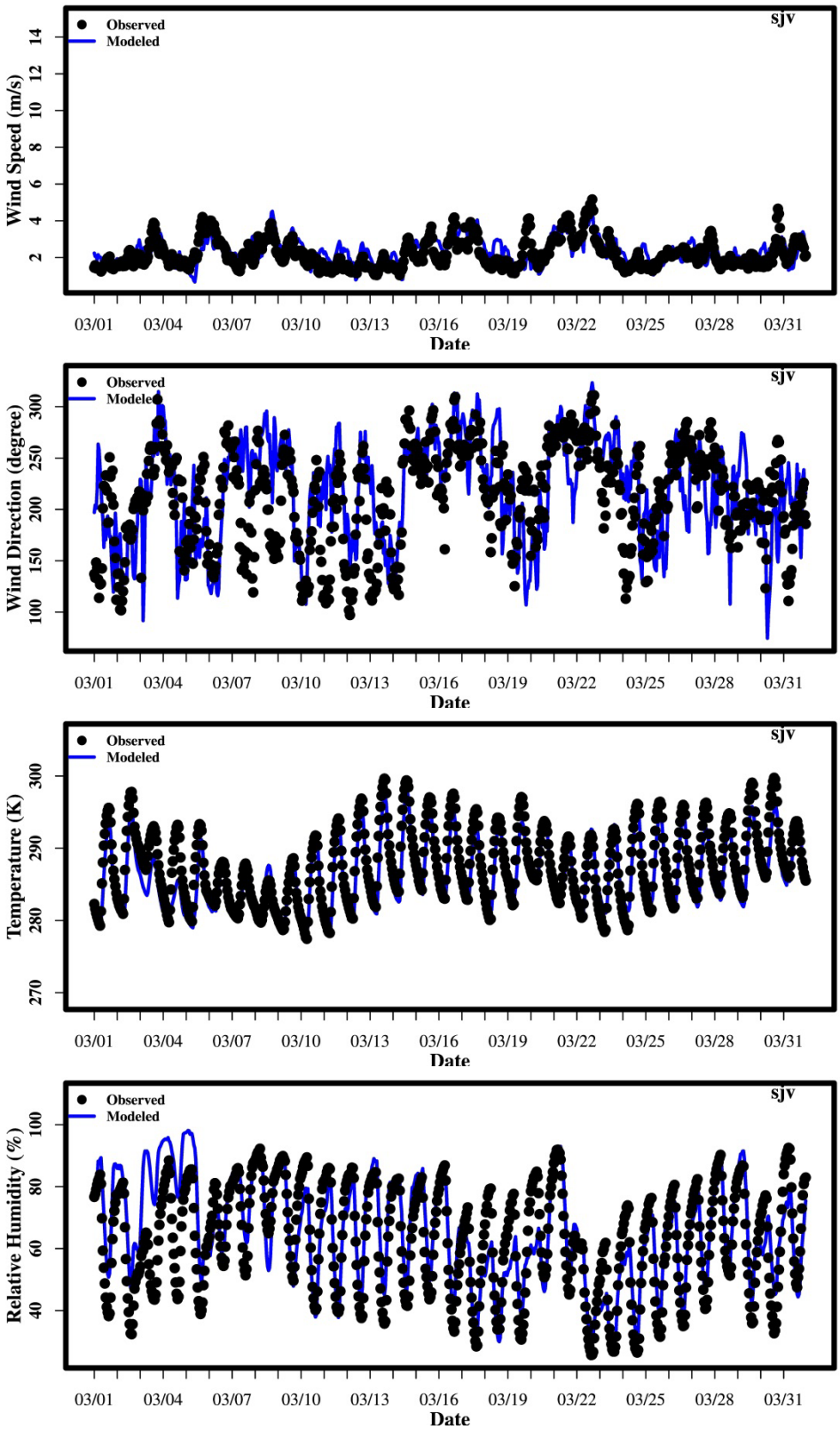

Figure S. 3 Time series of wind speed, direction, temperature and relative humidity for San Joaquin Valley in March 2013.

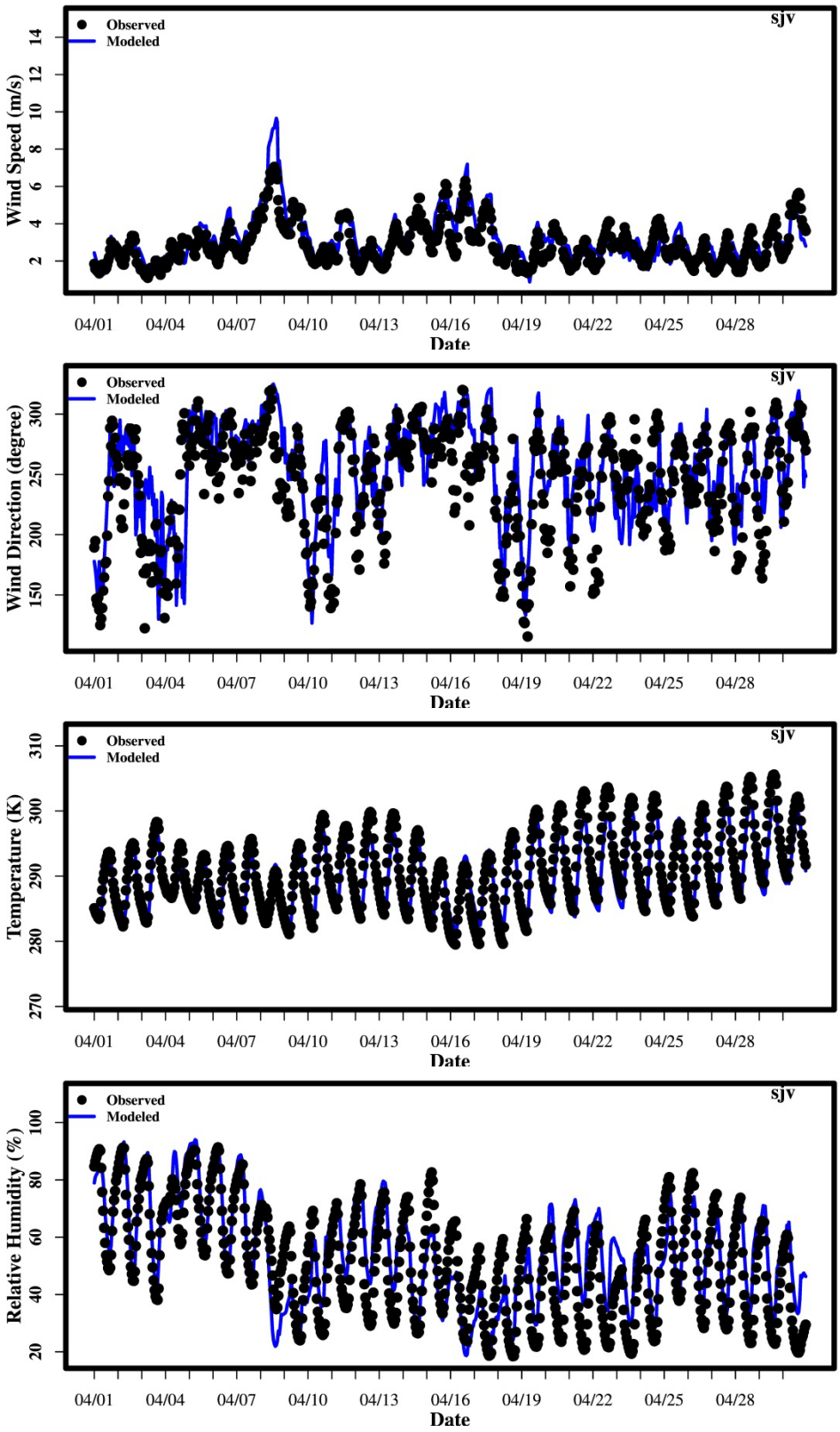

Figure S. 4 Time series of wind speed, direction, temperature and relative humidity for San Joaquin Valley in April 2013.

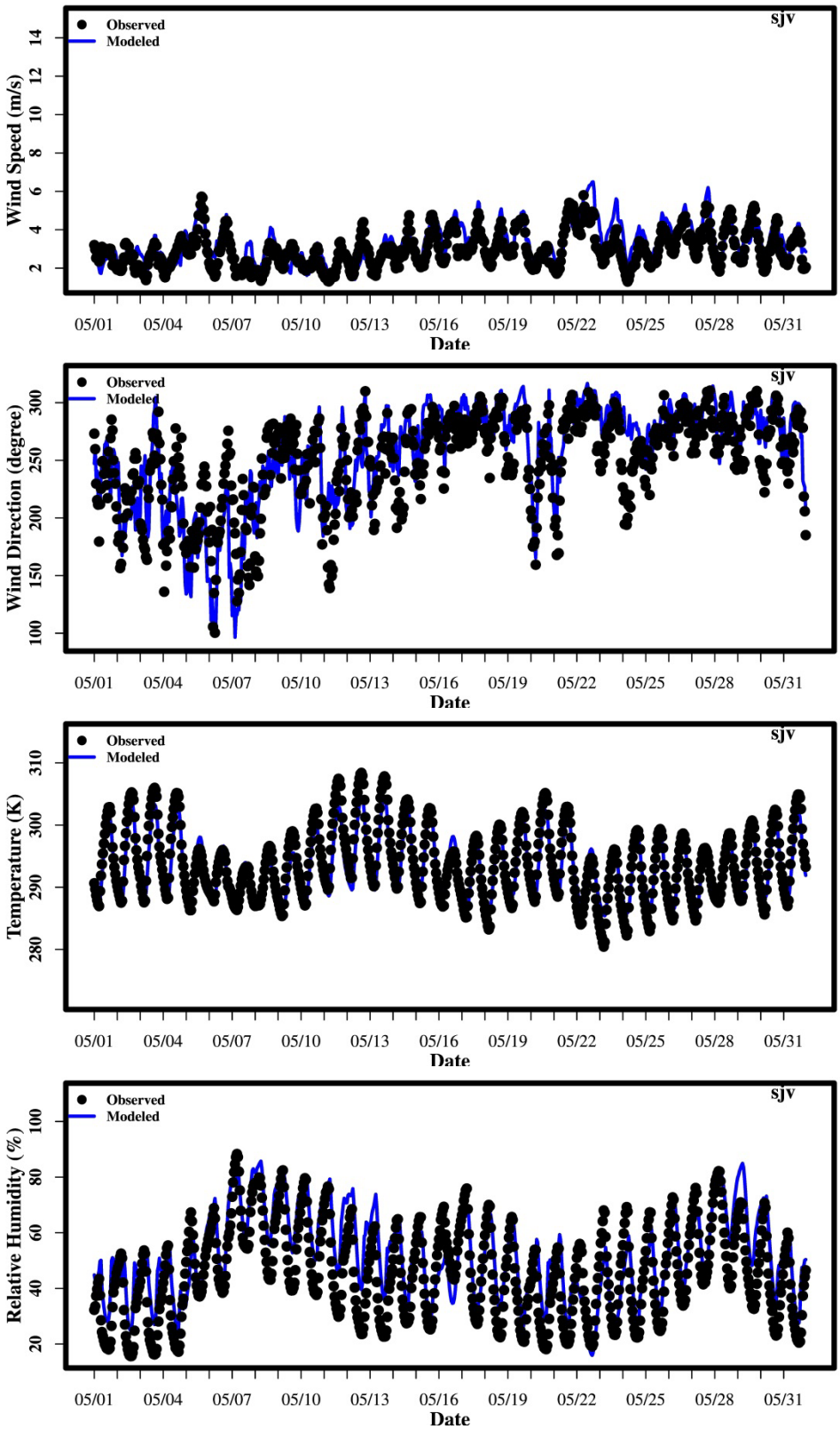

Figure S. 5 Time series of wind speed, direction, temperature and relative humidity for San Joaquin Valley in May 2013.

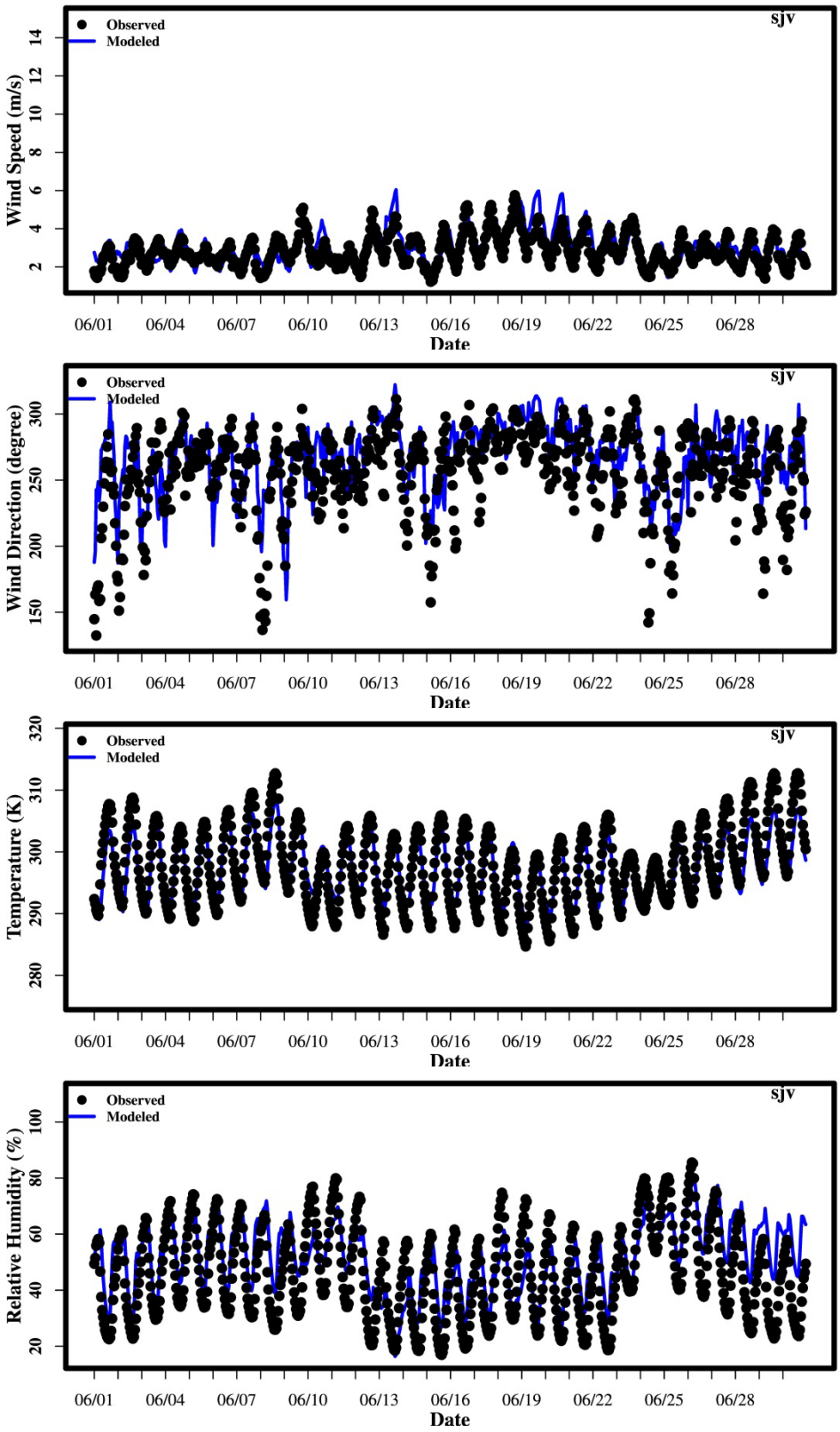

Figure S. 6 Time series of wind speed, direction, temperature and relative humidity for San Joaquin Valley in June 2013.

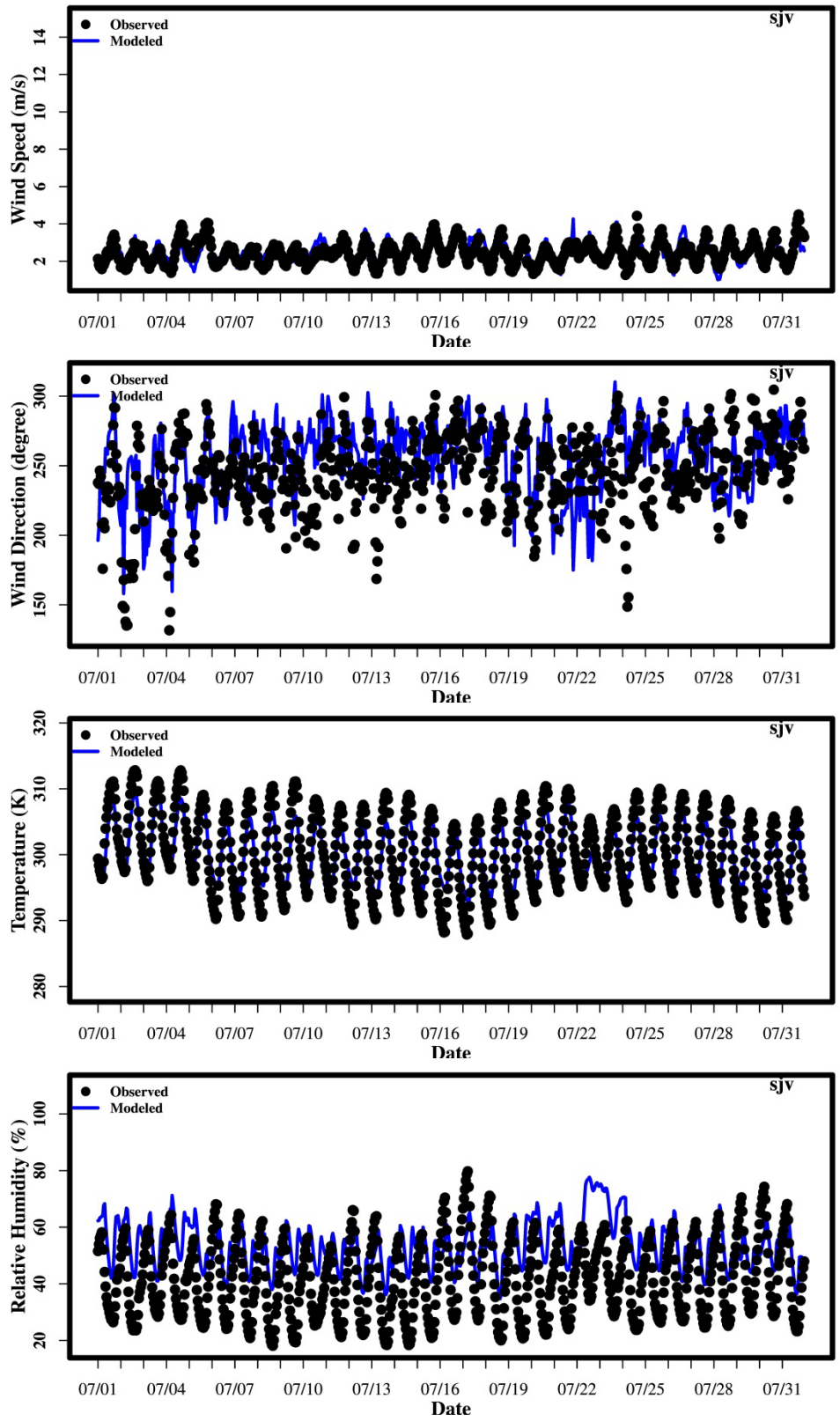

Figure S. 7 Time series of wind speed, direction, temperature and relative humidity for San Joaquin Valley in July 2013.

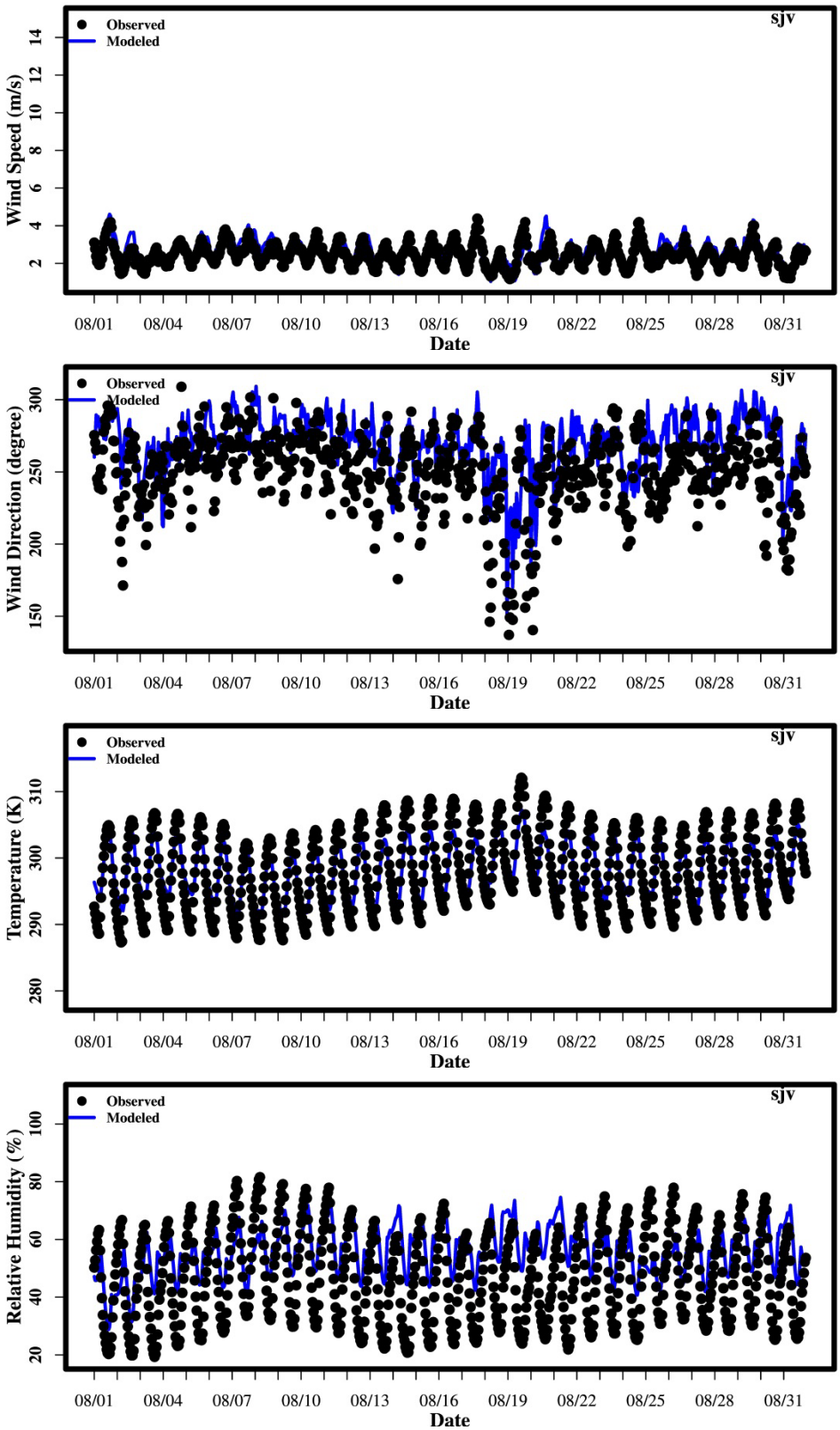

Figure S. 8 Time series of wind speed, direction, temperature and relative humidity for San Joaquin Valley in August 2013.

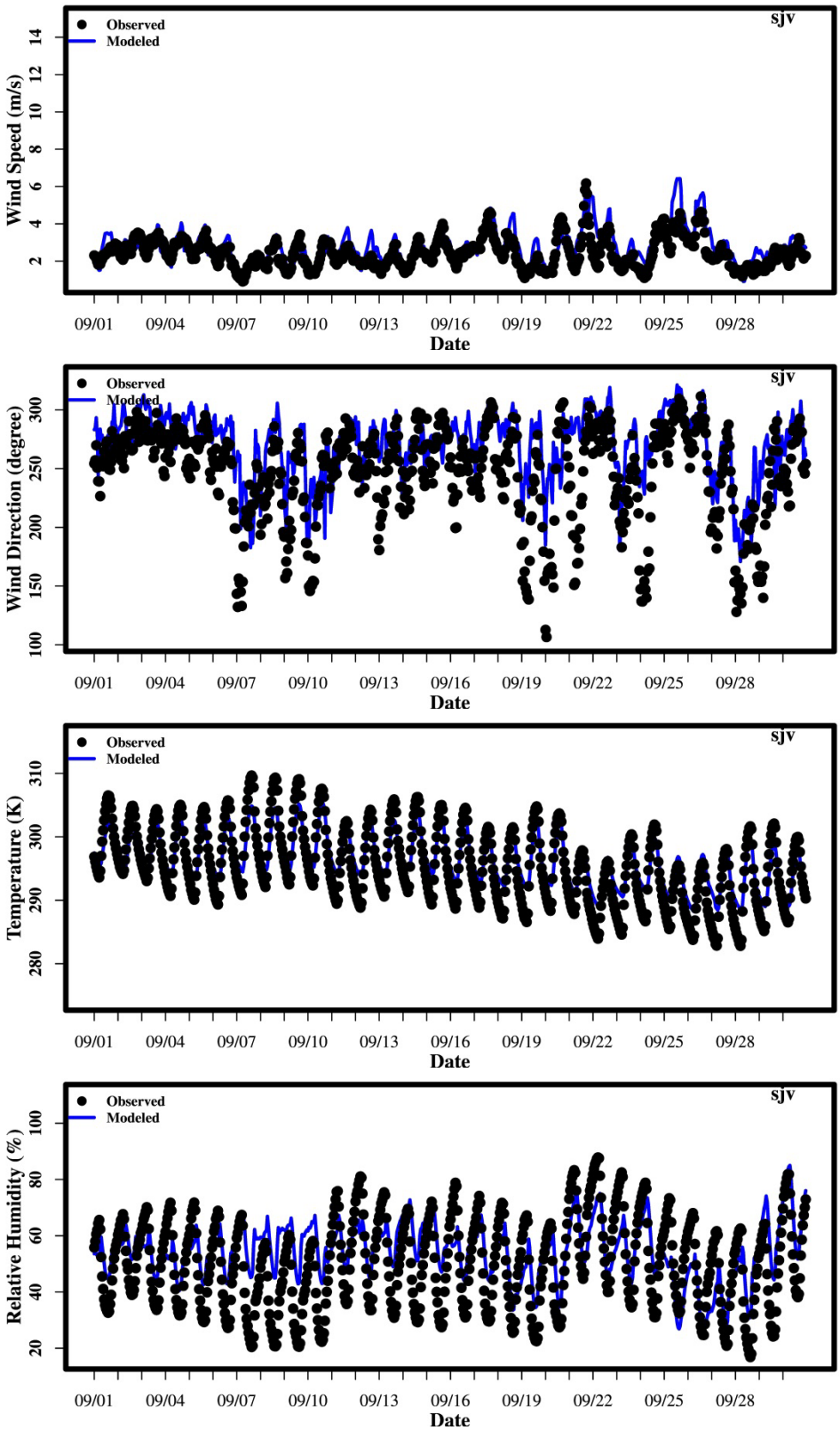

Figure S. 9 Time series of wind speed, direction, temperature and relative humidity for San Joaquin Valley in September 2013.

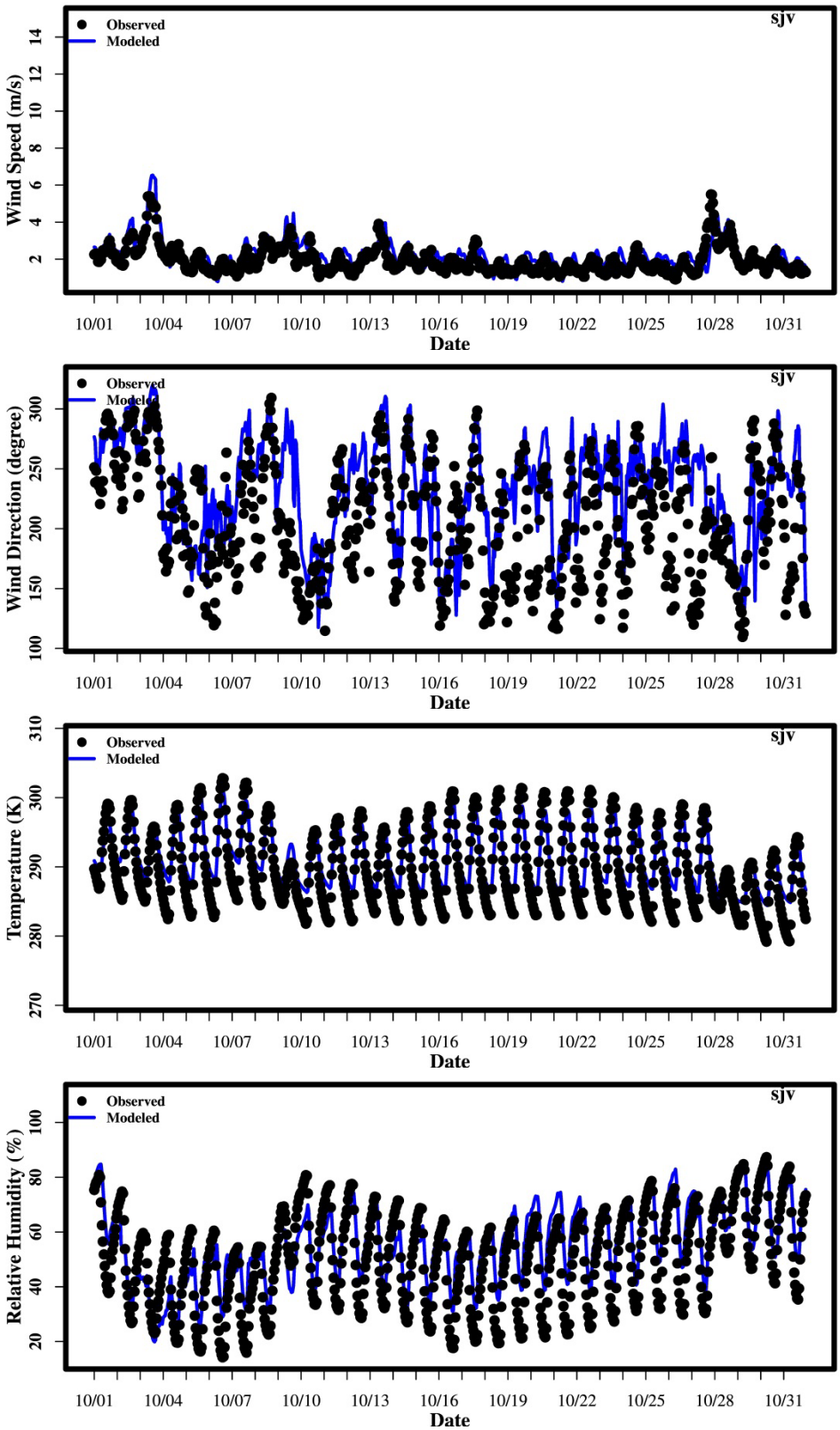

Figure S. 10 Time series of wind speed, direction, temperature and relative humidity for San Joaquin Valley in October 2013.

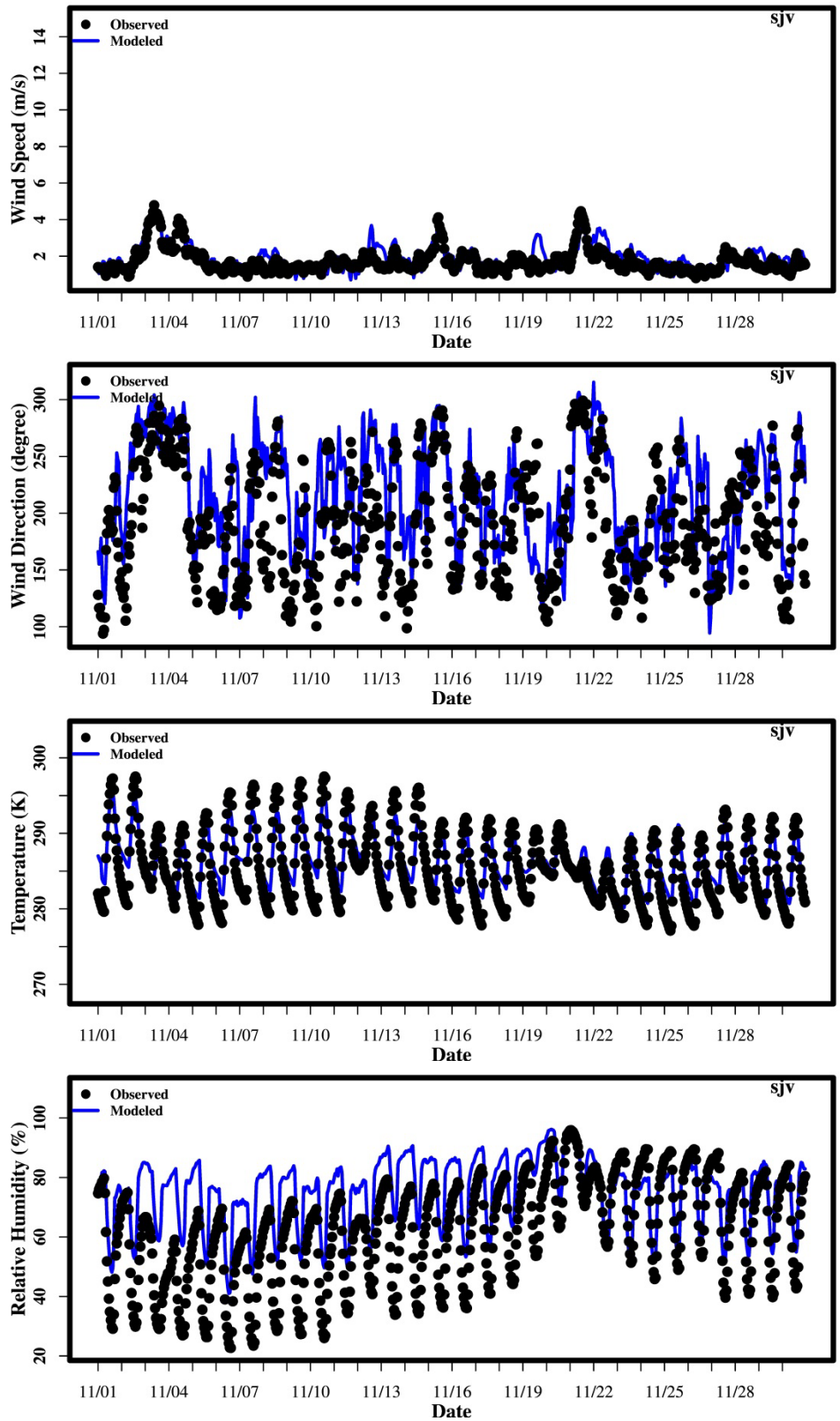

Figure S. 11 Time series of wind speed, direction, temperature and relative humidity for San Joaquin Valley in November 2013.

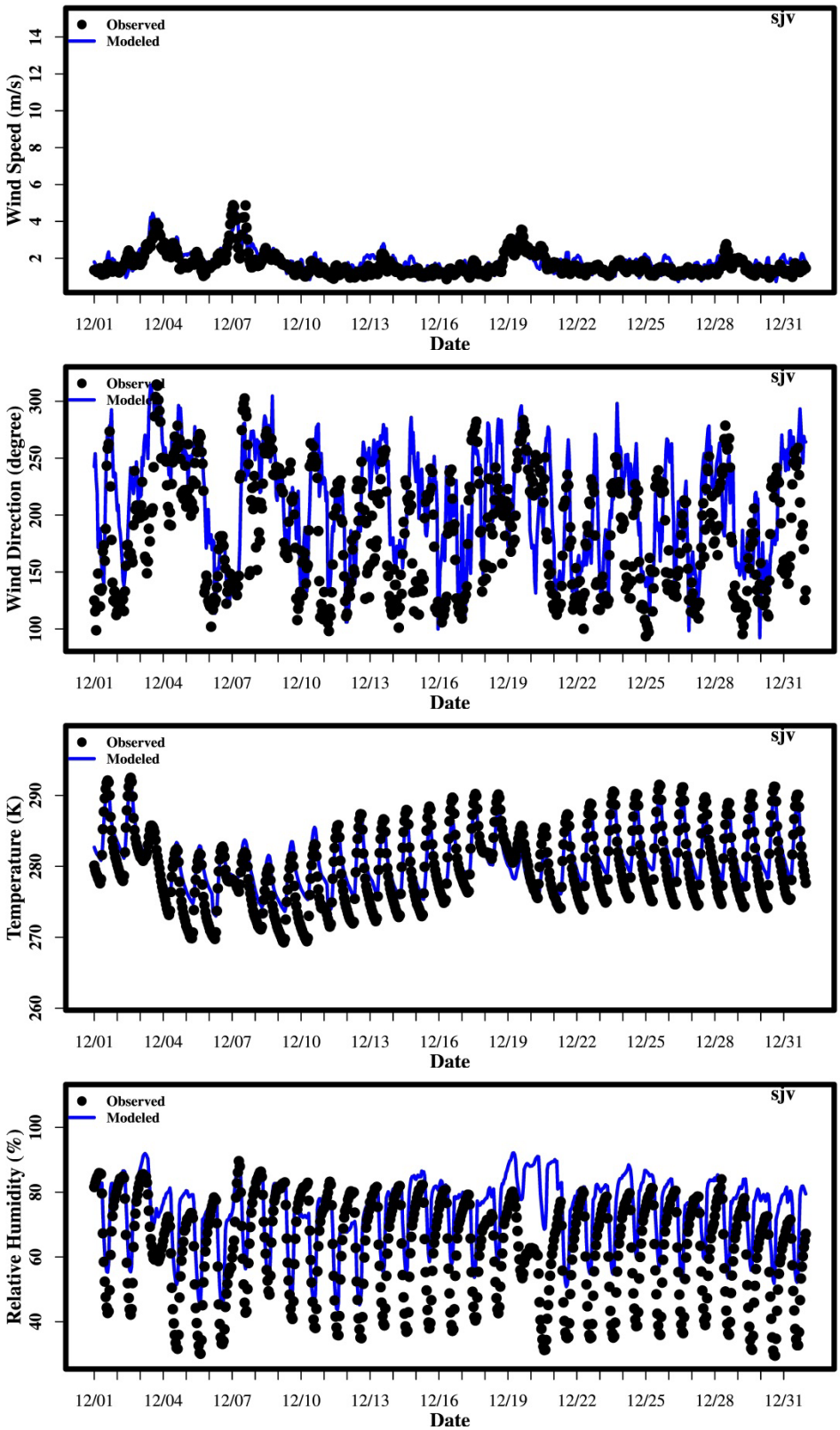

Figure S. 12 Time series of wind speed, direction, temperature and relative humidity for San Joaquin Valley in December 2013.

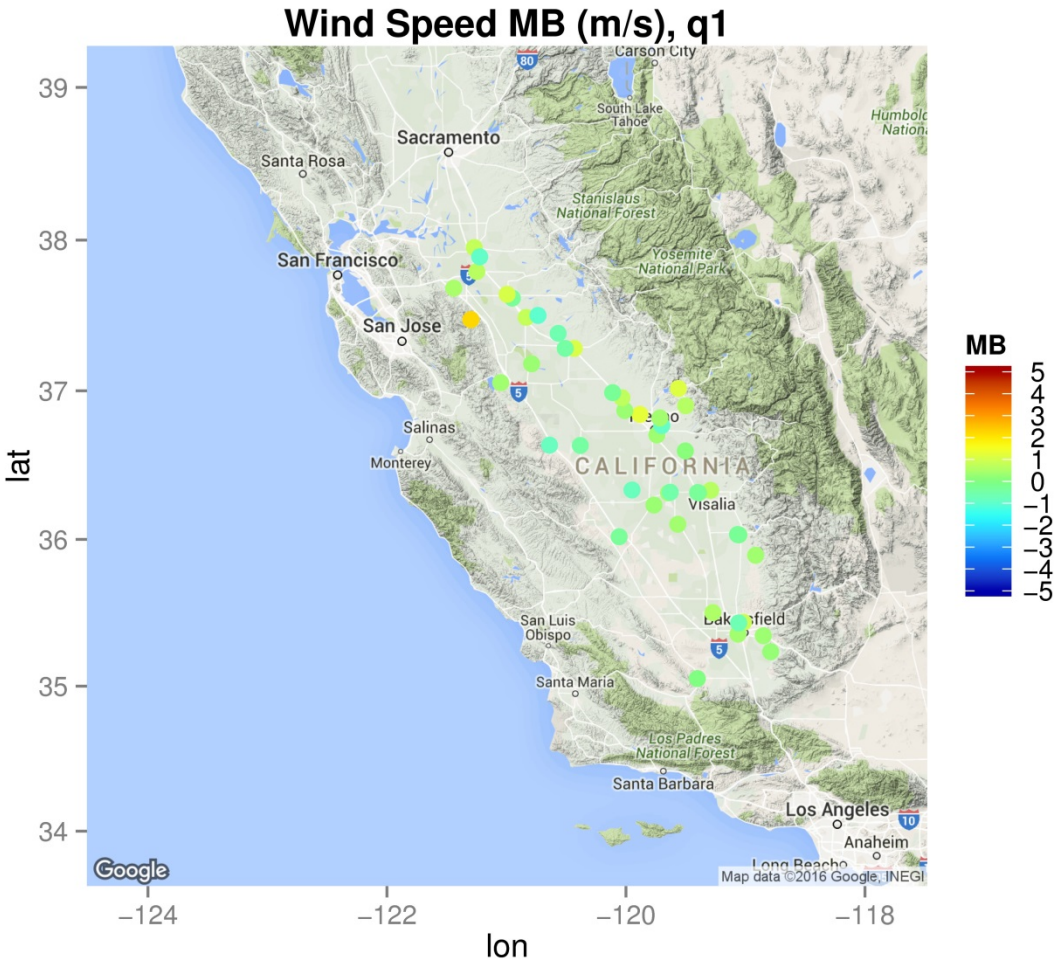

Figure S. 13 Hourly wind speed mean error in the first quarter of 2013

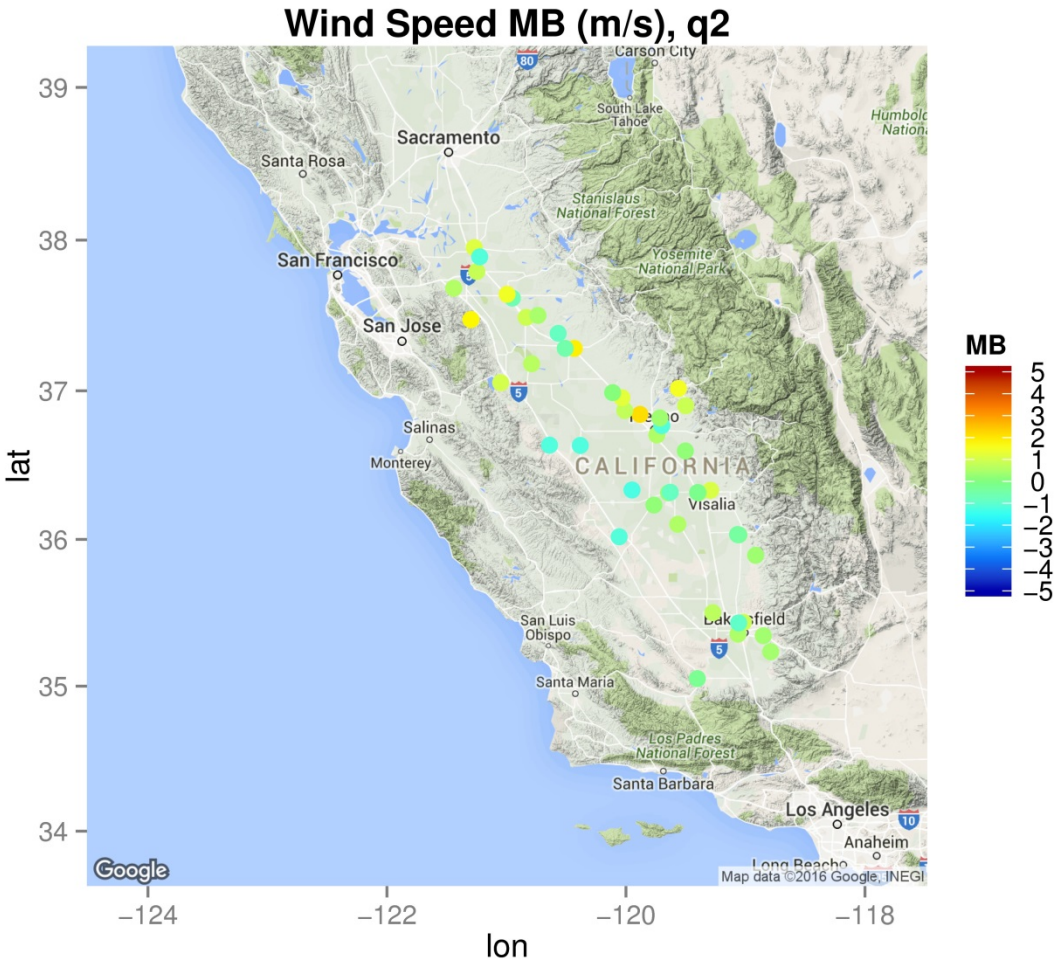

Figure S. 14 Hourly wind speed mean bias in the second quarter of 2013

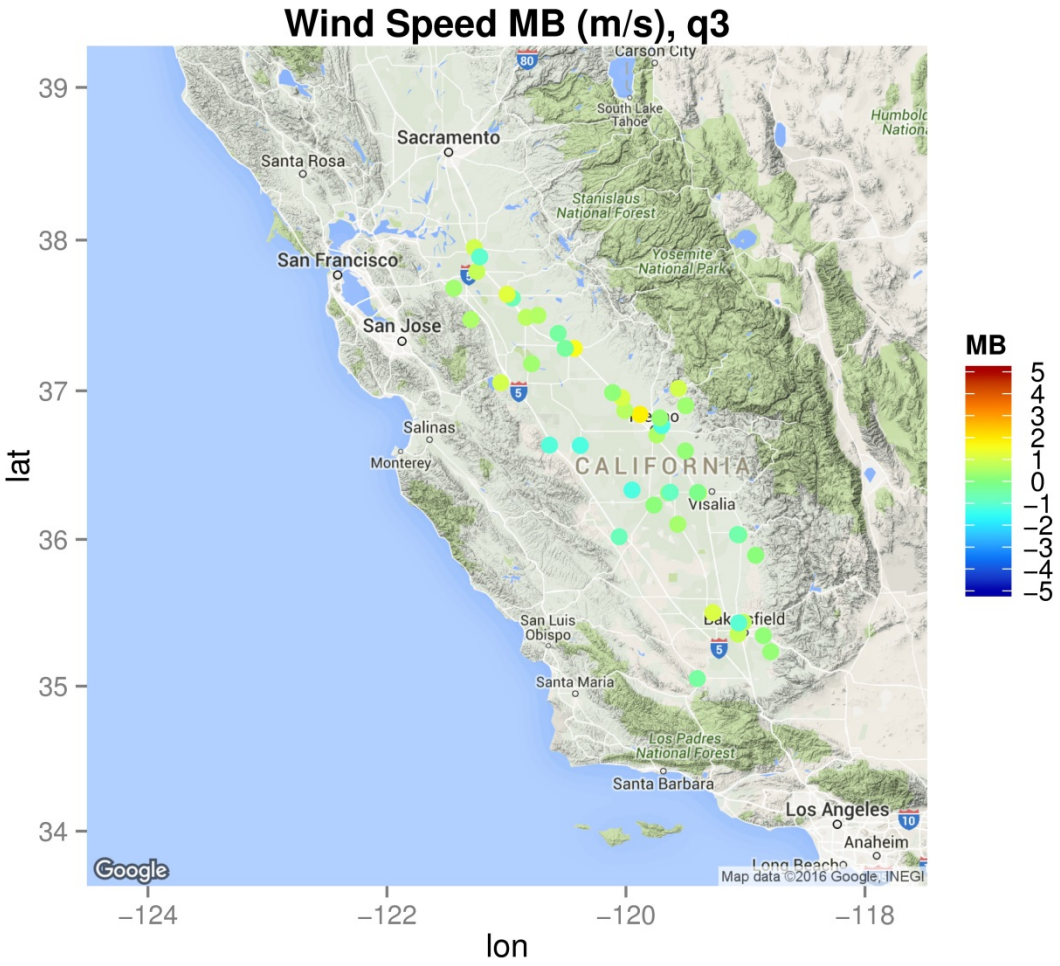

Figure S. 15 Hourly wind speed mean bias in the third quarter of 2013

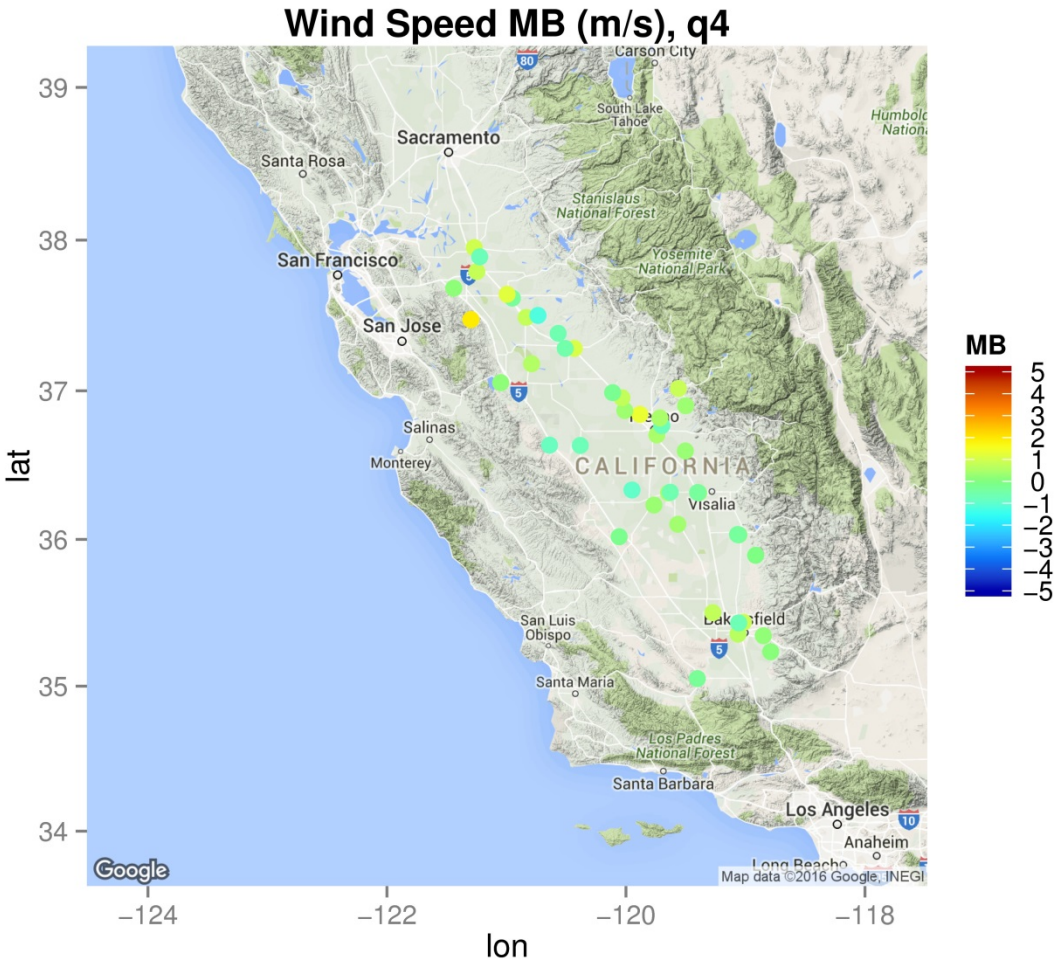

Figure S. 16 Hourly wind speed mean bias in the fourth quarter of 2013

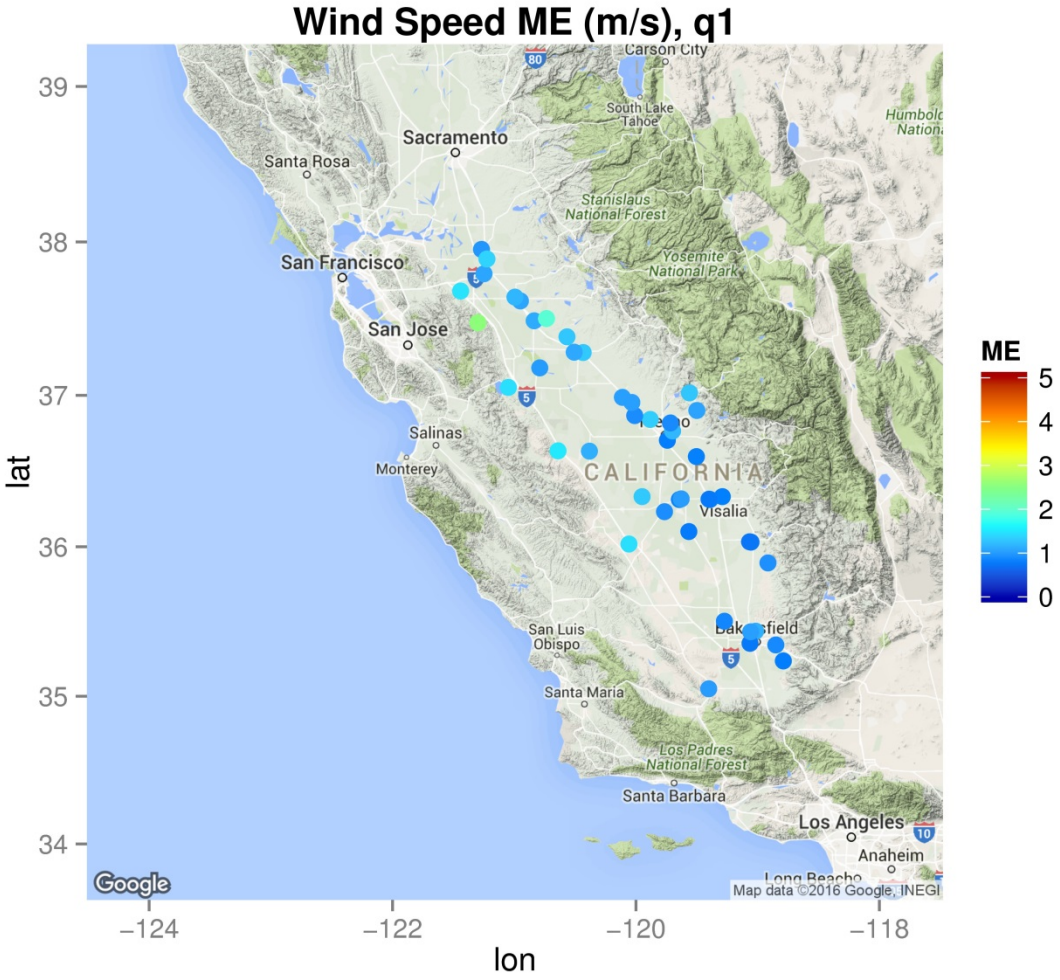

Figure S. 17 Hourly wind speed mean error in the first quarter of 2013

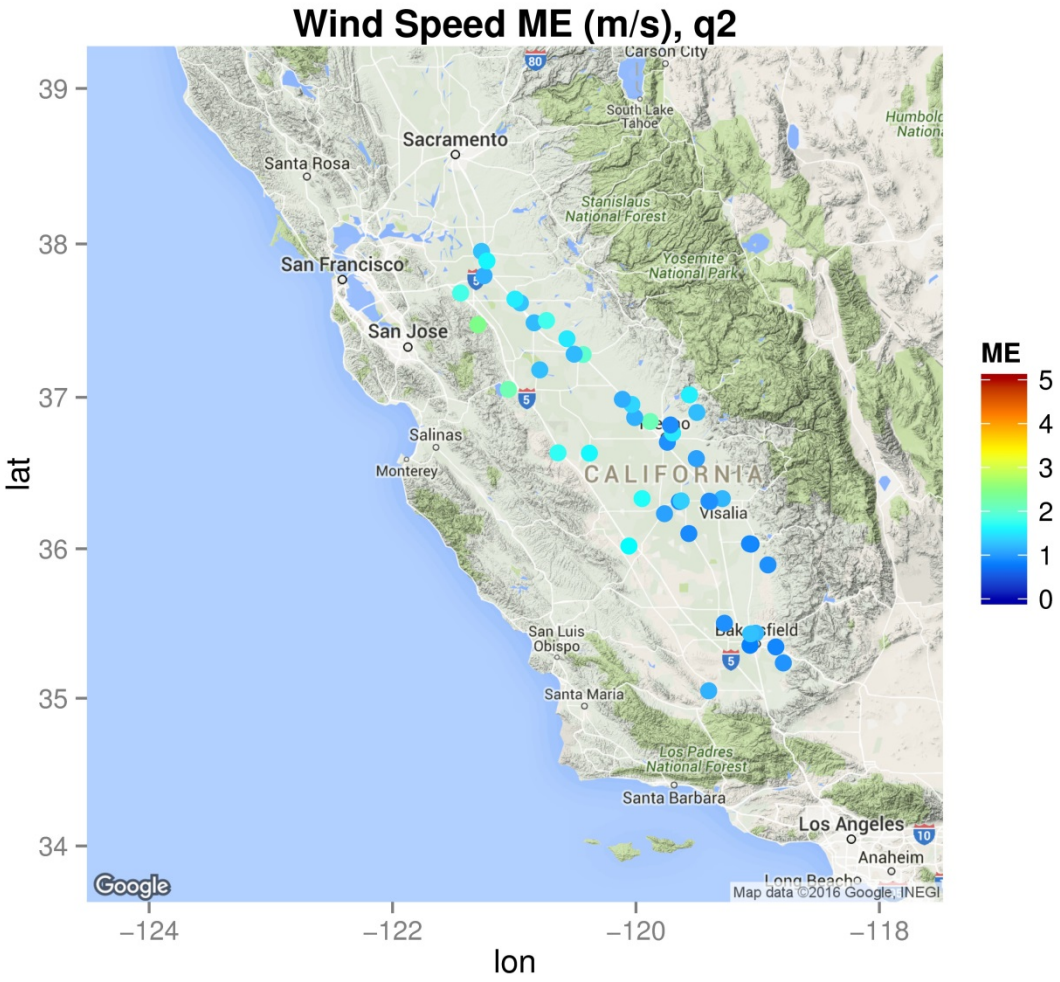

Figure S. 18 Hourly wind speed mean error in the second quarter of 2013

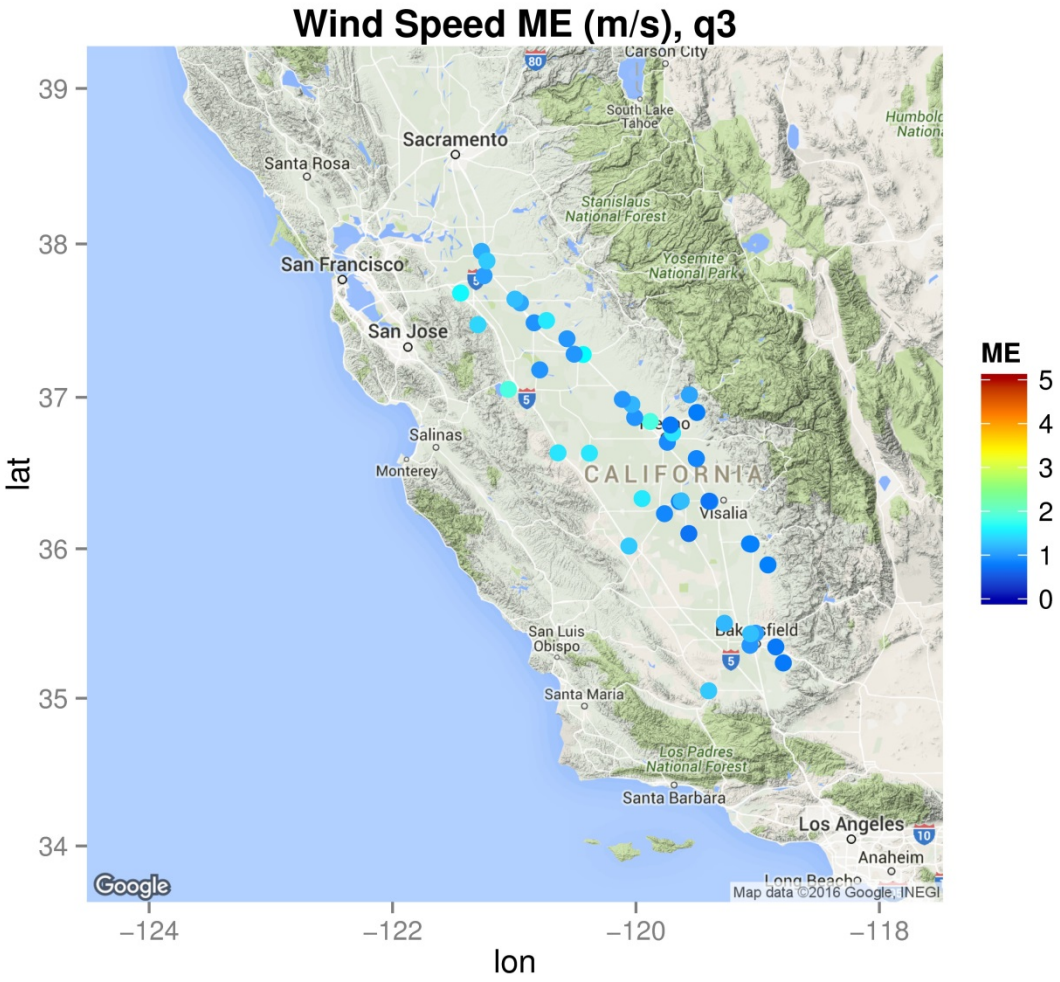

Figure S. 19 Hourly wind speed mean error in the third quarter of 2013

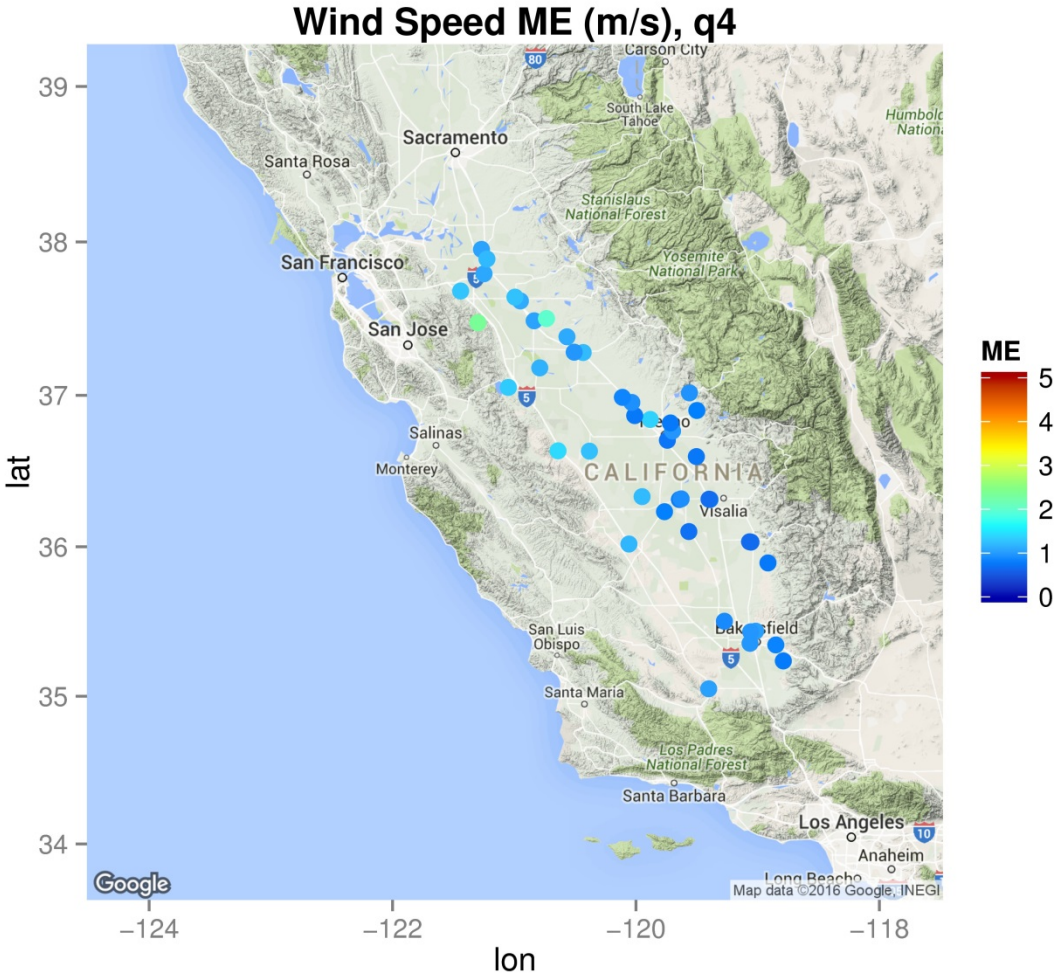

Figure S. 20 Hourly wind speed mean error in the fourth quarter of 2013

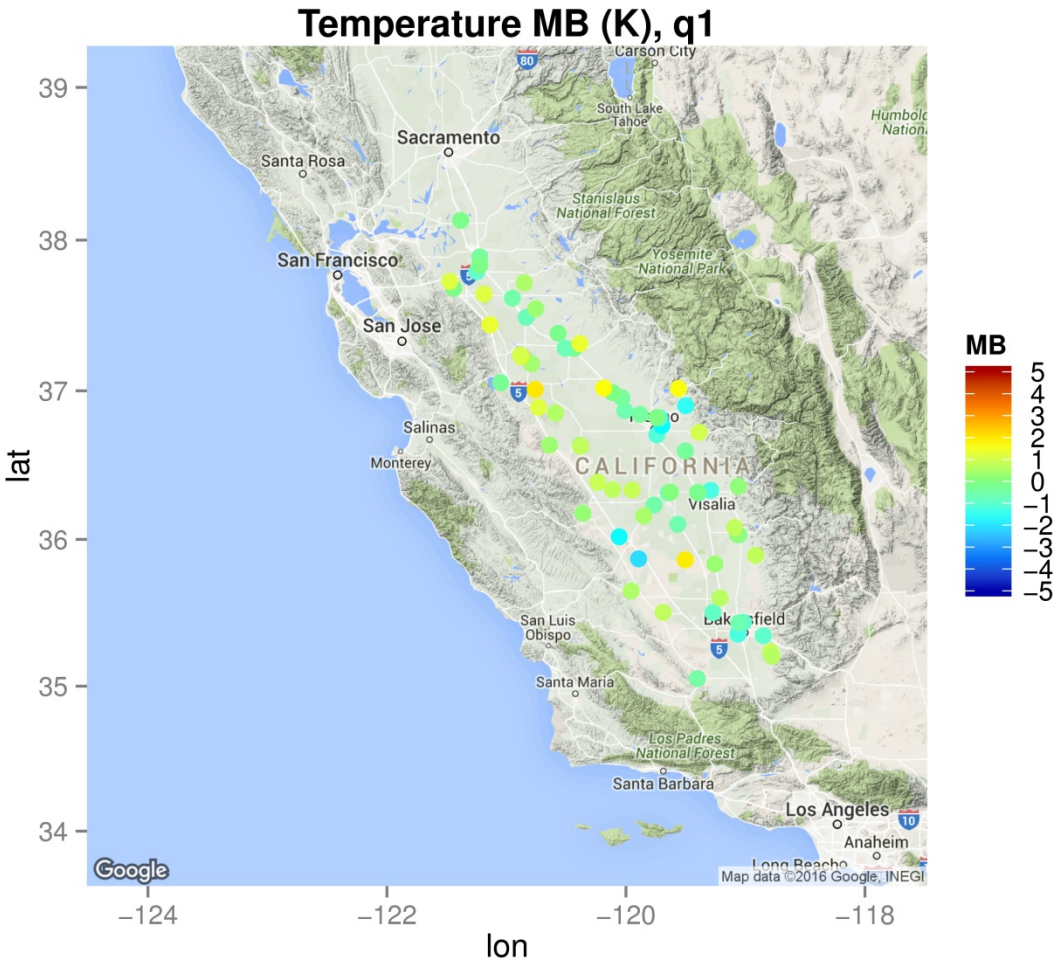

Figure S. 21 Hourly temperature mean bias in the first quarter of 2013

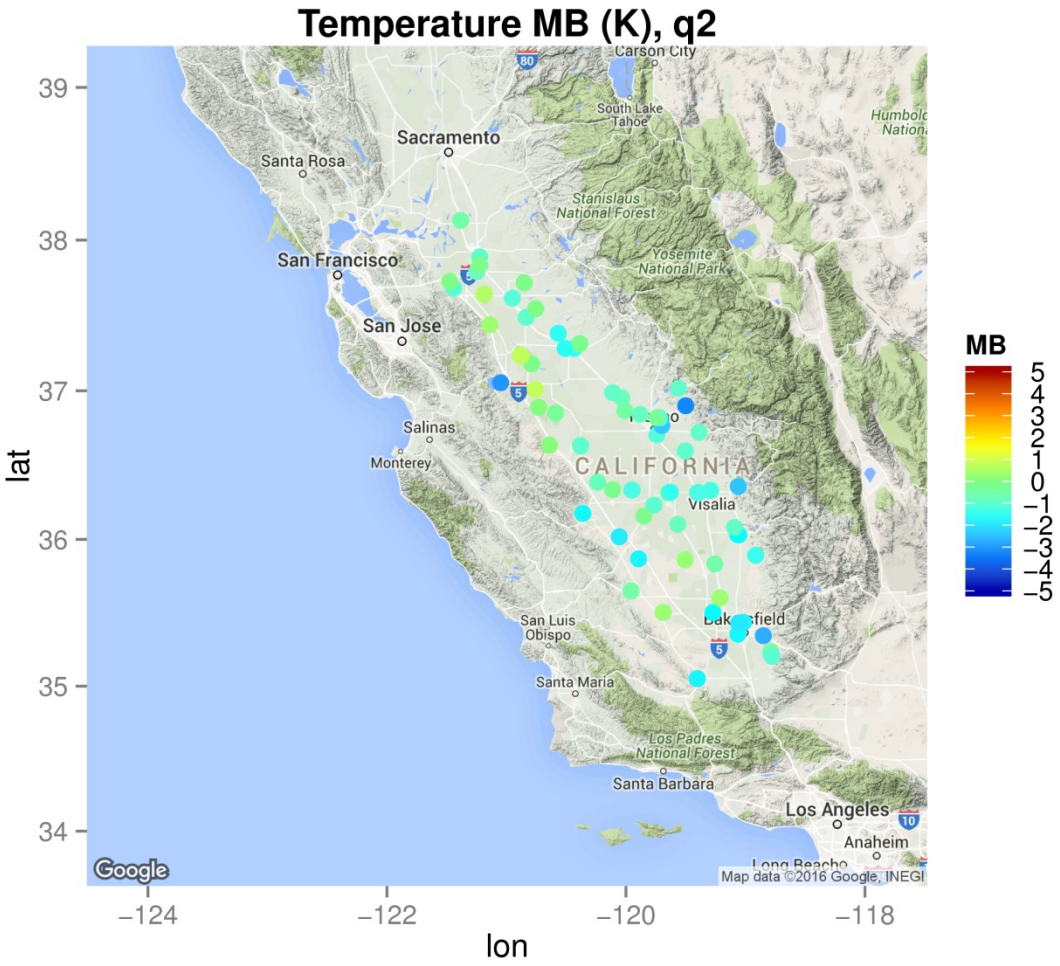

Figure S. 22 Hourly temperature mean bias in the second quarter of 2013

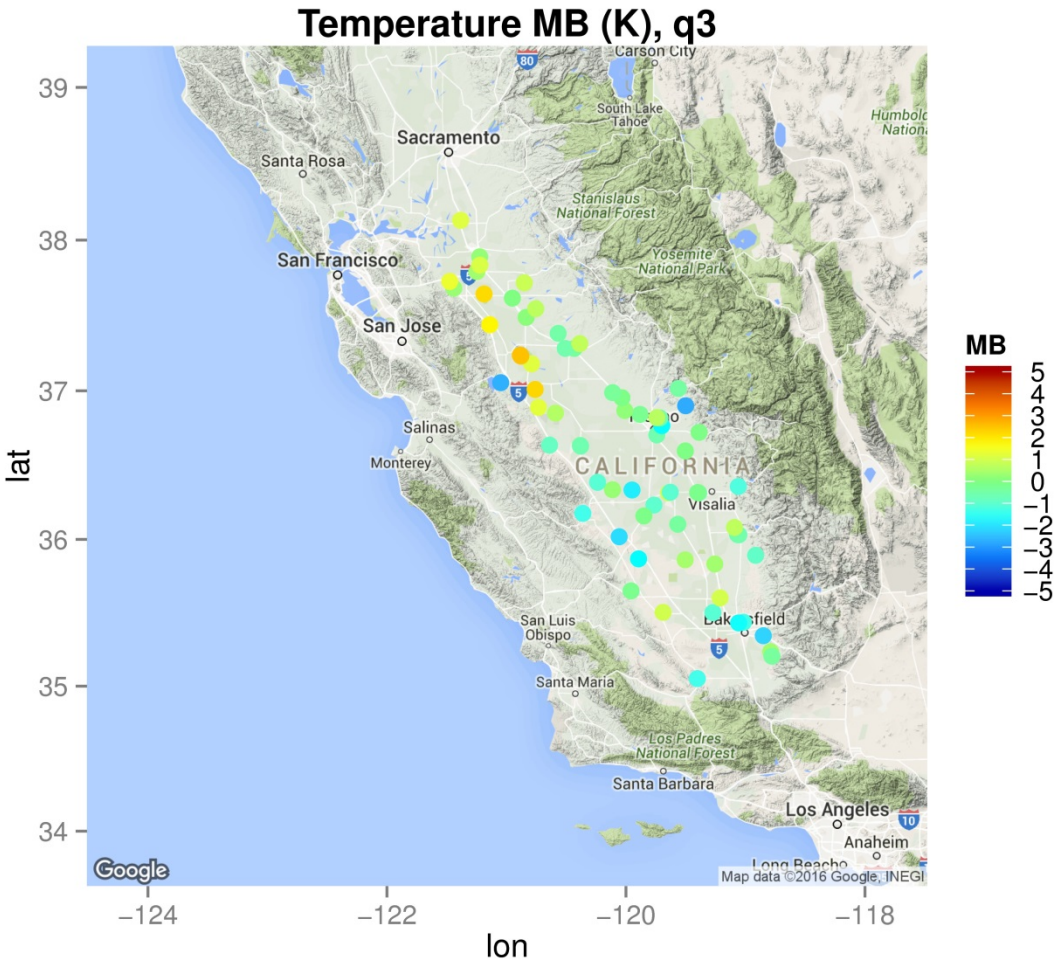

Figure S. 23 Hourly temperature mean bias in the third quarter of 2013

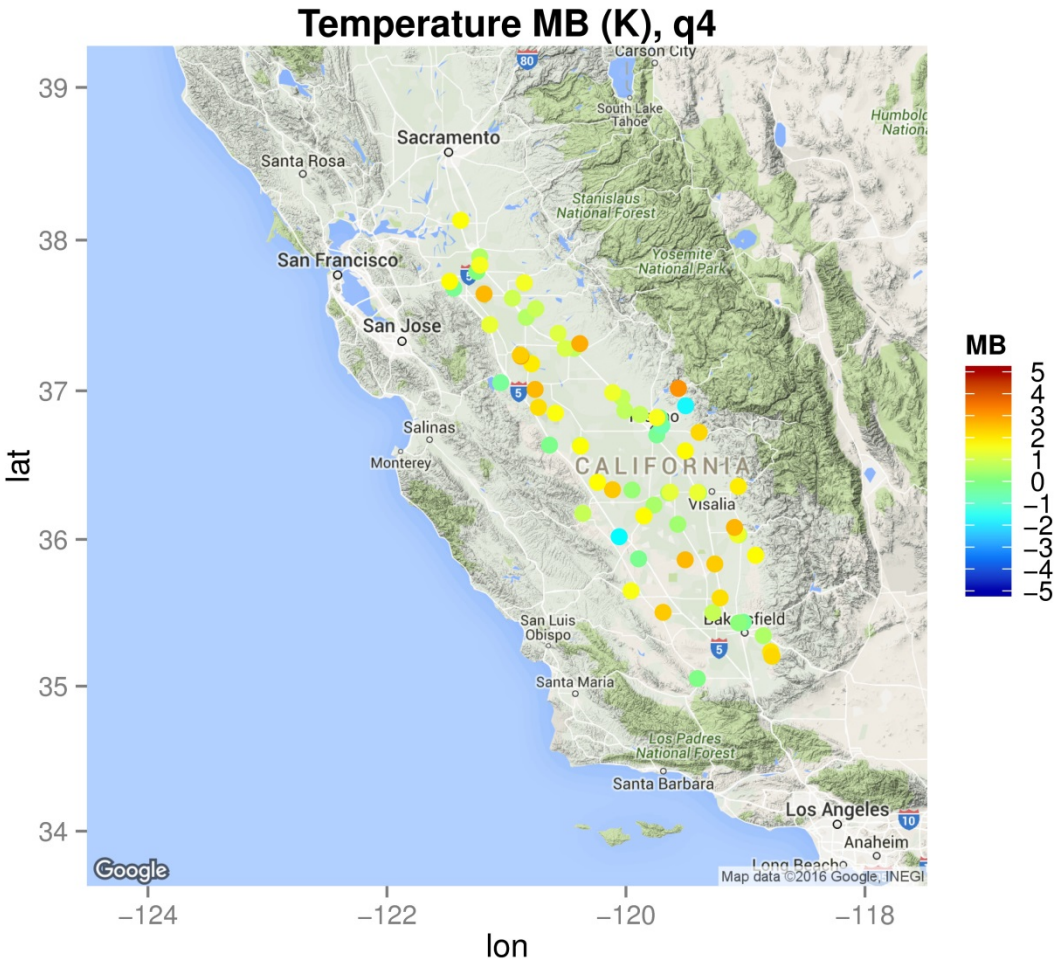

Figure S. 24 Hourly temperature mean bias in the fourth quarter of 2013

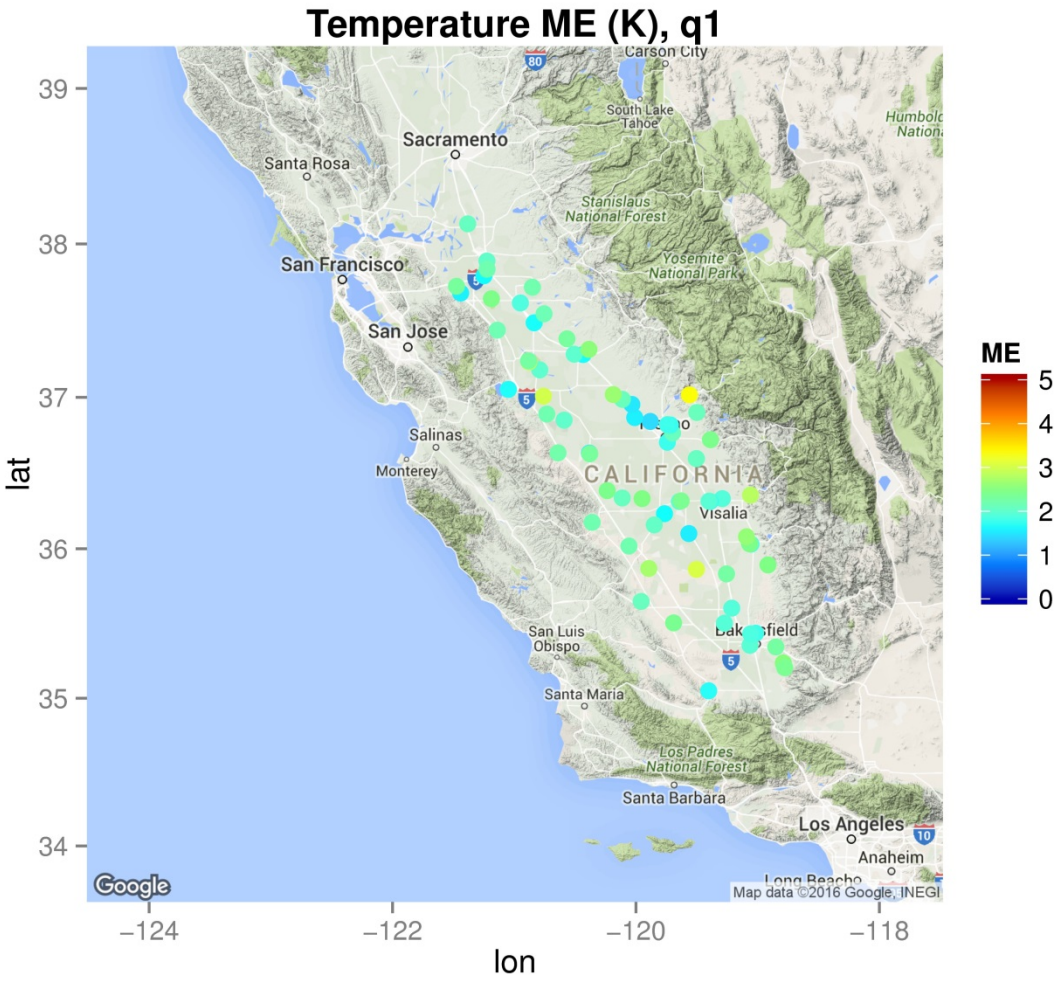

Figure S. 25 Hourly temperature mean error in the first quarter of 2013

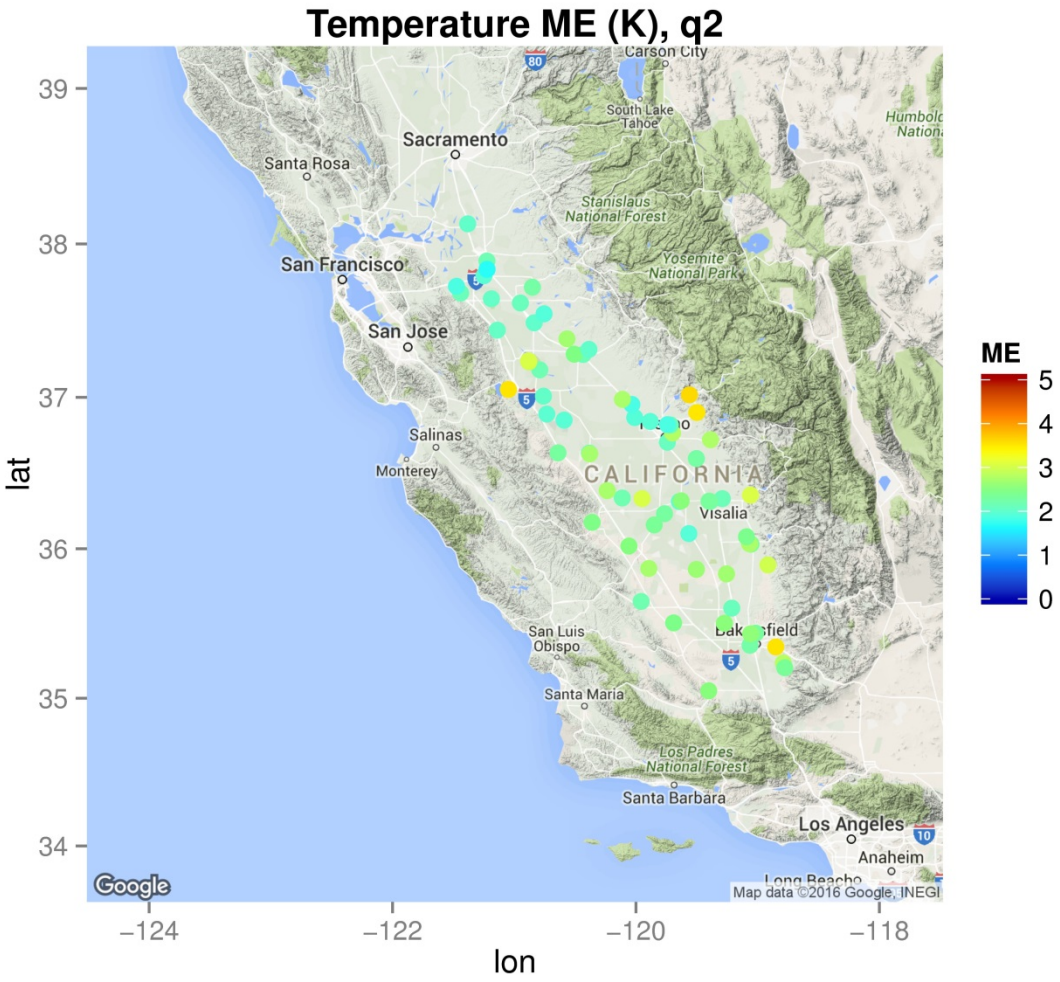

Figure S. 26 Hourly temperature mean error in the second quarter of 2013

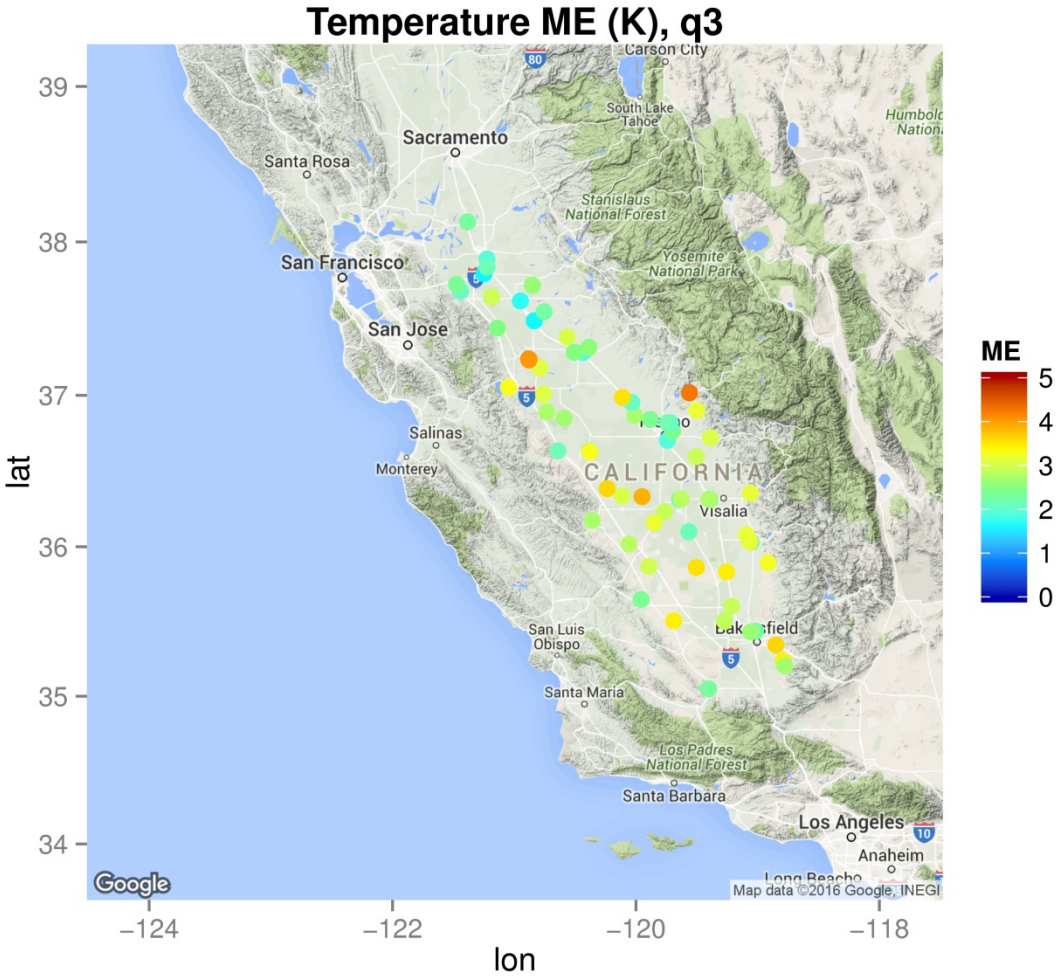

Figure S. 27 Hourly temperature mean error in the third quarter of 2013

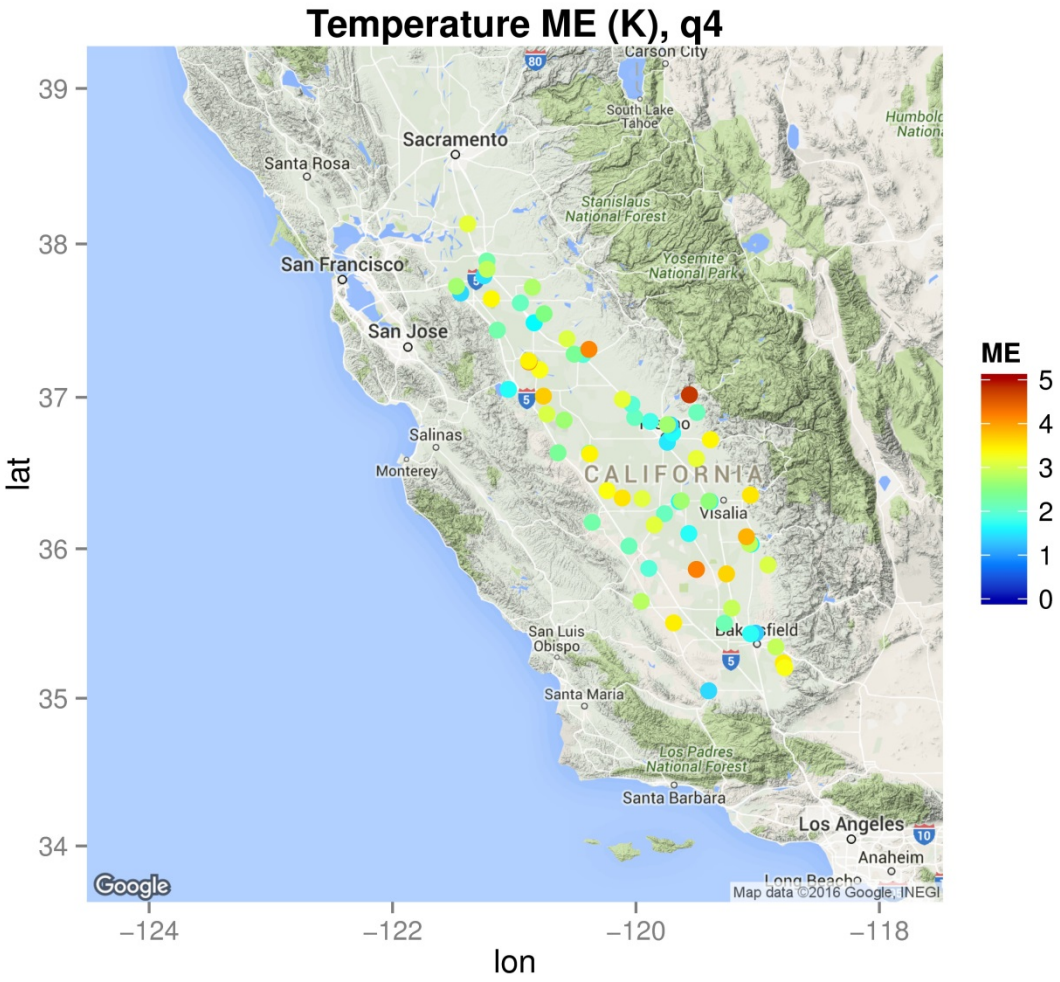

Figure S. 28 Hourly temperature mean error in the fourth quarter of 2013

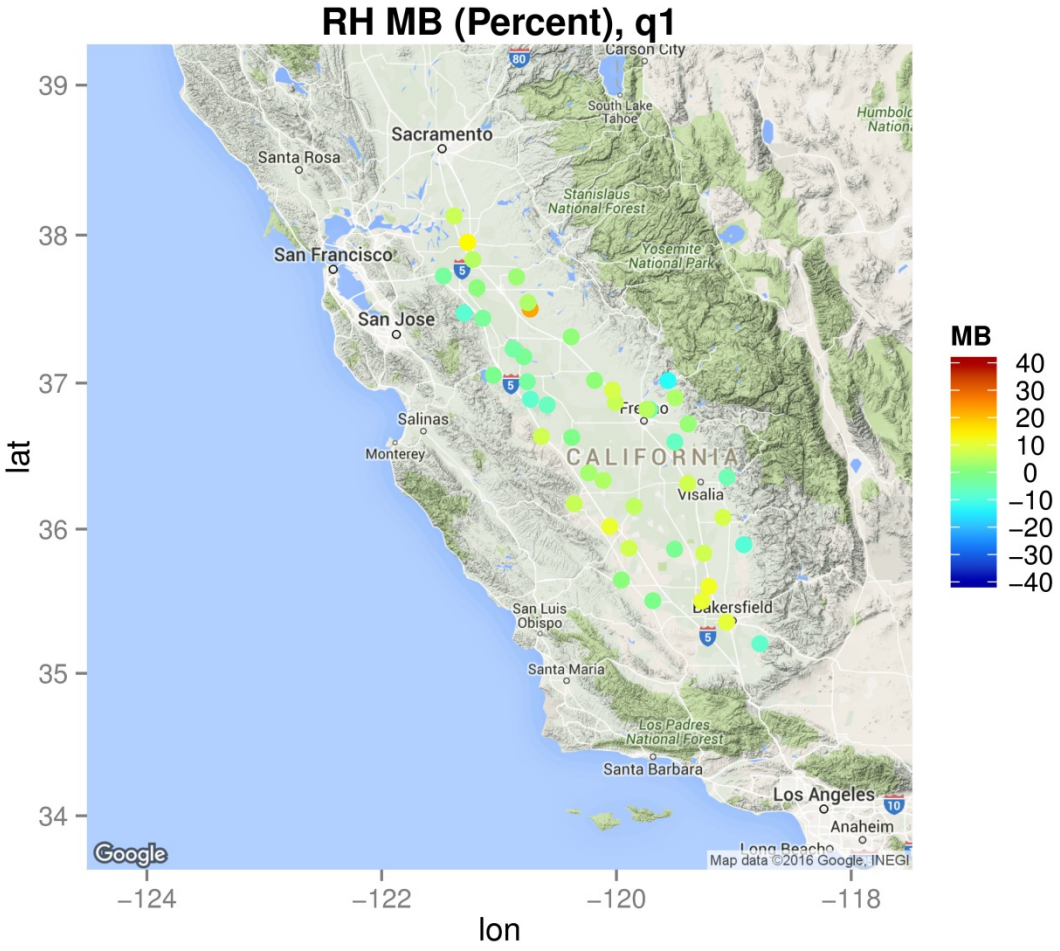

Figure S. 29 Hourly relative humidity mean bias in the first quarter of 2013

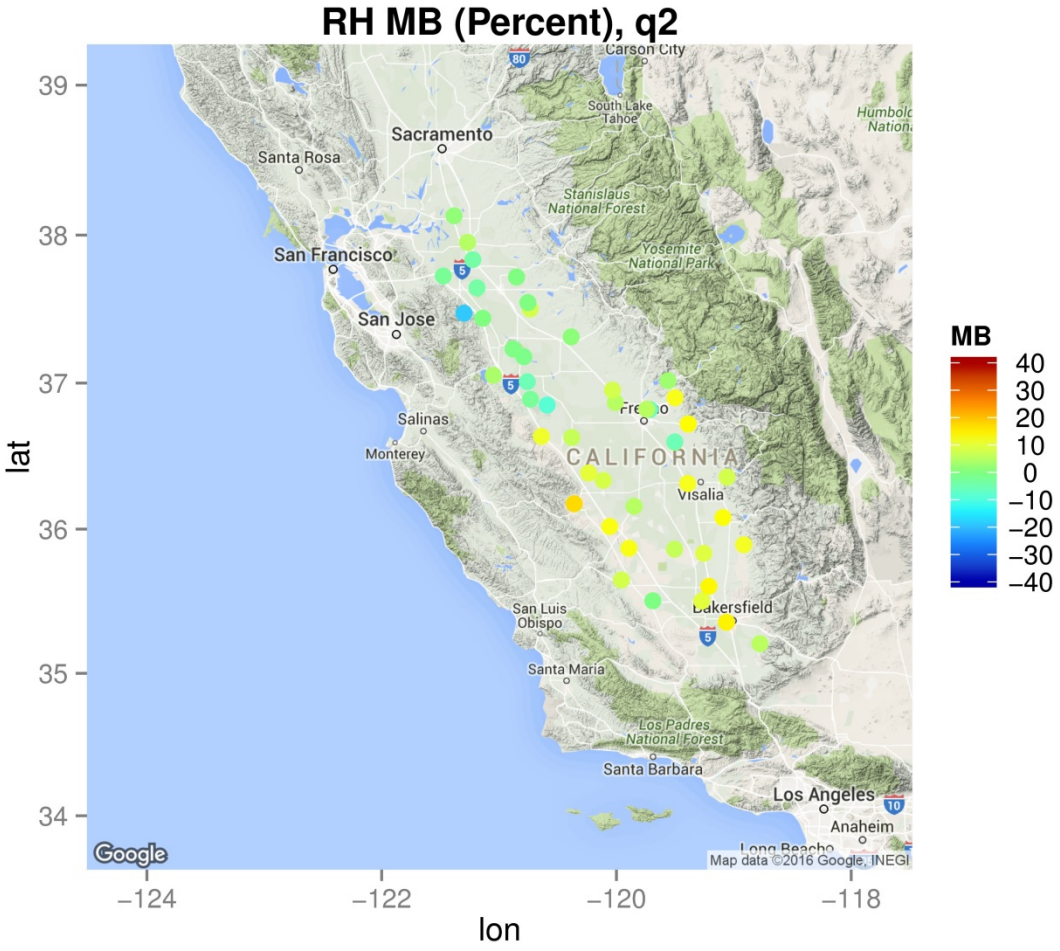

Figure S. 30 Hourly relative humidity mean bias in the second quarter of 2013

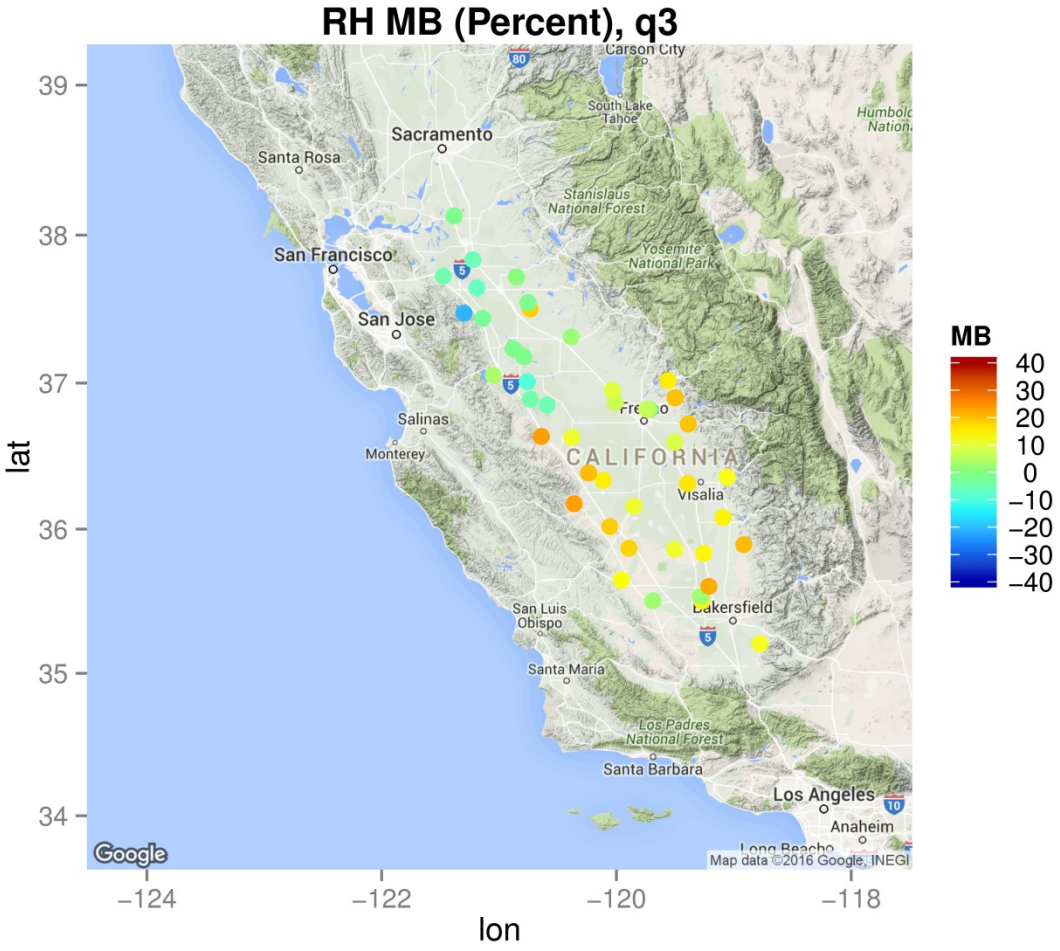

Figure S. 31 Hourly relative humidity mean bias in the third quarter of 2013

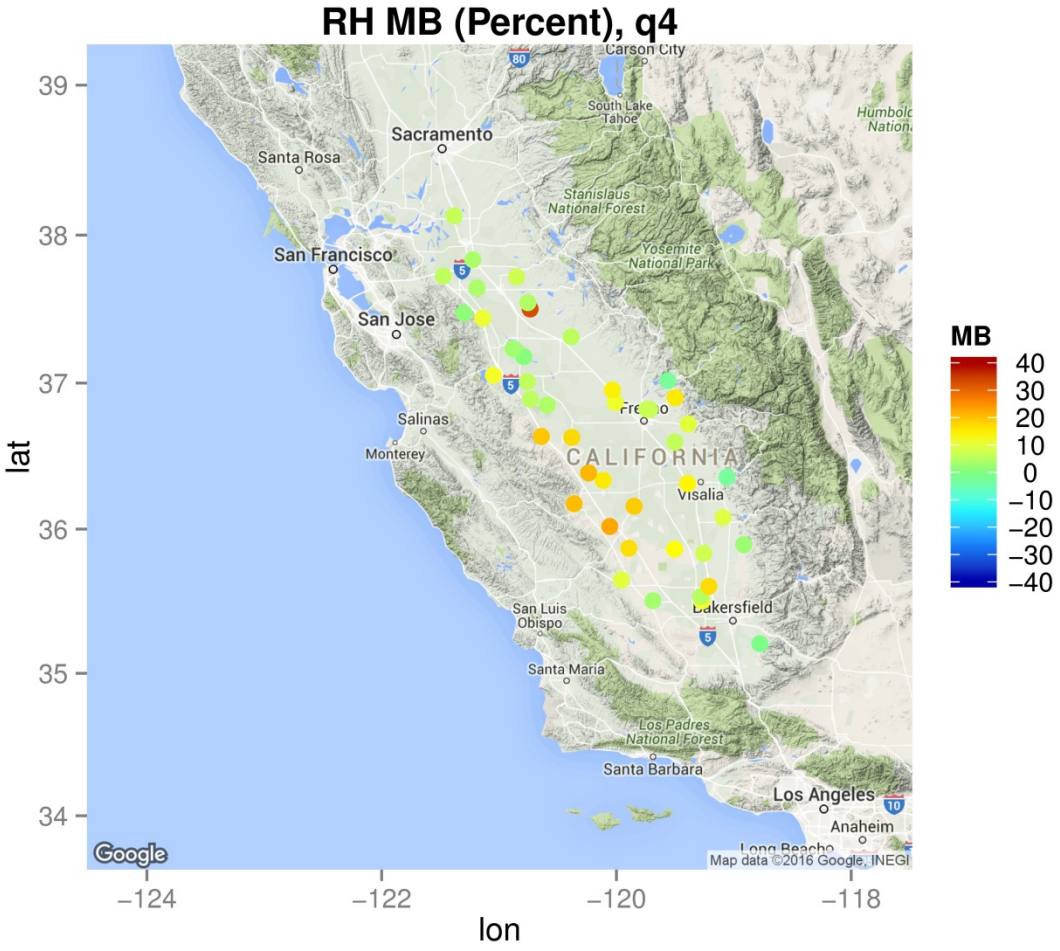

Figure S. 32 Hourly relative humidity mean bias in the fourth quarter of 2013

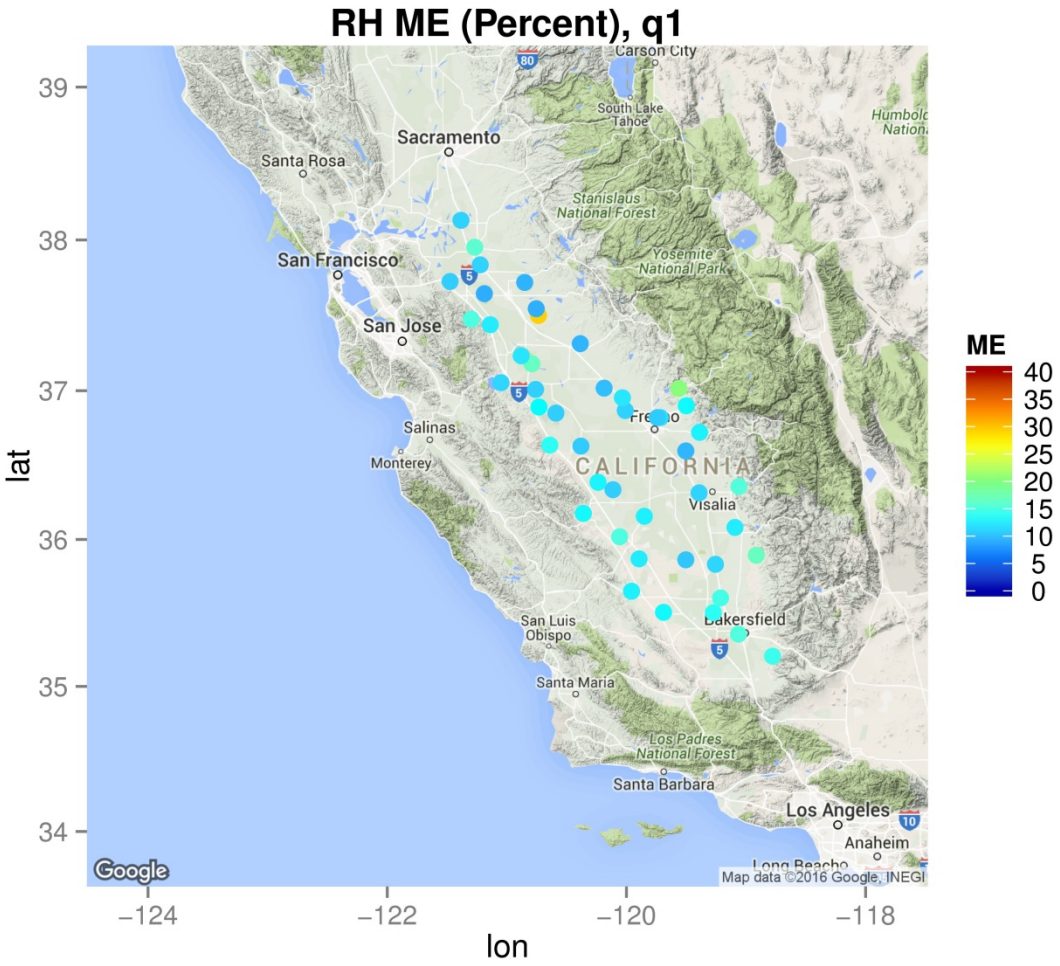

Figure S. 33 Hourly relative humidity mean error in the first quarter of 2013

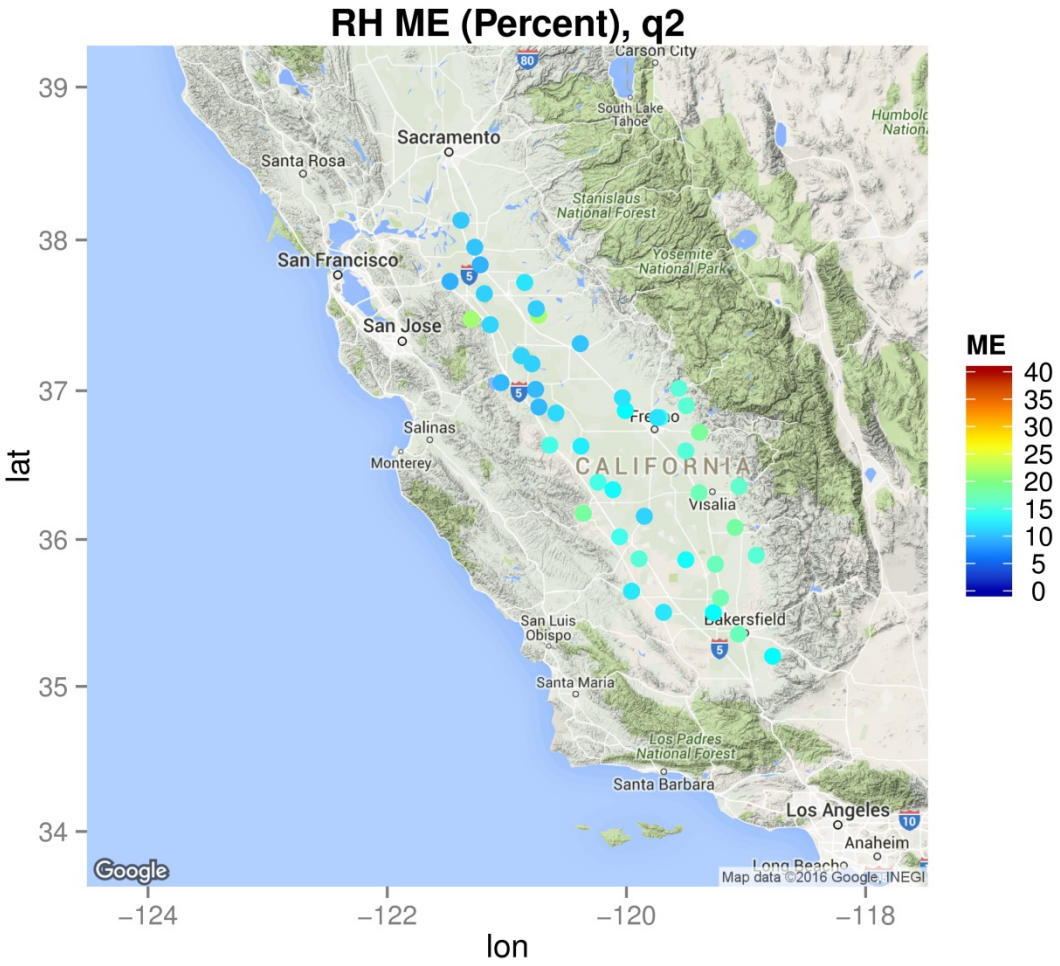

Figure S. 34 Hourly relative humidity mean error in the second quarter of 2013

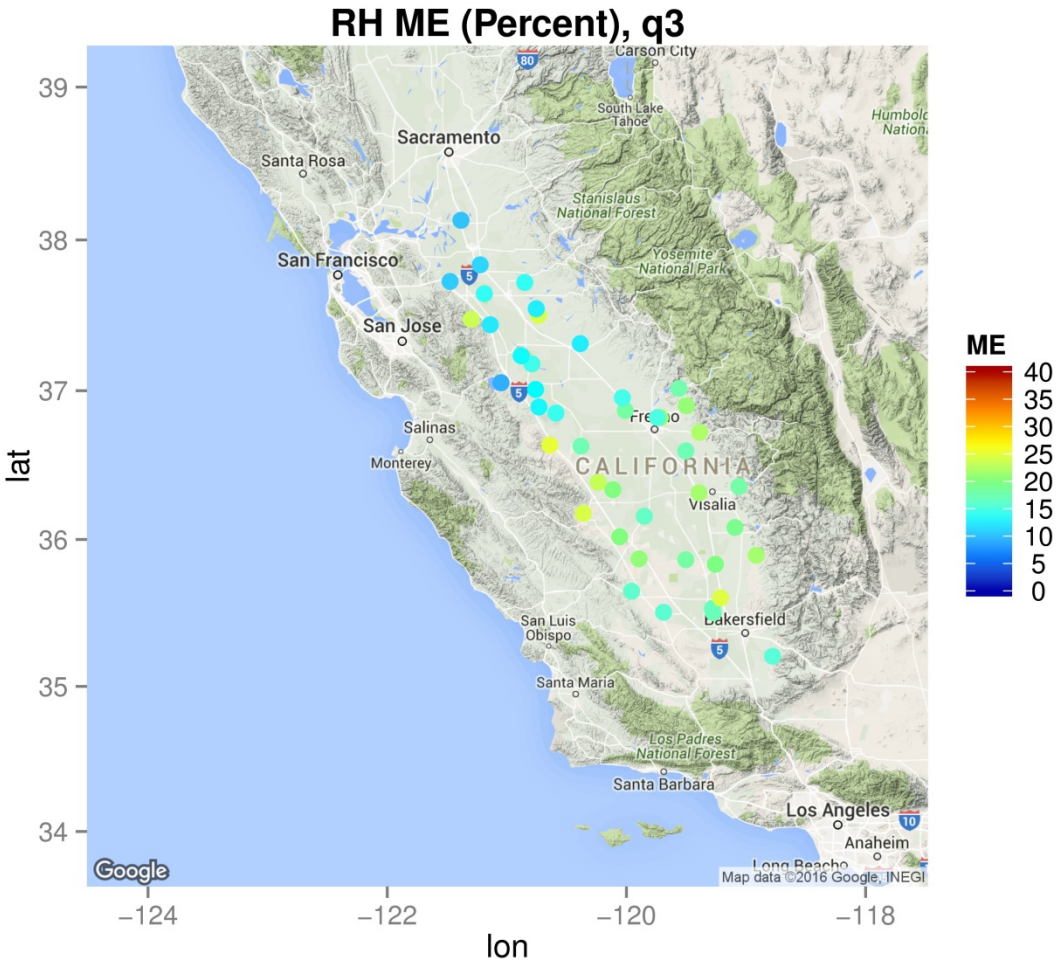

Figure S. 35 Hourly relative humidity mean error in the third quarter of 2013

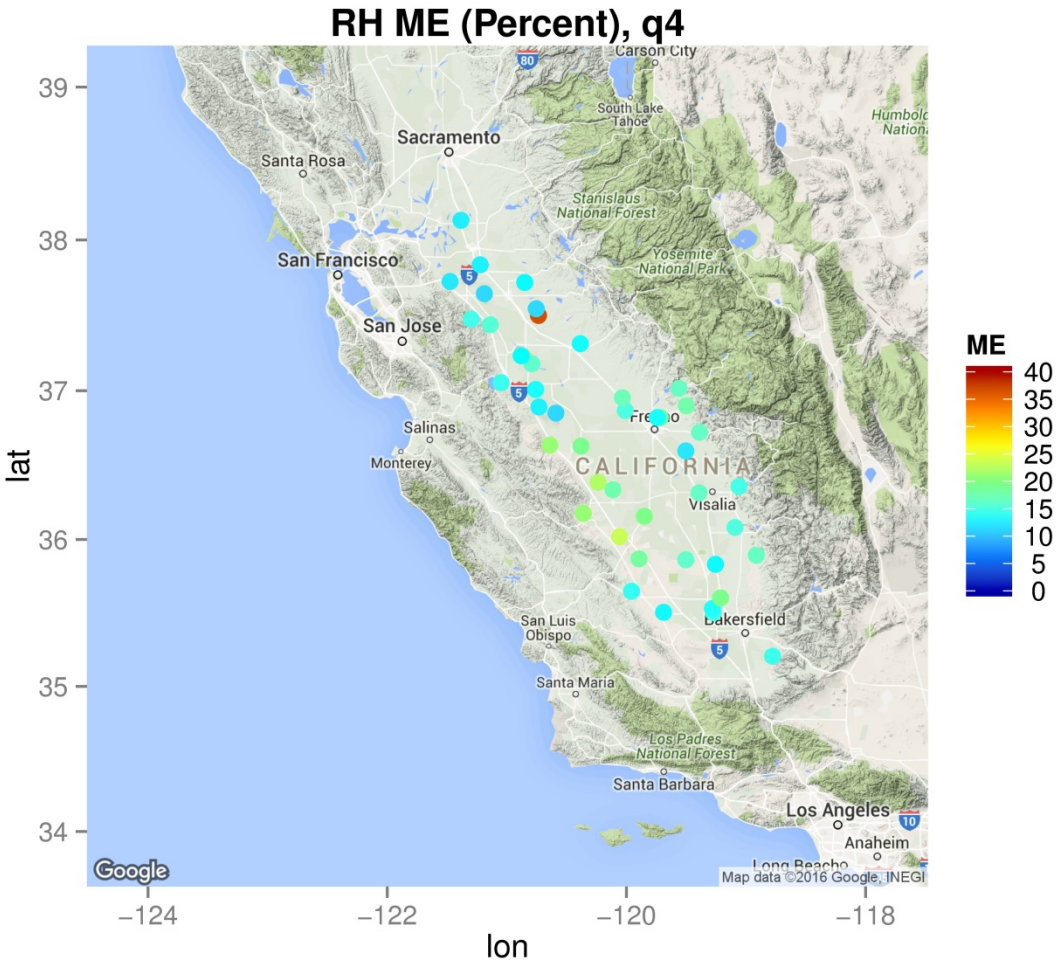

Figure S. 36 Hourly relative humidity mean error in the fourth quarter of 2013

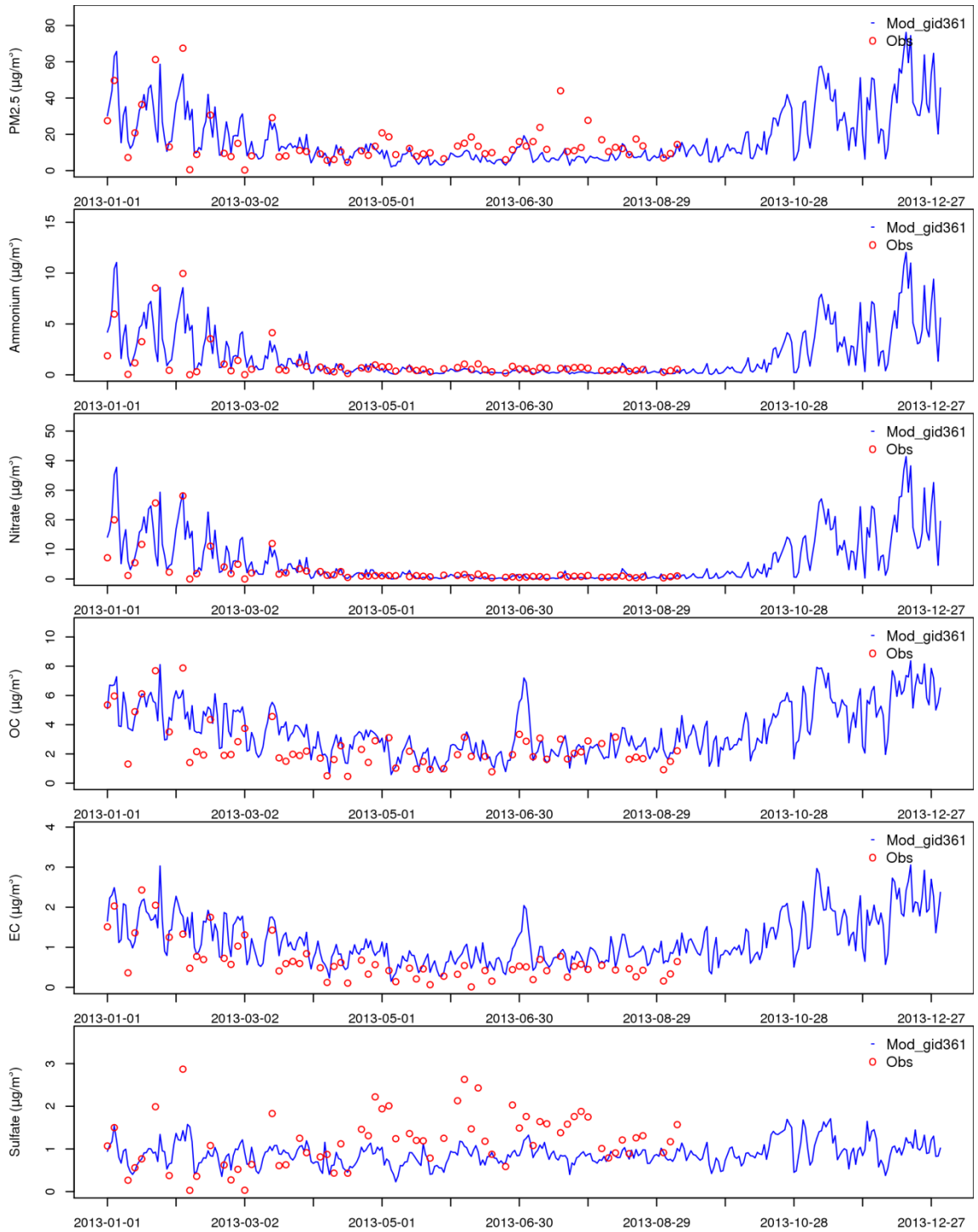

Figure S. 37 Comparison of time series of observed (from CSN measurement) and modeled $PM_{2.5}$ species at Bakersfield

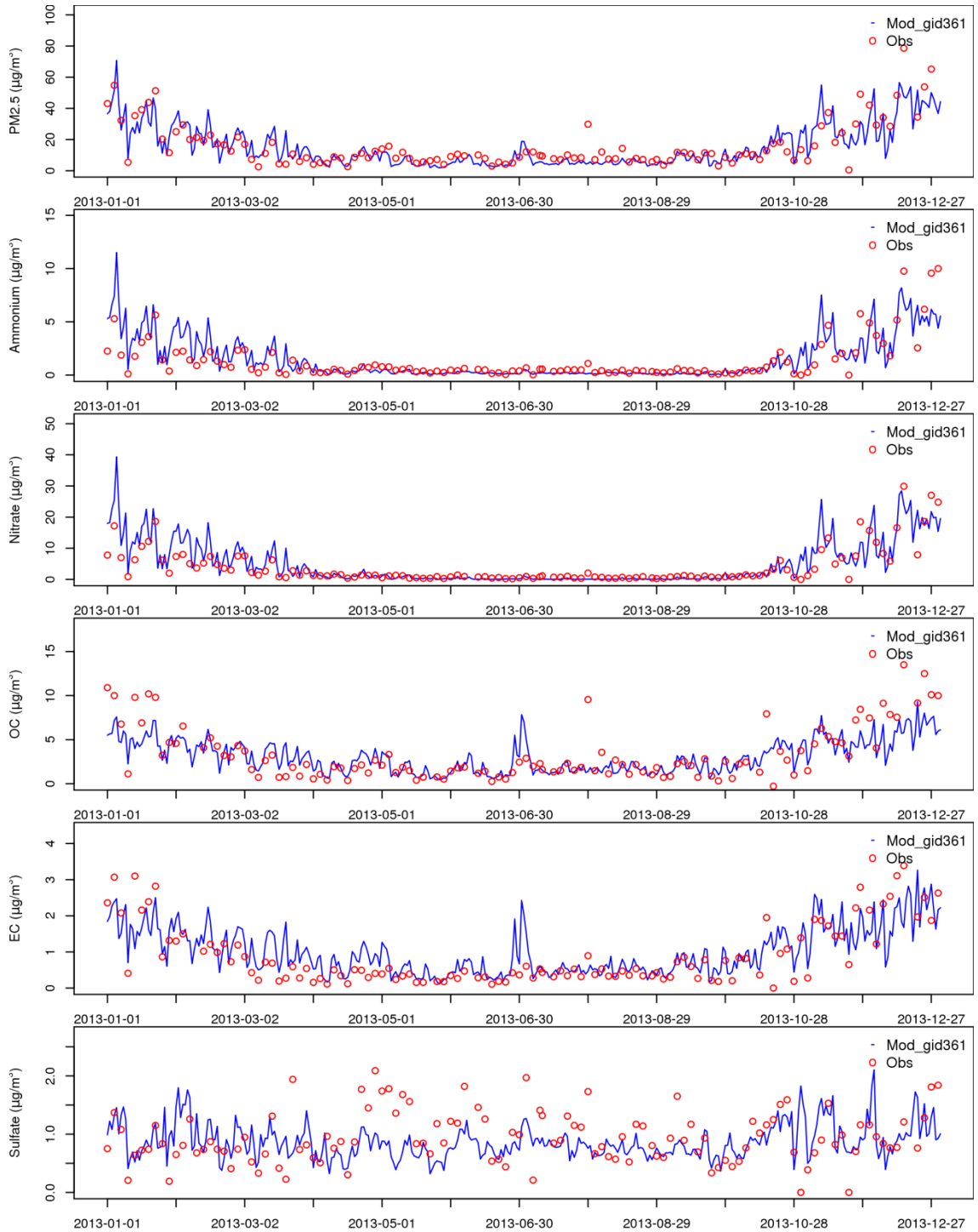

Figure S. 38 Comparison of time series of observed (from CSN measurement) and modeled $PM_{2.5}$ species at Fresno

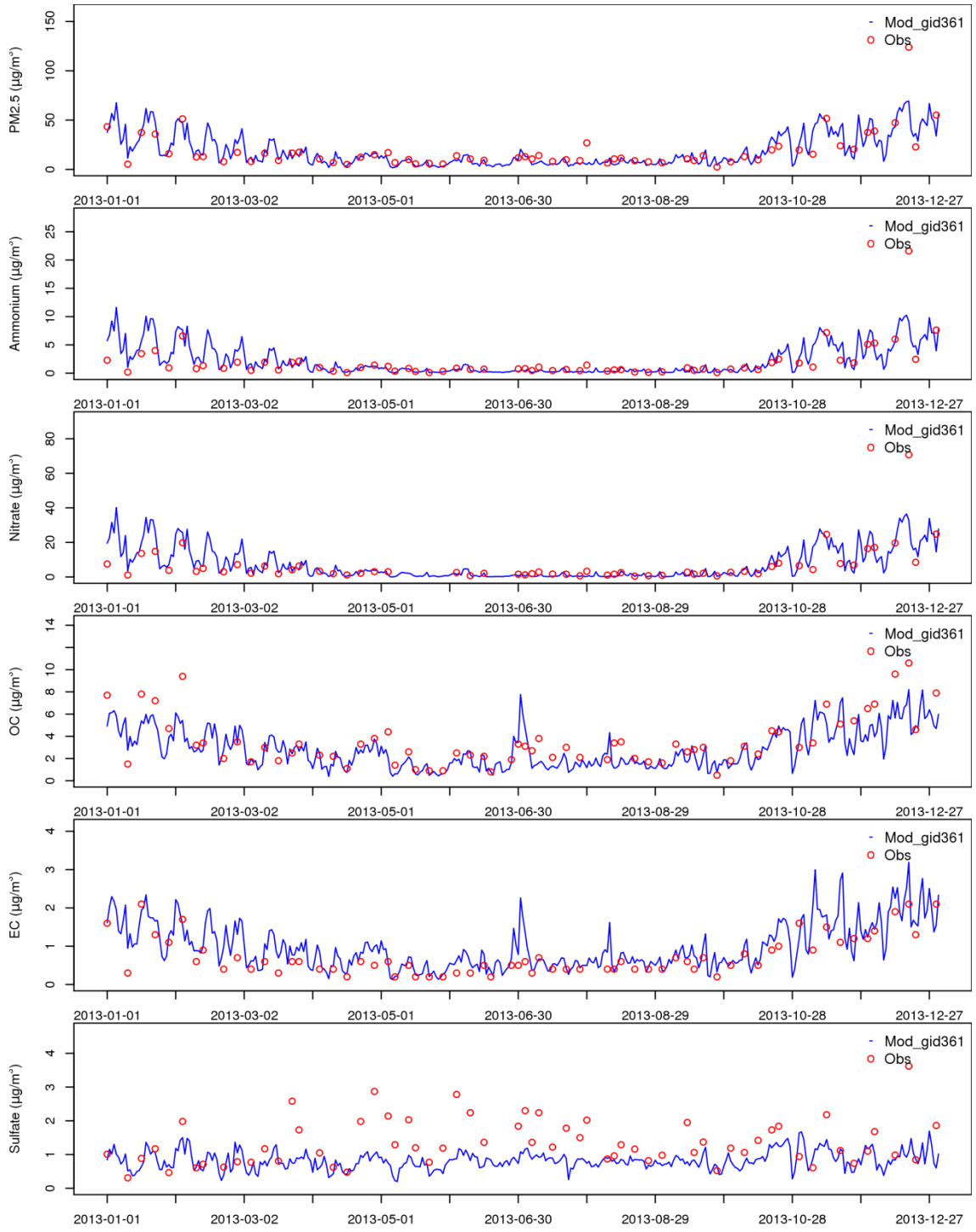

Figure S. 39 Comparison of time series of observed (from CSN measurement) and modeled $PM_{2.5}$ species at Visalia

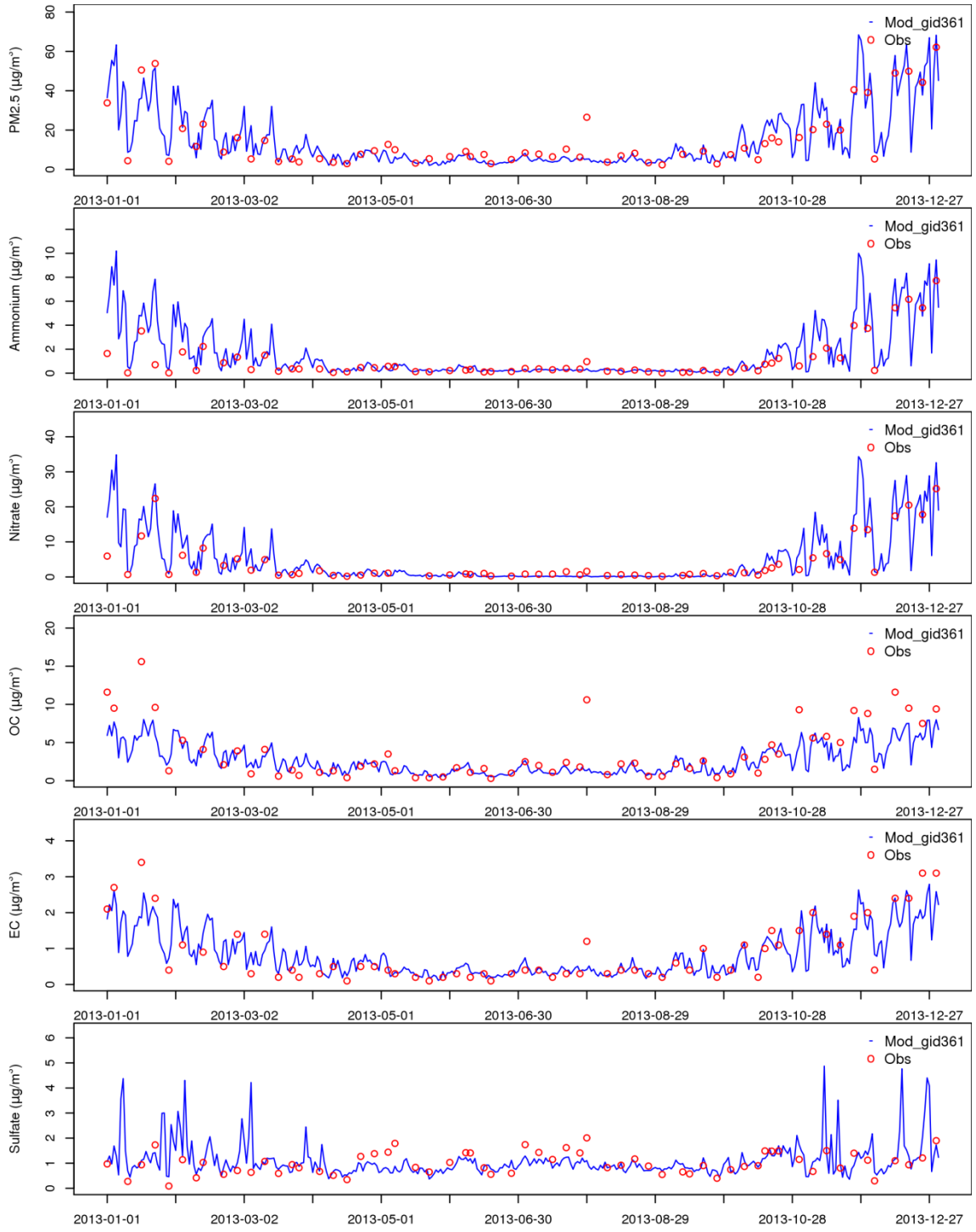

Figure S. 40 Comparison of time series of observed (from CSN measurement) and modeled $PM_{2.5}$ species at Modesto

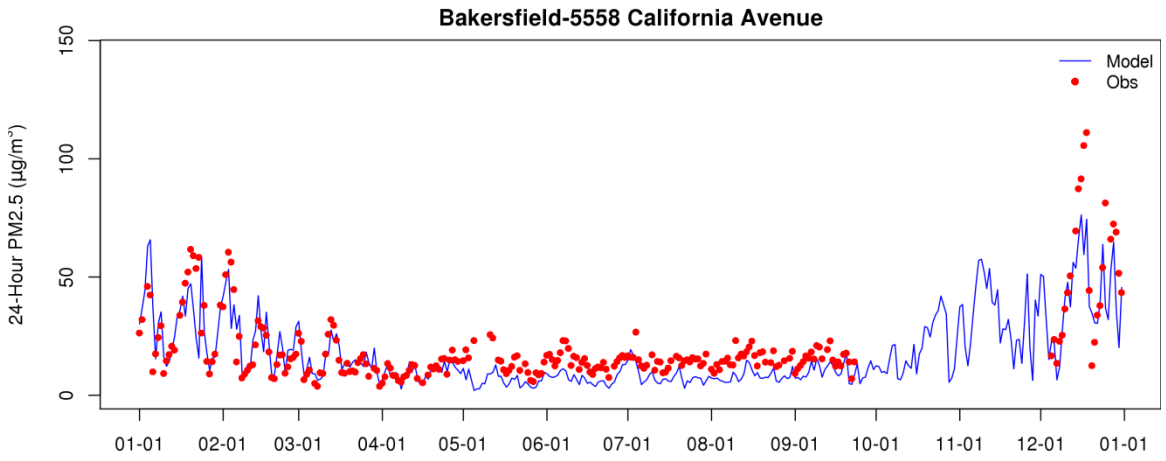

Figure S. 41 Observed and modeled 24-hour average $PM_{2.5}$ at Bakersfield – California Avenue.

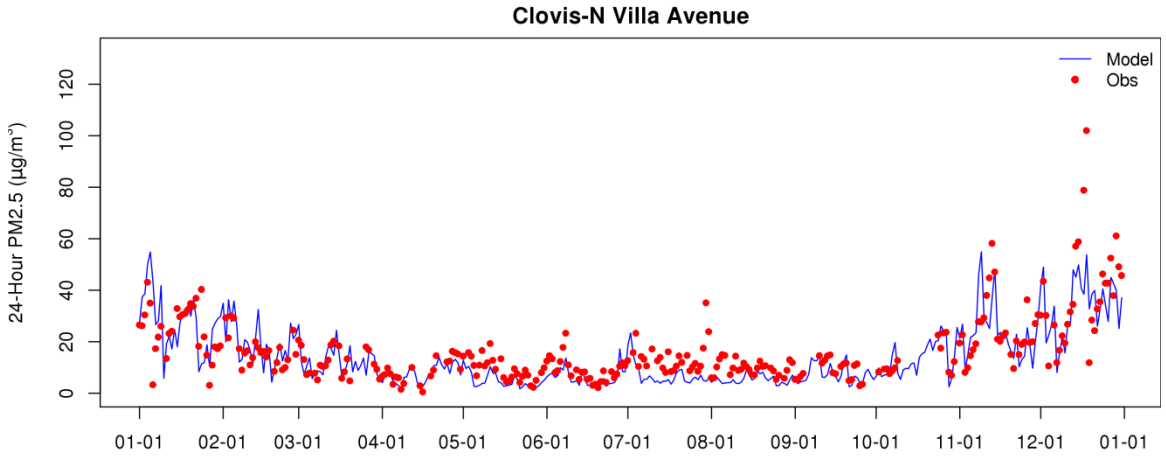

Figure S. 42 Observed and modeled 24-hour average $PM_{2.5}$ at Clovis – Villa Avenue

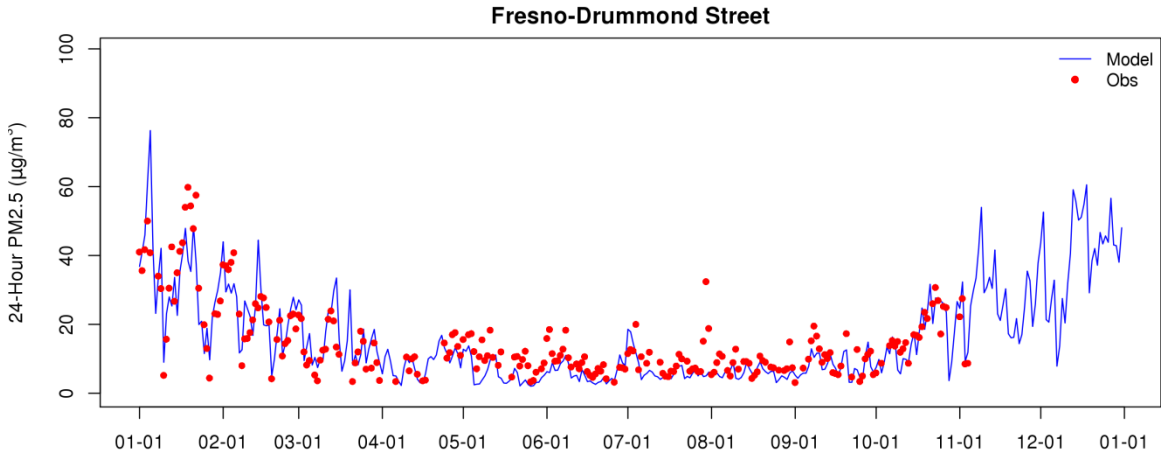

Figure S. 43 Observed and modeled 24-hour average $PM_{2.5}$ at Fresno – Drummond Street

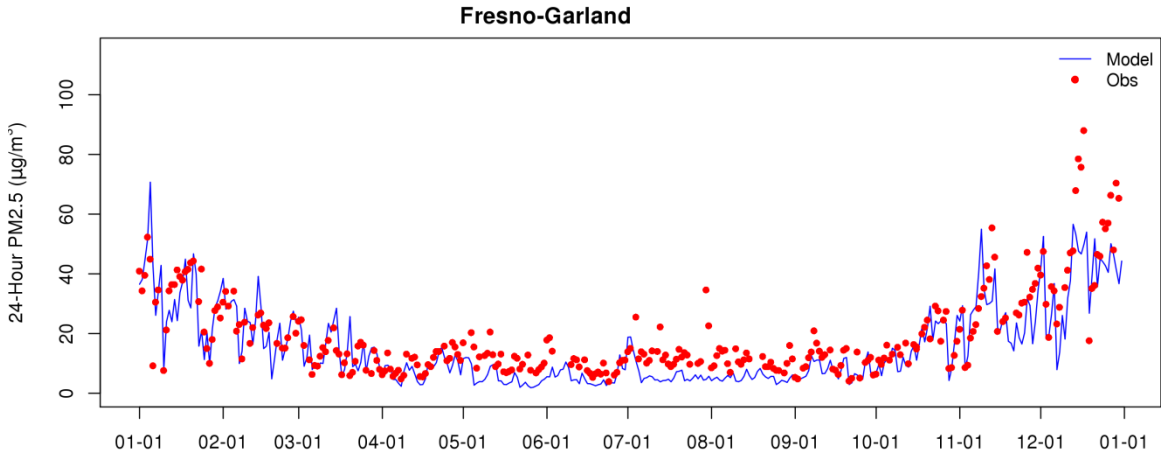

Figure S. 44 Observed and modeled 24-hour average $PM_{2.5}$ at Fresno – Garland

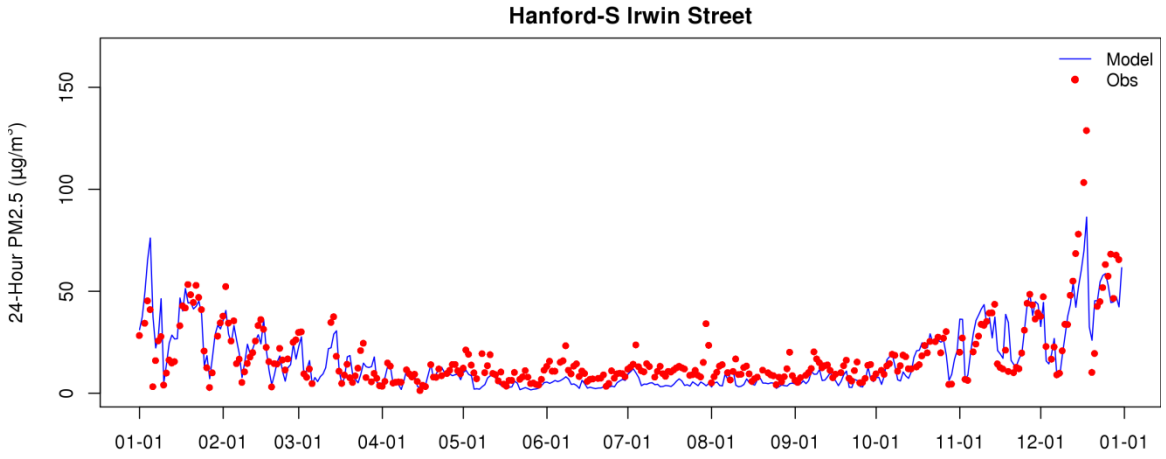

Figure S. 45 Observed and modeled 24-hour average $PM_{2.5}$ at Hanford – Irwin Street

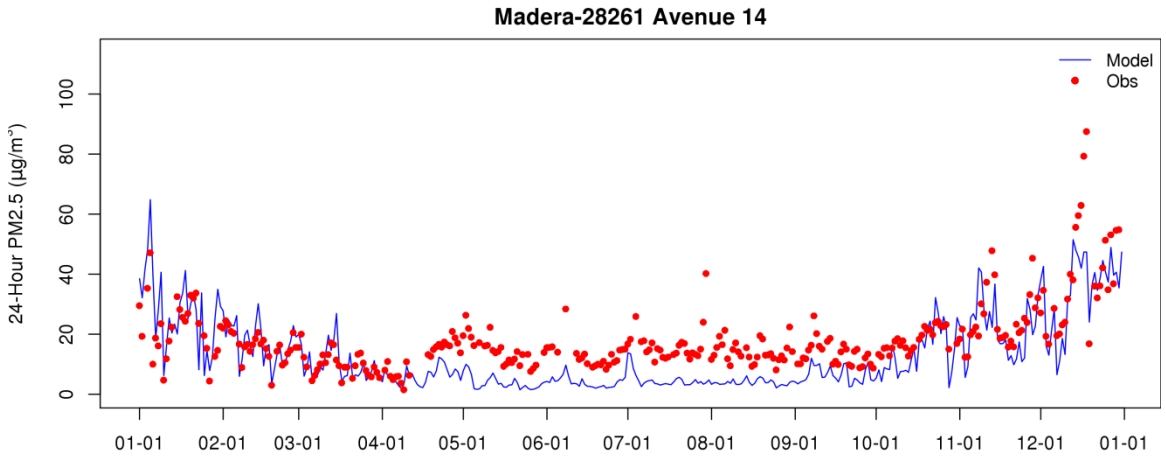

Figure S. 46 Observed and modeled 24-hour average $PM_{2.5}$ at Madera – Avenue 14

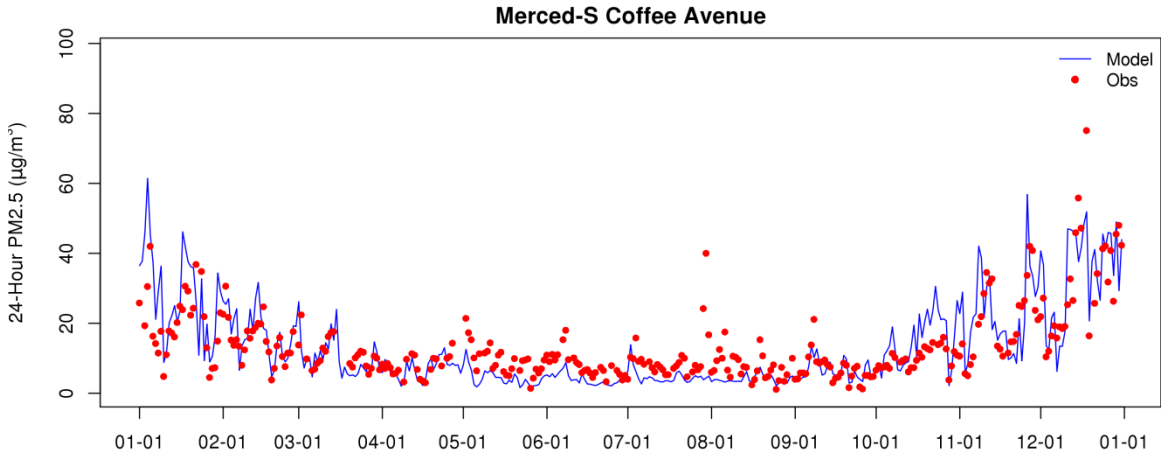

Figure S. 47 Observed and modeled 24-hour average $PM_{2.5}$ at Merced – S Coffee Avenue

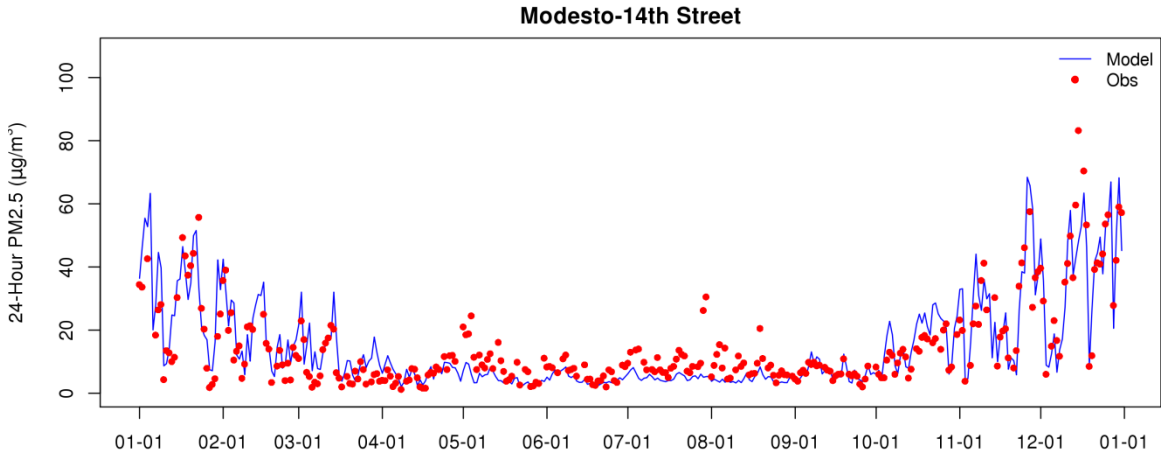

Figure S. 48 Observed and modeled 24-hour average $PM_{2.5}$ at Modesto – 14th Street

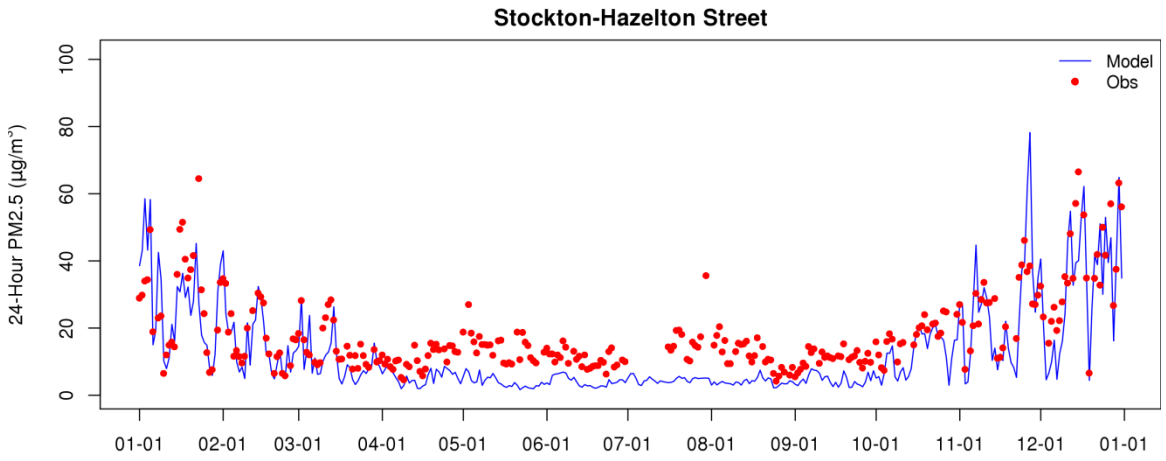

Figure S. 49 Observed and modeled 24-hour average $PM_{2.5}$ at Stockton – Hazelton Street

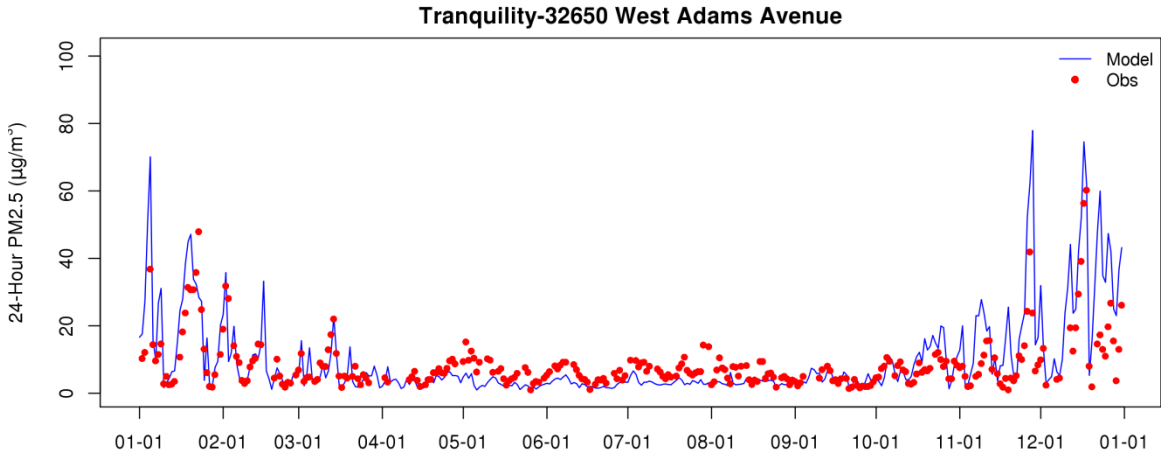

Figure S. 50 Observed and modeled 24-hour average $PM_{2.5}$ at Tranquility – West Adams Avenue

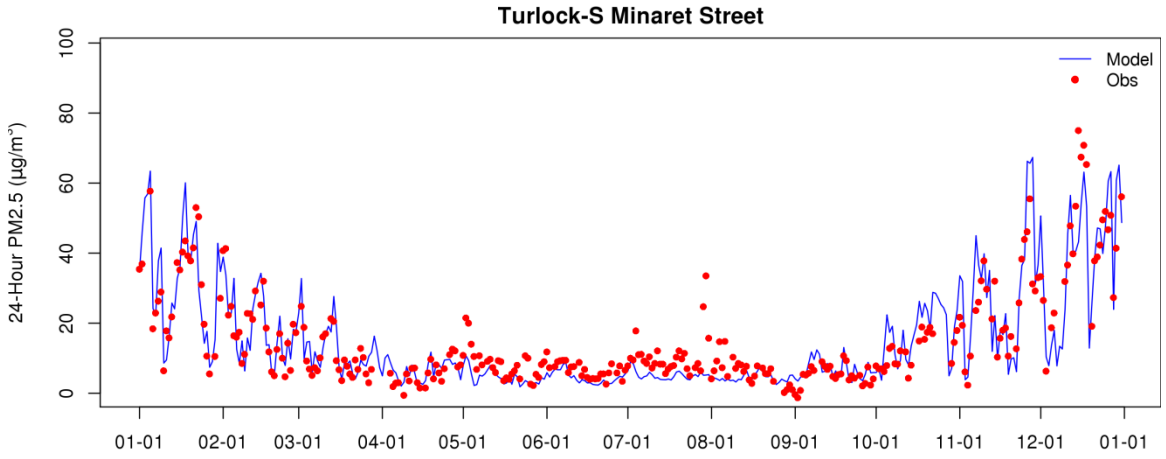

Figure S. 51 Observed and modeled 24-hour average $PM_{2.5}$ at Turlock – Minaret Street

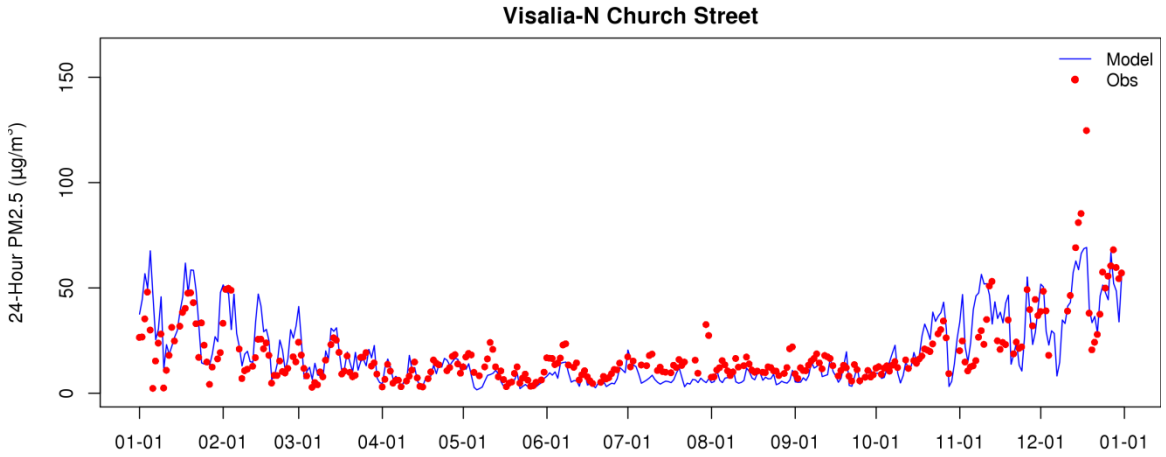

Figure S. 52 Observed and modeled 24-hour average $PM_{2.5}$ at Visalia – Church Street

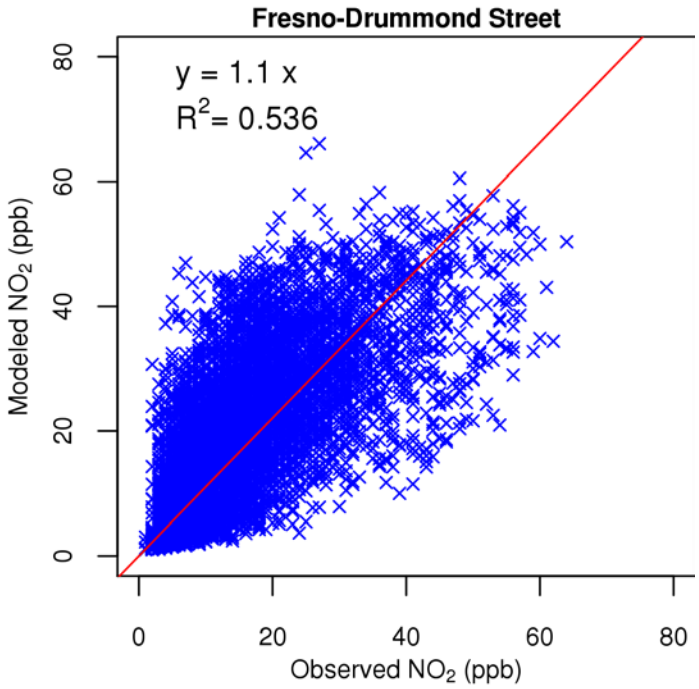

Figure S. 53 Scattering plot of observed and modeled 1-hour NO_2 mixing ratio at Fresno – Drummond Street

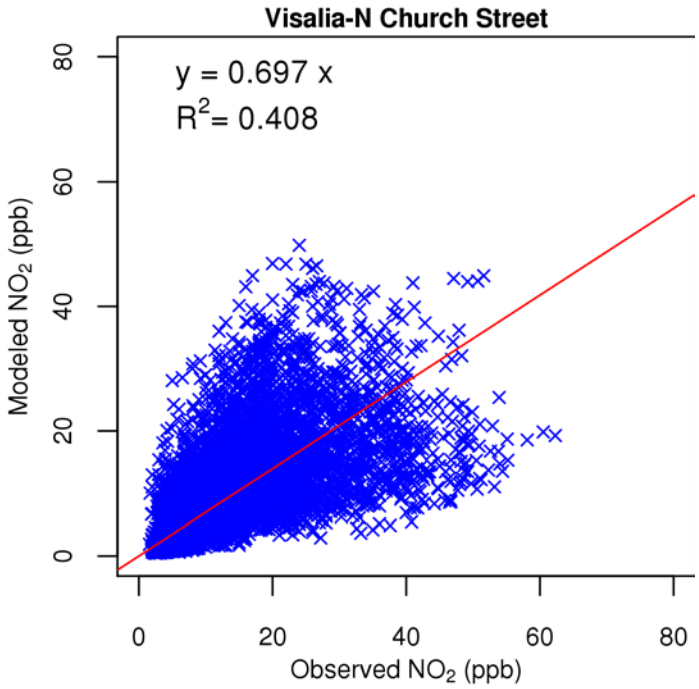

Figure S. 54 Scattering plot of observed and modeled 1-hour NO_2 mixing ratio at Visalia

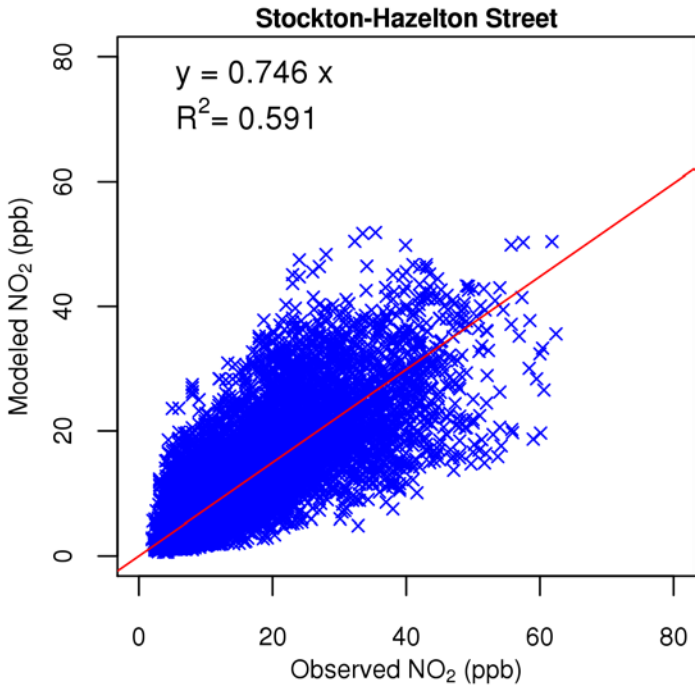

Figure S. 55 Scattering plot of observed and modeled 1-hour NO_2 mixing ratio at Stockton

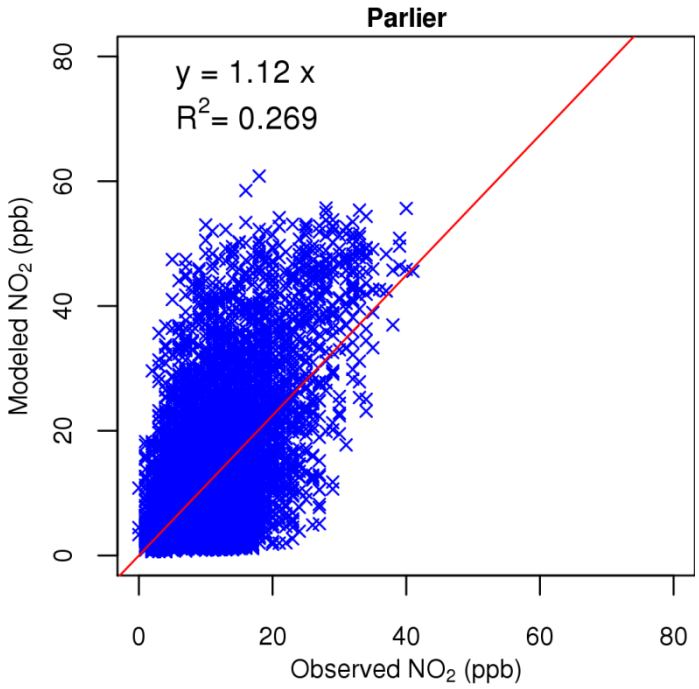

Figure S. 56 Scattering plot of observed and modeled 1-hour NO_2 mixing ratio at Parlier

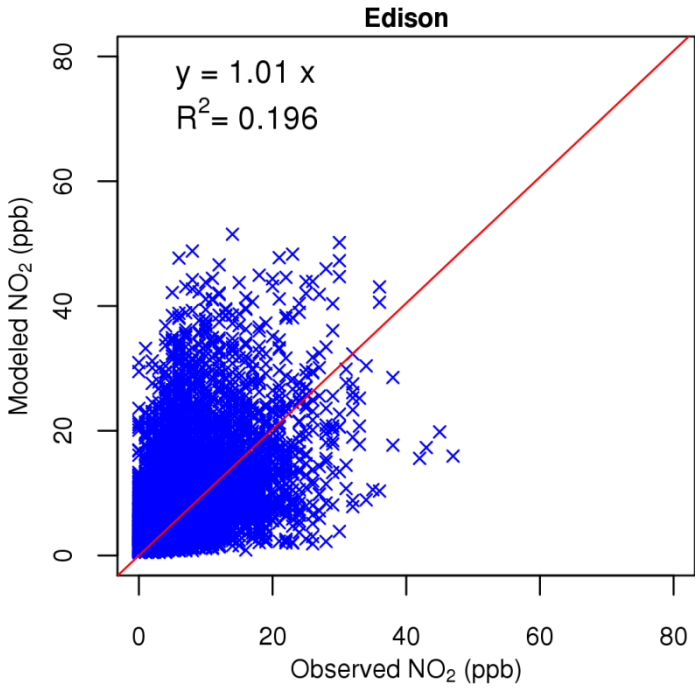

Figure S. 57 Scattering plot of observed and modeled 1-hour NO_2 mixing ratio at Edison

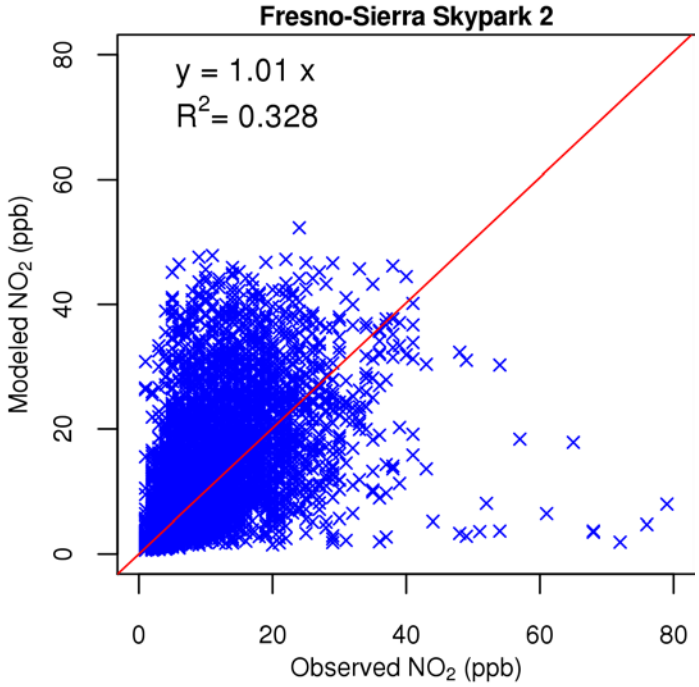

Figure S. 58 Scattering plot of observed and modeled 1-hour NO_2 mixing ratio at Fresno – Sierra Sky Park

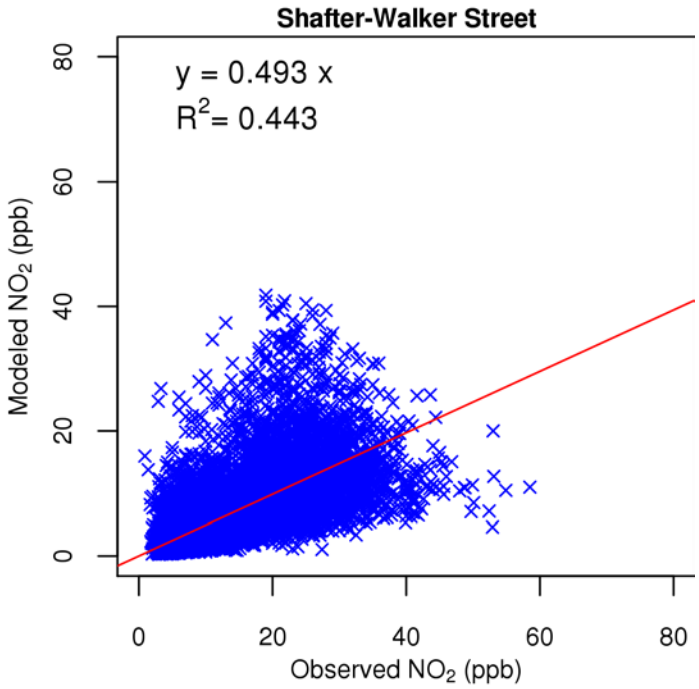

Figure S. 59 Scattering plot of observed and modeled 1-hour NO_2 mixing ratio at Shafter

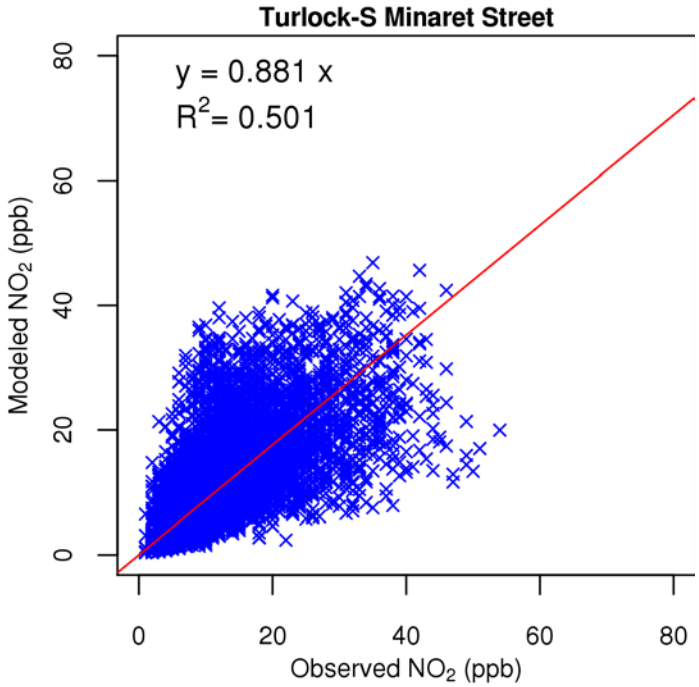

Figure S. 60 Scattering plot of observed and modeled 1-hour NO_2 mixing ratio at Turlock

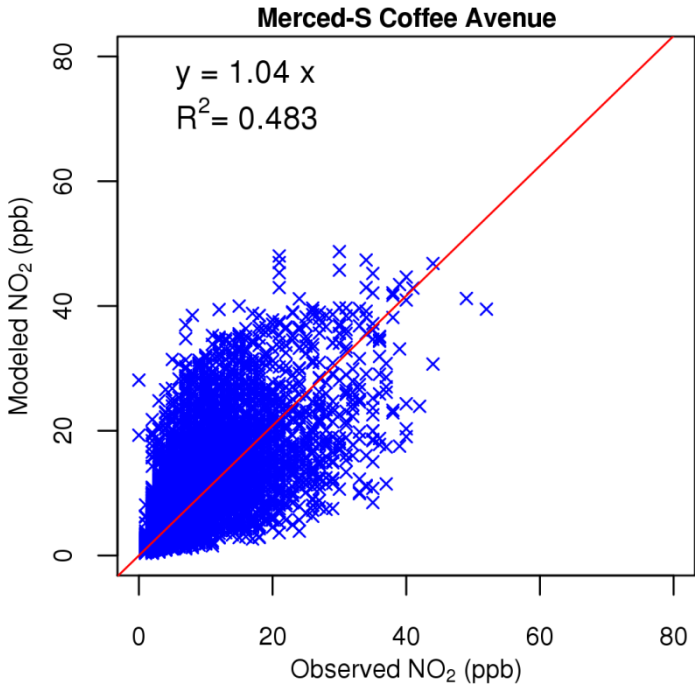

Figure S. 61 Scattering plot of observed and modeled 1-hour NO_2 mixing ratio at Merced

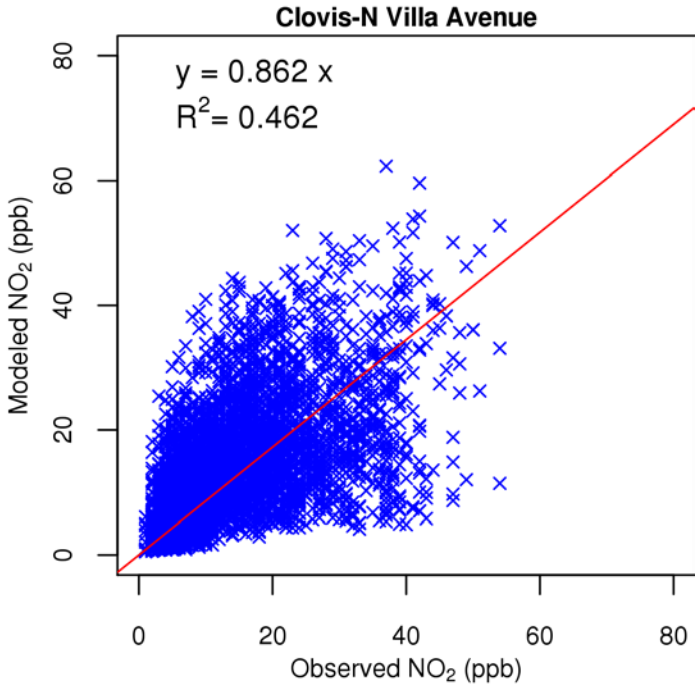

Figure S. 62 Scattering plot of observed and modeled 1-hour NO_2 mixing ratio at Clovis

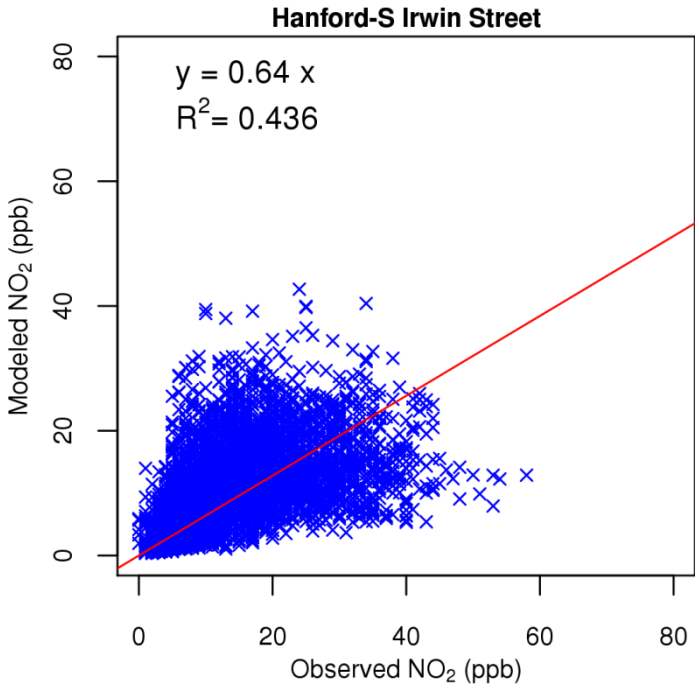

Figure S. 63 Scattering plot of observed and modeled 1-hour NO_2 mixing ratio at Hanford

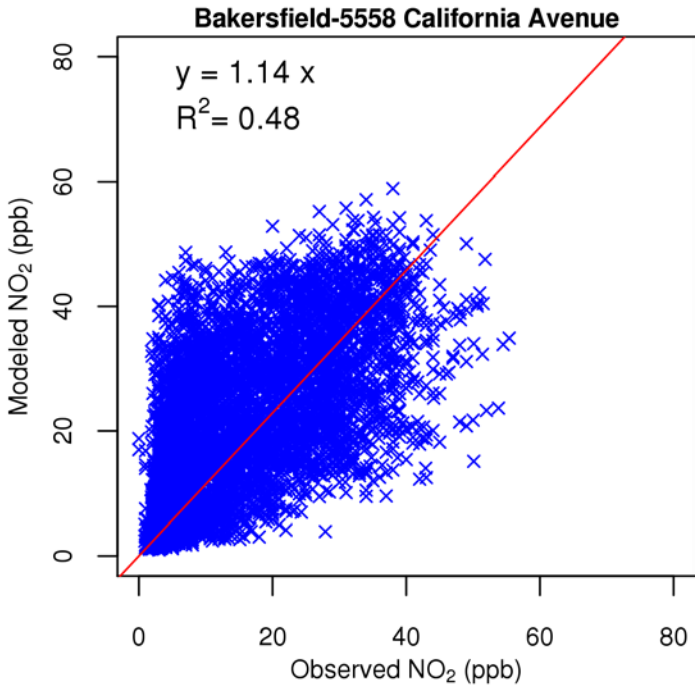

Figure S. 64 Scattering plot of observed and modeled 1-hour NO_2 mixing ratio at Bakersfield – California Avenue

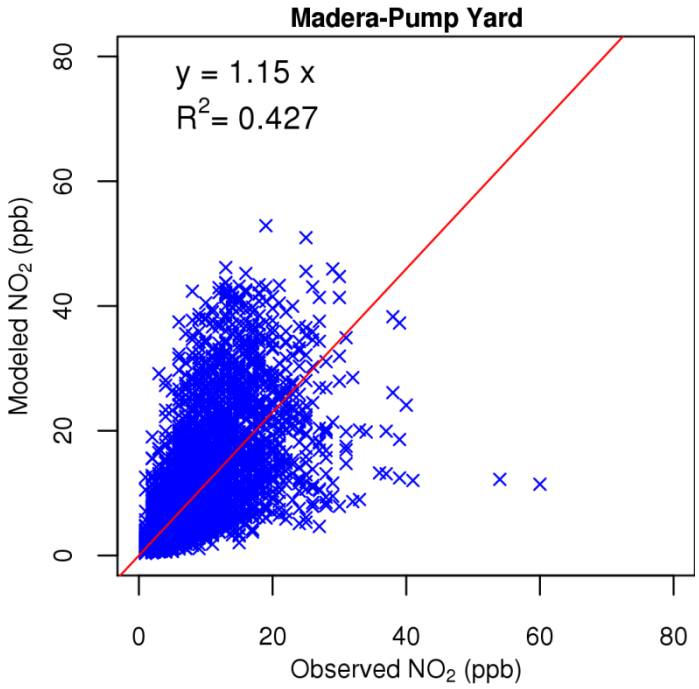

Figure S. 65 Scattering plot of observed and modeled 1-hour NO_2 mixing ratio at Madera

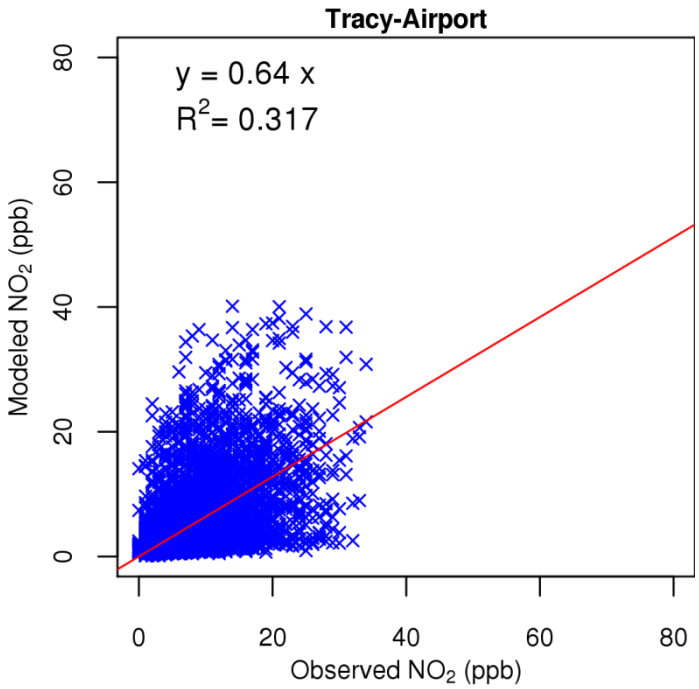

Figure S. 66 Scattering plot of observed and modeled 1-hour NO_2 mixing ratio at Tracy

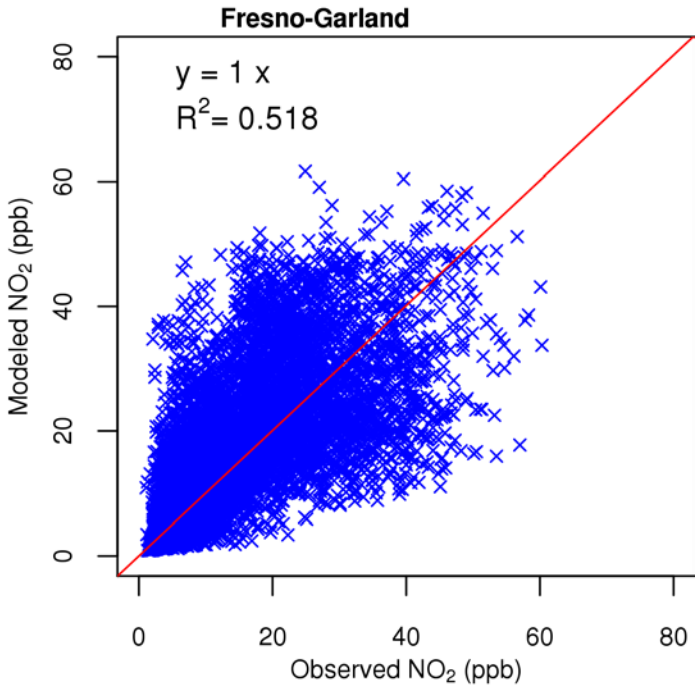

Figure S. 67 Scattering plot of observed and modeled 1-hour NO_2 mixing ratio at Fresno – Garland

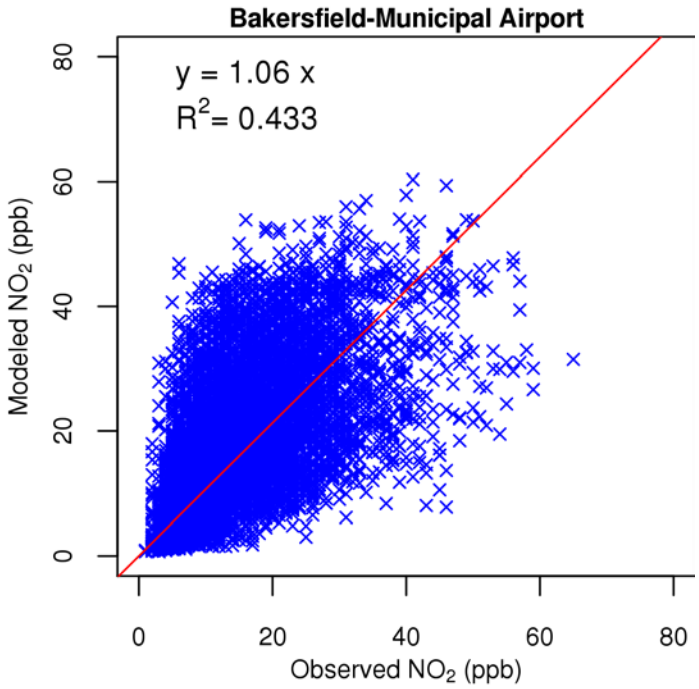

Figure S. 68 Scattering plot of observed and modeled 1-hour NO_2 mixing ratio at Bakersfield – Municipal Airport

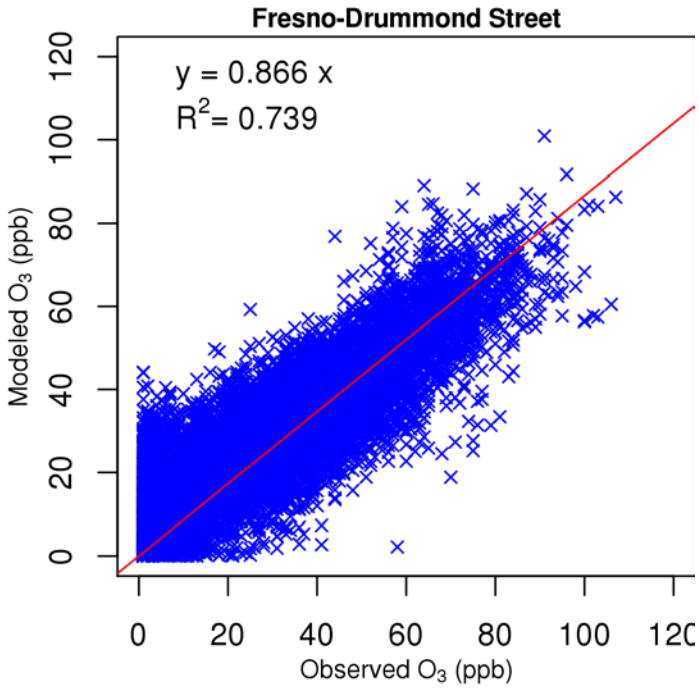

Figure S. 69 Scattering plot of observed and modeled 1-hour O_3 mixing ratio at Fresno – Drummond Street

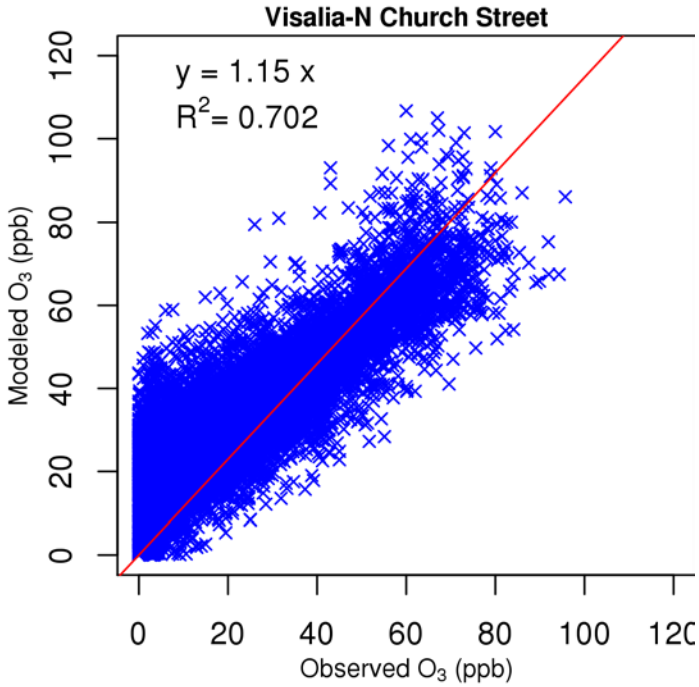

Figure S.70 Scattering plot of observed and modeled 1-hour O_3 mixing ratio at Visalia

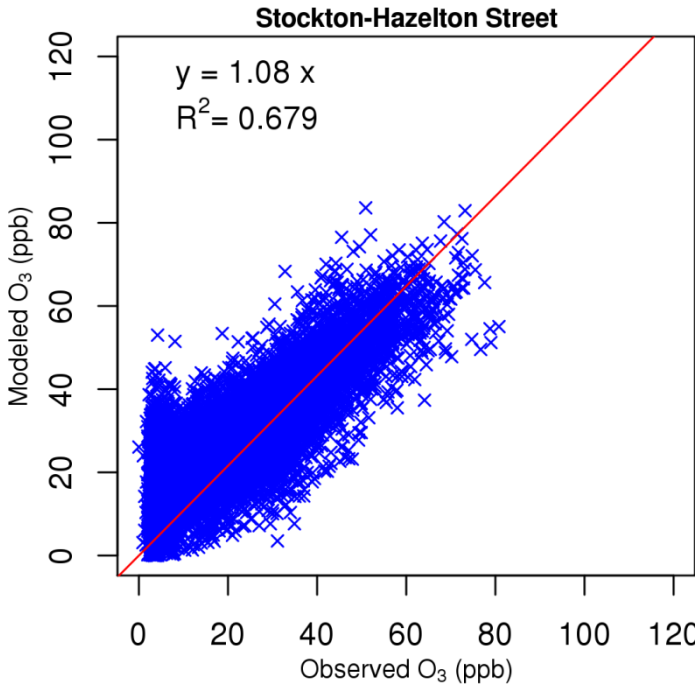

Figure S. 71 Scattering plot of observed and modeled 1-hour O_3 mixing ratio at Stockton

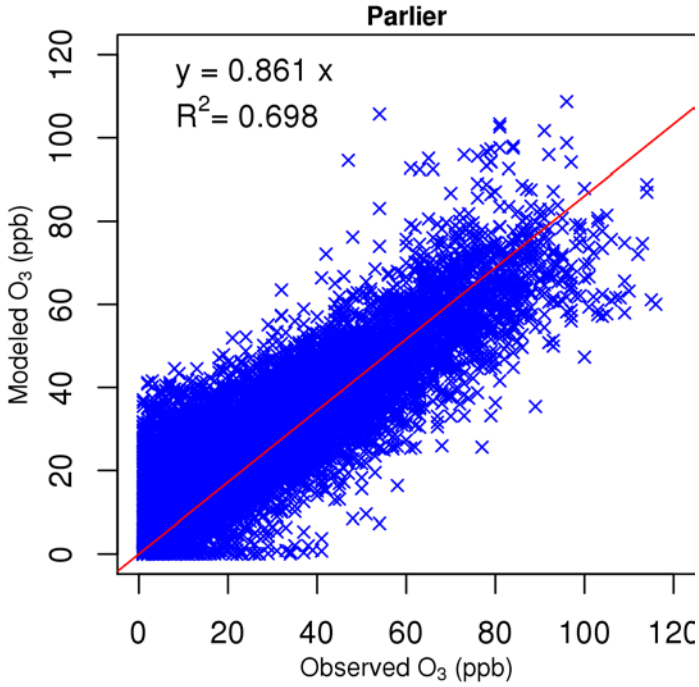

Figure S. 72 Scattering plot of observed and modeled 1-hour O_3 mixing ratio at Parlier

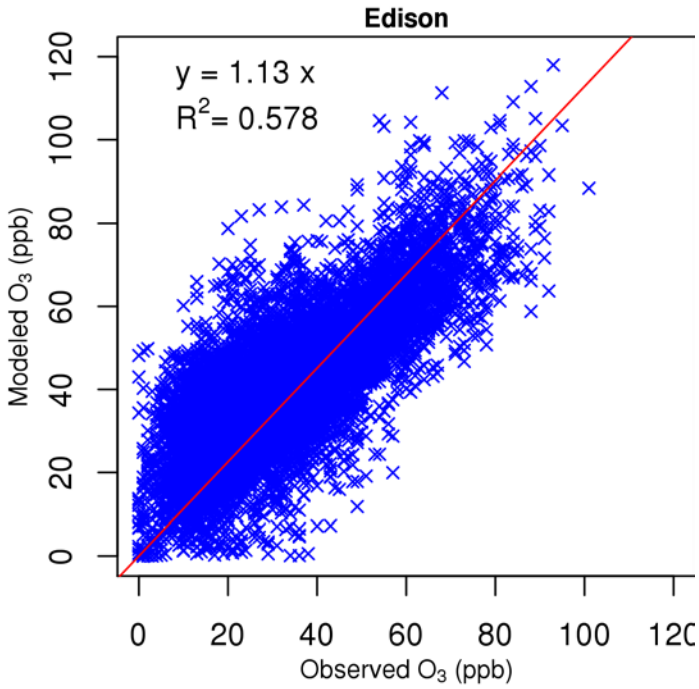

Figure S. 73 Scattering plot of observed and modeled 1-hour O_3 mixing ratio at Edison

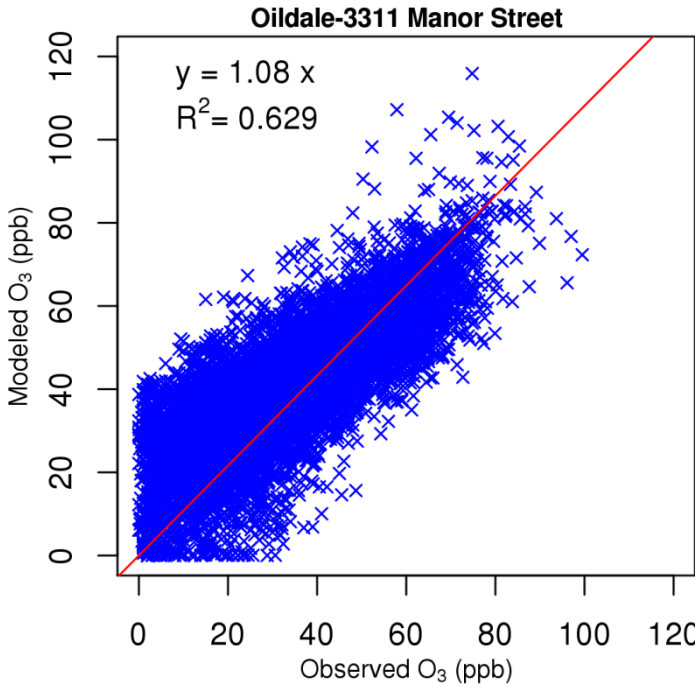

Figure S. 74 Scattering plot of observed and modeled 1-hour O_3 mixing ratio at Oildale

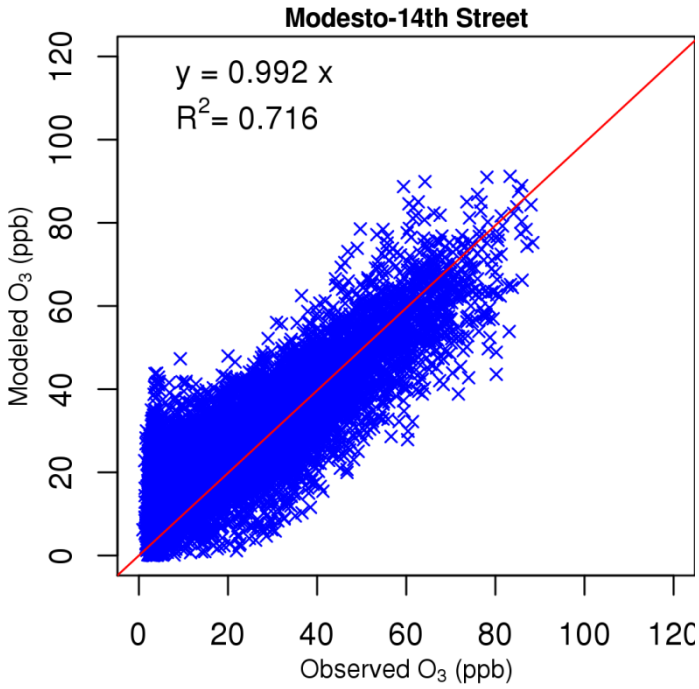

Figure S. 75 Scattering plot of observed and modeled 1-hour O_3 mixing ratio at Modesto -14th Street

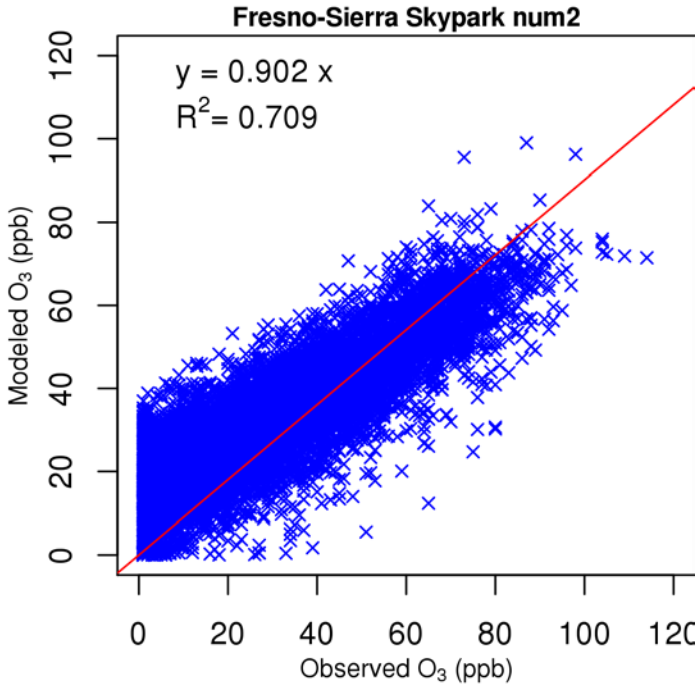

Figure S.76 Scattering plot of observed and modeled 1-hour O_3 mixing ratio at Fresno – Sierra Sky Park #2

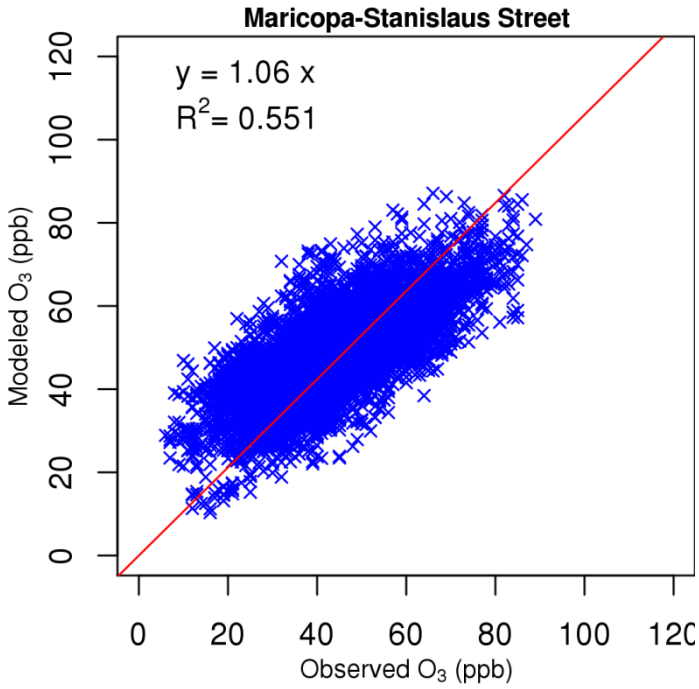

Figure S. 77 Scattering plot of observed and modeled 1-hour O_3 mixing ratio at Maricopa

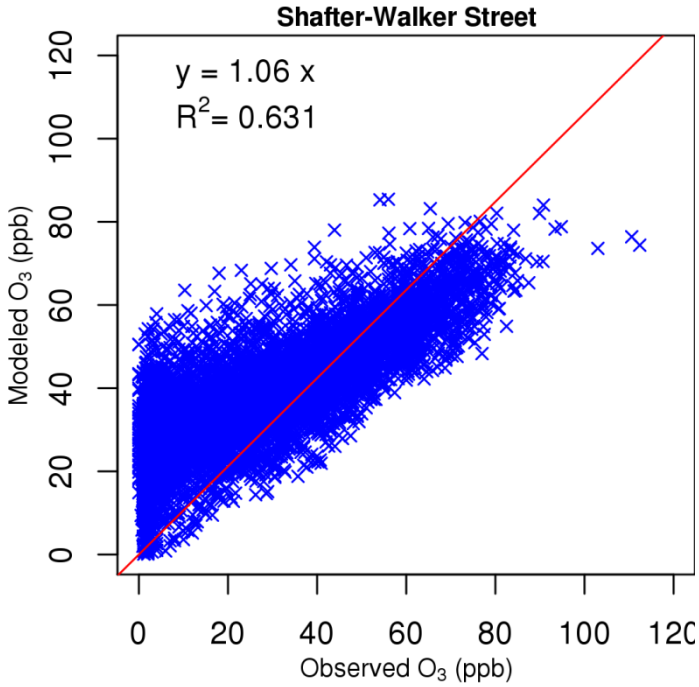

Figure S. 78 Scattering plot of observed and modeled 1-hour O_3 mixing ratio at Shafter

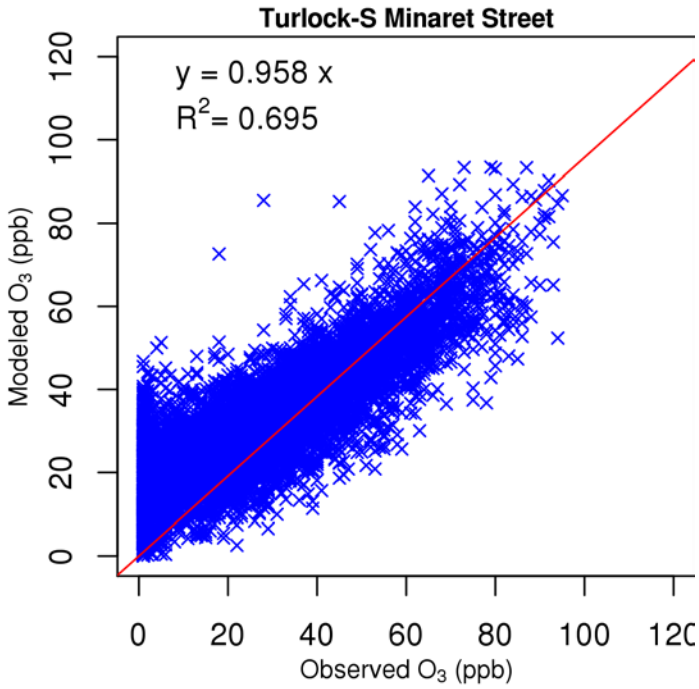

Figure S. 79 Scattering plot of observed and modeled 1-hour O_3 mixing ratio at Turlock

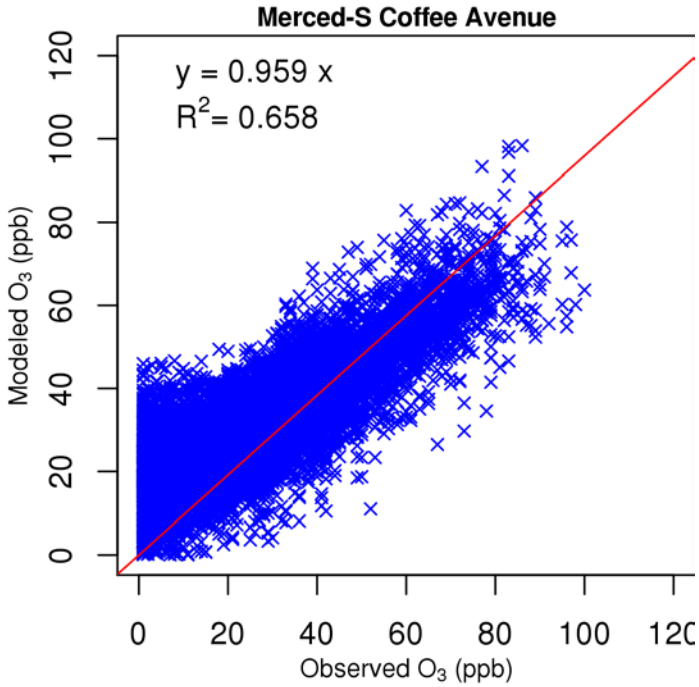

Figure S. 80 Scattering plot of observed and modeled 1-hour O_3 mixing ratio at Merced – S Coffee Avenue

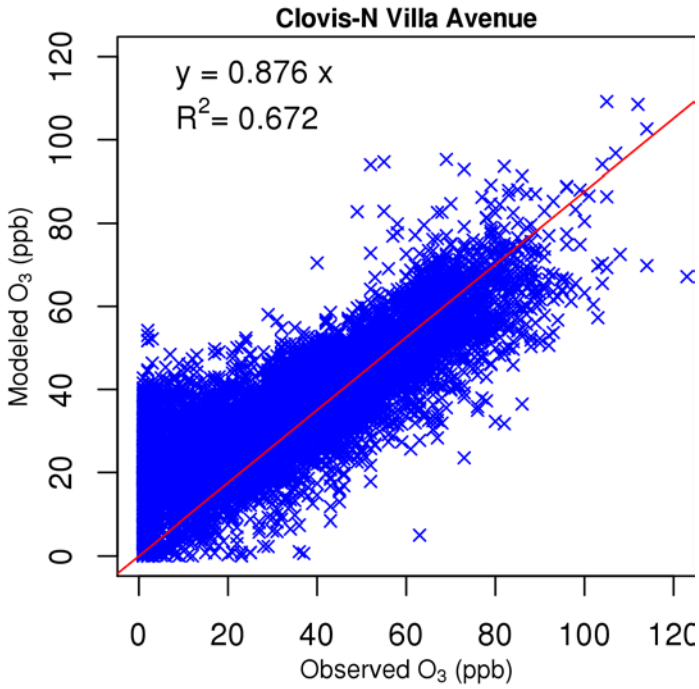

Figure S. 81 Scattering plot of observed and modeled 1-hour O_3 mixing ratio at Clovis

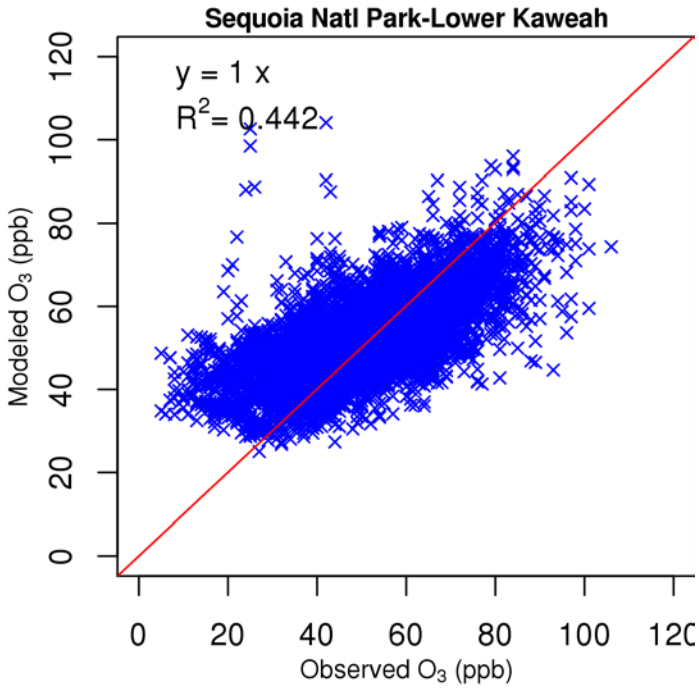

Figure S. 82 Scattering plot of observed and modeled 1-hour O_3 mixing ratio at Sequoia National Park

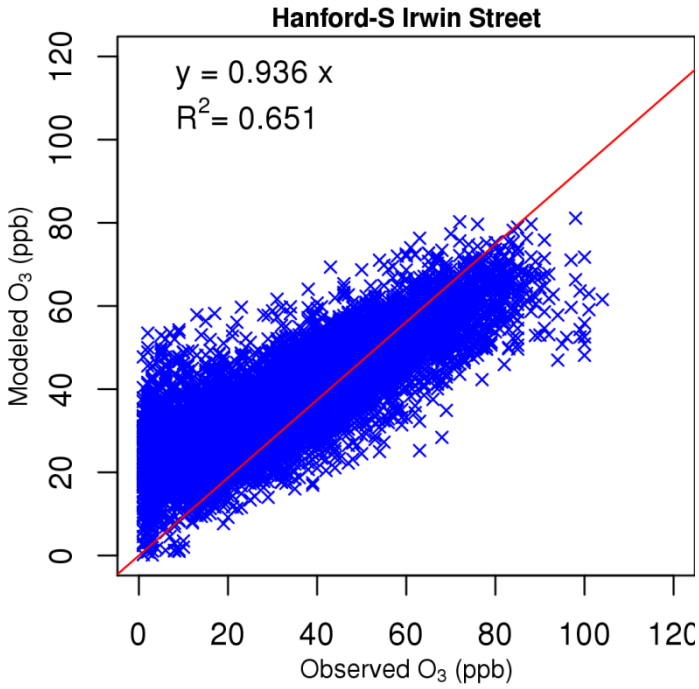

Figure S. 83 Scattering plot of observed and modeled 1-hour O_3 mixing ratio at Hanford

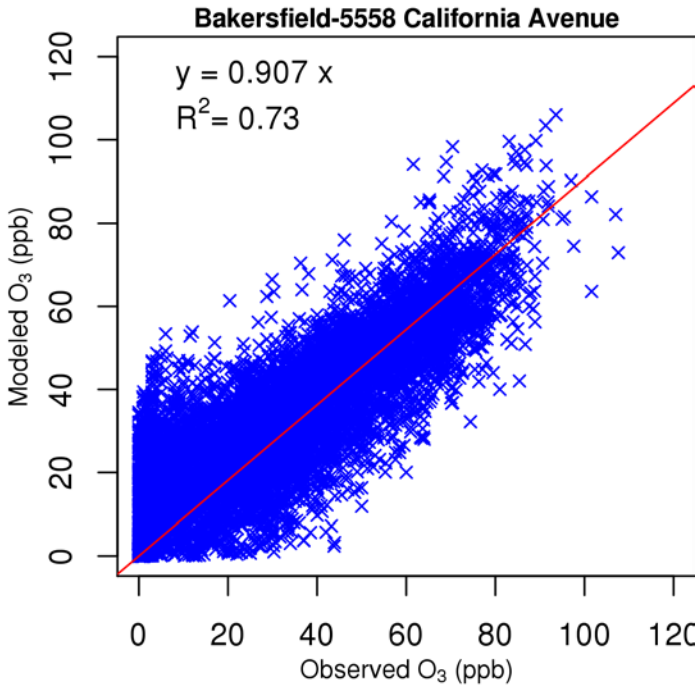

Figure S. 84 Scattering plot of observed and modeled 1-hour O_3 mixing ratio at Bakersfield – California Avenue

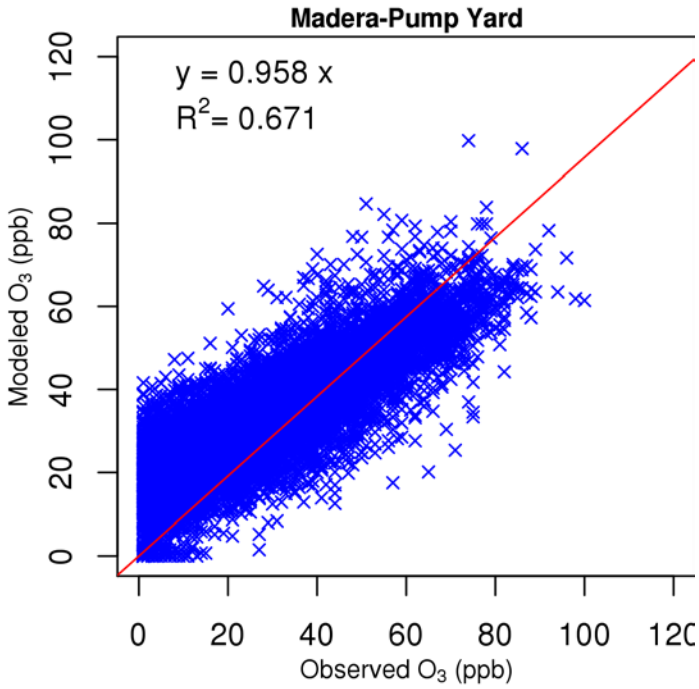

Figure S. 85 Scattering plot of observed and modeled 1-hour O_3 mixing ratio at Madera – Pump Yard

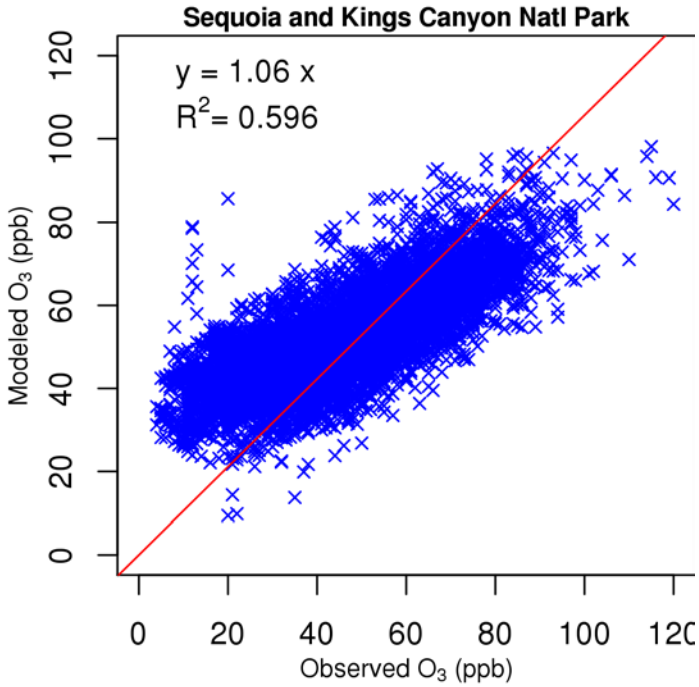

Figure S. 86 Scattering plot of observed and modeled 1-hour O_3 mixing ratio at Sequoia and Kings Canyon National Park

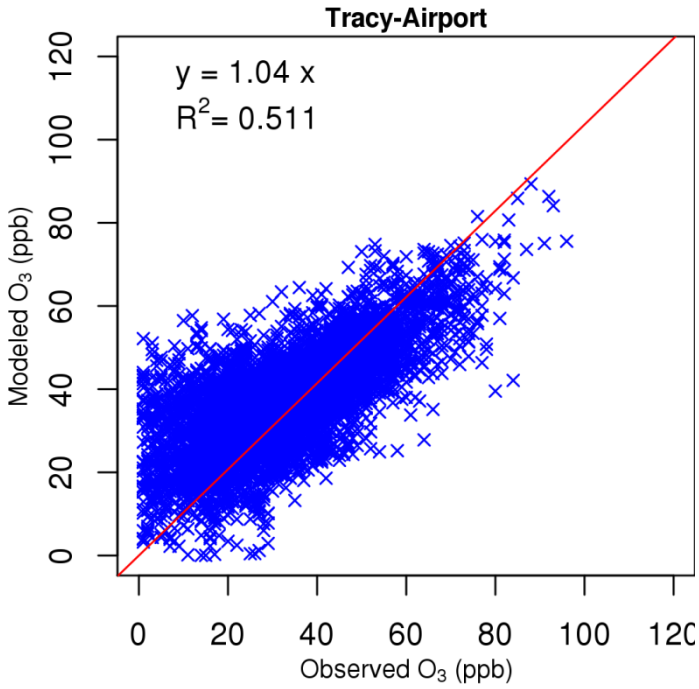

Figure S. 87 Scattering plot of observed and modeled 1-hour O_3 mixing ratio at Tracy

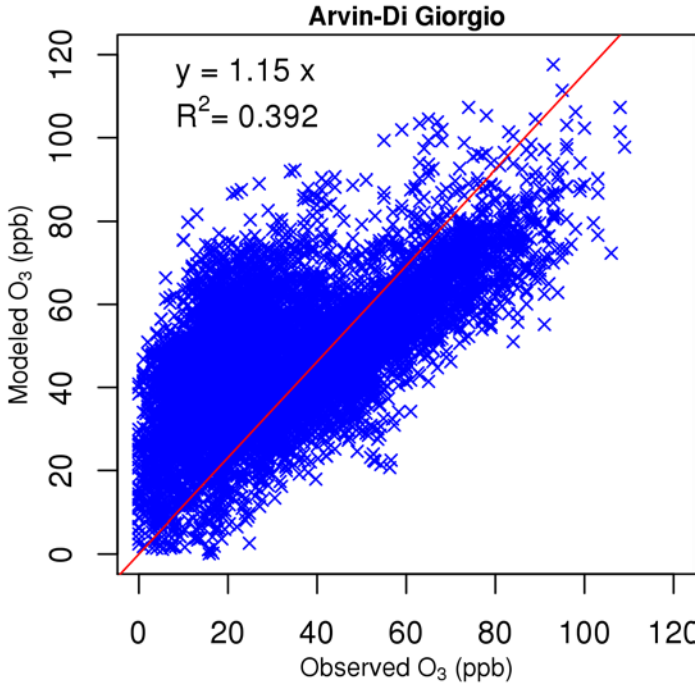

Figure S. 88 Scattering plot of observed and modeled 1-hour O_3 mixing ratio at Arvin

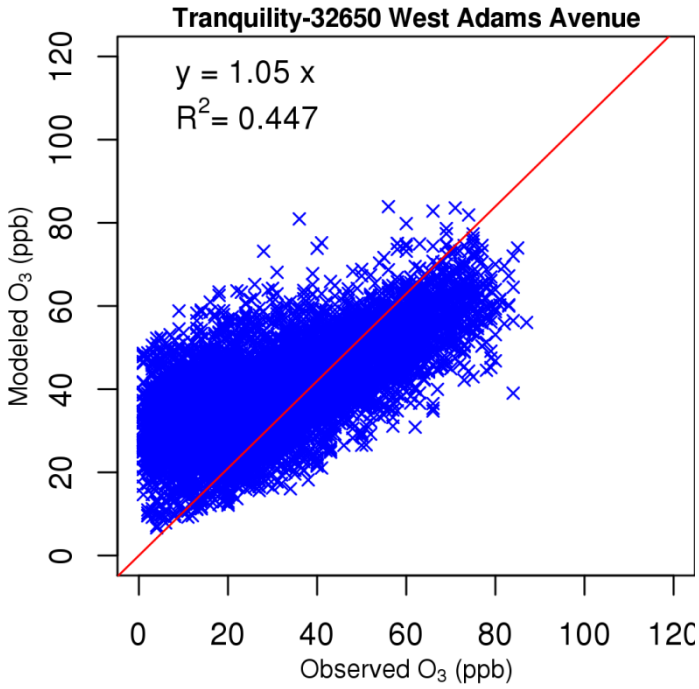

Figure S. 89 Scattering plot of observed and modeled 1-hour O_3 mixing ratio at Tranquility

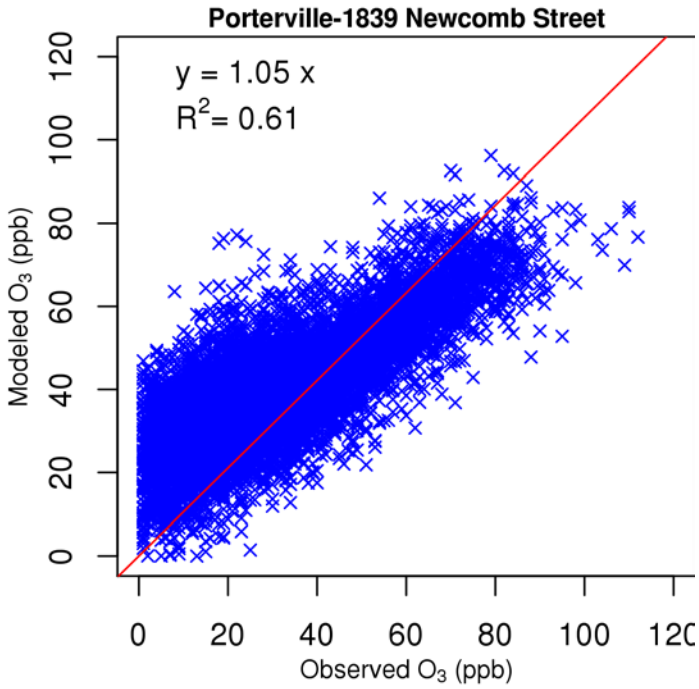

Figure S. 90 Scattering plot of observed and modeled 1-hour O_3 mixing ratio at Porterville

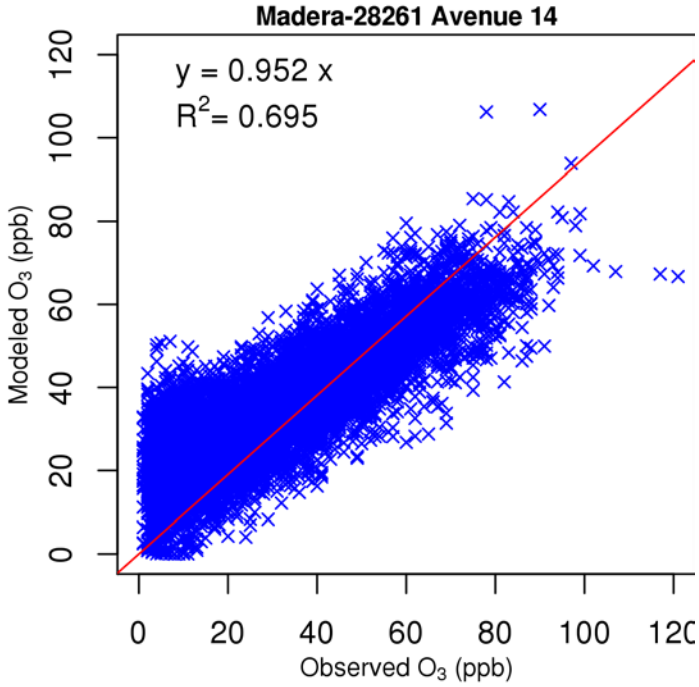

Figure S. 91 Scattering plot of observed and modeled 1-hour O_3 mixing ratio at Madera – 28261 Avenue 14

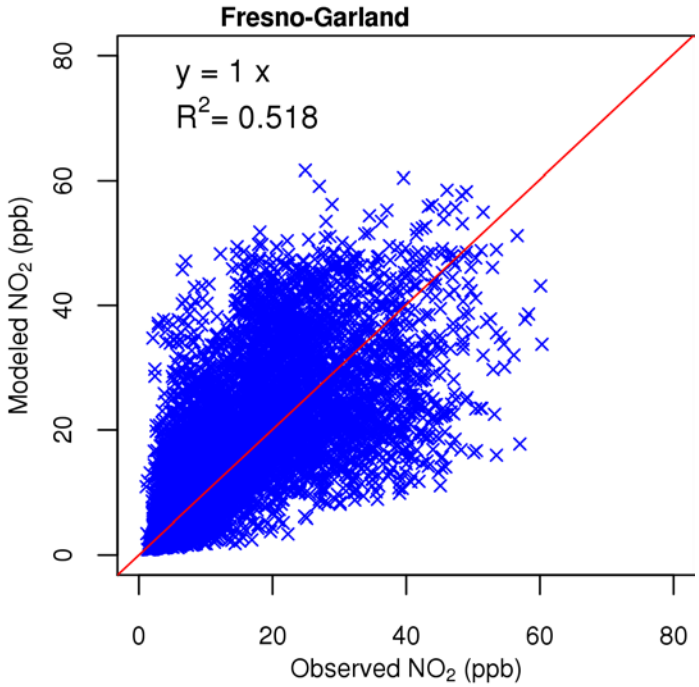

Figure S. 92 Scattering plot of observed and modeled 1-hour O_3 mixing ratio at Fresno-Garland

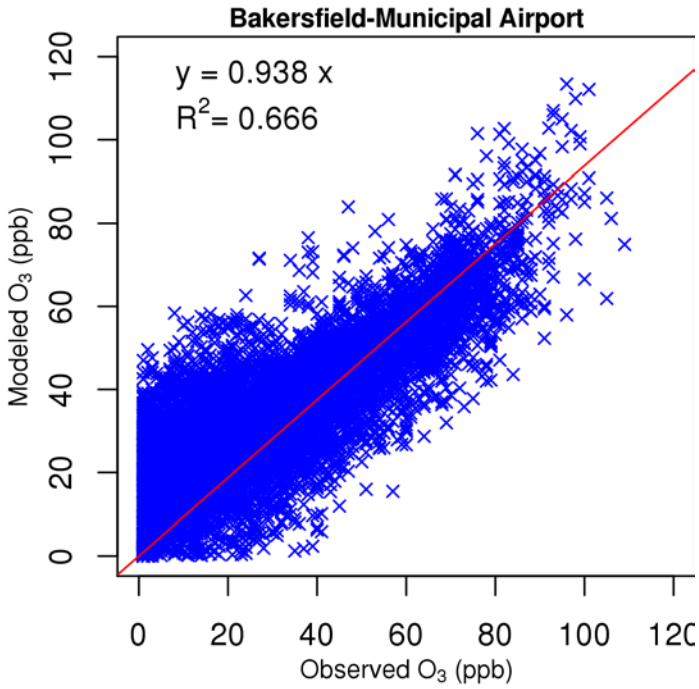

Figure S. 93 Scattering plot of observed and modeled 1-hour O_3 mixing ratio at Bakersfield – Municipal airport

PHOTOCHEMICAL MODELING PROTOCOL

Photochemical Modeling for the 8-Hour Ozone and Annual/24-hour $PM_{2.5}$ State Implementation Plans

Prepared by

California Air Resources Board

Prepared for

United States Environmental Protection Agency Region IX

July 26, 2016

TABLE OF CONTENTS

1. INTRODUCTION 9
1.1 Modeling roles for the current SIP 9
1.2 Stakeholder participation 9
1.3 Involvement of external scientific/technical experts and their input on the photochemical modeling 10
1.4 Schedule for completion of the Plan 11
2. DESCRIPTION OF THE CONCEPTUAL MODEL FOR THE NONATTAINMENT AREA 11
3. SELECTION OF MODELING PERIODS 11
3.1 Reference Year Selection and Justification 11
3.2 Future Year Selection and Justification 12
3.3 Justification for Seasonal/Annual Modeling Rather than Episodic Modeling 13
4. DEVELOPMENT OF EMISSION INVENTORIES 14
5. MODELS AND INPUTS 14
5.1 Meteorological Model 14
5.1.1 Meteorological Modeling Domain 15
5.2 Photochemical Model 18
5.2.1 Photochemical Modeling Domain 20
5.2.2 CMAQ Model Options 22
5.2.3 Photochemical Mechanism 22
5.2.4 Aerosol Module 23
5.2.5 CMAQ Initial and Boundary Conditions (IC/BC) and Spin-Up period 24
5.3 Quality Assurance of Model Inputs 26
6. METEOROLOGICAL MODEL PERFORMANCE 27
6.1 Ambient Data Base and Quality of Data 27
6.2 Statistical Evaluation 27
6.3 Phenomenological Evaluation 29
7. PHOTOCHEMICAL MODEL PERFORMANCE 29
7.1 Ambient Data 29
7.2 Statistical Evaluation 31

7.3 Comparison to Previous Modeling Studies 33
7.4 Diagnostic Evaluation 33
8. ATTAINMENT DEMONSTRATION 34
8.1 Base Year Design Values 34
8.2 Base, Reference, and Future Year Simulations 35
8.3 Relative Response Factors 36
8.3.1 8-hour Ozone RRF 36
8.3.2 Annual and 24-hour $PM_{2.5}$ RRF 37
8.4 Future Year Design Value Calculation 38
8.4.1 8-hour Ozone 38
8.4.2 Annual and 24-hour $PM_{2.5}$ 38
8.5 Unmonitored Area Analysis 45
8.5.1 8-hour Ozone 45
8.5.2 Annual $PM_{2.5}$ 46
8.5.3 24-hour $PM_{2.5}$ 47
8.6 Banded Relative Response Factors for Ozone 48
9. PROCEDURAL REQUIREMENTS 49
9.1 How Modeling and other Analyses will be Archived, Documented, and Disseminated 49
9.2 Specific Deliverables to U.S. EPA 49
REFERENCES 50

LIST OF FIGURES

Figure 5-1. The three nested grids for the WRF model (D01 36km; D02 12km; and D03 4km). 16

Figure 5-2. CMAQ modeling domains used in this SIP modeling platform. The outer domain (dashed black line) represents the extent of the California statewide domain (shown here with a 4 km horizontal resolution, but utilized in this modeling platform with a 12 km horizontal resolution). Nested higher resolution 4 km modeling domains are highlighted in green and red for the Northern/Central California and Southern California, respectively. The smaller SJV $PM_{2.5}$ 4 km domain (colored in blue) is nested within the Northern California 4 km domain..... 21

Figure 5-3. Comparison of MOZART (red) simulated CO (left), ozone (center), and PAN (right) to observations (black) along the DC-8 flight track. Shown are mean (filled symbol), median (open symbols), 10th and 90th percentiles (bars) and extremes (lines). The number of data points per 1-km wide altitude bin is shown next to the graphs. Adapted from Figure 2 in Pfister et al. (2011)..... 25

Figure 8-1. Example showing how the location of the MDA8 ozone for the top ten days in the reference and future years are chosen..... 37

LIST OF TABLES

Table 3-1. Future attainment year by non-attainment region and NAAQS. 0.08 ppm and 0.075 ppm refer to the 1997 and 2008 8-hour ozone standards, respectively. 15 ug/m^3 and 12 ug/m^3 refer to the 1997 and 2012 annual $PM_{2.5}$ standards, respectively. 35 ug/m^3 refers to the 2006 24-hour $PM_{2.5}$ standard, and 1-hr ozone refers to the revoked 1979 0.12 ppm 1-hour ozone standard. 13

Table 5-1. WRF vertical layer structure. 17

Table 5-2. WRF Physics Options. 18

Table 5-3. CMAQ v5.0.2 configuration and settings. 22

Table 7-1. Monitored species used in evaluating model performance. 30

Table 8-1. Illustrates the data from each year that are utilized in the Design Value calculation for that year (DV Year), and the yearly weighting of data for the weighted Design Value calculation (or DV_R). "obs" refers to the observed metric (8-hr O_3, 24-hour $PM_{2.5}$, or annual average $PM_{2.5}$). 35

ACRONYMS

ARB – Air Resources Board

ARCTAS-CARB – California portion of the Arctic Research of the Composition of the Troposphere from Aircraft and Satellites conducted in 2008

BCs – Boundary Conditions

CalNex – Research at the Nexus of Air Quality and Climate Change conducted in 2010

CCOS - Central California Ozone Study

CMAQ Model – Community Multi-scale Air Quality Model

CIT – California Institute of Technology

CRPAQS – California Regional PM_{10}/$PM_{2.5}$ Air Quality Study

DISCOVER-AQ - Deriving Information on Surface Conditions from Column and Vertically Resolved Observations Relevant to Air Quality

DV – Design Value

FDDA – Four-Dimensional Data Assimilation

FEM – Federal Equivalence Monitors

FRM – Federal Reference Monitors

HNO_3 – Nitric Acid

ICs – Initial Conditions

IMPROVE – Interagency Monitoring of Protected Visual Environments

IMS-95 – Integrated Monitoring Study of 1995

LIDAR – Light Detection And Ranging

MDA – Maximum Daily Average

MM5 – Mesoscale Meteorological Model Version 5

MOZART – Model for Ozone and Related chemical Tracers

NARR - North American Regional Reanalysis

NCAR – National Center for Atmospheric Research

NCEP – National Centers for Environmental Prediction

NH_3 – Ammonia

NOAA - National Oceanic and Atmospheric Administration

NO_x – Oxides of nitrogen

OC – Organic Carbon

OFP - Ozone Forming Potential

PAMS – Photochemical Assessment Monitoring Stations

PAN – Peroxy Acetyl Nitrate

$PM_{2.5}$ – Particulate Matter with aerodynamic diameter less than 2.5 micrometers

PM_{10} – Particulate Matter with aerodynamic diameter less than 10 micrometers

RH – Relative Humidity

ROG – Reactive Organic Gases

RRF – Relative Response Factor

RSAC – Reactivity Scientific Advisory Committee

SANDWICH – Application of the Sulfate, Adjusted Nitrate, Derived Water, Inferred Carbonaceous Material Balance Approach

SAPRC – Statewide Air Pollution Research Center

SARMAP – SJVAQS/AUSPEX Regional Modeling Adaptation Project

SCAQMD – South Coast Air Quality Management District

SIP – State Implementation Plan

SJV – San Joaquin Valley

SJVAB – San Joaquin Valley Air Basin (SJVAB)

SJVUAPCD – San Joaquin Valley Unified Air Pollution Control District

SJVAQS/AUSPEX – San Joaquin Valley Air Quality Study/Atmospheric Utilities Signatures Predictions and Experiments

SLAMS – State and Local Air Monitoring Stations

SMAQMD – Sacramento Metropolitan Air Quality Management District

SMAT – Application of the Speciated Modeled Attainment Test

SOA – Secondary Organic Aerosol

SO_x – Oxides of Sulfur

STN – Speciated Trend Network

UCD – University of California at Davis

U.S. EPA – United States Environmental Protection Agency

VOC – Volatile Organic Compounds

WRF Model – Weather and Research Forecast Model

1. INTRODUCTION

The purpose of this modeling protocol is to detail and formalize the procedures for conducting the photochemical modeling that forms the basis of the attainment demonstration for the 8-hour ozone and annual/24-hour $PM_{2.5}$ State Implementation Plans (SIPs) for California. The protocol is intended to communicate up front how the model attainment test will be performed. In addition, this protocol discusses analyses that are intended to help corroborate the findings of the model attainment test.

1.1 Modeling roles for the current SIP

The Clean Air Act (Act) establishes the planning requirements for all those areas that routinely exceed the health-based air quality standards. These nonattainment areas must adopt and implement a SIP that demonstrates how they will attain the standards by specified dates. Air quality modeling is an important technical component of the SIP, as it is used in combination with other technical information to project the attainment status of an area and to develop appropriate emission control strategies to achieve attainment.

ARB and local Air Districts will jointly develop the emission inventories, which are an integral part of the modeling. Working closely with the Districts, the ARB will perform the meteorological and air quality modeling. Districts will then develop and adopt their local air quality plan. Upon approval by the ARB, the SIP will be submitted to U.S.EPA for approval.

1.2 Stakeholder participation

Public participation constitutes an integral part of the SIP development. It is equally important in all technical aspects of SIP development, including the modeling. As the SIP is developed, the Air Districts and ARB will hold public workshops on the modeling and other SIP elements. Representatives from the private sector, environmental interest groups, academia, and the federal, state, and local public sectors are invited to attend and provide comments. In addition, Draft Plan documents will be available for public review and comment at various stages of plan development and at least 30 days before Plan consideration by the Districts' Governing Boards and subsequently by the ARB Board. These documents will include descriptions of the technical aspects of the SIP. Stakeholders have the choice to provide written and in-person comments at any of the Plan workshops and public Board hearings. The agencies take the comments into consideration when finalizing the Plan.

1.3 Involvement of external scientific/technical experts and their input on the photochemical modeling

During the development of the modeling protocol for the 2012 SJV 24-hour $PM_{2.5}$ SIP (SJVUAPCD, 2012), ARB and the San Joaquin Valley Air Pollution Control District (SJVAPCD) engaged a group of experts on prognostic meteorological modeling and photochemical/aerosol modeling to help prepare the modeling protocol document.

The structure of the technical expert group was as follows:

Conveners: John DaMassa – ARB
Samir Sheikh – SJVAPCD
Members: Scott Bohning – U.S. EPA Region 9
Ajith Kaduwela – ARB
James Kelly – U.S. EPA Office of Air Quality Planning and Standards
Michael Kleeman – University of California at Davis
Jonathan Pleim – U.S. EPA Office of Research and Development
Anthony Wexler – University of California at Davis

The technical consultant group provided technical consultations/guidance to the staff at ARB and SJVAPCD during the development of the protocol. Specifically, the group provided technical expertise on the following components of the protocol:

- Selection of the physics and chemistry options for the prognostic meteorological and photochemical air quality models
- Selection of methods to prepare initial and boundary conditions for the air quality model
- Performance evaluations of both prognostic meteorological and photochemical air quality models. This includes statistical, diagnostic, and phenomenological evaluations of simulated results.
- Selection of emissions profiles (size and speciation) for particulate-matter emissions.
- Methods to determine the limiting precursors for $PM_{2.5}$ formation.
- Application of the Sulfate, Adjusted Nitrate, Derived Water, Inferred Carbonaceous Material Balance Approach (SANDWICH) with potential modifications.
- Application of the Speciated Modeled Attainment Test (SMAT).
- Selection of methodologies for the determination of $PM_{2.5}$ precursor equivalency ratios.
- Preparation of Technical Support Documents.

The current approach to regional air quality modeling has not changed significantly since the 2012 SJV 24-hour $PM_{2.5}$ SIP (SJVUAPCD, 2012), so the expertise provided on the above components to the protocol remain highly relevant. In addition, since regional air quality modeling simulates ozone chemistry and PM chemistry/formation simultaneously, there is generally no difference in how the models are configured and simulations conducted for ozone vs. PM. Therefore, development of this modeling protocol will rely heavily on the recommendations made by this group of technical experts, as well as recently published work in peer-review journals related to regional air quality modeling.

1.4 Schedule for completion of the Plan

Final area designations kick-off the three year SIP development process. For the first two years, efforts center on updates and improvements to the Plan's technical and scientific underpinnings. These include the development of emission inventories, selection of modeling periods, model selection, model input preparation, model performance evaluation and supplemental analyses. During the last year, modeling, further supplemental analyses and control strategy development proceed in an iterative manner and the public participation process gets under way. After thorough review the District Board and subsequently the ARB Board consider the Plan. The Plan is then submitted to U.S. EPA. Table 1-1 in the Appendix corresponding to the appropriate region/standard (e.g., SJV 0.075 ppm 8-hour ozone) summarizes the overall anticipated schedule for Plan completion.

2. DESCRIPTION OF THE CONCEPTUAL MODEL FOR THE NONATTAINMENT AREA

See Section 2 in the Appendix corresponding to the appropriate region/standard (e.g., SJV 0.075 ppm 8-hour ozone).

3. SELECTION OF MODELING PERIODS

3.1 Reference Year Selection and Justification

From an air quality and emissions perspective, ARB and the Districts have selected 2012 as the base year for design value calculation and for the modeled attainment test.

For the SJV, the $PM_{2.5}$ model attainment test will utilize 2013 instead of 2012. These baseline values will serve as the anchor point for estimating future year projected design values.

The selection of 2012/13 is based on the following four considerations:

- Most complete and up to date emissions inventory, which reduces the uncertainty associated with future emissions projections.
- Analysis of meteorological adjusted air quality trends to determine recent years with meteorology most conducive to ozone and $PM_{2.5}$ formation and buildup.
- Availability of research-grade wintertime field measurements in the Valley, which captured two significant pollution episodes during the DISCOVER-AQ field study (January-February 2013).
- The SJV $PM_{2.5}$ design values for year 2013 were some of the highest in recent years, making 2013 a conservative choice for attainment demonstration modeling.

Details and discussion on these analyses can be found in the Weight of Evidence Appendix.

3.2 Future Year Selection and Justification

The future year modeled is determined by the year for which attainment must be demonstrated. Table 3-1 lists the year in which attainment must be demonstrated for the various ozone and $PM_{2.5}$ standards and non-attainment regions in California.

Table 3-1. Future attainment year by non-attainment region and NAAQS. 0.08 ppm and 0.075 ppm refer to the 1997 and 2008 8-hour ozone standards, respectively. 15 ug/m^3 and 12 ug/m^3 refer to the 1997 and 2012 annual $PM_{2.5}$ standards, respectively. 35 ug/m^3 refers to the 2006 24-hour $PM_{2.5}$ standard, and 1-hr ozone refers to the revoked 1979 0.12 ppm 1-hour ozone standard.

Area	Year								
	2031	2026	2025	2024	2023	2021	2020	2019	2017
Southern California Modeling Domain									
South Coast	0.075 ppm	--	--	--	0.08 ppm	12 µg/m^3	--	--	--
Mojave/Coachella	--	0.075 ppm	--	--	--	--	--	--	0.08 ppm
Imperial County	--	--	--	--	--	12 µg/m^3	--	--	0.075 ppm
Ventura County	--	--	--	--	--	--	0.075 ppm	--	--
San Diego	--	--	--	--	--	--	--	--	0.075 ppm
Northern California Modeling Domain									
San Joaquin Valley	0.075 ppm	--	[1]12 µg/m^3	35 µg/m^3	--	[2]12 µg/m^3	15 µg/m^3	35 µg/m^3	1-hr ozone
Sacramento Metropolitan	--	0.075 ppm	--	--	--	--	--	--	--
Portola-Plumas County	--	--	--	--	--	12 µg/m^3	--	--	--
East Kern	--	--	--	--	--	--	--	--	0.075 ppm
W. Nevada County	--	--	--	--	--	--	--	--	0.075 ppm

[1] Serious classification attainment date

[2] Moderate classification attainment date

3.3 Justification for Seasonal/Annual Modeling Rather than Episodic Modeling

In the past, computational constraints restricted the time period modeled for a SIP attainment demonstration to a few episodes (e.g., 2007 SJV 8-hr ozone SIP (SJVUAPCD, 2007), 2007 SC 8-hr ozone SIP (SCAQMD, 2012) and 2009 Sacramento 8-hr ozone SIP (SMAQMD, 2012)). However, as computers have become faster and

large amounts of data storage have become readily accessible, there is no longer a need to restrict modeling periods to only a few episodes. In more recent years, SIP modeling in California has covered the entire ozone or peak $PM_{2.5}$ seasons (2012 SC 8-hour ozone and 24-hour $PM_{2.5}$ SIP (SCAQMD, 2012), 2012 SJV 24-hour $PM_{2.5}$ SIP (SJVUAPCD, 2012) and 2013 SJV 1-hr ozone SIP (SJVUAPCD,2013)), or an entire year in the case of annual $PM_{2.5}$ (2008 SJV annual $PM_{2.5}$ SIP (SJVUAPCD, 2008)) The same is true for other regulatory modeling platforms outside of California (Boylan and Russell, 2006; Morris et al., 2006; Rodriguez et al., 2009; Simon et al., 2012; Tesche et al., 2006; U.S. EPA, 2011a, b).

Recent ozone based studies, which focused on model performance evaluation for regulatory assessment, have recommended the use of modeling results covering the full synoptic cycles and full ozone seasons (Hogrefe et al., 2000; Vizuete et al., 2011). This enables a more complete assessment of ozone response to emission controls under a wide range of meteorological conditions. The same is true for modeling conducted for peak 24-hour $PM_{2.5}$. Consistent with the shift to seasonal or annual modeling in most regulatory modeling applications, modeling for the 8-hour ozone standard will cover the entire ozone season (May – September), modeling for the annual 24-hour $PM_{2.5}$ standard will be conducted for the entire year, and modeling for the 24-hour $PM_{2.5}$ standard will, at a minimum, cover the months in which peak 24-hour $PM_{2.5}$ occurs (e.g., October – March in the SJV) and will be conducted annually whenever possible.

4. DEVELOPMENT OF EMISSION INVENTORIES

For a detailed description of the emissions inventory, updates to the inventory, and how it was processed from the planning totals to a gridded inventory for modeling, see the Modeling Emissions Inventory Appendix.

5. MODELS AND INPUTS

5.1 Meteorological Model

Meteorological model selection is based on a need to accurately simulate the synoptic and mesoscale meteorological features observed during the selected modeling period. The main difficulties in accomplishing this are California's extremely complex terrain and its diverse climate. It is desirable that atmospheric modeling adequately represent essential meteorological fields such as wind flows, ambient temperature variation, evolution of the boundary layer, and atmospheric moisture content to properly characterize the meteorological component of photochemical modeling.

In the past, the ARB has applied prognostic, diagnostic, and hybrid models to prepare meteorological fields for photochemical modeling. There are various numerical models that are used by the scientific community to study the meteorological characteristics of an air pollution episode. For this SIP modeling platform, the Weather and Research Forecasting (WRF) model (Skaramock et al, 2005) will be used to develop the meteorological fields that drive the photochemical modeling. The U.S. EPA (2014) recommends the use of a well-supported grid-based mesoscale meteorological model for generating meteorological inputs. The WRF model is a community-based mesoscale prediction model, which represents the state-of-the-science and has a large community of model users and developers who frequently update the model as new science becomes available. In recent years, WRF has been applied in California to generate meteorological fields for numerous air quality studies (e.g., Angevine, et al., 2012; Baker et al., 2015; Ensberg et al., 2013; Fast et al., 2014; Hu et al., 2014a, 2014b; Huang et al., 2010; Kelly et al., 2014; Lu et al., 2012; Mahmud et al., 2010), and has been shown to reasonably reproduce the observed meteorology in California.

5.1.1 Meteorological Modeling Domain

The WRF meteorological modeling domain consists of three nested grids of 36 km, 12 km and 4 km uniform horizontal grid spacing (illustrated in Figure 5-1). The purpose of the coarse, 36 km grid (D01) is to provide synoptic-scale conditions to all three grids, while the 12 km grid (D02) is used to provide finer resolution data that feeds into the 4 km grid (D03). The D01 grid is centered at 37 ˚N and 120.5 ˚W and was chosen so that the inner two grids, D02 and D03, would nest inside of D03 and be sufficiently far away from the boundaries to minimize boundary influences. The D01 grid consists of 90 x 90 grid cells, while the D02 and D03 grids encompass 192 x 192 and 327 x 297 grid cells, respectively, with an origin at -696 km x -576 km (Lambert Conformal projection). WRF will be run for the three nested domains simultaneously with two-way feedback between the parent and the nest grids. The D01 and D02 grids are meant to resolve the larger scale synoptic weather systems, while the D03 grid is intended to resolve the finer details of the atmospheric conditions and will be used to drive the air quality model simulations. All three domains will utilize 30 vertical sigma layers (defined in Table 5-1), as well as the various physics options listed in Table 5-2 for each domain.
The initial and boundary conditions (IC/BCs) for WRF will be prepared based on 3-D North American Regional Reanalysis (NARR) data that are archived at the National Center for Atmospheric Research (NCAR). These data have a 32 km horizontal resolution. Boundary conditions to WRF are updated at 6-hour intervals for the 36 km grid (D01). In addition, surface and upper air observations obtained from NCAR will be used to further refine the analysis data that are used to generate the IC/BCs. Analysis

nudging will be employed in the outer 36km grid (D01) to ensure that the simulated meteorological fields are constrained and do not deviate from the observed meteorology.

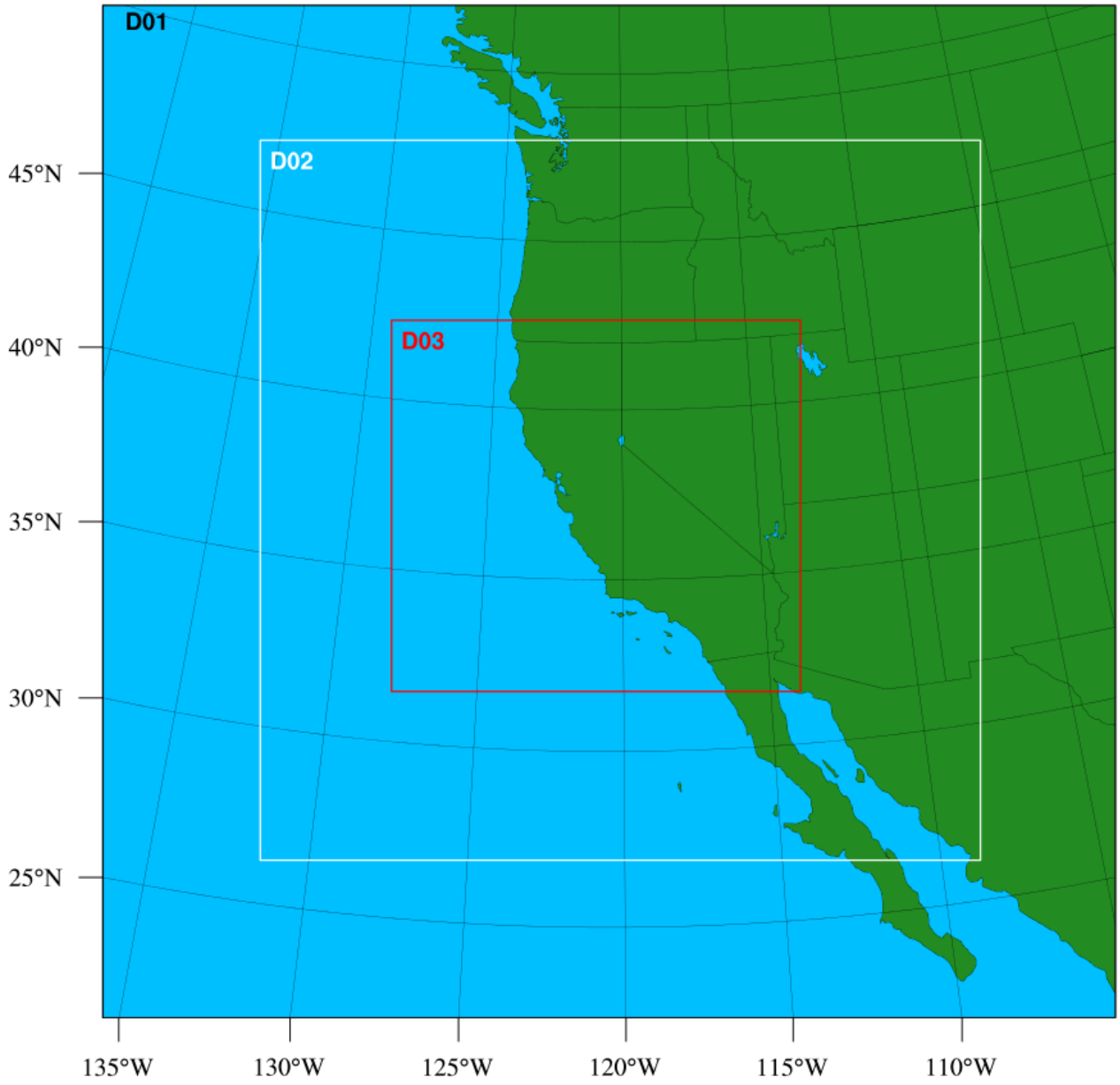

Figure 5-1. The three nested grids for the WRF model (D01 36km; D02 12km; and D03 4km).

Table 5-1. WRF vertical layer structure.

Layer Number	Height (m)	Layer Thickness (m)	Layer Number	Height (m)	Layer Thickness (m)
30	16082	1192	14	1859	334
29	14890	1134	13	1525	279
28	13756	1081	12	1246	233
27	12675	1032	11	1013	194
26	11643	996	10	819	162
25	10647	970	9	657	135
24	9677	959	8	522	113
23	8719	961	7	409	94
22	7757	978	6	315	79
21	6779	993	5	236	66
20	5786	967	4	170	55
19	4819	815	3	115	46
18	4004	685	2	69	38
17	3319	575	1	31	31
16	2744	482	0	0	0
15	2262	403			

Note: Shaded layers denote the subset of vertical layers to be used in the CMAQ photochemical model simulations. Further details on the CMAQ model configuration and settings can be found in subsequent sections.

Table 5-2. WRF Physics Options.

Physics Option	Domain		
	D01 (36 km)	D02 (12 km)	D03 (4 km)
Microphysics	WSM 6-class graupel scheme	WSM 6-class graupel scheme	WSM 6-class graupel scheme
Longwave radiation	RRTM	RRTM	RRTM
Shortwave radiation	Dudhia scheme	Dudhia scheme	Dudhia scheme
Surface layer	Revised MM5 Monin-Obukhov	Revised MM5 Monin-Obukhov	Revised MM5 Monin-Obukhov
Land surface	Pleim-Xiu LSM	Pleim-Xiu LSM	Pleim-Xiu LSM
Planetary Boundary Layer	YSU	YSU	YSU
Cumulus Parameterization	Kain-Fritsch scheme	Kain-Fritsch scheme	None

5.2 Photochemical Model

The U.S. EPA modeling guidance (U.S. EPA, 2014) requires several factors to be considered as criteria for choosing a qualifying air quality model to support the attainment demonstration. These criteria include: (1) It should have received a scientific peer review; (2) It should be appropriate for the specific application on a theoretical basis; (3) It should be used with databases which are available and adequate to support its application; (4) It should be shown to have performed well in past modeling applications; and (5). It should be applied consistently with an established protocol on methods and procedures (U.S. EPA, 2014). In addition, it should be well documented with a user's guide as well as technical descriptions. For the ozone modeled attainment test, a grid-based photochemical model is necessary to offer the best available representation of important atmospheric processes and the ability to analyze the impacts of proposed emission controls on ozone mixing ratios. In ARB's SIP modeling platform, the Community Multiscale Air Quality (CMAQ) Modeling System has been selected as the air quality model for use in attainment demonstrations of NAAQS for ozone and $PM_{2.5}$.

The CMAQ model, a state-of-the-science "one-atmosphere" modeling system developed by U.S. EPA, was designed for applications ranging from regulatory and policy analysis to investigating the atmospheric chemistry and physics that contribute to air pollution. CMAQ is a three-dimensional Eulerian modeling system that simulates ozone, particulate matter, toxic air pollutants, visibility, and acidic pollutant species throughout the troposphere (UNC, 2010). The model has undergone peer review every

few years and represents the state-of-the-science (Brown et al., 2011). The CMAQ model is regularly updated to incorporate new chemical and aerosol mechanisms, algorithms, and data as they become available in the scientific literature (e.g., Appel et al., 2013; Foley, et al., 2010; Pye and Pouliot, 2012;). In addition, the CMAQ model is well documented in terms of its underlying scientific algorithms as well as guidance on operational uses (e.g., Appel et al., 2013; Binkowski and Roselle, 2003; Byun and Ching, 1999; Byun and Schere, 2006; Carlton et al., 2010; Foley et al., 2010; Kelly, et al., 2010a; Pye and Pouliot, 2012; UNC, 2010).

The CMAQ model was the regional air quality model used for the 2008 SJV annual $PM_{2.5}$ SIP (SJVUAPCD, 2008), the 2012 SJV 24-hour $PM_{2.5}$ SIP (SJVUAPCD, 2012) and the 2013 SJV 1-hr ozone SIP (SJVUAPCD, 2013). A number of previous studies have also used the CMAQ model to study ozone and $PM_{2.5}$ formation in the SJV (e.g., Jin et al., 2008, 2010b; Kelly et al., 2010b; Liang and Kaduwela, 2005; Livingstone, et al., 2009; Pun et al, 2009; Tonse et al., 2008; Vijayaraghavan et al., 2006; Zhang et al., 2010). The CMAQ model has also been used for regulatory analysis for many of U.S. EPA's rules, such as the Clean Air Interstate Rule (U.S. EPA, 2005) and Light-duty and Heavy-duty Greenhouse Gas Emissions Standards (U.S. EPA, 2010, 2011a). There have been numerous applications of the CMAQ model within the U.S. and abroad (e.g., Appel, et al., 2007, 2008; Civerolo et al., 2010; Eder and Yu, 2006; Hogrefe et al., 2004; Lin et al., 2008, 2009; Marmur et al., 2006; O'Neill, et al., 2006; Philips and Finkelstein, 2006; Smyth et al., 2006; Sokhi et al., 2006; Tong et al., 2006; Wilczak et al., 2009; Zhang et al., 2004, 2006), which have shown it to be suitable as a regulatory and scientific tool for investigating air quality. Staff at the CARB has developed expertise in applying the CMAQ model, since it has been used at CARB for over a decade. In addition, technical support for the CMAQ model is readily available from the Community Modeling and Analysis System (CMAS) Center (http://www.cmascenter.org/) established by the U.S. EPA.

The version 5.0.2 of the CMAQ model released in May 2014, (http://www.airqualitymodeling.org/cmaqwiki/index.php?title=CMAQ_version_5.0.2_%28April_2014_release%29_Technical_Documentation), will be used in this SIP modeling platform. Compared to the previous version, CMAQv4.7.1, which was used for the 2012 SJV 24-hour $PM_{2.5}$ SIP (SJVUAPCD, 2012) and the 2013 SJV 1-hour ozone SIP (SJVUAPCD, 2013), CMAQ version 5 and above incorporated substantial new features and enhancements to topics such as gas-phase chemistry, aerosol algorithms, and structure of the numerical code (http://www.airqualitymodeling.org/cmaqwiki/index.php?title=CMAQ_version_5.0_%28February_2012_release%29_Technical_Documentation#RELEASE_NOTES_for_CMAQv5.0_-.C2.A0February_2012).

5.2.1 Photochemical Modeling Domain

Figure 5-2 shows the photochemical modeling domains used by ARB in this modeling platform. The larger domain (dashed black colored box), covering all of California, has a horizontal grid resolution of 12 km and extends from the Pacific Ocean in the west to Eastern Nevada in the east and runs from south of the U.S.-Mexico border in the south to north of the California-Oregon border in the north. The smaller 4 km Northern (green box) and Southern (red box) modeling domains are nested within the outer 12 km domain and utilized to better reflect the finer scale details of meteorology, topography, and emissions. Consistent with the WRF modeling, the 12 km and 4 km CMAQ domains are based on a Lambert Conformal Conic projection with reference longitude at -120.5°W, reference latitude at 37°N, and two standard parallels at 30°N and 60°N. The 30 vertical layers from WRF were mapped onto 18 vertical layers for CMAQ, extending from the surface to 100 mb such that the majority of the vertical layers fall within the planetary boundary layer. This vertical layer structure is based on the WRF sigma-pressure coordinates and the exact layer structure used can be found in Table 5-1. A third 4 km resolution modeling domain (blue box) is nested within the Northern California domain and covers the SJV air basin. This smaller SJV domain may be utilized for $PM_{2.5}$ modeling in the SJV if computational constraints (particularly for annual modeling) require the use of a smaller modeling domain. In prior work, modeling results from the smaller SJV domain were compared to results from the larger Northern California domain and no appreciable differences were noted, provided that both simulations utilized chemical boundary conditions derived from the same statewide 12 km simulation.

For the coarse portions of nested regional grids, the U.S. EPA guidance (U.S. EPA, 2014) suggests a grid cell size of 12 km if feasible but not larger than 36 km. For the fine scale portions of nested regional grids, it is desirable to use a grid cell size of ~4 km (U.S. EPA, 2014). Our selection of modeling domains and grid resolution is consistent with this recommendation. The U.S. EPA guidance (U.S. EPA, 2014) does not require a minimum number of vertical layers for an attainment demonstration, although typical applications of “one- atmosphere” models (with the model top at 50-100 mb) are anywhere from 14 to 35 vertical layers. In the ARB’s current SIP modeling platform, 18 vertical layers will be used in the CMAQ model. The vertical structure is based on the sigma-pressure coordinate, with the layers separated at 1.0, 0.9958, 0.9907, 0.9846, 0.9774, 0.9688, 0.9585, 0.9463, 0.9319, 0.9148, 0.8946, 0.8709, 0.8431, 0.8107, 0.7733, 0.6254, 0.293, 0.0788, and 0.0. As previously noted, this also ensures that the majority of the layers are in the planetary boundary layer.

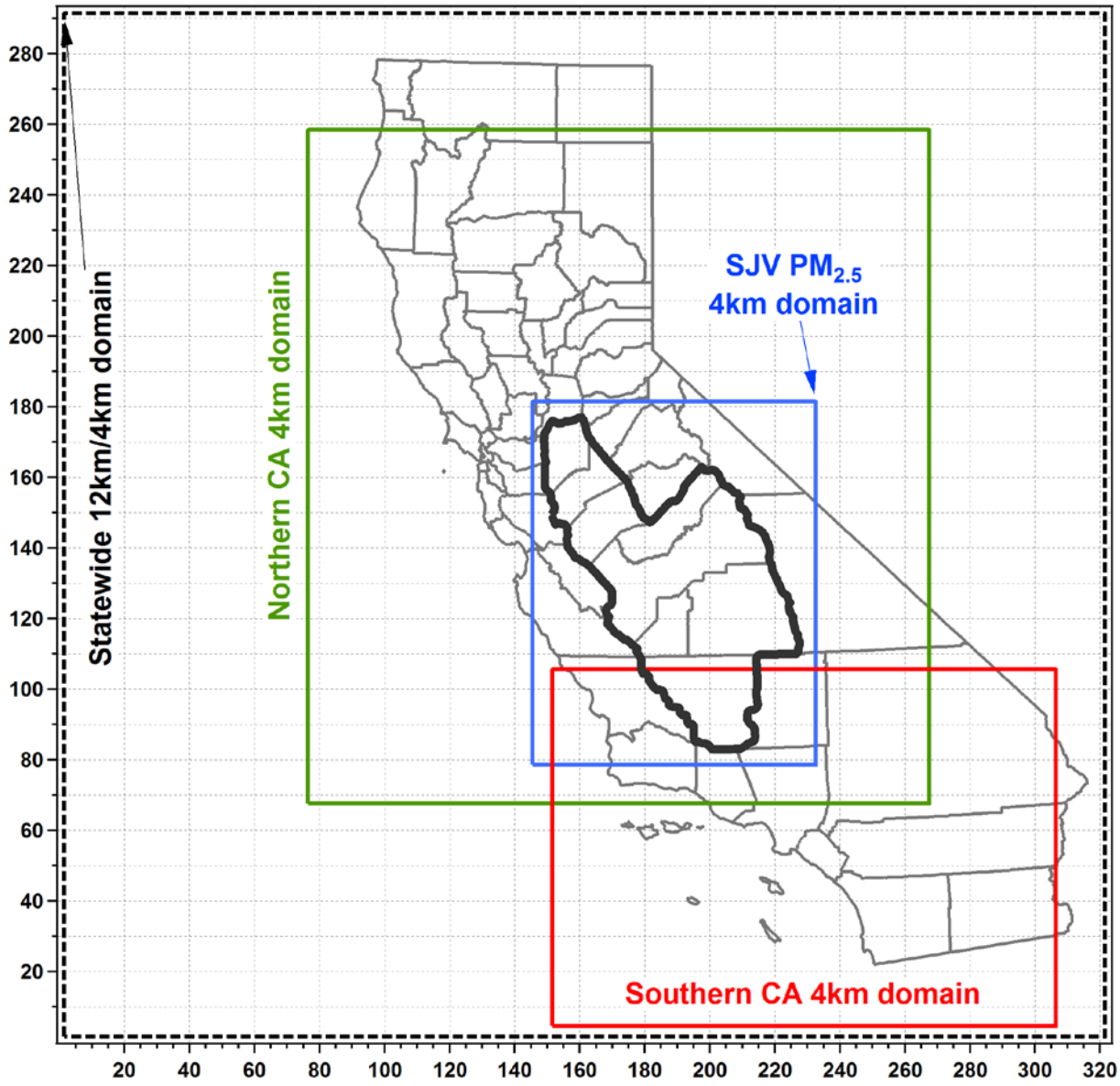

Figure 5-2. CMAQ modeling domains used in this SIP modeling platform. The outer domain (dashed black line) represents the extent of the California statewide domain (shown here with a 4 km horizontal resolution, but utilized in this modeling platform with a 12 km horizontal resolution). Nested higher resolution 4 km modeling domains are highlighted in green and red for Northern/Central California and Southern California, respectively. The smaller SJV $PM_{2.5}$ 4 km domain (colored in blue) is nested within the Northern California 4 km domain.

5.2.2 CMAQ Model Options

Table 5-3 shows the CMAQv5.0.2 configuration utilized in this modeling platform. The same configuration will be used in all simulations for both ozone and $PM_{2.5}$, and for all modeled years. The Intel FORTRAN compiler version 12 will be used to compile all source codes.

Table 5-3. CMAQ v5.0.2 configuration and settings.

Process	Scheme
Horizontal advection	Yamo (Yamartino scheme for mass-conserving advection)
Vertical advection	WRF-based scheme for mass-conserving advection
Horizontal diffusion	Multi-scale
Vertical diffusion	ACM2 (Asymmetric Convective Model version 2)
Gas-phase chemical mechanism	SAPRC07 gas-phase mechanism with version "C" toluene updates
Chemical solver	EBI (Euler Backward Iterative solver)
Aerosol module	Aero6 (the sixth-generation CMAQ aerosol mechanism with extensions for sea salt emissions and thermodynamics; includes a new formulation for secondary organic aerosol yields)
Cloud module	ACM_AE6 (ACM cloud processor that uses the ACM methodology to compute convective mixing with heterogeneous chemistry for AERO6)
Photolysis rate	phot_inline (calculate photolysis rates in-line using simulated aerosols and ozone)

5.2.3 Photochemical Mechanism

The SAPRC07 chemical mechanism will be utilized for all CMAQ simulations. SAPRC07, developed by Dr. William Carter at the University of California, Riverside, is a detailed mechanism describing the gas-phase reactions of volatile organic compounds (VOCs) and oxides of nitrogen (NO_x) (Carter, 2010a, 2010b). It represents a complete update to the SAPRC99 mechanism, which has been used for previous ozone SIP plans in the SJV. The well-known SAPRC family of mechanisms have been used widely in California and the U.S. (e.g., Baker, et al., 2015; Cai et al., 2011; Chen et

al., 2014; Dennis et al., 2008; Ensberg, et al., 2013; Hakami, et al., 2004a, 2004b; Hu et al., 2012, 2014a, 2014b; Jackson, et al., 2006; Jin et al., 2008, 2010b; Kelly, et al., 2010b; Lane et al., 2008; Liang and Kaduwela, 2005; Livingstone et al., 2009; Lin et al., 2005; Napelenok, 2006; Pun et al., 2009; Tonse et al., 2008; Ying et al., 2008a, 2008b; Zhang et al., 2010; Zhang and Ying, 2011).

The SAPRC07 mechanism has been fully reviewed by four experts in the field through an ARB funded contract. These reviews can be found at http://www.arb.ca.gov/research/reactivity/rsac.htm. Dr. Derwent's (2010) review compared ozone impacts of 121 organic compounds calculated using SAPRC07 and the Master Chemical Mechanism (MCM) v 3.1 and concluded that the ozone impacts using the two mechanisms were consistent for most compounds. Dr. Azzi (2010) used SAPRC07 to simulate ozone formation from isoprene, toluene, m-xylene, and evaporated fuel in environmental chambers performed in Australia and found that SAPRC07 performed reasonably well for these data. Dr. Harley discussed implementing the SAPRC07 mechanism into 3-D air quality models and brought up the importance of the rate constant of NO_2 + OH. This rate constant in the SAPRC07 mechanism in CMAQv5.0.2 has been updated based on new research (Mollner et al., 2010). Dr. Stockwell (2009) compared individual reactions and rate constants in SAPRC07 to two other mechanisms (CB05 and RADM2) and concluded that SAPRC07 represented a state-of-the-science treatment of atmospheric chemistry.

5.2.4 Aerosol Module

The aerosol mechanism with extensions version 6 with aqueous-phase chemistry (AE6-AQ) will be utilized for all SIP modeling. When coupled with the SAPRC07 chemical mechanism, AE6-AQ simulates the formation and evaporation of aerosol and the evolution of the aerosol size distribution (Foley et al., 2010). AE6-AQ includes a comprehensive, yet computationally efficient, inorganic thermodynamic model ISORROPIA to simulate the physical state and chemical composition of inorganic atmospheric aerosols (Fountoukis and Nenes, 2007). AE6-AQ also features the addition of new $PM_{2.5}$ species, an improved secondary organic aerosol (SOA) formation module, as well as new treatment of atmospheric processing of primary organic aerosol (Appel et al., 2013; Carlton et al., 2010; Simon and Bhave, 2011). These updates to AE6-AQ in CMAQv5.0.2 continue to represent state-of-the-art treatment of aerosol processes in the atmosphere (Brown et al., 2011).

5.2.5 CMAQ Initial and Boundary Conditions (IC/BC) and Spin-Up period

Air quality model initial conditions define the mixing ratio (or concentration) of chemical and aerosol species within the modeling domain at the beginning of the model simulation. Boundary conditions define the chemical species mixing ratio (or concentration) within the air entering or leaving the modeling domain. This section discusses the initial and boundary conditions utilized in the ARB modeling system.

U.S. EPA guidance recommends using a model "spin-up" period by beginning a simulation 3-10 days prior to the period of interest (U.S. EPA, 2014). This "spin-up" period allows the initial conditions to be "washed out" of the system, so that the actual initial conditions have little to no impact on the modeling over the time period of interest, as well as giving sufficient time for the modeled species to come to chemical equilibrium. When conducting annual or seasonal modeling, it is computationally more efficient to simulate each month in parallel rather than the entire year or season sequentially. For each month, the CMAQ simulations will include a seven day spin-up period (i.e., the last seven days of the previous month) for the outer 12 km domain to ensure that the initial conditions are "washed out" of the system. Initial conditions at the beginning of the seven day spin-up period will be based on the default initial conditions that are included with the CMAQ release. The 4 km inner domain simulations will utilize a three day spin-up period, where the initial conditions will be based on output from the corresponding day of the 12 km domain simulation.

In recent years, the use of global chemical transport model (CTM) outputs as boundary conditions (BCs) in regional CTM applications has become increasingly common (Chen et al., 2008; Hogrefe et al., 2011; Lam and Fu, 2009; Lee et al., 2011; Lin et al., 2010), and has been shown to improve model performance in many cases (Appel et al., 2007; Borge et al., 2010; Tang et al., 2007, 2009; Tong and Mauzerall, 2006). The advantage of using global CTM model outputs as opposed to fixed climatological-average BCs is that the global CTM derived BCs capture spatial, diurnal, and seasonal variability, as well as provide a set of chemically consistent pollutant mixing ratios. In the ARB's SIP modeling system, the Model for Ozone And Related chemical Tracers (MOZART; Emmons et al., 2010) will be used to define the boundary conditions for the outer 12 km CMAQ domain, while boundary conditions for the 4 km domain will be derived from the 12 km output. MOZART is a comprehensive global model for simulating atmospheric composition including both gases and bulk aerosols (Emmons et al., 2010). It was developed by the National Center for Atmospheric Research (NCAR), the Max-Planck-Institute for Meteorology (in Germany), and the Geophysical Fluid Dynamics Laboratory (GFDL) of the National Oceanic and Atmospheric Administration (NOAA), and is widely

used in the scientific community. In addition to inorganic gases and VOCs, BCs were extracted for aerosol species including elemental carbon, organic matter, sulfate, soil and nitrate. MOZART has been extensively peer-reviewed and applied in a range of studies that utilize its output in defining BCs for regional modeling studies within California and other regions of the U.S. (e.g., Avise et al., 2008; Chen et al., 2008, 2009a, 2009b; Fast et al., 2014; Jathar et al., 2015).

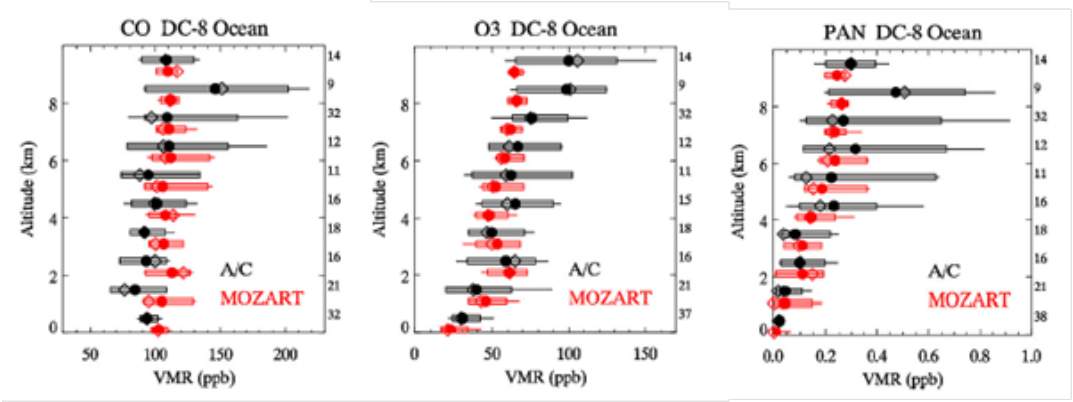

Figure 5-3. Comparison of MOZART (red) simulated CO (left), ozone (center), and PAN (right) to observations (black) along the DC-8 flight track. Shown are mean (filled symbol), median (open symbols), 10th and 90th percentiles (bars) and extremes (lines). The number of data points per 1-km wide altitude bin is shown next to the graphs. Adapted from Figure 2 in Pfister et al. (2011).

In particular, MOZART version 4 (MOZART-4) was recently used in a study characterizing summertime air masses entering California from the Pacific Ocean (Pfister et al., 2011). In their work, Pfister et al. (2011) compared MOZART-4 simulation results to measurements of CO, ozone, and PAN made off the California coast during the ARCTAS-CARB airborne field campaign (Jacob et al., 2010) and showed good agreement between the observations and model results (see Figure 5-3).
The specific MOZART simulations to be utilized in this modeling platform are the MOZART4-GEOS5 simulations by Louisa Emmons (NCAR) for the years 2012 and 2013, which are available for download at http://www.acom.ucar.edu/wrf-chem/mozart.shtml. These simulations are similar to those of Emmons et al. (2010), but with updated meteorological fields. Boundary condition data will be extracted from the MOZART-4 output and processed to CMAQ model ready format using the "mozart2camx" code developed by the Rambol-Environ Corporation (available at http://www.camx.com/download/support-software.aspx). The final BCs represent day-specific mixing ratios, which vary in both space (horizontal and vertical) and time (every six hours).

Per U.S. EPA guidance, the same MOZART derived BCs for the 12 km outer domain will be used for all simulations (e.g., Base Case, Reference, Future, and any sensitivity simulation).

5.3 Quality Assurance of Model Inputs

In developing the IC/BCs and Four Dimensional Data Assimilation (FDDA) datasets for WRF, quality control is performed on all associated meteorological data. Generally, all surface and upper air meteorological data are plotted in space and time to identify extreme values that are suspected to be "outliers". Data points are also compared to other, similar surrounding data points to determine whether there are any large relative discrepancies. If a scientifically plausible reason for the occurrence of suspected outliers is not known, the outlier data points are flagged as invalid and may not be used in the modeling analyses.

In addition, the model-ready emissions files used in CMAQ will be evaluated and compared against the planning inventory totals. Although deviations between the model-ready and planning inventories are expected due to temporal adjustments (e.g., month-of-year and day-of-week) and adjustments based on meteorology (e.g., evaporative emissions from motor vehicles and biogenic sources), any excessive deviation will be investigated to ensure the accuracy of the temporal and meteorology based adjustments. If determined to be scientifically implausible, then the adjustments which led to the deviation will be investigated and updated based on the best available science.

Similar to the quality control of the modeling emissions inventory, the chemical boundary conditions derived from the global CTM model will be evaluated to ensure that no errors were introduced during the processing of the data (e.g., during vertical interpolation of the global model data to the regional model vertical structure or mapping of the chemical species). Any possible errors will be evaluated and addressed if they are determined to be actual errors and not an artifact of the spatial and temporal dynamics inherent in the boundary conditions themselves.

6. METEOROLOGICAL MODEL PERFORMANCE

The complex interactions between the ocean-land interface, orographic induced flows from the mountain-valley topography, and the extreme temperature gradients between the ocean, delta region, valley floor, and mountain ranges surrounding the valley, make the SJV one of the most challenging areas in the country to simulate using prognostic meteorological models. Although there is a long history of prognostic meteorological model applications in California (e.g., Bao et al., 2008; Hu at al., 2010; Jackson et al., 2006; Jin et al., 2010a, 2010b; Livingstone et al., 2009; Michelson et al., 2010; Seaman, Stauffer, and Lario-Gibbs, 1995; Stauffer et al., 2000; Tanrikulu et al., 2000), there is no single model configuration that works equally well for all years and/or seasons, which makes evaluation of the simulated meteorological fields critical for ensuring that the fields reasonably reproduce the observed meteorology for any given time period.

6.1 Ambient Data Base and Quality of Data

Observed meteorological data used to evaluate the WRF model simulations will be obtained from the Air Quality and Meteorological Information System (AQMIS) database, which is a web-based source for real-time and official air quality and meteorological data (www.arb.ca.gov/airqualitytoday/). This database contains surface meteorological observations from 1969-2016, with the data through 2013 having been fully quality assured and deemed official. In addition ARB also has quality-assured upper-air meteorological data obtained using balloons, aircraft, and profilers.

6.2 Statistical Evaluation

Statistical analyses will be performed to evaluate how well the WRF model captured the overall structure of the observed atmosphere during the simulation period, using wind speed, wind direction, temperature, and humidity. The performance of the WRF model against observations will be evaluated using the METSTAT analysis tool (Emery et al, 2001) and supplemented using statistical software tools developed at ARB. The model output and observations will be processed, and data points at each observational site for wind speed, wind direction, temperature, and moisture data will be extracted. The following values will be calculated: Mean Obs, Mean Model, Mean Bias (MB), Mean (Gross) Error (ME/MGE), Normalized Mean Bias (NMB), Root Mean Squared error (RMSE), and the Index Of Agreement (IOA) when applicable. Additional statistical analysis may also be performed.

The mathematical expressions for these quantities are:

$$\mathrm{MB} = \frac{1}{\mathrm{N}}\sum_{1}^{\mathrm{N}}(\mathrm{Model} - \mathrm{Obs}) \tag{6-1}$$

$$\mathrm{ME} = \frac{1}{\mathrm{N}}\sum_{1}^{\mathrm{N}}\left|\mathrm{Model} - \mathrm{Obs}\right| \tag{6-2}$$

$$\mathrm{NMB} = \frac{\sum_{1}^{\mathrm{N}}(\mathrm{Model} - \mathrm{Obs})}{\sum_{1}^{\mathrm{N}}\mathrm{Obs}} \times 100\%, \tag{6-3}$$

$$\mathrm{RSME} = \sqrt{\frac{\sum_{1}^{\mathrm{N}}(\mathrm{Model} - \mathrm{Obs})^2}{\mathrm{N}}} \tag{6-4}$$

$$IOA = 1 - \frac{\sum_{1}^{N}(Model - Obs)^2}{\sum_{1}^{N}\left[(Model - Obs) + (Model + Obs)\right]^2}, \tag{6-5}$$

where, "*Model*" is the simulated values, "*Obs*" is the observed value, and *N* is the number of observations. These values will be tabulated and plotted for all monitoring sites within the air basin of interest, and summarized by subregion when there are distinct differences in the meteorology within the basin. Statistics may be compared to other prognostic model applications in California to place the current model performance within the context of previous studies. In addition to the statistics above, model performance may also be evaluated through metrics such as frequency distributions, time-series analysis, and wind-rose plots. Based on previous experience with meteorological simulations in California, it is expected that the analysis will show wind speed to be overestimated at some stations with a smaller difference at others. The diurnal variations of temperature and wind direction at most stations are likely to be captured reasonably well. However, the model will likely underestimate the larger magnitudes of temperature during the day and smaller magnitudes at night.

6.3 Phenomenological Evaluation

In addition to the statistical evaluation described above, a phenomenological based evaluation can provide additional insights as to the accuracy of the meteorological modeling. A phenomenological evaluation may include analysis such as determining the relationship between observed air quality and key meteorological parameters (e.g., conceptual model) and then evaluating whether the simulated meteorology and air quality is able to reproduce those relationships. Another possible approach would be to generate geopotential height charts at 500 and 850 mb using the simulated results and compare those to the standard geopotential height charts. This would reveal if the large-scale weather systems at those pressure levels were adequately simulated by the regional prognostic meteorology model. Another similar approach is to identify the larger-scale meteorological conditions associated with air quality events using the National Centers for Environmental Prediction (NCEP) Reanalysis dataset. These can then be visually compared to the simulated meteorological fields to determine whether those large-scale meteorological conditions were accurately simulated and whether the same relationships observed in the NCEP reanalysis are present in the simulated data.

7. PHOTOCHEMICAL MODEL PERFORMANCE

7.1 Ambient Data

Air quality observations are routinely made at state and local monitoring stations. Gas species and PM species are measured on various time scales (e.g., hourly, daily, weekly). The U.S. EPA guidance recommends model performance evaluations for the following gaseous pollutants: ozone (O_3), nitric acid (HNO_3), nitric oxide (NO), nitrogen dioxide (NO_2), peroxyacetyl nitrate (PAN), volatile organic compounds (VOCs), ammonia (NH_3), NO_y (sum of NO_x and other oxidized compounds), sulfur dioxide (SO_2), carbon monoxide (CO), and hydrogen peroxide (H2O2). The U.S. EPA recognizes that not all of these species are routinely measured (U.S. EPA, 2014) and therefore may not be available for evaluating every model application. Recognizing that $PM_{2.5}$ is a mixture, U.S. EPA recommends model performance evaluation for the following individual $PM_{2.5}$ species: sulfate (SO_4^{2-}), nitrate (NO_3^-), ammonium (NH_4^+), elemental carbon (EC), organic carbon (OC) or organic mass (OM), crustal, and sea salt constituent (U.S. EPA, 2014).

Table 7-1 lists the species for which routine measurements are generally available in 2012 and 2013. When quality assured data are available and appropriate for use, model performance for each species will be evaluated. Observational data will be

obtained from the Air Quality and Meteorological Information System (AQMIS), which is a web-based source for real-time and official air quality and meteorological data (www.arb.ca.gov/airqualitytoday/). This database contains surface air quality observations from 1980-2016, with the data through 2014 having been fully quality assured and deemed official.

Table 7-1. Monitored species used in evaluating model performance.

Species	Sampling frequency
O_3	1 hour
NO	1 hour
NO_2	1 hour
NO_x	1 hour
CO	1 hour
SO_2	1 hour
Selected VOCs from the PAMS measurement	3 hours (not every day)
$PM_{2.5}$ measured using FRM[1]	24 hours (daily to one in six days)
$PM_{2.5}$ measured using FEM	Continuously
$PM_{2.5}$ Speciation sites	24 hours (not every day)
Sulfate ion	24 hours (not every day)
Nitrate ion	24 hours (not every day)
Ammonium ion	24 hours (not every day)
Organic carbon	24 hours (not every day)
Elemental carbon	24 hours (not every day)
Sea salt constituents	24 hours (not every day)

[1] Direct comparison between modeled and FRM $PM_{2.5}$ may not be appropriate because of various positive and negative biases associated with FRM measurement procedures.

These species cover the majority of pollutants of interest for evaluating model performance as recommended by the U.S. EPA. Other species such as H_2O_2, HNO_3, NH_3, and PAN are not routinely measured. During the DISCOVER-AQ field campaign, which took place in January and February 2013 in the SJV, aircraft sampling provided daytime measurements for a number of species (including HNO_3, NH_3, PAN, alkyl nitrates, and selected VOC species) that are not routinely measured. Modeled concentrations will be compared to aircraft measurements for these species, except for the gaseous HNO_3 measurements, which were contaminated by particulate nitrate (Dr. Chris Cappa, personal communication).

7.2 Statistical Evaluation

As recommended by U.S. EPA, a number of statistical metrics will be used to evaluate model performance for ozone, speciated and total $PM_{2.5}$, as well as other precursor species. These metrics may include mean bias (MB), mean error (ME), mean fractional bias (MFB), mean fractional error (MFE), normalized mean bias (NMB), normalized mean error (NME), root mean square error (RMSE), correlation coefficient (R^2), mean normalized bias (MNB), and mean normalized gross error (MNGE). The formulae for estimating these metrics are given below.

$$\mathrm{MB} = \frac{1}{\mathrm{N}}\sum_{1}^{\mathrm{N}}(\mathrm{Model} - \mathrm{Obs}) \tag{7-1}$$

$$\mathrm{ME} = \frac{1}{\mathrm{N}}\sum_{1}^{\mathrm{N}}\left|\mathrm{Model} - \mathrm{Obs}\right| \tag{7-2}$$

$$\mathrm{MFB} = \frac{2}{\mathrm{N}}\sum_{1}^{\mathrm{N}}\left(\frac{\mathrm{Model} - \mathrm{Obs}}{\mathrm{Model} + \mathrm{Obs}}\right)\times 100\%, \tag{7-3}$$

$$\mathrm{MFE} = \frac{2}{\mathrm{N}}\sum_{1}^{\mathrm{N}}\left(\frac{\left|\mathrm{Model} - \mathrm{Obs}\right|}{\mathrm{Model} + \mathrm{Obs}}\right)\times 100\%, \tag{7-4}$$

$$NMB = \frac{\sum_{1}^{N}(Model - Obs)}{\sum_{1}^{N} Obs} \times 100\%, \quad (7\text{-}5)$$

$$NME = \frac{\sum_{1}^{N}|Model - Obs|}{\sum_{1}^{N} Obs} \times 100\%, \quad (7\text{-}6)$$

$$RSME = \sqrt{\frac{\sum_{1}^{N}(Model - Obs)^2}{N}} \quad (7\text{-}7)$$

$$R^2 = \left(\frac{\sum_{1}^{N}((Model - \overline{Model}) \times (Obs - \overline{Obs}))}{\sqrt{\sum_{1}^{N}(Model - \overline{Model})^2 \sum_{1}^{N}(Obs - \overline{Obs})^2}}\right)^2 \quad (7\text{-}8)$$

$$MNB = \frac{1}{N}\sum_{1}^{N}\left(\frac{Model - Obs}{Obs}\right) \times 100\%, \quad (7\text{-}9)$$

$$MNGE = \frac{1}{N}\sum_{1}^{N}\left(\frac{|Model - Obs|}{Obs}\right) \times 100\%. \quad (7\text{-}10)$$

where, "Model" is the simulated mixing ratio, "$\overline{Model}$" is the simulated mean mixing ratio, "Obs" is the observed value, "$\overline{Obs}$" is the mean observed value, and "N" is the number of observations.

In addition to the above statistics, various forms of graphics will also be created to visually examine and compare the model predictions to observations. These will include time-series plots comparing the predictions and observations, scatter plots for

comparing the magnitude of the simulated and observed mixing ratios, box plots to summarize the time series data across different regions and averaging times, as well as frequency distributions. For $PM_{2.5}$ the so called "bugle plots" of MFE and MFB from Boylan and Russell (2006) will also be generated. The plots described above will be created for paired observations and predictions over time scales dictated by the averaging frequencies of observations (i.e., hourly, daily, monthly, seasonally) for the species of interest. Together, they will provide a detailed view of model performance during different time periods, in different sub-regions, and over different concentrations and mixing ratio levels.

7.3 Comparison to Previous Modeling Studies

Previous U.S. EPA modeling guidance (U.S. EPA, 1991) utilized "bright line" criteria for the performance statistics that distinguished between adequate and inadequate model performance. In the latest modeling guidance from U.S. EPA (U.S EPA, 2014) it is now recommended that model performance be evaluated in the context of similar modeling studies to ensure that the model performance approximates the quality of those studies. The work of Simon et al. (2012) summarized photochemical model performance for studies published in the peer-reviewed literature between 2006 and 2012 and this work will form the basis for evaluating the modeling utilized in the attainment demonstration.

7.4 Diagnostic Evaluation

Diagnostic evaluations are useful for investigating whether the physical and chemical processes that control ozone and $PM_{2.5}$ formation are correctly represented in the modeling. These evaluations can take many forms, such as utilizing model probing tools like process analysis, which tracks and apportions ozone mixing ratios in the model to various chemical and physical processes, or source apportionment tools that utilize model tracers to attribute ozone formation to various emissions source sectors and/or geographic regions. Sensitivity studies (either "brute-force" or the numerical Direct Decoupled Method) can also provide useful information as to the response exhibited in the modeling to changes in various input parameters, such as changes to the emissions inventory or boundary conditions. Due to the nature of this type of analysis, diagnostic evaluations can be very resource intensive and the U.S. EPA modeling guidance acknowledges that air agencies may have limited resources and time to perform such analysis under the constraints of a typical SIP modeling application. To the extent possible, some level of diagnostic evaluation will be included in the model attainment demonstration for this SIP.

In addition to the above analysis, the 2013 DISCOVER-AQ field campaign in the SJV offers a unique dataset for additional diagnostic analysis that is not available in other areas, in particular, the use of indicator ratios in determining the sensitivity of secondary $PM_{2.5}$ to its limiting precursors. As an example, the ratio between free ammonia (total ammonia – 2 x sulfate) and total nitrate (gaseous + particulate) was proposed by Ansari and Pandis (1998) as an indicator of whether ammonium nitrate formation is limited by NO_x or ammonia emissions. The DISCOVER-AQ dataset will be utilized to the extent possible to investigate $PM_{2.5}$ precursor sensitivity in the SJV as well as analysis of upper measurements and detailed ground level AMS measurements (Young et al., 2016).

8. ATTAINMENT DEMONSTRATION

The U.S. EPA modeling guidance (U.S. EPA, 2014) outlines the approach for utilizing models to predict future attainment of the 0.075 ppm 8-hour ozone standard. Consistent with the previous modeling guidance (U.S. EPA, 2007) utilized in the most recent 8-hour ozone (2007), annual $PM_{2.5}$ (2008), and 24-hour $PM_{2.5}$ (2012) SIPs, the current guidance recommends utilizing modeling in a relative sense. A detailed description of how models are applied in the attainment demonstration for both ozone and $PM_{2.5}$, as prescribed by U.S. EPA modeling guidance, is provided below.

8.1 Base Year Design Values

The starting point for the attainment demonstration is with the observational based design value (DV), which is used to determine compliance with the standard at any given monitor. The DV for a specific monitor and year represents the three-year average of the annual 4^{th} highest 8-hour ozone mixing ratio, 98^{th} percentile of the 24-hour $PM_{2.5}$ concentration, or annual average $PM_{2.5}$ concentration, depending on the standard, observed at the monitor. For example, the 8-hr O_3 DV for 2012 is the average of the observed 4^{th} highest 8-hour ozone mixing ratio from 2010, 2011, and 2012.

The U.S. EPA recommends using an average of three DVs to better account for the year-to-year variability inherent in meteorology. Since 2012 has been chosen as the base year for projecting DVs to the future, site-specific DVs will be calculated for the three three-year periods ending in 2012, 2013, and 2014 and then these three DVs will be averaged. This average DV is called a weighted DV (in the context of this SIP, the weighted DV will also be referred to as the reference year DV or DV_R). Table 8-1 illustrates how the weighted DV is calculated.

Table 8-1. Illustrates the data from each year that are utilized in the Design Value calculation for that year (DV Year), and the yearly weighting of data for the weighted Design Value calculation (or DV_R). "obs" refers to the observed metric (8-hr O_3, 24-hour $PM_{2.5}$, or annual average $PM_{2.5}$).

DV Year	Years Averaged for the Design Value (4th highest observed 8-hr O_3, 98th percentile 24-hour $PM_{2.5}$, or annual average $PM_{2.5}$)				
2012	2010	2011	2012		
2013		2011	2012	2013	
2014			2012	2013	2014
Yearly Weightings for the Weighted Design Value Calculation					
2012-2014 Average	$\mathrm{DV_R} = \frac{\mathrm{obs_{2010}} + (2)\mathrm{obs_{2011}} + (3)\mathrm{obs_{2012}} + (2)\mathrm{obs_{2013}} + \mathrm{obs_{2014}}}{9}$				

8.2 Base, Reference, and Future Year Simulations

Projecting the weighted DVs to the future requires three photochemical model simulations as described below:

1. Base Year Simulation

The base year simulation for 2012 or 2013 is used to assess model performance (i.e., to ensure that the model is reasonably able to reproduce the observed ozone mixing ratios). Since this simulation will be used to assess model performance, it is essential to include as much day-specific detail as possible in the emissions inventory, including, but not limited to hourly adjustments to the motor vehicle and biogenic inventories based on observed local meteorological conditions, known wildfire and agricultural burning events, and exceptional events such as the Chevron refinery fire in 2012.

2. Reference Year Simulation

The reference year simulation is identical to the base year simulation, except that certain emissions events which are either random and/or cannot be projected to the future are removed from the emissions inventory. These include wildfires and events such as the 2012 Chevron refinery fire.

3. Future Year Simulation

The future year simulation is identical to the reference year simulation, except that the projected future year anthropogenic emission levels are used rather than the reference year emission levels. All other model inputs (e.g., meteorology, chemical boundary conditions, biogenic emissions, and calendar

for day-of-week specifications in the inventory) are the same as those used in the reference year simulation.

The base year simulation is solely used for evaluating model performance, while the reference and future year simulations are used to project the weighted DV to the future as described in subsequent sections of this document.

8.3 Relative Response Factors

As part of the model attainment demonstration, the fractional change in ozone or $PM_{2.5}$ between the model future year and model reference year are calculated for each monitor location. These ratios, called "relative response factors" or RRFs, are calculated based on the ratio of modeled future year ozone or $PM_{2.5}$ to the corresponding modeled reference year ozone or $PM_{2.5}$ (Equation 8-1).

$$RRF = \frac{\text{average } (O_3 \text{ or } PM_{2.5})_{\text{future}}}{\text{average } (O_3 \text{ or } PM_{2.5})_{\text{reference}}} \quad (8\text{-}1)$$

8.3.1 8-hour Ozone RRF

For 8-hour ozone, the modeled maximum daily average 8-hour (MDA8) ozone is used in calculating the RRF. These MDA8 ozone values are based on the maximum simulated ozone within a 3x3 array of cells surrounding the monitor (Figure 8-1). The future and base year ozone values used in RRF calculations are paired in space (i.e., using the future year MDA8 ozone value at the same grid cell where the MDA8 value for the reference? year is located within the 3x3 array of cells). The days used to calculate the average MDA8 for the reference and future years are inherently consistent, since the same meteorology is used to drive both simulations.

Not all modeled days are used to calculate the average MDA8 ozone from the reference and future year simulations. The form of the 8-hour ozone NAAQS is such that it is geared toward the days with the highest mixing ratios in any ozone season (i.e., the 4th highest MDA8 ozone). Therefore, the modeled days used in the RRF calculation should also reflect days with the highest ozone levels. As a result, the current U.S. EPA guidance (U.S. EPA, 2014) suggests using the top 10 modeled days when calculating the RRF. Since the relative sensitivity to emissions changes (in both the model and real world) can vary from day-to-day due to meteorology and emissions (e.g., temperature dependent emissions or day-of-week variability) using the top 10 days ensures that the

calculated RRF is robust and stable (i.e., not overly sensitive to any single day used in the calculation).

When choosing the top 10 days, the U.S. EPA recommends beginning with all days in which the simulated reference MDA8 is >= 60 ppb and then calculating RRFs based on the top 10 high ozone days. If there are fewer than 10 days with MDA8 ozone >= 60 ppb then all days >= 60 ppb are used in the RRF calculation, as long as there are at least 5 days used in the calculation. If there are fewer than 5 days >= 60 ppb, an RRF cannot be calculated for that monitor. To ensure that only modeled days which are consistent with the observed ozone levels are used in the RRF calculation, the modeled days are further restricted to days in which the reference MDA8 ozone is within ± 20% of the observed value at the monitor location.

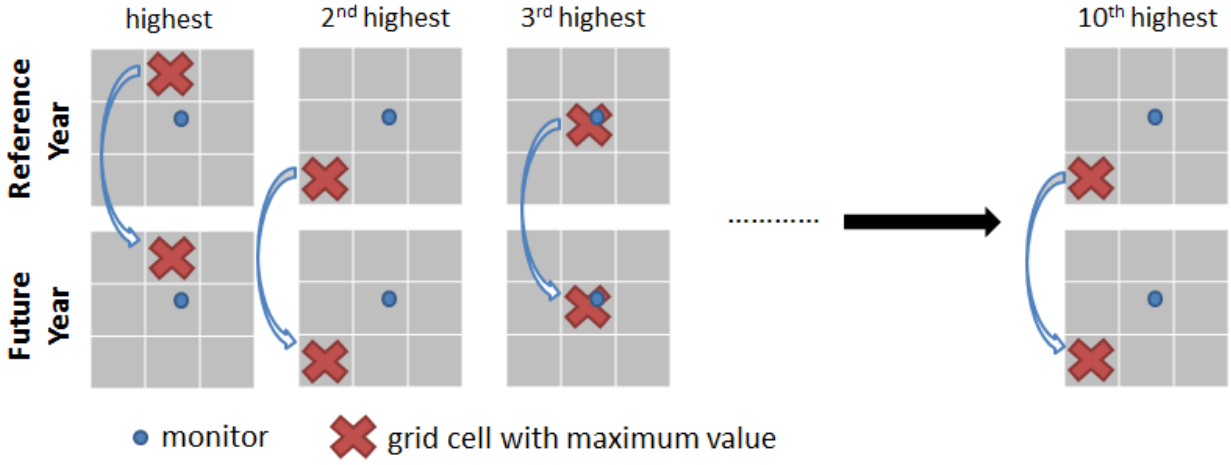

Figure 8-1. Example showing how the location of the MDA8 ozone for the top ten days in the reference and future years are chosen.

8.3.2 Annual and 24-hour $PM_{2.5}$ RRF

The U.S. EPA (2014) guidance requires RRFs for both the annual and 24-hour $PM_{2.5}$ attainment tests be calculated on a quarterly basis (January-March, April-June, July-September, and October-December) and for each $PM_{2.5}$ component (sulfate, nitrate, ammonium, organic carbon, elemental carbon, particle bound water, salt, and other primary inorganic components).

For annual $PM_{2.5}$, the quarterly RRFs are based on modeled quarterly mean concentrations for each component, where the concentrations are averaged over the 9 model grid cells within the 3x3 array of grid cells surrounding each monitor. For the 24-hour $PM_{2.5}$ attainment test, the quarterly RRFs are calculated based on the average for

each component over the top 10% of modeled days (or the top nine days per quarter) with the highest total 24-hour average $PM_{2.5}$ concentration. Peak $PM_{2.5}$ values are selected and averaged using the $PM_{2.5}$ concentration simulated at the single grid cell containing the monitoring site for calculating the 24-hour $PM_{2.5}$ RRF (as opposed to the 3x3 array average used in the annual $PM_{2.5}$ RRF calculation).

8.4 Future Year Design Value Calculation

8.4.1 8-hour Ozone

For 8-hour ozone, a future year DV at each monitor is calculated by multiplying the corresponding reference year DV by the site-specific RRF from Equation 8-1 (Equation 8-2).

$$DV_F = DV_R \times RRF \quad (8\text{-}2)$$

where,
DV_F = future year design value,
DV_R = reference year design value, and
RRF = the site specific RRF from Equation 8-1

The resulting future year DVs are then compared to the 8-hour ozone NAAQS to demonstrate whether attainment will be reached under the future emissions scenario utilized in the future year modeling. A monitor is considered to be in attainment of the 8-hour ozone standard if the estimated future design value does not exceed the level of the standard.

8.4.2 Annual and 24-hour $PM_{2.5}$

8.4.2.1 Sulfate, Adjusted Nitrate, Derived, Water, Inferred Carbonaceous Material Balance Approach (SANDWICH) and Potential Modifications

Federal Reference Method (FRM) $PM_{2.5}$ mass measurements provide the basis for the attainment/nonattainment designations. For this reason it is recommended that the FRM data be used to project future air quality and progress towards attainment. However, given the complex physicochemical nature of $PM_{2.5}$, it is necessary to consider individual $PM_{2.5}$ species as well. While the FRM measurements give the mass

of the bulk sample, a method for apportioning this bulk mass to individual $PM_{2.5}$ components is the first step towards determining the best emissions controls strategies to reach NAAQS levels in a timely manner.

The FRM measurement protocol finds its roots in the past epidemiological studies of health effects associated with $PM_{2.5}$ exposure. It is upon these studies that the NAAQS are based. The FRM protocol is sufficiently detailed so that results might be easily reproducible and involves the measurement of filter mass before and after sampling together with equilibrating at narrowly defined conditions. Filters are equilibrated for more than 24 hours at a standard relative humidity between 30 and 40% and temperature between 20 and 23 ºC. Due to the sampler construction and a lengthy filter equilibration period, FRM measurements are subjected to a number of known positive and negative artifacts. FRM measurements do not necessarily capture the $PM_{2.5}$ concentrations in the atmosphere and can differ substantially from what is measured by speciation monitors including the Speciation Trends Network (STN) monitors (see http://www.epa.gov/ttnamti1/specgen.html for more details). Nitrate and semi-volatile organic mass can be lost from the filter during the equilibration process, and particle bound water associated with hygroscopic species like sulfate provides a positive artifact. These differences present an area for careful consideration when one attempts to utilize speciated measurements to apportion the bulk FRM mass to individual species. Given that (1) attainment status is currently dependent upon FRM measurements and (2) concentrations of individual $PM_{2.5}$ species need to be considered in order to understand the nature of and efficient ways to ameliorate the $PM_{2.5}$ problem in a given region, a method has been developed to speciate bulk FRM $PM_{2.5}$ mass with known FRM limitations in mind. This method is referred to as the measured **S**ulfate, **A**djusted **N**itrate, **D**erived **W**ater, **I**nferred **C**arbonaceous material balance approach or "SANDWICH" (Frank, 2006). SANDWICH is based on speciated measurements from other (often co-located) samplers, such as those from STN, and the known sampling artifacts of the FRM. The approach strives to provide mass closure, reconciliation between speciated and bulk mass concentration measurements, and the basis for a connection between observations, modeled $PM_{2.5}$ concentrations, and the air quality standard (U.S. EPA, 2014).

The main steps in estimating the $PM_{2.5}$ composition are as follows:

(1) Calculate the nitrate retained on the FRM filter using hourly relative humidity and temperature together with the STN nitrate measurements,

The FRM does not retain all of the semi-volatile $PM_{2.5}$ mass, and at warmer temperatures, loss of particulate nitrate from filters has been commonly observed (Chow et al., 2005). In order to estimate how much nitrate is retained on the FRM filter,

simple thermodynamic equilibrium relations may be used. Necessary inputs include 24-hour average nitrate measurements and hourly temperature and relative humidity data. Frank (2006) suggests the following methodology for estimating retained nitrate. For each hour *i* of the day, calculate the dissociation constant, K_i from ambient temperature and relative humidity (RH).

For RH < 61%:

$$\ln(K_i) = 118.87 - (24084/T_i) - 6.025 \times \ln(T_i),$$

where, T_i is the hourly temperature in Kelvins and K_i is in nanobars.

For RH ≥ 61%, K_i is replaced by:

$$K_i' = [P_1 - P_2(1-a_i) + P_3(1-a_i)^2] \times (1-a_i)^{1.75} \times K_i,$$

where, a_i is "fractional" relative humidity and

$$\ln(P_1) = -135.94 + 8763/T_i + 19.12 \times \ln(T_i),$$
$$\ln(P_2) = -122.65 + 9969/T_i + 16.22 \times \ln(T_i),$$
$$\ln(P_3) = -182.61 + 13875/T_i + 24.46 \times \ln(T_i).$$

Using this information, calculate the nitrate retained on the filter as:

$$\text{Retained Nitrate} = \text{STN nitrate} - 745.7/T_R \times (\kappa - \gamma) \times \frac{1}{24} \sum_{i=1}^{24} \sqrt{K_i},$$

where, T_R is the daily average temperature for the sampled air volume in Kelvin, K_i is the dissociation constant for NH_4NO_3 at ambient temperature for hour i, and $(\kappa - \gamma)$ relates to the temperature rise of the filter and vapor depletion from the inlet surface and is assumed to have a value equal to one (Hering and Cass, 1999).

(2) Calculate quarterly averages for retained nitrate, sulfate, elemental carbon, sea salt, and ammonium,

(3) Calculate particle bound water using the concentrations of ammonium, sulfate, and nitrate, using an equilibrium model like the Aerosol Inorganic Model (AIM) or a polynomial equation derived from model output

Under the FRM filter equilibration conditions, hygroscopic aerosol will retain its particle bound water (PBW) and be included in the observed FRM $PM_{2.5}$ mass. PBW can be calculated using an equilibrium model like the Aerosol Inorganics Model (AIM). AIM requires the concentrations of ammonium, nitrate, sulfate, and estimated H^+ as inputs. In addition to inorganic concentrations, the equilibration conditions are also necessary model inputs. In this case, a temperature of 294.15 K and 35% RH is recommended. Alternatively, for simplification, a polynomial regression equation may be constructed by fitting the calculated water concentration from an equilibrium model and the concentrations of nitrate, ammonium, and sulfate. The AIM model will be used for more accurate calculation of PBW.

(4) Add 0.5 µg/m^3 as blank mass, and

(5) Calculate organic carbon mass (OCMmb) by difference, subtracting all inorganic species (including blank mass) from the $PM_{2.5}$ mass.

Other components that may be represented on the FRM filter include elemental carbon, crustal material, sea salt, and passively collected mass. Depending on location certain species may be neglected (e.g., sea salt for inland areas).

While carbonaceous aerosol may make up a large portion of airborne aerosol, speciated measurements of carbonaceous PM are considered highly uncertain. This is due to the large number of carbon compounds in the atmosphere and the measurement uncertainties associated with samplers of different configurations. In the SANDWICH approach, organic carbonaceous mass is calculated by difference. The sum of all nonorganic carbon components will be subtracted from the FRM $PM_{2.5}$ mass to estimate the mass of organic carbon.

After having calculated the species concentrations as outlined above, we will calculate the percentage contribution of each species to the measured FRM mass (minus the blank concentration of 0.5 µg/m^3) for each quarter of the years represented by the speciated data. Note that blank mass is kept constant at 0.5 µg/m^3 between the base and future years, and future year particle bound water needs to be calculated for the future year values of nitrate, ammonium, and sulfate.

8.4.2.2 Estimation of Species Concentrations at Federal Reference Method (FRM) Monitors that Lack Speciation Data

Speciation data from available STN (speciation) sites will be used to speciate the FRM mass for all FRM sites. For those sites not collocated with STN monitors, surrogate speciation sites will be determined based on proximity and evaluation of local emissions or based on similarity in speciation profiles if such data exists (e.g., such as the speciated data collected in the SJV during CRPAQS (Solomon and Magliano, 1998)).

8.4.2.3 Speciated Modeled Attainment Test (SMAT)

Following U.S. EPA modeling guidance (U.S. EPA, 2014), the model attainment test for the annual $PM_{2.5}$ standard will be performed with the following steps.

Step 1: For each year used in the design value calculation, determine the observed quarterly mean $PM_{2.5}$ and quarterly mean composition for each monitor by multiplying the monitored quarterly mean concentration of FRM derived $PM_{2.5}$ by the fractional composition of $PM_{2.5}$ species for each quarter.

Step 2: Calculate the component specific RRFs at each monitor for each quarter as described in section 8.3.2.

Step 3: Apply the component specific RRFs to the quarterly mean concentrations from Step 1 to obtain projected quarterly species estimates.

Step 4: Calculate future year annual average $PM_{2.5}$ estimates by summing the quarterly species estimates at each monitor and then compare to the annual $PM_{2.5}$ NAAQS. If the projected average annual arithmetic mean $PM_{2.5}$ concentration is ≤ the NAAQS, then the attainment test is passed.

For the 24-hour $PM_{2.5}$ standard, the attainment test is performed with the following steps (U.S. EPA, 2014):

Step 1: Determine the top eight days with the highest observed 24-hour $PM_{2.5}$ concentration (FRM sites) in each quarter and year used in the design value calculation (a total of 32 days per year), and calculate the 98^{th} percentile value for each year.

Step 2: Calculate quarterly ambient species fractions on "high" $PM_{2.5}$ days for each of the major $PM_{2.5}$ component species (i.e., sulfate, nitrate, ammonium, elemental carbon, organic carbon, particle bound water, salt, and blank mass). The "high" days are represented by the top 10% of days in each quarter. Depending on the sampling frequency, the number of days captured in the top 10% would range from three to nine. The species fractions of $PM_{2.5}$ are calculated using the "SANDWICH" approach which was described previously. These quarter-specific fractions along with the FRM $PM_{2.5}$ concentrations are then used to calculate species concentrations for each of the 32 days per year determined in Step 1.

Step 3: Apply the component and quarter specific RRF, described in Section 8.3.2, to observed daily species concentrations from Step 2 to obtain future year concentrations of sulfate, nitrate, elemental carbon, organic carbon, salt, and other primary $PM_{2.5}$.

Step 4: Calculate the future year concentrations for the remaining $PM_{2.5}$ components (i.e., ammonium, particle bound water, and blank mass). The future year ammonium is calculated based on the calculated future year sulfate and nitrate, using a constant value for the degree of neutralization of sulfate from the ambient data. The future year particle bound water is calculated from the AIM model.

Step 5: Sum the concentration of each of the species components to calculate the total $PM_{2.5}$ concentration for each of the 32 days per year and at each site. Sort the 32 days for each site and year, and calculate the 98^{th} percentile value corresponding to each year.

Step 6: Calculate the future design value at each site based on the 98^{th} percentile concentrations calculated in Step 5 and following the standard protocol for calculating design values (see Table 8-1). Compare the future-year 24-hour design values to the NAAQS. If the projected design value is ≤ the NAAQS, then the attainment test is passed.

8.4.2.4 Sensitivity Analyses

Model sensitivity analysis may be conducted if the model attainment demonstration does not show attainment of the applicable standard with the baseline future inventory, or for determining precursor sensitivities and inter-pollutant equivalency ratios. For both ozone and $PM_{2.5}$, the sensitivity analysis will involve domain wide fractional reductions of the appropriate anthropogenic precursor emissions using the future year baseline emissions scenario as a starting point. In the event that the model attainment demonstration does not show attainment for the applicable standard, it is important to know the precursor limitation to assess the level of emissions controls needed to attain the standard.

In order to identify what combinations of precursor emissions reductions is predicted to lead to attainment, a series of modeling sensitivity simulations with varying degrees of precursor reductions from anthropogenic sources are typically performed. These sensitivity simulations are identical to the baseline future year simulation discussed earlier except that domain-wide fractional reductions are applied to future year anthropogenic precursor emission levels and a new future year design value is calculated. The results of these sensitivity simulations are plotted on isopleth diagrams, which are also referred to as carrying capacity diagrams. The isopleths provide an estimate of the level of emissions needed to demonstrate attainment and thereby inform the development of a corresponding control strategy.

For ozone, this would likely entail reducing anthropogenic NO_x and VOC emissions in 25% increments including cross sensitivities (e.g., 0.75 x NO_x + 1.00 x VOC; 1.00 x NO_x + 0.75 x VOC; 0.75 x NO_x + 0.75 x VOC; 0.5 x NO_x + 1.00 x VOC; ….). Typically, a full set of sensitivities would include simulations for 25%, 50%, and 75% reduction in NO_x and VOC, along with the cross sensitivities (for a total of 16 simulations including the future base simulation). After design values are calculated for each new sensitivity simulation, an ozone isopleth (or carrying capacity diagram) as a function of NO_x and VOC emissions is generated and used to estimate the additional NO_x and VOC emission reductions needed to attain the standard. The approach for $PM_{2.5}$ is similar, except that additional precursor emissions must be considered. Typically, the precursors considered for $PM_{2.5}$ would include anthropogenic NO_x, SO_x, VOCs, NH_3, as well as direct $PM_{2.5}$ emissions (Chen et al., 2014). Cross sensitivities for generating $PM_{2.5}$ carrying capacity diagrams would be conducted with respect to NO_x, which would include the following precursor pairs: NO_x vs. primary $PM_{2.5}$, NO_x vs. VOC, NO_x vs. NH_3, and NO_x vs. SO_x.

In addition to the $PM_{2.5}$ carrying capacity simulations, precursor sensitivity modeling may be conducted for determining the significant precursors to $PM_{2.5}$ formation and for

developing inter-pollutant equivalency ratios. These simulations would follow a similar approach to the carrying capacity simulations described above, but would involve only a single sensitivity simulation for each precursor, where emissions of that precursor are reduced between 30% and 70% from the future base year. The "effectiveness" of reducing a given species can be quantified at each FRM monitor as the change in µg $PM_{2.5}$ (i.e., change in design value) per ton of precursor emissions (corresponding to the 15% change in emissions). Equivalency ratios between $PM_{2.5}$ precursors (i.e., NO_x, SO_x, VOCs, and NH_3) and primary $PM_{2.5}$ will be determined by dividing primary $PM_{2.5}$ effectiveness by the precursors' effectiveness.

8.5 Unmonitored Area Analysis

The unmonitored area analysis is used to ensure that there are no regions outside of the existing monitoring network that could exceed the NAAQS if a monitor was present at that location (U.S. EPA, 2014). The U.S. EPA recommends combining spatially interpolated design value fields with modeled gradients for the pollutant of interest (e.g. Ozone and $PM_{2.5}$) and grid-specific RRFs in order to generate gridded future year gradient adjusted design values. The spatial Interpolation of the observed design values is done only within the geographic region constrained by the monitoring network, since extrapolating to outside of the monitoring network is inherently uncertain. This analysis can be done using the Model Attainment Test Software (MATS) (Abt, 2014); however this software is not open source and comes as a precompiled software package. To maintain transparency and flexibility in the analysis, in-house R codes (https://www.r-project.org/) developed at ARB will be utilized in this analysis. The basic steps followed in the unmonitored area analysis for 8-hour ozone and annual/24-hour $PM_{2.5}$ are described below.

8.5.1 8-hour Ozone

In this section, the specific steps followed in 8-hr ozone unmonitored area analysis are described briefly:

Step 1: At each grid cell, the top-10 modeled maximum daily average 8-hour ozone mixing ratios from the reference year simulation will be averaged, and a gradient in this top-10 day average between each grid cell and grid cells which contain a monitor will be calculated.

Step 2: A single set of spatially interpolated 8-hr ozone DV fields will be generated based on the observed 5-year weighted base year 8-hr ozone DVs from the available monitors. The interpolation is done using normalized inverse

distance squared weightings for all monitors within a grid cell's Voronoi Region (calculated with the R tripack library; https://cran.r-project.org/web/packages/tripack/README), and adjusted based on the gradients between the grid cell and the corresponding monitor from Step 1.

Step 3: At each grid cell, the RRFs are calculated based on the reference- and future-year modeling following the same approach outlined in Section 8.3, except that the +/- 20% limitation on the simulated and observed maximum daily average 8-hour ozone is not applicable because observed data do not exist for grid cells in unmonitored areas.

Step 4: The future year gridded 8-hr ozone DVs are calculated by multiplying the gradient-adjusted interpolated 8-hr ozone DVs from Step 2 with the gridded RRFs from Step 3

Step 5: The future-year gridded 8-hr ozone DVs (from Step 4) are examined to determine if there are any peak values higher than those at the monitors, which could potentially cause violations of the applicable 8-hr ozone NAAQS.

8.5.2 Annual $PM_{2.5}$

The unmonitored area analysis for the annual $PM_{2.5}$ standard will include the following steps:

Step 1: At each grid cell, the quarterly average $PM_{2.5}$ (total and by species) will be calculated from the reference year simulation, and a gradient in these quarterly averages between each grid cell and grid cells which contain a monitor will be calculated.

Step 2: Interpolated spatial fields, based on the observed $PM_{2.5}$ (FRM) and each component species of $PM_{2.5}$, will be generated for each quarter using normalized inverse distance squared weightings for all monitors within a grid cell's Voronoi Region. The ambient interpolated spatial fields are then adjusted based on the gradients in predicted quarterly mean concentrations from Step 1.

Step 3: The component specific RRFs are calculated at each grid cell for each quarter as described in section 8.3.2.

Step 4: The quarterly mean concentrations from Step 2 are then multiplied by the corresponding component specific RRF (from Step 3) to obtain the corresponding projected quarterly species estimates.

Step 5: The future year annual average $PM_{2.5}$ estimates are calculated by summing the quarterly species estimates at each grid cell and then compared to the annual $PM_{2.5}$ NAAQS to determine compliance.

8.5.3 24-hour $PM_{2.5}$

The unmonitored area analysis for the 24-hour $PM_{2.5}$ standard will include the following steps:

Step 1: At each grid cell, the quarterly average of the top 10% of the modeled days for 24-hour $PM_{2.5}$ (total and by species for the same top 10% of days) will be calculated from the reference year simulation, and a gradient in these quarterly averages between each grid cell and grid cells which contain a monitor will be calculated.

Step 2: The top 8 days with observed high $PM_{2.5}$ (FRM) are identified for each quarter and for each of the five years (a total of 32 days per year), used in the base year DV calculation. The speciated $PM_{2.5}$ (FRM) values are then interpolated for each of the "high" $PM_{2.5}$ days (identified above) using normalized inverse distance squared weightings for all monitors within a grid cell's Voronoi Region. These ambient interpolated spatial fields are then adjusted based on the appropriate gradients in predicted concentrations from Step 1.

Step 3: The component specific RRFs are calculated at each grid cell for each quarter as described in section 8.3.2.

Step 4: The observed daily species concentrations from Step 2 are multiplied by the component and quarter specific RRF (from Step 3) to estimate the future year concentration of each $PM_{2.5}$ species using the method outlined in section 8.4.2.3

Step 5: The concentration of each of the component $PM_{2.5}$ species is summed to calculate the total $PM_{2.5}$ concentration for each of the 32 days per year (8 days per quarter) and at each grid cell. For each year, the 98^{th} percentile value is calculated by the sorting the 32 days for that particular year at each grid cell.

Step 6: The future design value at each grid cell is calculated based on the 98th percentile concentrations calculated in Step 5 and following the standard protocol for calculating design values (see Table 8-1). The future-year 24-hour design values are then compared to the 24-hour $PM_{2.5}$ NAAQS to determine compliance with that standard.

The R codes used in this analysis will be made available upon request.

8.6 Banded Relative Response Factors for Ozone

The "Band-RRF" approach expands upon the standard "Single-RRF" approach for 8-hour ozone to account for differences in model response to emissions controls at varying ozone levels. The most recent U.S. EPA modeling guidance (U. S. EPA, 2014) accounts for some of these differences by focusing on the top ten modeled days, but even the top ten days may contain a significant range of ozone mixing ratios. The Band-RRF approach accounts for these differences more explicitly by grouping the simulated ozone into bands of lower, medium, and higher ozone mixing ratios. Specifically, daily peak 8-hour ozone mixing ratios for all days meeting model performance criteria (+/- 20% with the observations) can be stratified into 5 ppb increments from 60 ppb upwards (bin size and mixing ratio range may vary under different applications). A separate RRF is calculated for each ozone band following a similar approach as the standard Single-RRF. A linear regression is then fit to the data resulting in an equation relating RRF to ozone band. Similar to the Single-RRF, this equation is unique to each monitor/location.

The top ten days for each monitor, based on observed 8-hour ozone, for each year that is utilized in the design value calculation (see Table 8-1) is then projected to the future using the appropriate RRF for the corresponding ozone band. The top ten future days for each year are then re-sorted, the fourth highest 8-hour ozone is selected, and the future year design value is calculated in a manner consistent with the base/reference year design value calculation. More detailed information on the Band-RRF approach can be found in Kulkarni et al. (2014) and the 2013 SJV 1-hour ozone SIP (SJVUAPCD, 2013).

9. PROCEDURAL REQUIREMENTS

9.1 How Modeling and other Analyses will be Archived, Documented, and Disseminated

The computational burden of modeling the entire state of California and its sub-regions requires a significant amount of computing power and large data storage requirements. For example, there are over half a million grid cells in total for each simulation based on the Northern CA domain (192 x 192 cells in the lateral direction and 18 vertical layers). The meteorological modeling system has roughly double the number of grid cells since it has 30 vertical layers. Archiving of all the inputs and outputs takes several terabytes (TB) of computer disk space (for comparison, one single-layer DVD can hold roughly 5 gigabytes (GB) of data, and it would require ~200 DVDs to hold one TB). Please note that this estimate is for simulated surface-level pollutant output only. If three-dimensional pollutant data are needed, it would add a few more TB to this total. Therefore, transferring the modeling inputs/outputs over the internet using file transfer protocol (FTP) is not practical.

Interested parties may send a request for model inputs/outputs to Mr. John DaMassa, Chief of the Modeling and Meteorology Branch at the following address.

John DaMassa, Chief
Modeling and Meteorology Branch
Air Quality Planning and Science Division
Air Resources Board
California Environmental Protection Agency
P.O. Box 2815
Sacramento, CA 95814, USA

The requesting party will need to send an external disk drive(s) to facilitate the data transfer. The requesting party should also specify what input/output files are requested so that ARB can determine the capacity of the external disk drive(s) that the requester should send.

9.2 Specific Deliverables to U.S. EPA

The following is a list of modeling-related documents that will be provided to the U.S. EPA.

- The modeling protocol

- Emissions preparation and results
- Meteorology
    - Preparation of model inputs
    - Model performance evaluation
- Air Quality
    - Preparation of model inputs
    - Model performance evaluation
- Documentation of corroborative and weight-of-evidence analyses
- Predicted future year Design Values
- Access to input data and simulation results

REFERENCES

Abt, 2014. Modeled Attainment Test Software: User's Manual. MATS available at: http://www.epa.gov/scram001/modelingapps_mats.htm

Angevine, W.M., Eddington, L., Durkee, K., Fairall, C., Bianco, L., and Brioude, J., 2012, Meteorological model evaluation for CalNex 2010, Monthly Weather Review, 140, 3885-3906.

Ansari, A.S., and Pandis, S.N., 1998, Response of inorganic PM to precursor concentrations, Environmental Science & Technology, 32, 2706-2714.

Appel, K. W., Pouliot, G. A., Simon, H., Sarwar, G., Pye, H. O. T., Napelenok, S. L., Akhtar, F., and Roselle, S. J., 2013, Evaluation of dust and trace metal estimates from the Community Multiscale Air Quality (CMAQ) model version 5.0, Geoscientific Model Development, 6, 883-899, doi:10.5194/gmd-6-883-2013, 2013.

Appel, W. K., Gilliland, A.B., Sarwar, G., and Gilliam, R.C., 2007, Evaluation of the Community Multiscale Air Quality (CMAQ) model version 4.5: Sensitivities impacting model performance: Part I – Ozone, Atmospheric Environment, 41, 9603-9615.

Appel, W.K., Bhave, P.V., Gilliland, A.B., Sarwar, G., and Roselle, S.J., 2008, Evaluation of the Community Multiscale Air Quality (CMAQ) model version 4.5: Sensitivities impacting model performance; Part II – Particulate Matter, Atmospheric Environment, 42, 6057-6066.

Avise, J., Chen, J., Lamb, B., Wiedinmyer, C., Guenther, A., Salathe, E., and Mass, C., 2009, Attribution of projected changes in summertime US ozone and $PM_{2.5}$ concentrations to global changes, Atmospheric Chemistry and Physics, 9, 1111-1124.

Azzi, M., White, S.J., Angove, D.E., Jamie, I. M., and Kaduwela, A., 2010, Evaluation of the SAPRC-07 mechanism against CSIRO smog chamber data, Atmospheric Environment, 44, 1707-1713.

Baker, K. R., Carlton, A. G., Kleindienst, T. E., Offenberg, J. H., Beaver, M. R., Gentner, D. R., Goldstein, A. H., Hayes, P. L., Jimenez, J. L., Gilman, J. B., de Gouw, J. A., Woody, M. C., Pye, H. O. T., Kelly, J. T., Lewandowski, M., Jaoui, M., Stevens, P. S., Brune, W. H., Lin, Y.-H., Rubitschun, C. L., and Surratt, J. D.: Gas and aerosol carbon in California: comparison of measurements and model predictions in Pasadena and Bakersfield, Atmos. Chem. Phys., 15, 5243-5258, doi:10.5194/acp-15-5243-2015, 2015.

Bao, J.W., Michelson, S.A., Persson, P.O.G., Djalalova, I.V., and Wilczak, J.M., 2008, Observed and WRF-simulated low-level winds in a high-ozone episode during the Central California Ozone Study, Journal of Applied Meteorology and Climatology, 47(9), 2372-2394.

Binkowski, F.S. and Roselle, S.J., 2003, Models-3 Community Multiscale Air Quality (CMAQ) model aerosol component, 2. Model description, Journal of Geophysical Research, 108, D6, doi:10.1029/2001jd001409.

Borge, R., Lopez, J., Lumbreras, J., Narros, A., and Rodriguez, E., 2010, Influence of boundary conditions on CMAQ simulations over the Iberian Peninsula, Atmospheric Environment, 44, 2681-2695 (doi:10.1016/j.atmosenv.2010.04.044).

Boylan, J.W., Russell, A.G., (2006), PM and light extinction model performance metrics, goals, and criteria for three-dimensional air quality models. Atmospheric Environment 40, 4946-4959.

Brown, N., Allen,D.T., Amar, P., Kallos, G., McNider, R., Russell, A.G., and Stockwell, W.R., 2011, Final report: Fourth peer review of the CMAQ model, Submitted to Community Modeling and Analysis System Center, The University of North Carolina at Chapel Hill.

Byun, D.W. and Ching, J.K.S., 1999, Science Algorithms of the EPA Models-3 Community Multiscale Air Quality (CMAQ) Modeling System, EPA/600/R-99/030, available at http://www.epa.gov/AMD/CMAQ/CMAQscienceDoc.html

Byun, D.W. and Schere, K.L., 2006, Review of the governing equations, computational algorithms, and other components of the Models-3 Community Multiscale Air Quality (CMAQ) modeling system, Applied Mechanics Review, 59, 51-77.

Cai, C., Kelly, J.T., Avise, J.C., Kaduwela, A.P., and Stockwell, W.R., 2011, Photochemical modeling in California with two chemical mechanisms: Model intercomparison and response to emission reductions, Journal of the Air & Waste Management Association, 61, 559-572.

Carlton, A.G., Bhave, P., Napelenok, S.L., Edney, E.O., Sarwar, G., Pinder, R.W., Pouliot, G.A., and Houyoux, M., 2010, Model representation of secondary organic aerosol in CMAQv4.7, Environmental Science Technology, 44, 8553-8560.

Carter, W.P.L., 2010a, Development of the SAPRC-07 chemical mechanism, Atmospheric Environment, 44(40), 5324-5335.

Carter, W.P.L., 2010b, Development of a condensed SAPRC-07 chemical mechanism, Atmospheric Environment, 44(40), 5336-5345.

Chen, J., Vaughan, J., Avise, J., O'Neill, S., and Lamb, B., 2008, Enhancement and evaluation of the AIRPACT ozone and $PM_{2.5}$ forecast system for the Pacific Northwest, Journal of Geophysical Research, 113, D14305, doi:10.1029/2007JD009554.

Chen, J., Avise, J., Guenther, A., Wiedinmyer, C., Salathe, E., Jackson, R.B., and Lamb, B., 2009a, Future land use and land cover influences on regional biogenic emissions and air quality in the United States, Atmospheric Environment, 43, 5771-5780.

Chen, J., Avise, J., Lamb, B., Salathe, E., Mass, C., Guenther, A., Wiedinmyer, C., Lamarque, J.-F., O'Neill, S., McKenzie, D., and Larkin, N., 2009b, The effects fo global changes upon regional ozone pollution in the United States, Atmospheric Chemistry and Physics, 9, 1125-1141.

Chen, J., Lu, J., Avise, J.C., DaMassa, J.A., Kleeman, M.J., and Kaduwela, A.P., 2014, Seasonal modeling of PM2.5 in California's San Joaquin Valley, Atmospheric Environment, 92, 182-190.

Chow J.C., Watson, J.G., Lowenthal, D.H., and Magliano, K., 2005, Loss of PM2.5 nitrate from filter samples in Central California, Journal of Air & Waste Management Association, 55, 1158-1168.

Civerolo, K., Hogrefe, C., Zalewsky, E., Hao, W., Sistla, G., Lynn, B., Rosenzweig, C., and Kinney, P., 2010, Evaluation of an 18-year CMAQ simulation: Seasonal variations and long-term temporal changes in sulfate and nitrate, Atmospheric Environment, 44, 3745-3752.

Dennis, R.L., Bhave, P., and Pinder, R.W., 2008, Observable indicators of the sensitivity of PM2.5 nitrate to emission reductions – Part II: Sensitivity to errors in total ammonia and total nitrate of the CMAQ-predicted non-linear effect of SO2 emission reductions, Atmospheric Environment, 42, 1287-1300.

Derwent, R. G., M. E. Jenkin, M. J. Pilling, W.P.L. Carter, and A. Kaduwela, 2010, Reactivity scales as comparative tools for chemical mechanisms, Journal of the Air & Waste Management Association, 60, 914-924.

Eder, B., Yu, S., 2006, A performance evaluation of the 2004 release of Models-3 CMAQ, Atmospheric Environment, 40, 4811-4824.

Emery, C., Tai, E., and Yarwood, G., 2001, Enhanced Meteorological Modeling and Performance Evaluation for Two Texas Ozone Episodes, Final report submitted to the Texas Natural Resources Conservation Commission.

Emmons, L.K., Walters, S., Hess, P.G., Lamarque, J.F., Pfister, G.G., Fillmore, D., Granier, C., Guenther, A., Kinnison, D., Laepple, T., Orlando, J., Tie, X., Tyndall, G., Wiedinmyer, C., Baughcum, S.L., and Kloster, S., 2010, Description and evaluation of the Model for Ozone and Related chemical Tracers, Version 4 (MOZART-4), Geoscientific Model Development, 3, 43-67.

Ensberg, J. J., et al., 2013, Inorganic and black carbon aerosols in the Los Angeles Basin during CalNex, Journal of Geophysical Research - Atmosphere, 118, 1777–1803, doi:10.1029/2012JD018136.

Fast, J.D., et al., 2014, Modeling regional aerosol and aerosol precursor variability over California and its sensitivity to emissions and long-range transport during the 2010 CalNex and CARES campaigns, Atmospheric Chemistry Physics, 14, 10013-10060.

Foley, K.M., Roselle, S.J., Appel, K.W., Bhave, P.V., Pleim, J.E., Otte, T.L., Mathur, R., Sarwar, G., Young, J.O., Gilliam, R.C., Nolte, C.G., Kelly, J.T., Gilliland, A.B., and Bash, J.O., 2010, Incremental testing of the Community Multiscale Air Quality (CMAQ) modeling system version 4.7, Geoscientific Model Development, 3, 205-226.

Fountoukis, C. and Nenes, A., 2007, ISORROPIA II: a computationally efficient thermodynamic equilibrium model for K+–Ca2+–Mg2+–NH4+–Na+–SO42−–NO3−–Cl−–H2O aerosols, Atmospheric Chemistry Physics, 7, 4639-4659.

Frank, N.H., 2006, Retained nitrate, hydrated sulfates, and carbonaceous mass in federal reference method fine particulate matter for six eastern U.S. cities, Journal of Air & Waste Management Association, 56, 500-511.

Hakami, A., Bergin, M.S., and Russell, A.G., 2004a, Ozone formation potential of organic compounds in the eastern United States: A comparison of episodes, inventories, and domain, Environmental Science & Technology, 38, 6748-6759.

Hakami, A., Harley, R.A., Milford, J.B., Odman, M.T., and Russell, A.G., 2004b, Regional, three-dimensional assessment of the ozone formation potential of organic compounds, Atmospheric Environment, 38, 121-134.

Hering, S. and Cass, G. 1999, The magnitude of bias in measurement of PM2.5 arising from volatilization of particulate nitrate from Teflon filters, Journal of Air & Waste Management Association, 49, 725-733.

Hogrefe, C., Hao, W., Zalewsky, E.E., Ku, J.Y., Lynn, B., Rosenzweig, C., Schultz, M.G., Rast, S., Newchurch, M.J., Wang, L., Kinney, P.L., and Sistla, G., 2011, An analysis of long-term regional-scale ozone simulations over the Northeastern United States: variability and trends, Atmospheric Chemistry and Physics, 11, 567-582.

Hogrefe,C., Biswas, J., Lynn, B., Civerolo, K., Ku, J.Y., Rosenthal, J. , Rosenweig, C., Goldberg, R., and Kinney, P.L., 2004, Simulating regional-scale ozone climatology over the eastern United States: model evaluation results, Atmospheric Environment, 38, 2627-2638.

Hogrefe, C., S. T. Rao, I. G. Zurbenko, and P. S. Porter, 2000 *Interpreting Information in Time Series of Ozone Observations and Model Predictions Relevant to Regulatory Policies in the Eastern United States*. Bull. Amer. Met. Soc., 81, 2083 – 2106

Hu, J., Howard, C.J., Mitloehner, F., Green, P.G., and Kleeman, M.J., 2012, Mobile source and livestock feed contributions to regional ozone formation in Central California, Environmental Science & Technology, 46, 2781-2789.

Hu, J., Ying, Q., Chen, J., Mahmud, A., Zhao, Z., Chen, S.H., and Kleeman, M.J., 2010, Particulate air quality model predictions using prognostic vs. diagnostic meteorology in central California, Atmospheric Environment, 44, 215-226.

Hu,J., Zhang, H., Chen, S. , Ying, Q., Wiedinmyer, C., Vandenberghe, F., and Kleeman, M.J., 2014a, Identifying PM2.5 and PM0.1 sources for epidemiological studies in California, Environmental Sciences & Technology, 48, 4980-4990.

Hu, J., Zhang, H., Ying, Q., Chen, S.-H., Vandenberghe, F., and Kleeman, M. J., 2014b, Long-term particulate matter modeling for health effects studies in California – Part 1: Model performance on temporal and spatial variations, Atmospheric Chemistry Physics Discussion, 14, 20997-21036.

Huang, M., Carmichael, G.R., Adhikary, B., Spak, S.N., Kulkarni, S., Cheng, Y.F., Wei, C., Tang, Y., Parrish, D.D., Oltmans, S.J., D'Allura, A., Kaduwela, A., Cai, C., Weinheimer, A.J., Wong, M., Pierce, R.B., Al-Saadi, J.A. Streets, D.G., and Zhang, Q., 2010, Impacts of transported background ozone on California air quality during the ARCTAS-CARB period - a multi-scale modeling study, Atmospheric Chemistry and Physics, 10(14), 6947-6968.

Jackson, B., Chau, D., Gürer, K., and Kaduwela, A, 2006, Comparison of ozone simulations using MM5 and CALMET/MM5 hybrid meteorological fields for the July/August 2000 CCOS episode, Atmospheric Environment, 40, 2812-2822.

Jacob, D.J., Crawford, J.H., Maring, H., Clarke, A.D., Dibb, J.E., Emmons, L.K., Ferrare, R.A., Hostetler, C.A., Russell, P.B., Singh, H.B., Thompson, A.M., Shaw, G.E., McCauley, E., Pederson, J.R., and Fisher, J.A., 2010, The Arctic Research of the Composition of the Troposphere from Aircraft and Satellites (ARCTAS) Mission: Design, Execution, and First Results, Atmospheric Chemistry and Physics, 10(11), 5191-5212.

Jathar, S. H., Cappa, C. D., Wexler, A. S., Seinfeld, J. H., and Kleeman, M. J.: Multi-generational oxidation model to simulate secondary organic aerosol in a 3-D air quality model, Geosci. Model Dev., 8, 2553-2567, doi:10.5194/gmd-8-2553-2015, 2015.

Jin L., Brown, N.J., Harley, R.A., Bao, J.W., Michelson, S.A., and Wilczak, J.M., 2010b, Seasonal versus episodic performance evaluation for an Eulerian photochemical air quality model, Journal of Geophysical Research, 115, D09302, doi:10.1029/2009JD012680.

Jin, L. Brown, N. and Harley, R.A. A Seasonal Perspective on Regional Air Quality in Central California, Draft Final Report, Lawrence Berkeley National Laboratory, Berkeley, CA, January, 2010a.

Jin, L., Tonse, S., Cohan, D.S., Mao, X., Harley, R.A., and Brown, N.J., 2008, Sensitivity analysis of ozone formation and transport for a central California air pollution episode, Environmental Science Technology, 42, 3683-3689.

Kelly, J. T., et al., 2014, Fine-scale simulation of ammonium and nitrate over the South Coast Air Basin and San Joaquin Valley of California during CalNex-2010, Journal of Geophysical Research - Atmosphere, 119, 3600–3614, doi:10.1002/2013JD021290.

Kelly, J.T., Avise, J., Cai, C., and Kaduwela, A., 2010b, Simulating particle size distributions over California and impact on lung deposition fraction, Aerosol Science & Technology, 45, 148-162.

Kelly, J.T., Bhave, P., Nolte, C.G., Shankar, U., and Foley, K.M., 2010a, Simulating emission and chemical evolution of coarse sea-salt particles in the Community Multiscale Air Quality (CMAQ) model, Geoscientific Model Development, 3, 257-273.

Kulkarni, S., Kaduwela, A.P., Avise, J.C., DaMassa, J.A., and Chau, D. , 2014, An extended approach to calculate the ozone relative response factors used in the attainment demonstration for the National Ambient Air Quality Standards, Journal of the Air & Waste Management Association, 64, 1204-1213.

Lam, Y.F. and Fu, J.S., 2009, A novel downscaling technique for the linkage of global and regional air quality modeling, Atmospheric Chemistry and Physics, 9, 9169-9185.

Lane, T.E., Donahue, N.M., and Pandis, S.N., 2008, Simulating secondary organic aerosol formation using the volatility basis-set approach in a chemical transport model, Atmospheric Environment, 42, 7439-7451.

Lee, S. H., Kim, S.W., Trainer, M., Frost, G.J., McKeen, S.A., Cooper, O.R., Flocke, F., Holloway, J.S., Neuman, J.A., Ryerson, T., Senff, C.J., Swanson, A.L., and Thompson, A.M., 2011, Modeling ozone plumes observed downwind of New York City over the North Atlantic Ocean during the ICARTT field campaign, Atmospheric Chemistry and Physics, 11, 7375-7397, doi:10.5194/acp-11-7375-2011.

Liang, J. and Kaduwela, A., 2005, Micro-development of CMAQ for California Regional Particulate Matter Air Quality Study, Proceedings of the 4th Annual CMAQ Models-3 User's Conference, Chapel Hill, NC.

Lin, C. J., Ho, T. C., Chu, H. W.,, Yang, H., Chandru, S., Krishnarajanagar, N., Chiou, P., Hopper J. R., June 2005,Sensitivity analysis of ground-level ozone concentration to emission changes in two urban regions of southeast Texas, Journal of Environ. Manage., 75 315-323, http://dx.doi.org/10.1016/j.jenvman.2004.09.012.

Lin, M., Holloway, T., Carmichael, G.R., and Fiore, A.M., 2010, Quantifying pollution inflow and outflow over East Asia in spring with regional and global models, Atmospheric Chemistry and Physics, 10, 4221-4239, doi:10.5194/acp-10-4221-2010.

Lin, M., Holloway, T., Oki, T., Streets, D. G., and Richter, A., 2009, Multi-scale model analysis of boundary layer ozone over East Asia, Atmospheric Chemistry Physics, 9, 3277-3301, 2009.

Lin, M., Oki, T., Holloway, T., Streets, D.G., Bengtsson, M., and Kanae, S., 2008, Long-range transport of acidifying substances in East Asia - Part I: Model evaluation and sensitivity studies, Atmospheric Environment, 42, 5939-5955.

Livingstone, P.L., Magliano, K.,Guerer, K., Allen, P.D., Zhang, K.M., Ying, Q., Jackson, B.S., Kaduwela, A., Kleeman, M., Woodhouse, L.F., Turkiewicz, K., Horowitz, L.W., Scott, K., Johnson, D., Taylor, C., O'Brien, G., DaMassa, J., Croes, B.E., Binkowski, F., and Byun, D., 2009, Simulating PM concentration during a winter episode in a subtropical valley: Sensitivity simulations and evaluation methods, Atmospheric Environment, 43, 5971-5977.

Lu, W., Zhong, S., Charney, J.J., Bian, X., and Liu, S., 2012, WRF simulation over complex terrain during a southern California wildfire event, Climate and Dynamics, 117, D05125, doi:10.1029/2011JD017004.

Mahmud, A., Hixson, M., Hu, J., Zhao, Z., Chen, S.H., and Kleeman, M.J., 2010, Climate impact on airborne particulate matter concentrations in California using seven year analysis periods, Atmospheric Chemistry Physics, 10, 11097-11114.

Marmur, A., Park, S.K., Mulholland, J.A., Tolbert, P.E., and Russell, A.G., 2006, Source apportionment of PM2.5 in the southeastern United States using receptor and emissions-based models: Conceptual differences and implications for time-series health studies, Atmospheric Environment, 40, 2533-2551.

Michelson, S.A.,Djalalova, I.V.,and Bao, J.W., 2010, Evaluation of the Summertime Low-Level Winds Simulated by MM5 in the Central Valley of California, Journal of Applied Meteorology and Climatology, 49(11), 2230-2245.

Mollner, A.K., Valluvadasan, S., Feng, L., Sprague, M.K., Okumura, M., Milligan, D.B., Bloss, W.J., Sander, S.P., Martien, P.T., Harley, R.A., McCoy, A.B., and Carter, W.P.L., 2010, Rate of Gas Phase Association of Hydroxyl Radical and Nitrogen Dioxide, Sciences, 330, 646-649.

Morris, R.E., Koo, B., Guenther, A., Yarwood, G., McNally, D., Tesche, T.W., Tonnesen, G., Boylan, J., Brewer, P., (2006), Model sensitivity evaluation for organic carbon using two multi-pollutant air quality models that simulate regional haze in the southeastern United States, Atmospheric Environment 40, 4960-4972.

Napelenok, S.L., Cohan, D.S., Hu, Y., and Russell, A.G., 2006, Decoupled direct 3D sensitivity analysis for particulate matter (DDM-3D/PM), Atmospheric Environment, 40, 6112-6121.

O'Neill, S.M., Lamb, B.K., Chen, J., Claiborn, C., Finn, D., Otterson, S., Figueroa, C., Bowman, C., Boyer, M., Wilson, R., Arnold, J., Aalbers, S., Stocum, J., Swab, C., Stoll, M., Dubois, M., and Anderson, M., 2006, Modeling ozone and aerosol formation and transport in the Pacific Northwest with the Community Multi-Scale Air Quality (CMAQ) Modeling System, Environmental Science Technology, 40, 1286 – 1299.

Seinfeld J. H. and Pandis S. N. (1998) Atmospheric Chemistry and Physics: From Air Pollution to Climate Change, 1st edition, J. Wiley, New York

.Pfister, G.G., Parrish, D.D., Worden, H., Emmons, L.K., Edwards, D.P., Wiedinmyer, C., Diskin, G.S., Huey, G., Oltmans, S.J., Thouret, V., Weinheimer, A., and Wisthaler, A., 2011, Characterizing summertime chemical boundary conditions for airmasses entering the US West Coast, Atmospheric Chemistry and Physics, 11(4), 1769-1790.

Philips, S.B., Finkelstein, P.L., 2006, Comparison of spatial patterns of pollutant distribution with CMAQ predictions, Atmospheric Environment, 40, 4999-5009.

Pun, B.K., Balmori, R.T.F., Seigneur, C., 2009, Modeling wintertime particulate matter formation in central California, Atmospheric Environment, 43, 402-409.

Pye, H.O.T. and Pouliot, G.A., 2012, Modeling the role of alkanes, polycyclic aromatic hydrocarbons, and their oligomers in secondary organic aerosol formation, Environmental Science & Technology, 46, 6041-6047.

Rodriguez, M.A., Barna, M.G., Moore, T., (2009), Regional Impacts of Oil and Gas Development on Ozone Formation in the Western United States. J. Air Waste Manage. Assoc. 59, 1111-1118.

SCAQMD 8-hr ozone SIP, 2007, available at http://www.aqmd.gov/home/library/clean-air-plans/air-quality-mgt-plan/2007-air-quality-management-plan

SCAQMD 8-hr ozone and 24-hour $PM_{2.5}$ SIP, 2012, available at http://www.aqmd.gov/home/library/clean-air-plans/air-quality-mgt-plan/final-2012-air-quality-management-plan

Seaman, N.L., Stauffer, D.R., and Lario-Gibbs, A.M., 1995, A Multiscale Four-Dimensional Data Assimilation System Applied in the San Joaquin Valley during SARMAP. Part I: Modeling Design and Basic Performance Characteristics, Journal of Applied Meteorology 34(8), 1739-1761.

Simon, H., and Bhave, P.V., 2011, Simulating the degree of oxidation in atmospheric organic particles, Environmental Science & Technology, 46, 331-339.

Simon, H., Baker, K.R., and Phillips, S., 2012, Compilation and interpretation of photochemical model performance statistics published between 2006 and 2012, Atmospheric Environment, 61, 124-139.

SJVUAPCD 8-hour ozone Plan, 2007, available at http://www.valleyair.org/Air_Quality_Plans/AQ_Final_Adopted_Ozone2007.htm

SJVUAPCD Annual $PM_{2.5}$ Plan, 2008, available at http://www.valleyair.org/Air_Quality_Plans/AQ_Final_Adopted_PM25_2008.htm

SJVUAPCD 24-hour $PM_{2.5}$ Plan, 2012, available at http://www.valleyair.org/Air_Quality_Plans/PM25Plans2012.htm

SJVUAPCD 1-hour ozone Plan, 2013, available at http://www.valleyair.org/Air_Quality_Plans/Ozone-OneHourPlan-2013.htm

Skamarock, W. C., J. B. Klemp, J. Dudhia, D. O. Gill, D. M. Barker, W. Wang, and J. G. Powers, 2005: A description of the Advanced Research WRF Version 2. NCAR Tech Notes-468+STR

SMAQMD 8-hour ozone Plan, 2009, available at http://airquality.org/plans/federal/ozone/8hr1997/index.shtml

Smyth, S.C., Jiang, W., Yin, D., Roth, H., and Giroux, E., 2006, Evaluation of CMAQ O3 and PM2.5 performance using Pacific 2001 measurement data, Atmospheric Environment, 40, 2735-2749.

Sokhi, R.S., Jose, R.S., Kitwiroon, N., Fragkoua, E., Perez, J.L., and Middleton, D.R., 2006, Prediction of ozone levels in London using the MM5–CMAQ modeling system. Environmental Modeling & Software, 21, 566–576.

Solomon, P.A. and Magliano, K.L., 1998, The 1995-Integrated Monitoring Study (IMS95) of the California Regional PM10/PM2.5 air quality study (CRPAQS): Study overview, Atmospheric Environment, 33(29), 4747-4756.

Stauffer, D.R., Seaman, N.L. Hunter, G.K., Leidner, S.M., Lario-Gibbs, A., and Tanrikulu, S., 2000, A field-coherence technique for meteorological field-program design for air quality studies. Part I: Description and interpretation, Journal of Applied Meteorology,39(3), 297-316.

Stockwell, W. R., 2009, Peer review of the SAPRC-07 chemical mechanism of Dr. William Carter, Report to the California Air Resources Board, March 9.

Tang, Y., Carmichael, G.R., Thongboonchoo, N., Chai, T.F., Horowitz, L.W., Pierce, R.B., Al-Saadi, J.A., Pfister, G., Vukovich, J.M., Avery, M.A., Sachse, G.W., Ryerson, T.B., Holloway, J.S., Atlas, E.L., Flocke, F.M., Weber, R.J., Huey, L.G., Dibb, J.E., Streets, D.G., and Brune, W.H., 2007, Influence of lateral and top boundary conditions on regional air quality prediction: A multiscale study coupling regional and global chemical transport models, Journal of Geophysical Research 112, D10S18, doi:10.1029/2006JD007515.

Tang, Y.H., Lee, P., Tsidulko, M., Huang, H.C., McQueen, J.T., DiMego, G.J., Emmons, L.K., Pierce, R.B., Thompson, A.M., Lin, H.M., Kang, D.W., Tong, D., Yu, S.C., Mathur, R., Pleim, J.E., Otte, T.L., Pouliot, G., Young, J.O., Schere, K.L., Davidson, P.M., and Stajner, I., 2009, The impact of chemical lateral boundary conditions on CMAQ predictions of tropospheric ozone over the continental United States, Environmental Fluid Mechanics, 9, 43-58, doi:10.1007/s10652-008-9092-5.

Tanrikulu, S., Stauffer, D.R., Seaman, N.L., and Ranzieri, A.J., 2000, A Field-Coherence Technique for Meteorological Field-Program Design for Air Quality Studies. Part II: Evaluation in the San Joaquin Valley, Journal of Applied Meteorology, 39(3), 317-334.

Tesche, T.W., Morris, R., Tonnesen, G., McNally, D., Boylan, J., Brewer, P., 2006. CMAQ/CAMx annual 2002 performance evaluation over the eastern US. Atmospheric Environment 40, 4906-4919.

Tong, D.Q., and Mauzerall, D.L., 2006, Spatial variability of summertime tropospheric ozone over the continental United States: Implications of an evaluation of the CMAQ model, Atmospheric Environment, 40, 3041-3056.

Tonse, S.R., Brown, N.J., Harley, R.A., and Jin, L. 2008, A process-analysis based study of the ozone weekend effect, Atmospheric Environment, 42, 7728-7736.

U.S. EPA, 2005, Technical Support Document for the Final Clean Air Interstate Rule, Air Quality Modeling, prepared by the U.S. EPA Office of Air Quality Planning and Standards, RTP, NC.

U.S. EPA, 2007, Guidance on the Use of Models and Other Analyses for Demonstrating Attainment of Air Quality Goals for Ozone, PM2.5, and Regional Haze, EPA-454/B07-002.

U.S. EPA, 2010, Air Quality Modeling Technical Support Document: Light-Duty Vehicle Greenhouse Gas Emission Standards Final Rule, EPA Report 454/4-10-003.

U.S. EPA, (2011a), Air Quality Modeling Final Rule Technical Support Document, http://www.epa.gov/airquality/transport/pdfs/AQModeling.pdf, Research Triangle Park, North Carolina.

U.S. EPA, (2011b), Air Quality Modeling Technical Support Document: Final EGU NESHAP (EPA-454/R-11-009), Research Triangle Park, North Carolina.

U.S. EPA, 2014, Draft Modeling Guidance for Demonstrating Attainment of Air Quality Goals for Ozone, PM2.5 and Regional Haze, available at http://www.epa.gov/scram001/guidance/guide/Draft_O3-PM-RH_Modeling_Guidance-2014.pdf

U.S. EPA. 1991. Guideline for Regulatory Application of the Urban Airshed Model. EPA-450/4-91-013. Found at http://www.epa.gov/ttn/scram/guidance_sip.htm

UNC, 2010, Operational Guidance for the Community Multiscale Air Quality (CMAQ) Modeling System Version 4.7.1., available at http://www.cmascenter.org/help/model_docs/cmaq/4.7.1/CMAQ_4.7.1_OGD_28june10.pdf.

Vijayaraghavan, K., Karamchadania, P., and Seigneur, C., 2006, Plume-in-grid modeling of summer air pollution in Central California, Atmospheric Environment, 40, 5097-5109.

Vizuete, W., Jeffries, H.E., Tesche, T.W., Olaguer, E., Couzo, E., 2011. Issues with Ozone Attainment Methodology for Houston, TX. Journal of the Air and Waste Management Association 61 (3), 238-253.

Wilczak, J. M., Djalalova, I., McKeen, S., Bianco, L., Bao, J., Grell, G, Peckham, S., Mathur, R., McQueen, J., and Lee, P., 2009, Analysis of regional meteorology and surface ozone during the TexAQS II field program and an evaluation of the NMM-CMAQ and WRF-Chem air quality models, Journal of Geophysical Research, 114, D00F14, doi:10.1029/2008JD011675.

Ying, Q., Lu, J., Allen, P., Livingstone, P., Kaduwela, A., and Kleeman, M., 2008a, Modeling air quality during the California Regional PM_{10}/$PM_{2.5}$ Air Quality Study (CRPAQS) using the UCD/CIT source-oriented air quality model – Part I. Base case model results, Atmospheric Environment, 42, 8954-8966.

Ying, Q., Lu, J., Kaduwela, A., and Kleeman, M., 2008b, Modeling air quality during the California Regional PM_{10}/$PM_{2.5}$ Air Quality Study (CPRAQS) using the UCD/CIT Source Oriented Air Quality Model - Part II. Regional source apportionment of primary airborne particulate matter, Atmospheric Environment, 42(39), 8967-8978.

Young, D. E., Kim, H., Parworth, C., Zhou, S., Zhang, X., Cappa, C. D., Seco, R., Kim, S., and Zhang, Q.: Influences of emission sources and meteorology on aerosol chemistry in a polluted urban environment: results from DISCOVER-AQ California, Atmos. Chem. Phys., 16, 5427-5451, doi:10.5194/acp-16-5427-2016, 2016.

Zhang, H., and Ying, Q., 2011, Secondary organic aerosol formation and source apportionment in Southeast Texas, Atmospheric Environment, 45, 3217-3227.

Zhang, Y., Liu, P., Liu, X., Pun, B., Seigneur, C., Jacobson, M.Z., and Wang, W., 2010, Fine scale modeling of wintertime aerosol mass, number, and size distributions in Central California, Journal of Geophysical Research, 115, D15207, doi:10.1029/2009JD012950.

Zhang, Y., Liu, P., Queen, A., Misenis, C., Pun, B., Seigneur, C., and Wu, S.Y., 2006, A Comprehensive performance evaluation of MM5-CMAQ for the summer 1999 Southern Oxidants Study Episode, Part-II. Gas and aerosol predictions, Atmospheric Environment, 40, 4839-4855.

Zhang, Y., Pun, B., Wu, S.Y., Vijayaraghavan, K., and Seigneur, C., 2004, Application and Evaluation of Two Air Quality Models for Particulate Matter for a Southeastern U.S. Episode, Journal of Air & Waste Management Association, 54, 1478-1493.

APPENDIX: San Joaquin Valley 12 µg/m^3 Annual $PM_{2.5}$ (2016)

Table of Contents

1. TIMELINE OF THE PLAN 7

2. DESCRIPTION OF THE CONCEPTUAL MODEL FOR THE NONATTAINMENT AREA 8

2.1 History of Field Studies in the Region 8

2.2 Description of the Ambient Monitoring Network 13

2.3 $PM_{2.5}$ Air Quality Trends 20

2.4 Major $PM_{2.5}$ Components 24

2.5 Seasonality of $PM_{2.5}$ and Meteorological Conditions Leading to Elevated $PM_{2.5}$ 26

REFERENCES 29

LIST OF TABLES

Table 1-1. Timeline for Completion of the Plan 7

Table 2-1. Major Field Studies in Central California and surrounding areas. 11

Table 2-2. 2012-2015 San Joaquin Valley $PM_{2.5}$, ozone, NO_x, and PAMS Sites 16

Table 2-3. Annual Average $PM_{2.5}$ ($\mu g/m^3$) 21

Table 2-4. Annual $PM_{2.5}$ Design Value (three year average, $\mu g/m^3$) 22

LIST OF FIGURES

Figure 2-1. Map of the ambient monitoring network in the San Joaquin Valley. 15

Figure 2-2. Trends in valley-wide annual average, 24-hour 98th percentile $PM_{2.5}$, and approximate number of days above the 24-hour standard (http://www.arb.ca.gov/adam/index.html). 23

Figure 2-3. San Joaquin Valley trends in $PM_{2.5}$, NO_x, and VOC emissions. 23

Figure 2-4. Three-year average (2011-2013) and average peak day (top 10 percent over the same three years) $PM_{2.5}$ composition at Bakersfield, Fresno, and Modesto. .. 25

Figure 2-5. 24-hour $PM_{2.5}$ concentrations at Bakersfield- California Avenue in 2013. ... 26

ACRONYMS

ACHEX - Aerosol Characterization Experiment

ARCTAS - Arctic Research of the Composition of the Troposphere from Aircraft and Satellites

BEARPEX - Biosphere Effects on Aerosols and Photochemistry Experiment

CABERNET - California Airborne BVOC Emission Research in Natural Ecosystem Transects

CalNex - Research at the Nexus of Air Quality and Climate Change

CARB – California Air Resources Board

CARES - Carbonaceous Aerosols and Radiative Effects Study

CCOS - Central California Ozone Study

CIRPAS - Center for Interdisciplinary Remotely-Piloted Aircraft Studies

CRPAQS - California Regional PM_{10}/$PM_{2.5}$ Air Quality Study

CSN – Chemical Speciation Network

DISCOVER-AQ - Deriving Information on Surface Conditions from Column and Vertically Resolved Observations Relevant to Air Quality

FEM – Federal Equivalent Method

FRM – Federal Reference Method

IMPROVE - Interagency Monitoring of Protected Visual Environments

IMS - Integrated Monitoring Study

NASA – National Aeronautics and Space Administration

NOAA – National Oceanic and Atmospheric Administration

OC – Organic Carbon

OM – Organic Matter

PAMS - Photochemical Assessment Monitoring Stations

$PM_{2.5}$ – Particulate matter with aerodynamic diameter less than 2.5 µm

SJV - San Joaquin Valley

SJVAB - San Joaquin Valley Air Basin

SJVAPCD - San Joaquin Valley Air Pollution Control District

SJVAQS/AUSPEX - San Joaquin Valley Air Quality Study/Atmospheric Utilities Signatures Predictions and Experiments

SLAMS - State and Local Air Monitoring Stations

SOA – Secondary Organic Aerosol

SoCAB - Southern California Air Basin

U.S. EPA – United States Environmental Protection Agency

VOC – Volatile Organic Compounds

1. TIMELINE OF THE PLAN

Table 1-1. Timeline for Completion of the Plan

Timeline	Action
Late 2015/Early 2016	Emission Inventory Completed
Spring/Summer 2016	Modeling Completed
September 15, 2016	San Joaquin Valley Governing Board Hearing to consider the Draft Plan
October 20, 2016	ARB Board Hearing to consider the SJV Adopted Plan
October 15, 2016	Plan is due to U.S. EPA

2. DESCRIPTION OF THE CONCEPTUAL MODEL FOR THE NONATTAINMENT AREA

2.1 History of Field Studies in the Region

The San Joaquin Valley (SJV) air basin is perhaps the second most studied air basin in the world, in terms of the number of publications in peer-reviewed international scientific/technical journals and other major reports, with the Los Angeles air basin being the first. Major Field studies that have taken place in the SJV and surrounding areas are listed in Table 2-1.

The first major air quality study in the SJV, dubbed Project Lo-Jet, took place in 1970 and resulted in the identification of the Fresno Eddy (Lin and Jao, 1995 and references therein). The first Valley-wide study that formed the foundation for a SIP was the San Joaquin Valley Air Quality Study/Atmospheric Utilities Signatures Predictions and Experiments (SJVAQS/AUSPEX) study, also known as SARMAP (SJVAQS/AUSPEX Regional Modeling Adaptation Project). A 1-hour Extreme Ozone Attainment Demonstration Plan based on the SARMAP Study was submitted to the U.S. EPA in 2004 and was approved in 2010 (74 FR 33933; 75 FR 10420). The next major study was the Integrated Monitoring Study in 1995 (IMS-95), which was the pilot study for the subsequent California Regional $PM_{10}/PM_{2.5}$ Air Quality Study (CRPAQS) in 2000 (Solomon and Magliano, 1998). IMS-95 formed the technical basis for the 2003 PM10 SIP which was approved by the U.S. EPA in 2006 (71 FR 63642). The area was re-designated as attainment in 2008 (73 FR 66759). The first annual field campaign in the SJV was CRPAQS, and embedded in it was the Central California Ozone Study (CCOS) that took place during the summer of 2000 (Fujita et al., 2001). CRPAQS was a component of the technical foundation for the 2008 annual $PM_{2.5}$ SIP which was approved by the U.S. EPA in 2011 (76 FR 41338; 76 FR 69896), and CCOS was part of the technical basis for the 2007 8-hour O_3 SIP (76 FR 57846). While CRPAQS is still highly relevant to the current annual 24-hour $PM_{2.5}$ SIP, there are additional, more recent studies with relevance to $PM_{2.5}$ formation in the Valley and surrounding regions: 1) ARCTAS-CARB 2008, 2) CalNex 2010, 3) CARES 2010, 4) BEARPEX 2007 & 2009, 5) CABERNET 2011, and 6) DISCOVER-AQ 2013. Each of these studies has contributed significantly to our understanding of various atmospheric processes in the Valley.

The ARCTAS-CARB aircraft field campaign was a joint research effort by NASA and CARB and took place from June 18 to 24, 2008. During the study, DC-8 aircraft performed two flights over southern California on June 18 and 24 with a focus on the Southern California Air Basin (SoCAB), one flight over northern California with a focus

on the San Joaquin Valley Air Basin (SJVAB) on June 20, and one flight off shore on June 22 to quantify the pollutant levels in air masses entering California from the Pacific Ocean. During the campaign, large wildfires occurred in California, particularly in the north. The DC-8 aircraft encountered many of the fire plumes, which allowed for the study of fire emissions and their chemical composition, as well as evaluation of the simulated fire impacts. The ARCTAS-CARB campaign provided a unique dataset for evaluating the impacts of wildfires on ozone levels through photochemical modeling studies and for evaluating the distribution of reactive nitrogen species in California (Huang et al., 2011; Cai et al., 2016).

The CalNex May-July 2010 field campaign was organized by NOAA (NOAA, 2014) and CARB. The focus of this field study included airborne measurements using the NOAA WP-3D aircraft and the Twin Otter Remote Sensing aircraft, and surface measurements using the R/V *Atlantis* mobile platform as well as two stationary ground supersites, one of which was located in Bakersfield. Analysis of the data collected during CalNex has shown that photochemical ozone production in the southern and central portions of the Valley is transitioning to a NO_x-limited chemistry regime, where further NO_x reductions are expected to lead to a more rapid reduction in ozone than what was observed over the past decade or more (Pusede and Cohen, 2012). Studies have also shown that there is evidence for an unidentified temperature-dependent VOC emissions source on the hottest days (Pusede and Cohen, 2012; Pusede et al., 2014) and large sources of hydrocarbon compounds from petroleum extraction/processing, dairy (and other cattle) operations, and agricultural crops in SJV (Gentner et al., 2014a,b). In addition, findings also suggest that NO_x emissions control nighttime secondary organic aerosol formation in Bakersfield, thus reductions in NOx emissions should reduce organic aerosol concentrations in Bakersfield and the surrounding region (Rollins et al., 2012).

The CARES field campaign took place in the central California region, to the northeast of Sacramento in June 2010. Comprehensive data sets of trace gases and aerosols were taken from the daily evolving Sacramento urban plume under relatively well-defined and regular meteorological conditions using multiple suites of ground-based and airborne instruments onboard the Gulfstream (G-1) research aircraft. The ground-based measurements were conducted at two sites: one within the Sacramento urban source area and the other in a downwind area about 70 km to the northeast in Cool, CA. A combination of measurement and model data during CARES (Fast et al., 2012) shows that emissions from the San Francisco Bay area transported by intrusions of marine air contributed a large fraction of the carbon monoxide in the vicinity of Sacramento. The study also showed that mountain venting processes contributed to aged pollutants aloft in the valley atmosphere which are then entrained into the growing boundary layer the following day. Although the CARES study did not take place within the SJV itself, it

remains relevant to the SJV for two reasons: 1) CARES took place within the delta region north of the SJV, which can influence air quality in the northern SJV (see Section 2.4), and 2) the improved scientific understanding of the interaction between urban emissions and downwind biogenic emissions gained during CARES is applicable to the SJV, which experiences a similar confluence of anthropogenic and biogenic emissions.

BEARPEX was conducted at the University of California's Blodgett Forest Research Station during June-July 2007 and September-October 2009. Blodgett Forest is located 65 miles northeast of Sacramento. The project was designed to study chemistry downwind of urban areas where there is high VOC reactivity (due to biogenic emissions sources) and low NO_x, to understand the full oxidation sequence and subsequent fate of biogenic VOC and the processes leading to formation and removal of biogenic secondary organic aerosol (SOA) and the associated chemical and optical properties of SOA. A study by Bouvier-Brown et al., (2009) suggests that reactive and semi-volatile compounds, especially sesquiterpenes, significantly impact the gas- and particle-phase chemistry of the atmosphere at Blodgett Forest. An analysis of absolute PANs mixing ratios by Lafranchi et al. (2009) reveals a missing PANs sink that can be resolved by increasing the peroxy acetyl radicals + RO2 rate constant by a factor of three. At the BEARPEX field site, the sum of the individual biogenically derived nitrates account for two-thirds of the organic nitrate, confirming the importance of biogenic nitrates to the NO_y budget (Beaver et al., 2012).

The CABERNET field campaign was conducted in June 2011 in California. The objectives were to develop and evaluate new approaches for regional scale measurements of biogenic VOC emissions, quantify the response of biogenic VOC emissions to land cover change, investigate the vertical transport of isoprene and oxidation products, and evaluate biogenic emission models. Isoprene fluxes were measured on board the Center for Interdisciplinary Remotely-Piloted Aircraft Studies (CIRPAS) Twin Otter (http://www.cirpas.org/twinOtter.html) using the virtual disjunct eddy covariance method (Karl et al. 2013). Isoprene flux measurements from CABERNET have formed the basis for evaluating the biogenic emissions inventory used in California's SIP modeling (Misztal et al., 2016).

The DISCOVER-AQ (Deriving Information on Surface Conditions from Column and Vertically Resolved Observations Relevant to Air Quality) field campaign took place in the SJV from January 16th through mid-February 2013. The campaign was organized by NASA, with the primary goal of relating column observations (e.g., from satellites) to surface measurements of $PM_{2.5}$ and key trace gases such as O_3, NO_2, and formaldehyde. The campaign captured two elevated $PM_{2.5}$ episodes in the SJV when 24-hour $PM_{2.5}$ concentrations in Bakersfield exceeded 60 µg/m^3. During the campaign,

sampling by two aircrafts focused on agricultural and vehicle traffic emission sources from Bakersfield to Fresno. In addition to the aircraft measurements there were also intensive ground-based data collection in Fresno and Porterville. The field campaign provided unprecedented observations of $PM_{2.5}$ and its precursors with broad horizontal spatial coverage, at the surface as well as aloft, and also at a finer temporal resolution (i.e., minutes compared to daily or multiple hours in the past) than was previously available. The combination of highly resolved spatial and temporal measurements presented a unique opportunity to update the conceptual model for wintertime $PM_{2.5}$ formation in the SJV that was initially developed from CRPAQS field study. Pusede et al. (2016) analyzed the DISCOVER-AQ dataset and historical ammonium nitrate records in the SJV and concluded that NO_x emissions control in the valley in the past decade has substantially decreased nighttime ammonium nitrate formation in the nocturnal residual layer and continued reduction in NO_x emissions in the SJV will lead to fewer wintertime exceedances of the 24-hour $PM_{2.5}$ standard. This study lends support to the emissions control policies in the SJV that have historically focused on NO_x emissions.

Table 2-1. Major Field Studies in Central California and surrounding areas.

Year	Study	Significance
1970	Project Lo-Jet	Identified summertime low-level jet and Fresno eddy
1972	Aerosol Characterization Experiment (ACHEX)	First TSP chemical composition and size distributions
1979-1980	Inhalable Particulate Network	First long-term $PM_{2.5}$ and PM_{10} mass and elemental measurements in Bay Area, Five Points
1978	Central California Aerosol and Meteorological Study	Seasonal TSP elemental composition, seasonal transport patterns
1979-1982	Westside Operators	First TSP sulfate and nitrate compositions in western Kern County
1984	Southern SJV Ozone Study	First major characterization of O_3 and meteorology in Kern County
1986-1988	California Source Characterization Study	Quantified chemical composition of source emissions

1988-1989	Valley Air Quality Study	First spatially diverse, chemical characterized, annual and 24-hour $PM_{2.5}$ and PM_{10}
Summer 1990	San Joaquin Valley Air Quality Study/Atmospheric Utilities Signatures Predictions and Experiments (SJVAQS/AUSPEX) – Also known as SARMAP (SJVAQS/AUSPEX Regional Modeling Adaptation Project)	First central California regional study of O_3 and $PM_{2.5}$
July and August 1991	California Ozone Deposition Experiment	Measurements of dry deposition velocities of O_3 using the eddy correlation technique made over a cotton field and senescent grass near Fresno
Winter 1995	Integrated Monitoring Study (IMS-95, the CRPAQS Pilot Study)	First sub-regional winter study
December 1999 – February 2001	California Regional $PM_{10}/PM_{2.5}$ Air Quality Study (CRPAQS) and Central California Ozone Study (CCOS)	First year-long, regional-scale effort to measure both O_3 and $PM_{2.5}$
December 1999 to present	Fresno Supersite	First multi-year experiment with advanced monitoring technology
July 2003	NASA high-resolution lidar flights	First high-resolution airborne lidar application in SJV in the summer
February 2007	U.S. EPA Advanced Monitoring Initiative	First high-resolution airborne lidar application in SJV in the winter
August-October 2007; June-July 2009	BEARPEX (Biosphere Effects on Aerosols and Photochemistry Experiment)	Research-grade measurements to study the interaction of the Sacramento urban plume with downwind biogenic emissions
June 2008	ARCTAS - CARB	First measurement of high-time resolution (1-10s) measurements of organics

		and free radicals in SJV
May-July 2010	CalNex 2010 (Research at the Nexus of Air Quality and Climate Change)	Expansion of ARCTAS-CARB type research-grade measurements to multi-platform and expanded geographical area including the ocean.
June 2010	CARES (Carbonaceous Aerosols and Radiative Effects Study)	Research-grade measurements of trace gases and aerosols within the Sacramento urban plume to investigate SOA formation
June 2011	CABERNET (California Airborne BVOC Emission Research in Natural Ecosystem Transects)	Provided the first ever airborne flux measurements of isoprene in California
January- February 2013	DISCOVER-AQ (Deriving Information of Surface Conditions from Column and Vertically Resolved Observations Relevant to Air Quality)	Research-grade measurements of trace gases and aerosols during two $PM_{2.5}$ pollution episodes in the SJV

2.2 Description of the Ambient Monitoring Network

The San Joaquin Valley covers an area of 23,490 square miles and is home to approximately 4 million residents. The Valley is bordered on the west by the coastal mountain ranges and on the east by the Sierra Nevada range. These ranges converge at the southern end of the basin at the Tehachapi Mountains. The majority of the population is centered in the large urban areas of Bakersfield, Fresno, Modesto, and Stockton. The nonattainment area includes seven full counties (San Joaquin, Stanislaus, Merced, Madera, Fresno, Kings, and Tulare) and one partial county Kern (only the western portion of Kern County, which lies in the jurisdiction of the SJVAPCD, is included).

The Valley can be divided into three regions that are characterized by distinct geography, meteorology, and air quality: 1) northern SJV (San Joaquin, Stanislaus, and Merced counties), 2) central SJV (Madera, Fresno, and King counties), and 3) southern SJV (Tulare and Western Kern counties). A third of the Valley population lives in the

northern SJV. This lowland area is bordered by the Sacramento Valley and Delta lowland to the north, the central portion of the SJV to the south, and mountain ranges to the east and west. Because of the marine influence, which extends into this area through gaps in the coastal mountains to the west, the northern SJV experiences a more temperate climate than the rest of the Basin. These more moderate temperatures (cooler in the summer and warmer in the winter) and the predominant air flow patterns generally favor better air quality. Similar to the northern SJV, the central and southern SJV are also low lying areas, flanked by mountains on their west and east sides. The worst air quality within the Valley occurs in these two regions, where the population is primarily clustered around the Fresno and Bakersfield urban areas. In these regions the interaction between geography, climate, and a mix of natural (biogenic) and anthropogenic emissions pose significant challenges to air quality progress. The southern SJV represents the terminus of the Valley and is flanked by mountains on the south, as well. The surrounding mountains in both areas act as barriers to air flow, and combined with recirculation patterns and stable air to trap emissions and pollutants near the valley floor. The more extreme temperatures and stagnant conditions in these two regions lead to a build-up of $PM_{2.5}$ and ozone, and overall poorer air quality. In addition to the urban air quality problems, emissions and pollutants from these areas are transported downwind, resulting in poor air quality in downwind areas.

As discussed above, the Valley's diverse area includes several major metropolitan areas, vast expanses of agricultural land, industrial sources, and highways, all of which pose many issues to air quality. The San Joaquin Valley Air Pollution Control District (SJVAPCD or District), the California Air Resources Board (CARB), and the National Park Service work together and operate an extensive network of air quality monitors throughout the Valley to help improve and protect public health. The data collected from the Valley air monitoring network is used to generate daily air quality forecasts, issue health advisories as needed, support compliance with various ambient air quality standards and serves as the basis for developing long-term attainment strategies and tracking progress towards health-based air quality standards.

Figure 2-1 shows the spatial distribution of the $PM_{2.5}$, ozone, NO_x, and PAMS (Photochemical Assessment Monitoring Stations) monitors in the Valley (see Table 2-2 for longitude/latitude information for each monitor). The monitors are located throughout the Valley floor, at higher elevation locations, and within higher population density urban areas, and have been shown to sufficiently capture the highest ozone mixing ratios and the corresponding precursors under various weather conditions and in all major population centers. A detailed discussion about the monitoring network and its adequacy can be found in the Valley's 2015 Air Monitoring Network Plan (http://www.valleyair.org/aqinfo/Docs/2015-Air-Monitoring-Network-Plan.pdf) and 2014 California Infrastructure SIP (http://www.arb.ca.gov/planning/sip/infrasip/docs/i-sip.pdf).

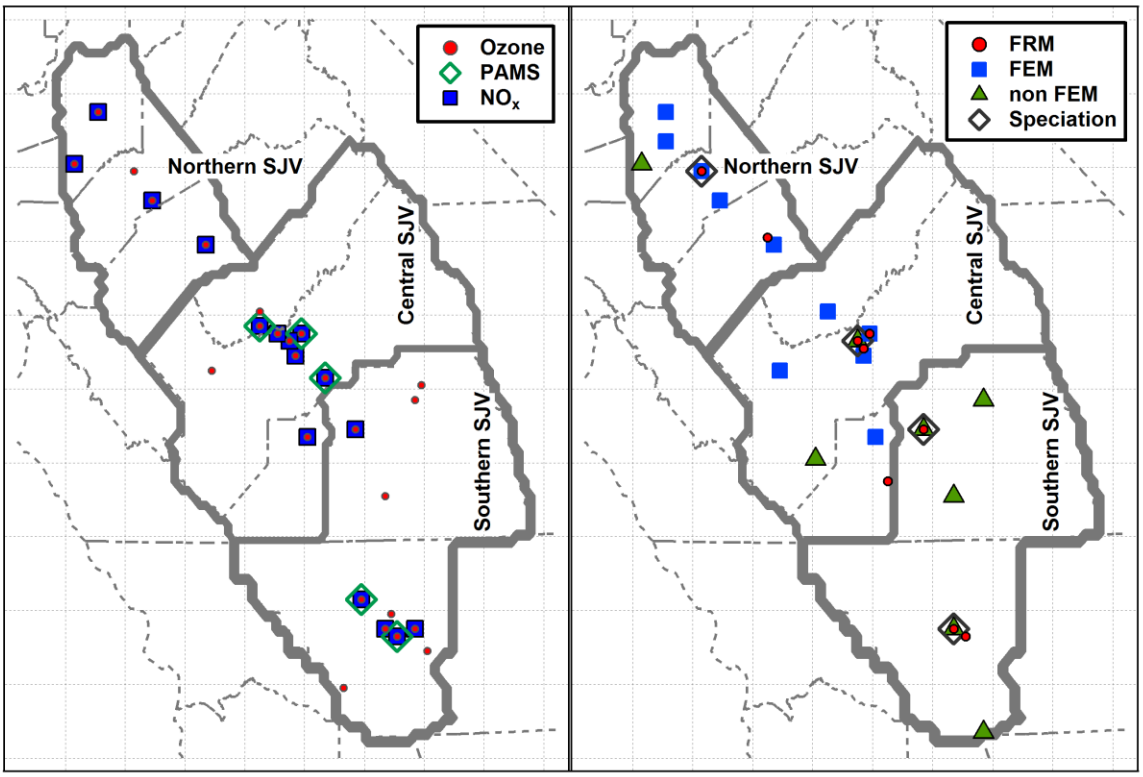

Figure 2-1. Map of the ambient monitoring network in the San Joaquin Valley.

Table 2-2. 2012-2015 San Joaquin Valley $PM_{2.5}$, ozone, NO_x, and PAMS Sites

Site ID (AQS/ARB)	Sub Region	Site	Particulate Matter				Gaseous			Location	
			FRM	FEM	non-FEM	Speciation	NO_x	Ozone	PAMS	Latitude	Longitude
Fresno County											
060195001 3026	Central SJV	Clovis-N Villa Avenue	X	X			X	X	X	36.8194	-119.7164
060190008 3009	Central SJV	Fresno-1st Street					X	X		36.7819	-119.7731
060190007 2013	Central SJV	Fresno-Drummond Street		X			X	X		36.7053	-119.7413
060190011 3781	Central SJV	Fresno-Garland	X		X	X	X	X		36.7853	-119.7742
060195025 3485	Central SJV	Fresno – Hamilton and Winery	X							36.7436	-119.7486
060190242 2844	Central SJV	Fresno-Sierra Skypark #2					X	X		36.8417	-119.8828
060192008 3768	Central SJV	Huron-16875 4th Street			X					36.1986	-120.1010
060194001 2114	Central SJV	Parlier					X	X	X	36.5974	-119.5039
060192009 3759	Central SJV	Tranquility-32650 West Adams Avenue		X				X		36.6342	-120.3823

Kern County										
060295002 3758	Southern SJV	Arvin-Di Giorgio					X		35.2367	-118.7894
060290016 3496	Southern SJV	Bakersfield-410 E Planz Road	X						35.3246	-118.9976
060290014 3146	Southern SJV	Bakersfield-5558 California Avenue	X	X	X	X	X		35.3567	-119.0628
060292012 3787	Southern SJV	Bakersfield-Municipal Airport				X	X	X	35.3313	-119.001
060290007 2312	Southern SJV	Edison				X	X		35.3458	-118.8506
060292009 3769	Southern SJV	Lebec-Beartrap Road		X					34.8415	-118.8605
060290008 2919	Southern SJV	Maricopa-Stanislaus Street					X		35.0514	-119.4028
060290232 2772	Southern SJV	Oildale-3311 Manor Street					X		35.4381	-119.0167
060296001 2981	Southern SJV	Shafter-Walker Street				X	X	X	35.5033	-119.2728
Kings County										
060310004 3194	Central SJV	Corcoran-Patterson Avenue	X						36.1022	-119.5658

060311004 3129	Central SJV	Hanford-S Irwin Street		X			X	X		36.3147	-119.6436
Madera County											
060392010 3771	Central SJV	Madera-28261 Avenue 14		X				X		36.9533	-120.0342
060390004 3211	Central SJV	Madera-Pump Yard					X	X	X	36.8672	-120.01
Merced County											
060470003 3022	Northern SJV	Merced-S Coffee Avenue		X			X	X		37.2817	-120.4336
060472510 3253	Northern SJV	Merced-2334 M Street	X							37.3092	-120.4806
San Joaquin County											
060772010 3772	Northern SJV	Manteca-530 Fishback Rd		X						37.7934	-121.2478
060771002 2094	Northern SJV	Stockton-Hazelton Street		X			X	X		37.9517	-121.2689
060773005 3696	Northern SJV	Tracy-Airport			X		X	X		37.6825	-121.4406
Stanislaus County											
060990005 2833	Northern SJV	Modesto-14th Street	X	X		X		X		37.6419	-120.9942
060990006 2996	Northern SJV	Turlock-S Minaret Street		X			X	X		37.4882	-120.8359

Tulare County									
061072010 3763	Southern SJV	Porterville -1839 Newcomb Street		X			X	36.0318	-119.055
061070009 3484	Southern SJV	Sequoia and Kings Canyon Natl Park		X			X	36.4911	-118.8342
061070002 3036	Southern SJV	Sequoia Natl Park-Lower Kaweah					X	36.564	-118.773
061072002 2032	Southern SJV	Visalia-N Church Street	X	X	X	X	X	36.3325	-119.2908

2.3 $PM_{2.5}$ Air Quality Trends

Tables 2-3 and 2-4 show the annual average $PM_{2.5}$ concentration and the annual $PM_{2.5}$ design values (i.e., 3-year average), from 1999 to 2013, for FRM and FEM sites in the SJV, respectively. Based on the 2013 design value, 13 out of the 16 FRM/FEM sites exceeded the annual $PM_{2.5}$ standard of 12 µg/m^3, with the Madera-city site having the highest design value at 18.1 µg/m^3. Figure 2-2 shows the trend in peak valley-wide annual average $PM_{2.5}$ concentration and 98th percentile of the 24-hour $PM_{2.5}$ concentration, as well as the approximate number of days above the 24-hour standard in the valley from 1999 to 2015. The extreme drought conditions experienced by much of California since 2012 coupled with persistent and strong high pressure systems over the SJV in recent winters, has led to elevated levels of $PM_{2.5}$ in the SJV that have not been seen in over a decade. This is clearly illustrated by the "U" shaped curve of the 98th percentile 24-hour $PM_{2.5}$ shown in Figure 2-2. Despite the recent increase in peak 24-hour $PM_{2.5}$ levels, the SJV has seen significant improvement in $PM_{2.5}$ concentrations over the last 15 years, with steady decreases in both annual average $PM_{2.5}$ and in the number of days above the 24-hour standard, which coincide with the large emission reductions experienced in the valley (Figure 2-3).

Table 2-3: Annual Average $PM_{2.5}$ ($\mu g/m^3$)

SJV Monitoring Site	1999	2000	2001	2002	2003	2004	2005	2006	2007	2008	2009	2010	2011	2012	2013
Stockton	19.7	15.5	13.9	16.7	13.6	13.2	12.5	13.1	12.9	14.4	11.3	11.0	11.3	12.4	17.7
Manteca													10.8	8.3	11.7
Modesto	24.9	18.7	15.6	18.7	14.5	13.6	13.9	14.8	15.0	16.0	13.0	12.3	14.7	11.9	14.3
Turlock											16.1	12.7	17.1	14.8	15.1
Merced-Coffee												16.3	15.6	11.0	13.3
Merced-M		16.7	14.5	18.7	15.7	15.2	14.1	14.8	15.2		13.6	11.2	10.4	9.5	13.5
Madera-City													20.4	16.0	17.8
Fresno-First	27.6		19.8	21.5	17.8	16.3	16.7	16.8	18.8	17.4	15.1	13.0	15.5		
Fresno-Garland														14.1	16.8
Fresno-Winery		18.4	18.6	21.3	17.8	17.0	16.9	17.6	16.8	16.5	14.6	13.4	15.4	12.7	15.9
Clovis	19.8	16.3	18.0	16.2	18.5	16.4	16.3	16.4	16.4	16.2	18.3	14.7	17.9	15.4	15.9
Tranquility												7.0	8.2	7.1	8.4
Corcoran		16.4	19.2	21.5	16.2	17.4	17.5	16.9	18.4	15.8	17.7	17.9			15.6
Hanford													18.0	14.8	18.2
Visalia	27.6	23.9	22.5	23.2	18.2	17.0	18.8	18.8	20.4	19.8	16.0	13.6	16.1	14.8	18.9
Bakersfield-Golden	26.2	22.6	21.8	24.1	19.6	18.2	19.1	18.6	19.9	17.9					
Bakersfield-California	27.4	22.5	21.2	22.7	17.1	18.9	18.0	18.7	22.0	21.9	19.0	14.2	16.2	13.0	20.0
Bakersfield-Planz		20.3	20.8	23.5	17.8	17.4	19.8	19.3	21.8	23.5	22.5	17.6	14.4	14.7	21.7

Table 2-4: Annual $PM_{2.5}$ Design Value (three year average, $\mu g/m^3$)

SJV Monitoring site	2001	2002	2003	2004	2005	2006	2007	2008	2009	2010	2011	2012	2013
Stockton	16.4	15.3	14.7	14.5	13.1	12.9	12.8	13.5	12.9.	12.2	11.2	11.6	13.8
Manteca													10.2
Modesto	19.7	17.7	16.2	15.6	14.0	14.1	14.6	15.3	14.7	13.8	13.3	12.9	13.6
Turlock											15.3	14.9	15.7
Merced-Coffee												14.3	13.3
Merced-M		16.6	16.3	16.5	15.0	14.7	14.7				11.7	10.4	11.1
Madera-City													18.1
Fresno-First			19.7	18.6	16.9	16.6	17.4	17.7	17.1	15.2	14.5		
Fresno-Garland													15.4
Fresno-Winery		19.4	19.2	18.7	17.2	17.2	17.1	17.0	16.0	14.9	14.5	13.9	14.7
Clovis	18.0	16.8	17.6	17.0	17.1	16.4	16.4	16.4	17.0	16.4	17.0	16.0	16.4
Tranquility												7.5	7.9
Corcoran		19.0	19.0	18.4	17.0	17.2	17.6	17.0	17.3	17.1			
Hanford												15.8	17.0
Visalia	24.7	23.2	21.3	19.5	18.0	18.2	19.3	19.7	18.8	16.5	15.2	14.8	16.6
Bakersfield-Golden	23.6	22.8	21.8	20.6	19.0	18.6	19.2	18.8					
Bakersfield-California	23.7	22.1	20.3	19.6	18.0	18.5	19.6	20.9	21.0	18.4	16.5	14.5	16.4
Bakersfield-Planz		21.5	20.7	19.6	18.4	18.9	20.3	21.5	22.6	21.2	18.2	15.6	16.9

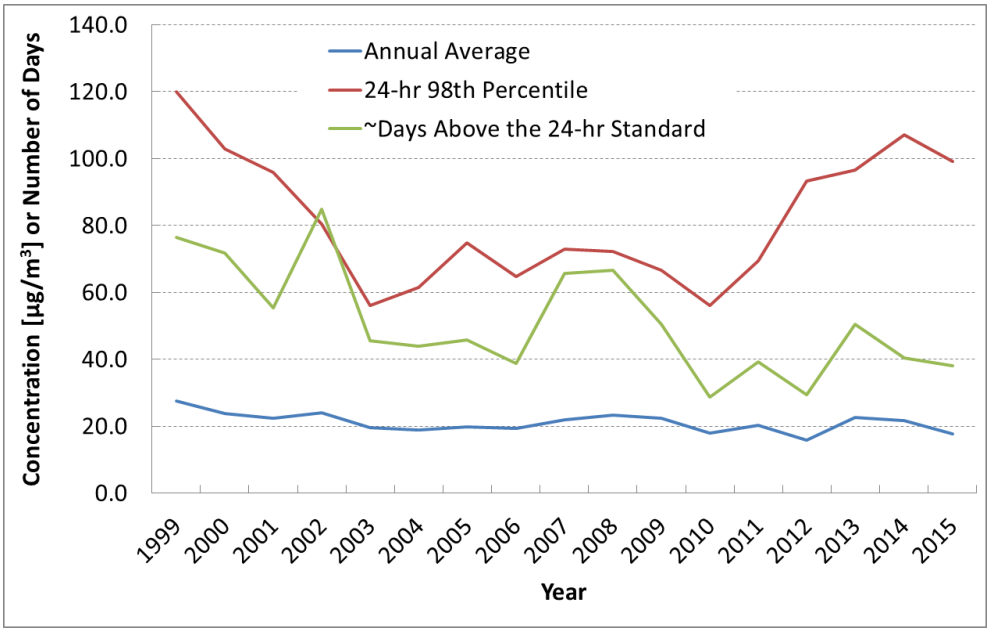

Figure 2-2. Trends in valley-wide annual average, 24-hour 98th percentile $PM_{2.5}$, and approximate number of days above the 24-hour standard (http://www.arb.ca.gov/adam/index.html).

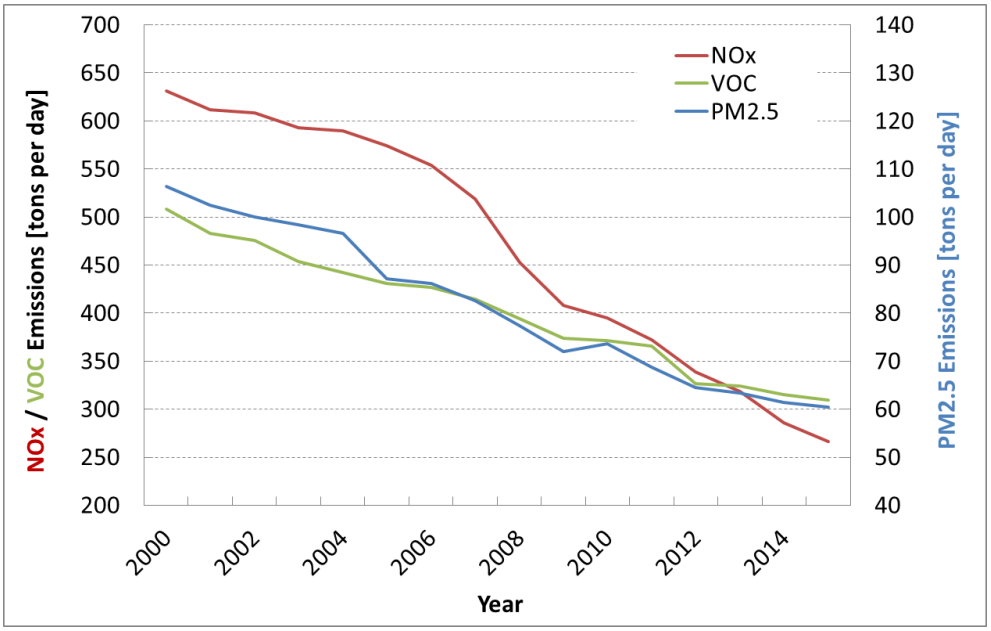

Figure 2-3. San Joaquin Valley trends in $PM_{2.5}$, NO_x, and VOC emissions.

2.4 Major $PM_{2.5}$ Components

Four monitoring sites collect $PM_{2.5}$ chemical composition data in the San Joaquin Valley: Bakersfield-California, Fresno-Garland, Modesto, and Visalia. The Bakersfield and Fresno speciation monitors are part of the national Chemical Speciation Network (CSN) while Modesto and Visalia are part of the State and Local Air Monitoring Stations (SLAMS) network. All four sites use SASS samplers (Spiral Aerosol Speciation Sampler, Met One, Grants Pass, OR.) for data collection. The CSN data are analyzed by the Research Triangle Institute and the SLAMS data are analyzed by ARB. In recent years, changes were made to the carbon sampling and analysis method. The collection method changed from the MetOne SASS to the URG3000N sampler, which is very similar to the IMPROVE module C sampler. The analytical method was changed from the NIOSH-like thermal optical transmittance method to IMPROVE_A thermal optical reflectance. At Bakersfield, Modesto, and Visalia these changes were implemented in May of 2007, and the Fresno site switched to the new carbon system in April of 2009.

Figure 2-4 illustrates the average of the 2011-2013 annual average $PM_{2.5}$ composition, as well as average of the top 10 percent of days at Bakersfield, Fresno, and Modesto over the same time period. Organic matter (OM) was calculated by multiplying measured OC by 1.5 according to the OM/OC ratio measured at Fresno (Ge et al., 2012). Ammonium nitrate is the largest contributor to $PM_{2.5}$ on annual basis, accounting for approximately 40% of the $PM_{2.5}$ mass. Its contribution is even higher on peak $PM_{2.5}$ days, accounting for 55-60% of $PM_{2.5}$ mass. Formation mechanisms for ammonium nitrate are discussed in Section 2.5. OM is the second most abundant component, constituting approximately 30% of the $PM_{2.5}$ mass on an annual basis. Activities such as residential wood combustion, cooking, biomass burning, and mobile sources contribute to OM levels in the atmosphere. In addition, OM can also be formed in the atmosphere from oxidation of VOCs. Ammonium sulfate contributes approximately 10% of the $PM_{2.5}$ on an annual basis. Its contribution is half that on peak days, at approximately 5%. Elemental carbon and crustal materials typically contribute less than 10% to $PM_{2.5}$ levels in these cities, except at Bakersfield, where crustal materials contributed more than 10% on an annual basis.

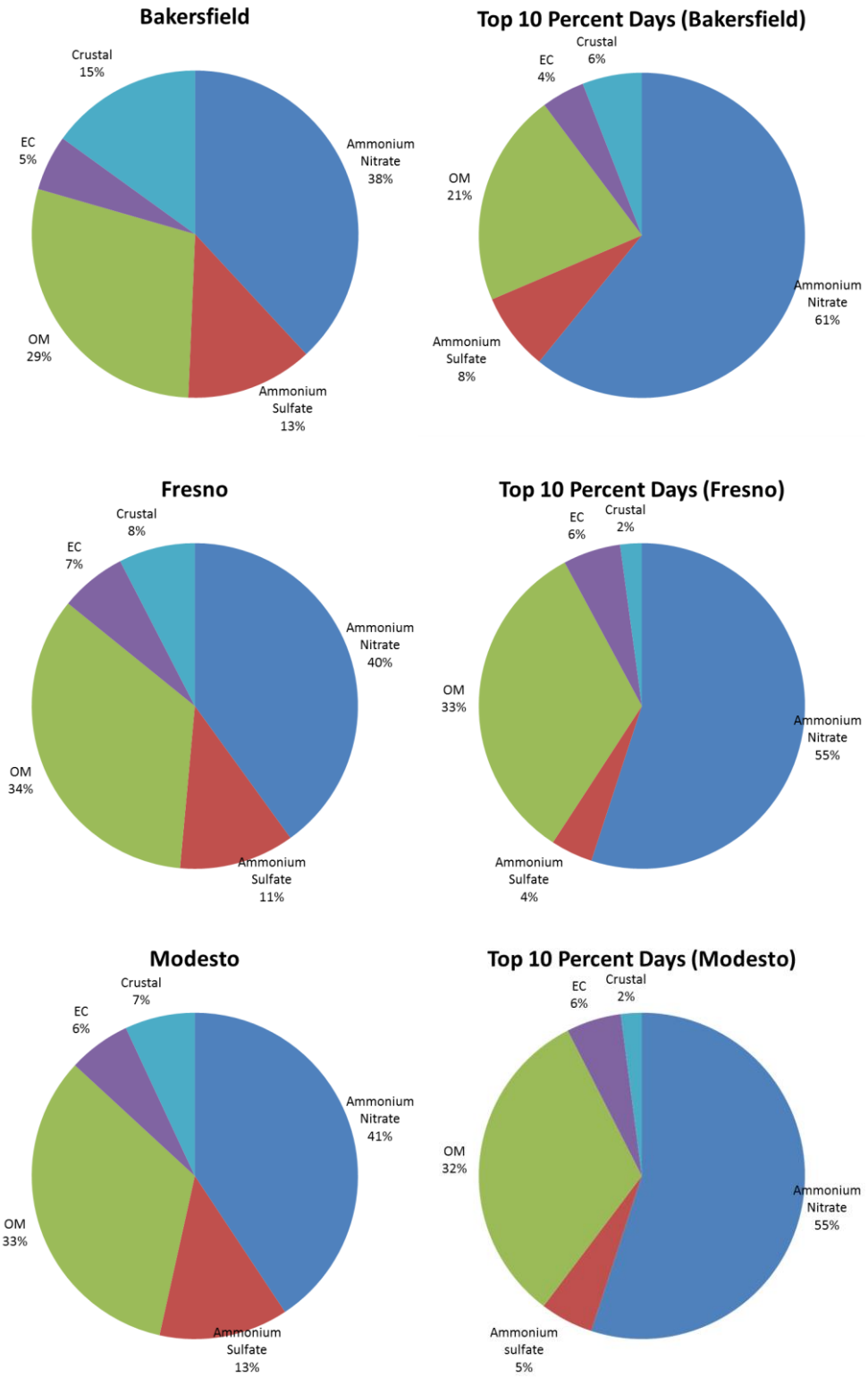

Figure 2-4. Three-year average (2011-2013) and average peak day (top 10 percent over the same three years) $PM_{2.5}$ composition at Bakersfield, Fresno, and Modesto.

2.5 Seasonality of $PM_{2.5}$ and Meteorological Conditions Leading to Elevated $PM_{2.5}$

$PM_{2.5}$ concentrations in the San Joaquin Valley exhibit a strong seasonal variability, with the highest concentrations occurring during the months of November through February. For example, Figure 2-5 represents the time series of 24-hour $PM_{2.5}$ concentrations at Bakersfield - California Avenue in 2013, which shows a vast majority of the elevated $PM_{2.5}$ episodes occurred in the first two and last two months of the year. The predominance of elevated $PM_{2.5}$ episodes during winter months results from a confluence of meteorological conditions conducive to the formation and buildup of $PM_{2.5}$, as well as wintertime sources of directly emitted $PM_{2.5}$.

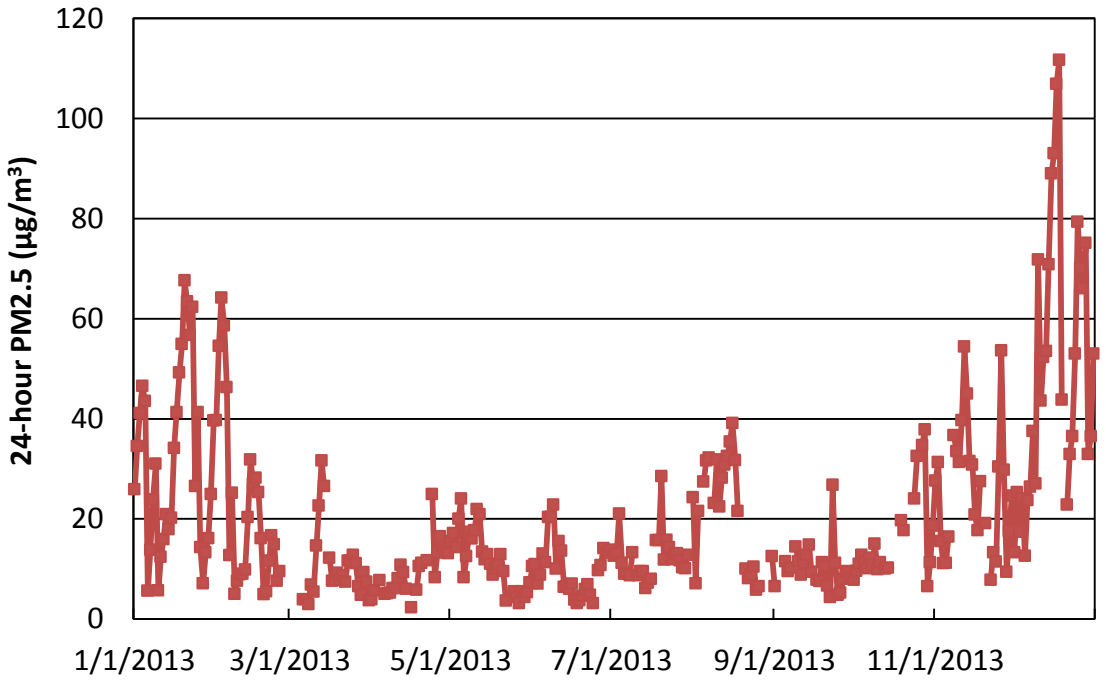

Figure 2-5. 24-hour $PM_{2.5}$ concentrations at Bakersfield- California Avenue in 2013.

High $PM_{2.5}$ concentrations typically build up during multiday episodes under stagnant winter weather when a high pressure system (the Great Basin High) reduces the ventilation in the Valley (Ferreria et al., 2005). These stagnation events, sandwiched between two weather systems, are characterized by low wind speeds, moderate temperatures, vertical atmospheric stability, and high relative humidity. This stable atmosphere prevents precursor gases and primary (or directly emitted) $PM_{2.5}$ released at the surface in the Valley from rapidly dispersing. The moderate temperatures and

high relative humidity also enhance the formation of secondary particulate matter, especially ammonium nitrate and sulfate. In contrast, hotter and drier weather conditions in summer favor the evaporation of semi-volatile species from particles. Greater mixing height in summer can also help the ventilation of air pollutants. As a result, summertime $PM_{2.5}$ concentrations in the SJV are typically much lower compared to wintertime.

Wintertime $PM_{2.5}$ episodes can last for many days. At the beginning of an episode, concentrations are low but increase daily because of both the accumulation of primary pollutants and formation of secondary pollutants (Watson et al, 2002). Concentrations continue to build until there is a change in the weather significant enough to wash out particles through rainfall or increased ventilation of the Valley. For example, the two main episodes captured during the CRPAQS field study (starting in late 1999) had up to 18 days with $PM_{2.5}$ concentrations exceeding 65 $\mu g/m^3$ (Turkiewicz et al., 2006). At the end of 2013 and the beginning of 2014, Bakersfield experienced 18 days with $PM_{2.5}$ concentrations greater than 35 $\mu g/m^3$. During such episodes, urban sites typically record elevated concentrations earlier than rural sites, and as a consequence, have a greater number of days with high concentrations. However, due to the buildup of $PM_{2.5}$ concentrations, rural sites can achieve concentrations with similar magnitude as urban sites by the end of an episode.

The elevated wintertime $PM_{2.5}$ concentrations observed during pollution episodes are the result of both directly emitted particulates (known as primary particulate matter) and particulate matter formed via chemical and physical processes in the atmosphere (known as secondary particulate matter). Ammonium nitrate, the dominant $PM_{2.5}$ component throughout the Valley, is formed in the atmosphere as a result of chemical reactions between precursor pollutants such as NO_x, VOC, and ammonia. Carbonaceous aerosol, the second most abundant component, is mostly directly emitted, and is the result of contributions from wood combustion (e.g., wood burning for heating), mobile sources, and cooking.

As shown in Figure 2-4, carbonaceous aerosols and ammonium nitrate together comprise approximately 80 percent of the $PM_{2.5}$ mass. In winter, most of the carbonaceous aerosol is emitted into the atmosphere as directly emitted particles, and its transport is much more limited compared to gaseous precursors of ammonium nitrate. Ammonium nitrate can be formed both at the surface and aloft and can be fairly uniform across urban and rural sites. The spatial homogeneity of ammonium nitrate is influenced by higher wind speeds aloft (which allow more efficient transport), and the diurnal variation in mixing heights (which allow entrainment of ammonium nitrate down to the surface).

Ammonium nitrate is also formed via both daytime and nighttime chemistry. The amount of ammonium nitrate produced will be limited by the relative abundance of its precursors in the atmosphere. In the San Joaquin Valley, the nighttime formation is considered to be the most important pathway (Lurmann et al., 2006). The nighttime pathway involves oxidation of NO_2, followed by reaction with ammonia to form ammonium nitrate. Since ammonia is abundant in the Valley in the winter, NO_x is considered to be the limiting precursor. In contrast, the daytime pathway also involves VOCs. Modeling studies that investigated winter episodes in the Valley estimated that reductions in VOC emissions have a small impact on nitrate concentrations only at very high $PM_{2.5}$ concentrations (Pun, et al., 2009). However, at current $PM_{2.5}$ levels the impact was very limited, and in some cases VOC reductions lead to an increase in $PM_{2.5}$ concentrations (Chen et al., 2014; Kleeman, et al., 2005).

REFERENCES

Beaver, M.R. et al., 2012 Importance of biogenic precursors to the budget of organic nitrates: observations of multifunctional organic nitrates by CIMS and TD-LIF during BEARPEX 2009, Atmos. Chem. Phys., 12, 5773-5785.

Bouvier-Brown, N.C., Goldstein, A.H., Gilman, J.B., Kuster, W.C., and de Gouw, J.A., 2009, Atmos. Chem. Phys., 9, 5505-5518.

Cai C. et al., 2016 Simulating reactive nitrogen, carbon monoxide, and ozone in California during ARCTAS-CARB 2008 with high wildfire activity, Atmos. Environ. 128, 28-44.

Chen, J., Lu, J., Avise, J.C., DaMassa, J.A., Kleeman, M.J., and Kaduwela, A.P., 2014, Seasonal modeling of PM2.5 in California's San Joaquin Valley, Atmospheric Environment, 92, 182-190.

Fast JD, WI Gustafson, Jr, LK Berg, WJ Shaw, MS Pekour, MKB Shrivastava, JC Barnard, R Ferrare, CA Hostetler, J Hair, MH Erickson, T Jobson, B Flowers, MK Dubey, PhD, SR Springston, BR Pirce, L Dolislager, JR Pederson, and RA Zaveri. 2012. "Transport and Mixing Patterns over Central California during the Carbonaceous Aerosol and Radiative Effects Study (CARES)." Atmospheric Chemistry and Physics 12(4):1759-1783. doi:10.5194/acp-12-1759-2012

Federal Register, 2006, Approval and Promulgation of Implementation Plans; Designation of Areas for Air Quality Planning Purposes; State of California; PM-10; Determination of Attainment for the San Joaquin Valley Nonattainment Area; Determination Regarding Applicability of Certain Clean Air Act Requirements, Final Rule, October 30th, 63642-63664.

Federal Register, 2008, Approval and Promulgation of Implementation Plans; Designation of Areas for Air Quality Planning Purposes; State of California; PM-10; Revision of Designation; Redesignation of the San Joaquin Valley Air Basin PM-10 Nonattainment Area to Attainment; Approval of PM-10 Maintenance Plan for the San Joaquin Valley Air Basin; Approval of Commitments for the East Kern PM-10 Nonattainment Area, Final Rule, November 12th, 66759-66775.

Federal Register, 2009, Approval and Promulgation of Implementation Plans: 1-Hour Ozone Extreme Area Plan for San Joaquin Valley, CA, Proposed Rule, July 14th, 33933-33947.

Federal Register, 2010, Approval and Promulgation of Implementation Plans: 1-Hour Ozone Extreme Area Plan for San Joaquin Valley, CA, March 8th, 10420-10438.

Federal Register, 2011, Approval and Promulgation of Implementation Plans; California; 2008 San Joaquin Valley PM2.5 Plan and 2007 State Strategy, Proposed Rule, July 13th, 41338-41363.

Federal Register, 2011, Approval and Promulgation of Implementation Plans; California; 2008 San Joaquin Valley PM2.5 Plan and 2007 State Strategy, Final Rule, November 9th, 69896-69926.

Ferreria, S.R. and Shipp, E.M., 2005, Historical Meteorological Analysis in Support of the 2003 San Joaquin Valley PM10 State Implementation Plan, San Joaquin Valley Air Pollution District, Fresno, CA.

Fujita, E., D. Campbell, R. Keisler, J. Brown, S. Tanrikulu, and A. J. Ranzieri, 2001, Central California Ozone Study (CCOS)-Final report, volume III:Summary of field operations, Technical Report, California Air Resources Board, Sacramento.

Ge, X., A. Setyan, Y. Sun, and Q. Zhang (2012), Primary and secondary organic aerosols in Fresno, California during wintertime: Results from high resolution aerosol mass spectrometry, J. Geophys. Res., 117, D19301, doi:10.1029/2012JD018026.

Gentner, D.R. et al., 2014a, Emissions of organic carbon and methane from petroleum and dairy operations in California's San Joaquin Valley Atmos. Chem. Phys., 14, 4955-4978.

Gentner, D.R., Ormeño, Fares, E.S., Ford, T.B., Weber, R., Park, J.-H., Brioude, J., Angevine, W.M., Karlik, J.F., and Goldstein, A.H., 2014b, Emissions of terpenoids, benzenoids, and other biogenic gas-phase organic compounds from agricultural crops and their potential implications for air quality Atmos. Chem. Phys., 14, 5393–5413.

Huang, M., Carmichael, G.R., Adhikary, B., Spak, S.N., Kulkarni, S., Cheng, Y.F., Wei, C., Tang, Y., Parrish, D.D., Oltmans, S.J., D'Allura, A., Kaduwela, A., Cai, C., Weinheimer, A.J., Wong, M., Pierce, R.B., Al-Saadi, J.A. Streets, D.G., and Zhang, Q., 2010, Impacts of transported background ozone on California air quality during the ARCTAS-CARB period - a multi-scale modeling study, Atmospheric Chemistry and Physics, 10(14), 6947-6968.

Karl, T, Misztal, P.K., Jonsson, H.H., Shertz, S., Goldstein, A.H., and Guenther, A.B., 2013, Airborne Flux Measurements of BVOCs above Californian Oak Forests: Experimental Investigation of Surface and Entrainment Fluxes, OH Densities, and Damköhler Numbers, JOURNAL OF THE ATMOSPHERIC SCIENCES, 70, 3277-3287

Kleeman, M.J., Ying, Q., and Kaduwela, A., 2005, Control strategies for the reduction of airborne particulate nitrate in California’s San Joaquin Valley, Atmospheric Environment, 39, 5325-5341.

LaFranchi, B.W. et al., 2009, Closing the peroxy acetyl nitrate budget: observations of acyl peroxy nitrates (PAN, PPN, and MPAN) during BEARPEX 2007, Atmos. Chem. Phys., 9, 7623–7641.

Lin, Y.L., and Jao, I.C., 1995, A Numerical Study of Flow Circulations in the Central Valley of California and Formation Mechanisms of the Fresno Eddy, Monthly Weather Review, 123(11), 3227-3239.

Lurmann, F.W., Brown, S.G., McCarthy, M.C., and P.T. Roberts. Processes Influencing Secondary Aerosol Formation in the San Joaquin Valley During Winter JAWMA, 2006, 56:1679-1693

Misztal, P. K., Avise, J. C., Karl, T., Scott, K., Jonsson, H. H., Guenther, A. B., and Goldstein, A. H., 2016, Evaluation of regional isoprene emission factors and modeled fluxes in California, Atmos. Chem. Phys. Discuss., doi:10.5194/acp-2016-130, in review.

NOAA (2014), Synthesis of Policy Relevant Findings from the CalNex 2010 Field Study, Final report to the California Air Resources Board, available at http://www.esrl.noaa.gov/csd/projects/calnex/synthesisreport.pdf

Pun, B.K., Balmori, R.T.F., Seigneur, C., 2009, Modeling wintertime particulate matter formation in central California, Atmospheric Environment, 43, 402-409.

Pusede, S. E., and R. C. Cohen, 2012, On the observed response of ozone to NOx and VOC reactivity reductions in San Joaquin Valley California 1995–present, Atmos. Chem. Phys., 12, 8323–8339.

Pusede, S. E., Gentner, D. R., Wooldridge, P. J., Browne, E. C., Rollins, A. W., Min, K.-E., Russell, A. R., Thomas, J., Zhang, L., Brune, W. H., Henry, S. B., DiGangi, J. P., Keutsch, F. N., Harrold, S. A., Thornton, J. A., Beaver, M. R., St. Clair, J. M., Wennberg, P. O., Sanders, J., Ren, X., VandenBoer, T. C., Markovic, M. Z., Guha, A., Weber, R., Goldstein, A. H., and Cohen, R. C.: On the temperature dependence of organic reactivity, nitrogen oxides, ozone production, and the impact of emission controls in San Joaquin Valley, California, Atmos. Chem. Phys., 14, 3373-3395, doi:10.5194/acp-14-3373-2014, 2014.

Pusede, S. E., Duffey, K. C., Shusterman, A. A., Saleh, A., Laughner, J. L., Wooldridge, P. J., Zhang, Q., Parworth, C. L., Kim, H., Capps, S. L., Valin, L. C., Cappa, C. D., Fried, A., Walega, J., Nowak, J. B., Weinheimer, A. J., Hoff, R. M., Berkoff, T. A., Beyersdorf, A. J., Olson, J., Crawford, J. H., and Cohen, R. C.: On the effectiveness of nitrogen oxide reductions as a control over ammonium nitrate aerosol, Atmos. Chem. Phys., 16, 2575-2596, doi:10.5194/acp-16-2575-2016, 2016.

Rollins, A.W., et al., 2012, Evidence for NOx control over nighttime SOA formation, Science, 337, 1210-1212.

Solomon, P.A. and Magliano, K.L., 1998, The 1995-Integrated Monitoring Study (IMS95) of the California Regional PM10/PM2.5 air quality study (CRPAQS): Study overview, Atmospheric Environment, 33(29), 4747-4756.

Turkiewicz, K., Magliano, K; and Najita, T., 2006, Comparison of Two Winter Air Quality Episodes during the California Regional Particulate Air Quality Study, Journal of Air & Waste Management Association, 56, 467-473

Watson, J.G., and Chow, J.C.A., 2002, Wintertime PM2.5 Episode at the Fresno, CA, Supersite; Atmospheric Environment, 36, 465-475.